Macromolecules For Protein Binding Using Dendrimer and Graphene Oxide

Amal Alageel

Department of Chemistry

The University of Sheffield

Submitted to the University of Sheffield

In fulfilment of the requirements for the degree of

Doctor of Philosophy

2024

Acknowledgements

I would like to express my profound gratitude to my supervisor, Dr. Lance Twyman, whose unwavering support and encouragement made this work possible. His insightful guidance and expert advice were invaluable in shaping both the direction and quality of this research.

I am also deeply thankful to the members of the research group—Dr. Abdulfatah, Dr. Khalid, Dr. Enas, Dr. Abdullah, and Dr. Reyad—for their consistent collaboration, constructive suggestions, and shared expertise, which significantly enriched my academic experience.

My appreciation extends to additional group members including Mr. Abdul Latif, Mr. Nayef, Ms. Manar, Ms. Leema, Ms. Nada, and especially Ms. Ohoud and Mr. Chen, whose collegiality and support were greatly valued throughout the research process.

I would like to thank Dr. Ibrahim Althobaiti for recommending Dr. Twyman as my supervisor and for his continued guidance and encouragement throughout my doctoral studies.

I am also grateful to the Iraqi Group, particularly Dr. Saif, for his collaborative spirit and generous support. Special thanks go to Miss. Fatimah Asseri, whose generosity, professionalism, and steadfast support were deeply appreciated.

I extend my sincere thanks to the technical staff whose assistance contributed significantly to the completion of this research. In particular, I would like to thank Mr. Alan, Mr. Michael, Dr. Simon Parker, Mr. Joseph, Mr. Samuel, Mr. Luke, and Dr. Anna Foster for their technical expertise. I also acknowledge Nick and Sharon in the stores; Dr. David Griffin and Dr. Deeba Zahoor in the Departmental Safety Office; Denise and Louise on the C-floor; Dr. Craig Robertson for his support with X-ray analysis; Sharon Spey for her assistance with mass spectrometry; and Dr. Khalid Doudin for his generous guidance and expertise in NMR spectroscopy, which was essential to the success of this research

To all who have influenced me—through support, challenge, or simply presence—thank you. I am especially grateful to my family, whose encouragement and belief in me, in every form, helped shape this journey.

I am especially grateful to Shaqra University and Imam Muhammad ibn Saud Islamic University for their financial support, without which this research would not have been possible. I also extend my sincere appreciation to the Saudi Cultural Attaché in London for their continuous support of Saudi students pursuing studies abroad.

Finally, I would like to express heartfelt thanks to my dear friend **Reem**. Though our academic paths have diverged, her enduring friendship and encouragement remained a constant source of strength throughout this journey.

*To my beloved **Sara** and **Lena**, you are the greatest blessings in my life.*

Abstract

This research explored non-covalently functionalized dendrimers and graphene oxide as macromolecular ligands for protein binding. Their structures were functionalized with amino acids to modulate protein recognition and binding.

Developing macro-ligands to target large protein binding surfaces is an effective strategy for inhibiting protein-protein interactions. While covalently functionalized macromolecules have shown potential, their synthesis and control over the positioning of binding groups can be challenging. Therefore, in the first area of research, dendrimers that had been functionalized using non-covalent methods were examined. This involved synthesizing neutral PAMAM dendrimers that could not bind to the surface of α-chymotrypsin (Chy) and a series of linear chains that could bind the protein. These chains were originally synthesised using a simple Boc protection strategy that involved a considerable amount of aqueous workup. However, the use of water resulted in very low yields and poor purity. This thesis describes a new CBz protection method that avoids the use of aqueous workup and was able to generate the required chains in excellent yield and high purity. Linear chains with either tyrosine or valine were prepared and up to 6 of these could be encapsulated within the G3.5 OH ended dendrimer, with a further 4 or 5 remaining dissolved in the bulk water. The resulting complexes were tested for their ability to bind the protein cytochrome-c. To facilitate a quantitative analysis, the quencher zinc-tetra(4-hydroxyphenyl) porphyrin (Zn-THPP) was also encapsulated. Using a fluorescence titration technique a dissociation constant (K_d) of 33 nM was measured for the G3.5 dendrimer encapsulated with the tyrosine chains. In contrast, no binding could be detected using the dendrimer alone, or the dendrimer encapsulated with the valine chains.

The next part of this project examined a similar "dynamic" approach to protein binding, using graphene oxides (GO) functionalized through both covalent and non-covalent approaches. This involved synthesising a series of anthracenes modified with various amino acids. These could be added to GO covalently, via a Diels-Alder reaction. In this case the functional groups were fixed in specific positions on the GO surface, and any biding would involve the protein moving around, which would limit the binding efficiency. The same anthracenes could also be added to the GO surface using non-covalent π-π interactions (by simply mixing the GO and functionalized anthracenes together in water). In this case the functional groups were free to move around the surface of the GO, allowing for maximum binding efficiency. As expected, the non-covalently functionalized anthracenes demonstrated enhanced binding to chymotrypsin through a series of inhibitory experiments.

The research was extended to the study of GO systems functionalized with a mixture of functional groups (using covalent and non-covalent methods). Subsequent binding studies indicated that these mixed systems were more effective than corresponding systems functionalised with a single functional group, highlighting the benefits of combining amino acids for better binding affinity. Overall, the work described presents a proof of principle that addresses the difficulties in controlling functional group placement in precise 3D locations on the surface of protein binding ligands.

Abbreviations

^{13}C-NMR - Carbon-13 nuclear magnetic resonance

Ala - Alanine

Anthracene -AA - anthracene-amino acid ligands

BTNA - N-benzoyltyrosine-p-nitroanilide

CD - Circular Dichroism

$CDCl_3$ - Deuterated chloroform

Chy - α-Chymotrypsin

Cyt *c* - Cytochrome *c*

D_2O - Deuterated Water

d^6-DMSO - Deuterated dimethyl sulfoxide

DCC -Dynamic combinatorial chemistry

DCLs -Dynamic combinatorial libraries

DMAP -4-Dimethylaminopyridine

EDA - Ethylene diamine

ES MS - Electrospray Ionisation Mass Spectrometry

FTIR - Fourier Transform Infrared Spectroscopy

G – Generation

Glu - Glutamic acid

GO- Graphene Oxide

MA- Methyl Acrylate

PAMAM- Poly (amido amine)

PAMAM-OH- Neutral Hydroxyl Terminated PAMAM

Tyr - Tyrosine

Val – Valine

NMR Abbreviations

d - doublet
m - multiplet
q - quartet
s- singlet
t - triplet
m - meta
p – para
o - ortho

Table of Contents

Chapter 1

Introduction

1.0 Introduction to Protein-Protein Interactions

Proteins are crucial molecules in all living organisms, serving a wide range of important biological functions. They consist of long chains of amino acids, which are encoded by genes. In order to create functional proteins, these amino acids are linked to form peptides, which subsequently fold into intricate three-dimensional structures. These proteins contribute to the formation of tissues and organs and participate in a range of vital biological processes, including catalysing metabolic reactions, transporting critical substances such as oxygen, supporting the immune system, and facilitating cellular communication through signal transduction.

Moreover, proteins are involved in a variety of basic cellular activities including DNA replication, transcription, translation, and transmembrane signalling, all of which are essential to life and directly affect human health. Many of these biological functions are controlled by specific protein-protein interactions (PPIs)[1] within protein complexes. It is essential for maintaining cellular homeostasis and ensuring the efficiency of biological processes for these complexes to function properly. Any misregulation or malfunction of these PPIs can lead to various diseases, including cancers, neurodegenerative disorders, and autoimmune conditions.

In general, PPIs can be divided into two main types: homocomplexes and heterocomplexes. Homocomplexes, which formed when identical proteins interact and are typically stable as well as able to carry out structural or long-term enzymatic functions. In contrast, heterocomplexes are composed of interactions between different proteins, which are often responsible for regulating transient and dynamic processes such as signalling and immune responses. Because heterocomplexes have a regulatory nature, they frequently participate in processes that require the assembly and disassembly of protein units, making them particularly important for cellular regulation and adaptation.

The specificity of protein interactions is determined by distinctive interfacial regions, which allow proteins to recognize and bind to the appropriate partners. These interactions can be disrupted by protein aggregation, where misfolded proteins clump together. As a result of abnormal protein folding, this aggregation is a hallmark of many diseases, including Alzheimer's disease, in which amyloid plaques are formed.[2] To develop therapeutic interventions, it is imperative to understand the mechanisms involved in these interactions as well as the environmental conditions that lead to their failure.[3,4]

Currently, scientists are working on developing synthetic agents capable of inhibiting harmful protein aggregates or promoting beneficial interactions with PPIs. Research using this approach may lead to the development of cures for diseases related to protein misfolding and aggregation, including Alzheimer's disease, Parkinson's disease, and rheumatoid arthritis (Figure 1).[5]

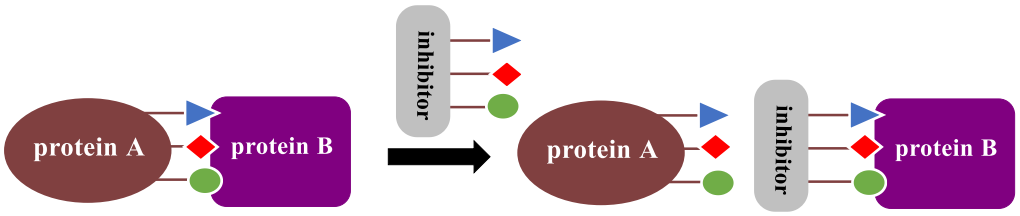

Figure 2-Illustration of the proteomimetic concept for disrupting protein-protein interactions (PPIs).[5]

1.1 Amino acid and protein

The word "protein" is derived from the Greek word "proteios", meaning "primary," emphasizing the essential role that proteins play in every biological system.[5] Proteins are polymers composed of 20 amino acids, each of which contributes to their unique chemical and structural properties. These amino acids fold into specific tertiary structures (figure 2), which enable proteins to perform a variety of biological functions. The most abundant elements found in proteins are carbon, hydrogen, oxygen, and nitrogen, with nitrogen constituting approximately 16% of its weight. Additionally, minor elements, such as sulphur and phosphorus, are present, but in small amounts.

In order to synthesize proteins, amino acids are polymerized, a process which involves the formation of covalent bonds known as peptide bonds. These bonds link the carboxyl group of one amino acid and the amino group of another amino acid. A dipeptide is formed when two amino acids are combined; similarly, a tripeptide is formed when three amino acids are joined, and polypeptides are formed when longer chains of amino acids are connected. "Protein" is a term used in biochemistry to refer to a chain of polypeptide chain containing more than 50 amino acids. The polypeptide backbones consist of repetitive sequences of atoms, with side chains attached to the amino acids. These side chains are unique to each amino acid and are responsible for determining whether the amino acid is hydrophobic, polar, or reactive.

Amino acid side chains possess distinctive properties that determine how proteins fold, interact with other molecules, and perform their biological functions. As a result of their versatility, proteins are involved in a wide range of processes, such as catalysing biochemical reactions (as enzymes), transporting molecules, providing structural support, and regulating cellular functions via signal transduction.

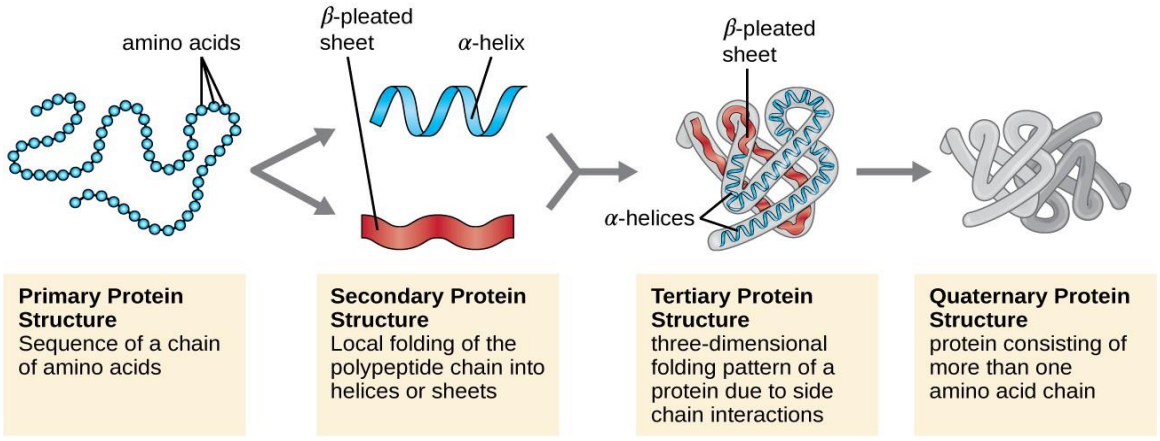

Figure 2- Different Protein structure: primary, secondary, tertiary, and quaternary.

1.2 Understanding hot spots and interfacial area.

The structure of a protein is determined by its unique sequence of amino acids, which directs the protein to fold into a specific three-dimensional shape. This folding process is critical, as it directly affects the protein's function. Each protein's function is based on its amino acid sequence and conformation. These conformations create distinct surface topographies of chemical groups, which are essential for the protein's interactions with other molecules and its overall biological function.[6]

The first step in designing molecules that disrupt protein-protein interactions is understanding the characteristics of protein interfaces.[7] The protein-protein interfacial area is a large accessible surface that becomes buried and inaccessible to solvents once a protein complex form. This area is primarily hydrophobic, with non-polar residues playing a key role in stabilizing the interaction. However, polar groups surrounding this hydrophobic core contribute to the specificity and affinity of the interactions. Understanding these features is essential for developing targeted inhibitors.[8]

Protein-protein interactions occur through weak non-covalent bonds, allowing proteins to fold into specific shapes and bind together to form larger cellular structures. These interactions are

driven by electrostatic forces, hydrogen bonds, van der Waals forces, and hydrophobic effects. Various theories have been proposed to explain the mechanisms behind these interactions and the conformational changes that occur.

One of the earliest theories was introduced by Emil Fischer in 1894, known as the "lock and key" model. Fischer suggested that a protein fits its ideal partner, much like a key fits into a lock, with minimal structural changes.[9] However, this theory has limitations, as it does not account for interactions involving flexible proteins or ligands with varying shapes.

To address this, Daniel Koshland proposed the "induced fit" model in 1958,[10]which argues that the active site of a protein is somewhat flexible and can adjust its conformation to accommodate a binding ligand. As a result, conformational changes occur in response to ligand binding, allowing for more diverse protein-protein interactions.

Following this, the pre-existing equilibrium hypothesis was introduced. This model suggests that proteins exist in an ensemble of conformations at the active site, and ligand binding shifts the equilibrium towards the most active conformation. This theory highlights the dynamic nature of proteins and how they can adopt multiple conformations before binding with ligands, adding another layer of complexity to our understanding of protein-protein interactions.[2]

Understanding protein-protein interactions is complex due to several contributing factors, including the large surface areas involved, electrostatic forces, and hydrophobic effects. No single factor can perfectly predict these interactions, but considering all of them together offers reasonable insight. The binding mechanism is highly specific, with proteins selecting partners of similar size and three-dimensional shape. Intermolecular forces such as hydrogen bonding, van der Waals interactions, and electrostatic forces, along with the specific arrangement of amino acids, play key roles in determining which proteins bind together. Figure 3 illustrates this selection process, highlighting how proteins identify and interact with compatible partners, demonstrating the importance of shape complementarity and molecular forces in these interactions.

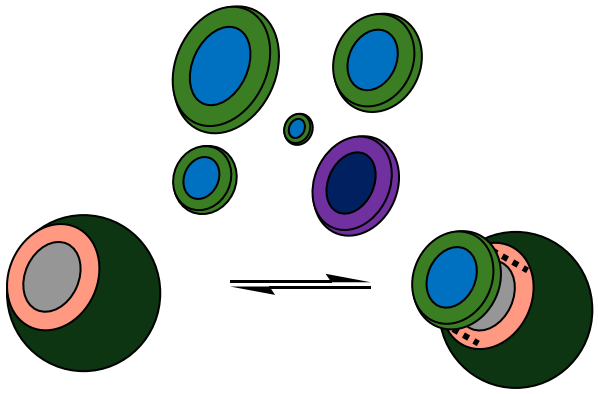

Figure 3-The selection of a compatible partner in protein-protein binding mechanism.

Binding sites on proteins play a critical role in facilitating interactions with other molecules through non-covalent bonds. These sites are typically composed of specific regions on a protein's surface where complementary molecular shapes and electrostatic properties allow for effective binding. Numerous studies have focused on identifying the key residues that contribute to these binding interactions, commonly referred to as "hot spots." This concept was first introduced by Clackson and Wells,[11] who found that the free energy of binding is concentrated within a limited region of amino acid residues on the protein's surface.

To investigate these hot spots, researchers often employ alanine scanning, a technique that involves systematically mutating amino acid residues at the binding interface to alanine. This approach helps determine the impact of each residue on the binding free energy of the protein complex. Bogan and Thorn[12] utilized this method in their analysis of protein interactions, examining a total of 2,325 mutations of surface residues containing alanine. Their findings revealed that hot spots represent a small, pre-organized surface area of the protein, enriched with specific amino acids that play a pivotal role in binding.

Moreover, Bogan and Thorn's research indicated that the energetic contributions of these hot spots are not uniformly distributed. Instead, they found that the hot spots are typically located at the center of the binding interface, while some surrounding residues do not directly participate in the binding process. These non-binding residues, which are less energetically stable, function like "O-rings," creating a barrier that prevents bulk solvent from interfering with the interactions necessary for optimal binding.

The study also explored the amino acid preferences within the hot spot regions, revealing that certain residues are overrepresented compared to their abundance in the overall protein structure. For instance, tryptophan was found to constitute 21% of the residues in these regions, followed by arginine at 13.3% and tyrosine at 12.3%. This enrichment of specific amino acids

suggests that they may confer distinct advantages, such as enhanced binding affinity or specificity, contributing to the overall stability of the protein-ligand complex (Figure 4).[13]

In summary, understanding the structural and energetic characteristics of binding sites, especially the hot spots within them, is crucial for deciphering protein-protein interactions and developing targeted therapeutic strategies. The insights gained from alanine scanning and the analysis of amino acid preferences pave the way for further investigations into protein interactions, potentially leading to advancements in drug design and protein engineering.

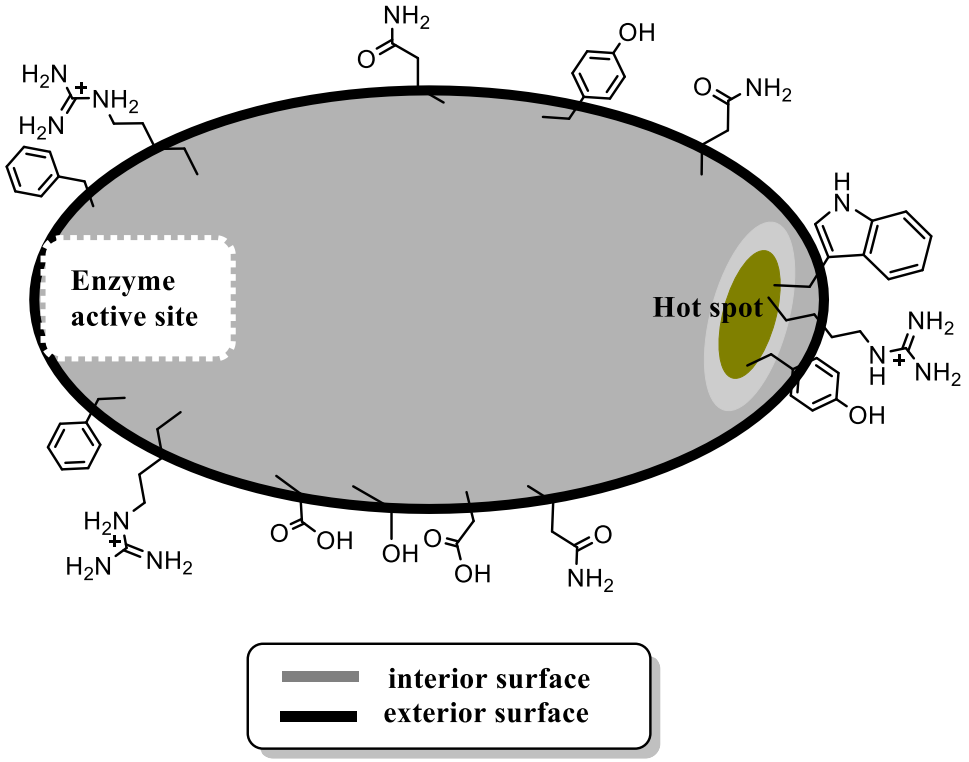

Figure 4 -An illustration of the interior, exterior, and hot spots of a protein (enzyme).[12]

Due to their hydrophobic effects, certain amino acids play a crucial role in contributing to the binding energy of protein-protein interactions and are more commonly found at the interaction interface or "hot spot." These amino acids, such as tryptophan, tyrosine, and arginine, are preferred within hot spots because they help stabilize the binding interaction through their side chains. The structural depressions and concavities in these regions facilitate the fitting of complementary proteins, creating a highly specific and stable interaction. While a protein may have multiple hot spots, successful binding typically requires that the resulting protein complex achieves a low-energy, highly stable conformation. This specificity ensures that hot spots do

not contain arbitrary amino acids, but rather, are composed of residues optimized for binding efficiency and stability.

Despite the weak nature of individual protein-protein interactions, cooperative binding plays a crucial role in achieving a wide range of biological and biochemical functions. Cooperative binding occurs when the binding of one molecule to a site on a macromolecule (such as a protein) influences the binding of additional molecules, either enhancing or inhibiting their attachment. This process provides stability to molecule-molecule interactions, resulting in stronger combined forces than when molecules act independently.

Positive cooperative binding, in particular, increases the apparent affinity of a molecule, meaning that the likelihood of binding for subsequent molecules rises once the initial binding occurs. This can be understood as a substantial increase in the effective local concentration of the ligand for the second binding event. Initially, a bond forms between the first binding site and the ligand at a rate denoted by K_1, which represents the dissociation constant for the first interaction. Once this bond forms, the subsequent interaction occurs more quickly and with greater strength, represented by a dissociation constant K_2. Because the relative concentration of the second ligand near the binding site becomes higher than that of other molecules, K_2 is significantly smaller than K_1. This demonstrates that the effects of cooperative binding are not simply additive, but rather synergistic, resulting in a much stronger overall binding affinity.

The concept of cooperative binding is vital to understanding how proteins and other macromolecules function in a biological context. For example, hemoglobin, the oxygen-carrying protein in red blood cells, exhibits positive cooperative binding when interacting with oxygen molecules. The binding of one oxygen molecule to hemoglobin enhances the affinity of the protein for additional oxygen molecules, allowing efficient oxygen uptake and transport throughout the body.[14]

From a thermodynamic perspective, positive cooperative binding typically increases enthalpy and decreases entropy, meaning that the system becomes more structured and ordered as additional molecules bind (Figure 5). The ordered arrangement of molecules due to cooperative binding allows for stronger, more stable interactions between molecules. This increased stability is reflected in biological processes where efficient and regulated binding is crucial, such as enzyme-substrate interactions, signal transduction, and cellular adhesion.

In summary, cooperative binding plays a key role in amplifying the stability and strength of molecular interactions in biological systems. Its ability to enhance affinity and promote stronger bonds through positive cooperation is fundamental to the function of many proteins and macromolecular assemblies. This mechanism explains how weak individual interactions can collectively lead to significant biological effects.

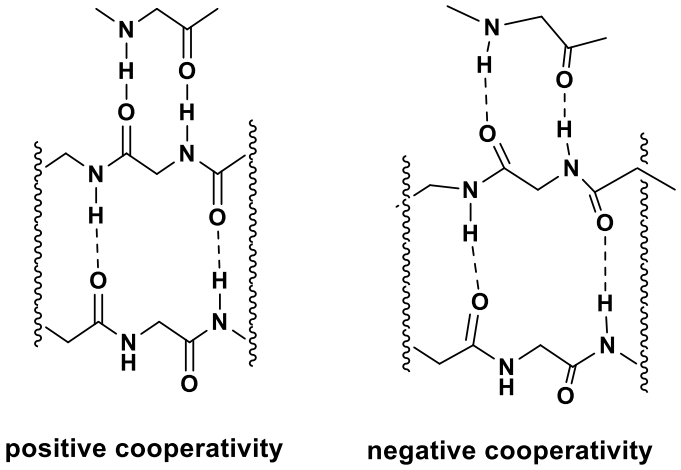

Figure 5- Schematic representation structural models for positive and negative cooperativity, where positive shows more stable bonds.

1.3 Inhibition of protein-protein interactions

A wide range of biological processes reliant on protein-protein interactions, including enzymatic activity, signal transduction, and the maintenance of cellular structure. Disruption of these interactions has emerged as a key strategy for the development of novel therapeutic agents, especially in the treatment of diseases associated with improper protein function, such as cancer and neurodegenerative diseases. Significant progress has been made in the development of synthetic inhibitors that can target and modulate these interactions in recent years due to advancements in molecular biology. Several small and large biomolecules have been investigated as potential PPI inhibitors, such as peptides and antibodies.

The majority of PPI interactions take place through non-covalent forces, including Van der Waals interactions, electrostatic attractions, hydrophobic effects, and hydrogen bonds. Protein complexes benefit from these interactions because they ensure specificity and stability, while also providing a dynamic response to cellular signals. It is possible to inhibit PPIs in two ways, depending on the structural features of the target protein.

The first approach involves targeting the protein's interior active sites, which are often buried. The active sites of small molecules typically bind small substrates and are not accessible to bulk solvents, making them particularly useful for the inhibition of enzyme activity.

The second approach focuses on disrupting exterior surface interactions between proteins. The exterior regions are more exposed to solvents and often the sites of transient regulatory interactions, such as those in signal transduction pathways and immune responses. This case can be overcome by using larger biomolecules, such as antibodies, to block these exposed binding interfaces, inhibiting the PPI process.

The development of effective therapeutic agents requires a thorough understanding of the structural and mechanistic nuances of these interactions. Researchers continue to investigate inhibitors that target both interior and exterior protein surfaces as potential therapeutics to modulate PPIs across a wide range of disease settings.

1.4 Small molecule inhibitors

The development of small molecules, typically with molecular weights below 500 Da, has gained significant attention as potential inhibitors for a range of diseases, including cancer, autoimmune disorders, and infections. These molecules are often designed to interact with specific regions of proteins, particularly enzyme active sites. Within these active sites, hydrogen bonds, salt bridges, and electrostatic interactions predominate, allowing small molecules with hydrophilic motifs, hydrogen-bond donors, and receptors to be effective. The ability of these molecules to mimic natural substrates or inhibitors enables them to bind tightly to target enzymes, disrupting normal biological processes.

However, designing synthetic agents that effectively target protein-protein interactions presents several challenges. One major obstacle is the size of the surface area involved in these interactions, typically ranging from 700 to 1500 $Å^2$ per protein. This large surface area makes it difficult for small molecules to fully engage the protein interface. Moreover, the interacting surfaces of proteins tend to lack distinctive features like deep pockets or grooves, which are common in enzyme-ligand interactions. Instead, these surfaces often consist of shallow depressions, making it harder to achieve selective targeting with small molecules.

Another significant challenge is the non-contiguous nature of binding regions on protein partners. In protein-protein interactions, the contact areas are often spread across different regions of the protein surface, rather than being confined to a single, well-defined pocket. This

makes it difficult for synthetic peptides or small molecules to effectively mimic these interactions, as they lack the spatial structure to bridge multiple contact points simultaneously.

Protein-protein interactions are also more complex than enzyme-ligand interactions. Instead of one partner fitting neatly into a binding pocket of the other, both proteins in a complex may contribute protrusions and sub-pockets. This interlocking arrangement complicates the design of inhibitors because small molecules may struggle to occupy all the necessary binding sites simultaneously.

Moreover, even if a small molecule is successfully designed to inhibit a target protein, it must still be validated for efficacy in vivo, ensuring minimal toxicity, sufficient bioavailability, and appropriate pharmacokinetics. Small molecules must not only demonstrate the ability to bind effectively to their target but also maintain high selectivity to minimize off-target effects. As a result, the process of designing, testing, and optimizing small molecule inhibitors is complex and requires careful consideration of both molecular structure and biological function. Despite these challenges, small molecule inhibitors remain a promising approach for drug development, particularly when addressing diseases with known protein targets.

Despite the challenges, extensive research has been dedicated to developing small synthetic compounds that can inhibit protein-protein interactions. Although these small molecules may not match the binding efficacy of a protein's natural partners, they offer a promising avenue for therapeutic intervention, particularly due to their potential for oral bioavailability and ease of chemical modification. Advances in structure-based drug design and high-throughput screening have also contributed to the identification of small molecule inhibitors capable of targeting specific protein-protein interactions, despite the inherent complexity of such interactions.

Maraviroc is a commercially available small molecule inhibitor known for its selective and slowly reversible antagonistic action against the chemokine receptor CCR5 (Figure 6). This receptor plays a crucial role in the entry of the Human Immunodeficiency Virus (HIV) into host cells. By binding to the CCR5 receptor, Maraviroc effectively blocks the interaction between the receptor and HIV, preventing the virus from entering CD4 T cells. CD4 T cells are vital components of the immune system, and their infection by HIV leads to the deterioration of immune function in individuals with HIV. Maraviroc, by blocking this critical entry pathway, significantly reduces the ability of HIV to infect these cells and helps slow the progression of HIV infection. This mechanism highlights Maraviroc’s importance as a

therapeutic agent in the management of HIV, particularly for patients whose HIV strain uses the CCR5 receptor for cell entry.[15]

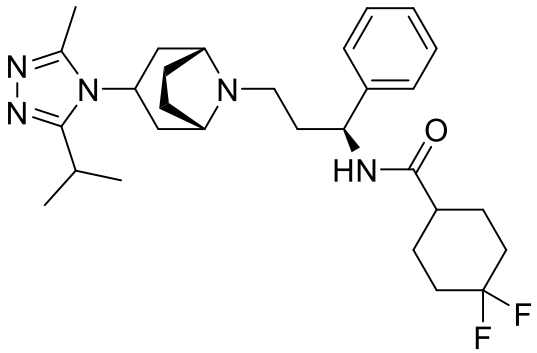

Figure 6- Chemical structure of Maraviroc

Inhibiting protein-protein interactions is a critical approach in cancer therapy, particularly in targeting the p53 tumour suppressor pathway. One notable advancement in this area is the discovery of Nutlins, a class of imidazoline-containing compounds, by Vassilev et al. in 2004. Nutlins are small molecules designed to disrupt the interaction between MDM2 and p53, which is essential for the regulation of p53's tumour suppressor activity. Normally, MDM2 binds to p53, leading to its degradation and consequently inhibiting its function in controlling cell growth and apoptosis. By disrupting this interaction, Nutlins prevent MDM2 from degrading p53, allowing p53 levels to accumulate in the cell. This increase in p53 activates critical cellular pathways responsible for promoting apoptosis (programmed cell death) and arresting the cell cycle, essential processes for eliminating cancerous cells.

Nutlins achieve this by binding to the hydrophobic pockets of MDM2 (specifically targeting residues Phe19, Trp23, and Leu26), blocking its interaction with p53. After extensive chemical optimization, Nutlin-3 (Figure 7), emerged as a potent inhibitor, with an IC50 value of 90 nM, making it highly effective in disrupting MDM2-p53 complexes. In addition to its molecular efficacy, Nutlin-3 has shown promising activity in preclinical studies, including its ability to inhibit tumour growth in xenograft models in vivo. This demonstrates Nutlin-3's potential as a therapeutic agent in cancers where the p53 pathway is dysregulated, offering hope for targeted cancer therapies aimed at restoring p53 function.[16]

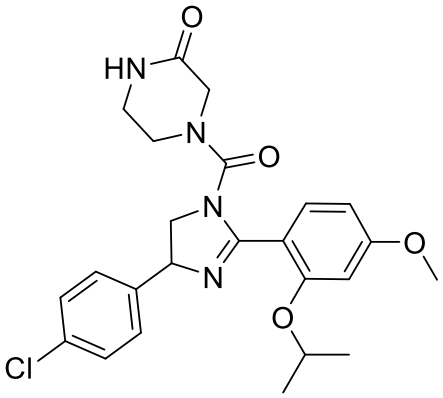

Figure 7 - The chemical structure of Nutlin-3

One of the most significant protein targets in the field of biomedicine is inducible nitric oxide synthase (iNOS). This enzyme plays a crucial role in signal transduction by producing nitric oxide (NO), a signalling molecule that is vital for various physiological processes. The dimeric enzyme nitric oxide synthase consists of different isoforms, among which iNOS is particularly noteworthy due to its association with tissue damage in various autoimmune diseases, including rheumatoid arthritis and multiple sclerosis. Given its involvement in these pathological conditions, the selective inhibition of iNOS (Figure 8) presents a promising therapeutic strategy.

Research conducted by McMillan and colleagues focused on developing a small-molecule inhibitor of iNOS using combinatorial chemistry techniques. The study utilized X-ray crystallography to explore the enzyme's structure, specifically examining the dimerization interface and substrate binding site. Their findings revealed that the inhibitor effectively perturbed these critical areas, disrupting the formation of the iNOS dimer through an allosteric mechanism. This innovative approach not only blocks the enzyme's function but also offers a pathway to more selective targeting, reducing potential side effects.

In vivo studies on rat models demonstrated that this novel inhibitor exhibited an effective dose (ED50) of less than 2 mg/kg, confirming its therapeutic potential for treating conditions associated with elevated iNOS activity. These findings underscore the importance of targeting iNOS in the development of new therapeutic agents aimed at managing autoimmune diseases.[17,18]

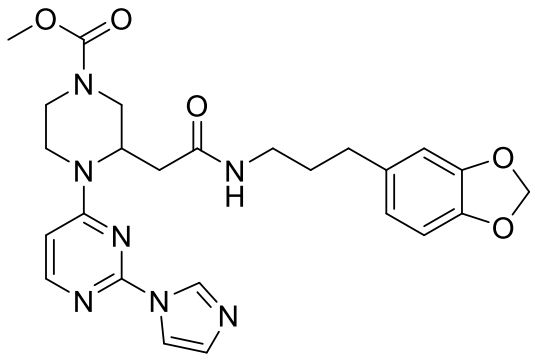

Figure 8- Chemical structure of iNOS inhibitor

Tumour necrosis factor alpha (TNF-α) is a cytokine that was originally associated with inducing tumour necrosis. However, more recently, it has been recognized for its role in the pathology of autoimmune diseases. TNF-α plays a key role in inflammatory processes, making it a prime therapeutic target in disorders such as rheumatoid arthritis. To inhibit TNF-α, various therapeutic antibodies have been developed, including well-known drugs like Enbrel, Remicade, and Humira. These biologic therapies have proven highly effective in reducing inflammation and disease symptoms in patients with autoimmune conditions, particularly rheumatoid arthritis.

A recent advancement in TNF-α inhibition was made by He et al., [19] who developed a potent TNF-α inhibitor. The mechanism by which this inhibitor works involves displacing a biologically active subunit within the TNF-α trimer, leading to the formation of an inactive dimer. This effectively neutralizes TNF-α activity, preventing it from exerting its inflammatory effects.[19,20] Figure 9 demonstrates the structure of this novel inhibitor. These developments underscore the importance of targeting TNF-α in the treatment of autoimmune diseases, as well as the ongoing research efforts to improve the efficacy and specificity of TNF-α inhibitors.

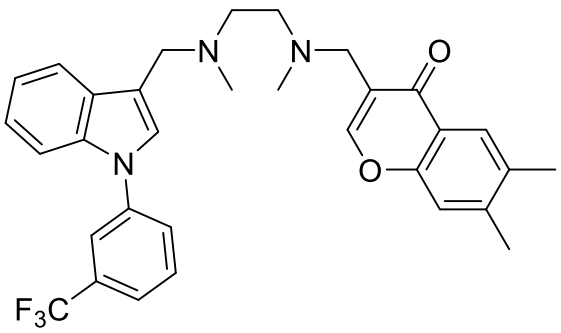

Figure 9- The chemical structure of TNF-α inhibitor

1.5 α-Helix Mimetics

α-Helices are common protein secondary structures and serve as recognition regions for numerous protein–protein, protein–DNA, and protein–RNA interactions (Figure 10). The development of peptide mimics that adopt stable helices has become a powerful tool for modulating PPI activity in vitro as well as in vivo. Specific features of the α-helix which are important in considering factors involved in mimetic design. The α-helix is usually associated with sequences of hydrophobic amino acids, including Ala, Ile, Leu, Met, Phe, Pro, Trp, Tyr, and Val, with up to 16 residues. Many crucial interactions occur in alpha-helix-protein complexes along one face of the structure. This involves side chains from residues i, i + 3, and i + 7 (Figure 9)[21].

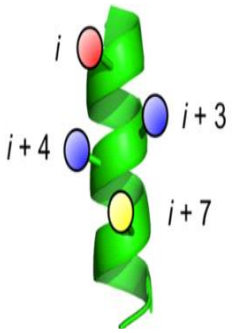

Figure 10- structure of α-Helix with i, i + 3/4, and i + 7 side chains.

Hamilton et al. presented an innovative method for disrupting protein-protein interactions through an α-helix-mimicking approach. [22]This technique involves the utilization of terphenyl scaffolds to develop synthetic mimics that replicate the hydrophobic face of an α-helix, a crucial feature in many protein interactions (Figure 11(A)). One noteworthy example is a tris-pyridylamide scaffold (Figure 11(C)), which showcases a preferred conformation in which all three functional groups are oriented on the same face of the molecule. This specific arrangement is made possible by the inclusion of iso-propoxy groups, which contribute to the stability and functionality of the structure. Additionally, a bifurcated hydrogen-bonding network plays a pivotal role in maintaining this optimal conformation, effectively mimicking the α-helical BH3 domain of Bak. This approach not only enhances the understanding of protein interactions but also opens avenues for developing targeted therapeutic strategies to disrupt detrimental protein-protein interactions in various diseases, including cancer. By mimicking the structural characteristics of α-helices, such scaffolds can provide valuable insights into the design of new molecules that can interfere with specific protein interactions, paving the way for novel drug discovery.

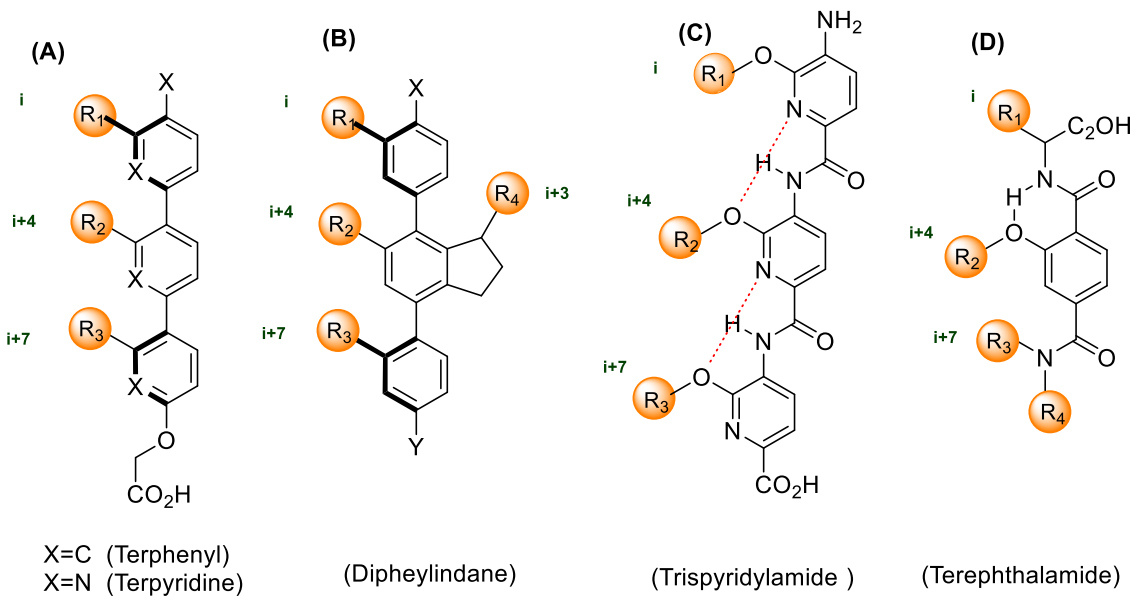

Figure 11- general structure of non-peptide, single-face α-helix mimetics based on the terphenyl scaffold derivatives with residues positioned at i, i + 3, i + 4, and i + 7.

Hamilton et al. have further enhanced the solubility and synthesis simplicity of the mimetics by designing scaffolds based on terephthalamide (Figure 11(D)). Human HEK293 cells treated with terephthalamide derivatives showed disruption of Bcl-xL-Bak interactions. This outcome confirms that terephthalamide serves as a successful alternative scaffold to terphenyl for mimicking α-helical structures.

Furthermore, considerable attention has also been dedicated in the creation of non-peptidic small molecule α-helical mimics as inhibitors of protein-protein interactions. Lee et al presented in 2011 a novel pyrrolopyrimadine-based receptor, which is shown in Figure 12.

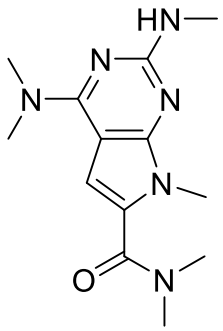

Figure 12- The pyrrolopyramidine chemical structure based α-helix mimic.

This scaffold was monitored for its ability to disrupt the p53-MDMX interaction as an α-helical mimic. To accomplish this, the scaffold was screened against a library of 900 compounds, followed by the selection of primary amines comprising hydrophobic groups. The latter played essential role in replicating the side chains of the three amino acids found in p53. The scaffold exhibits good aqueous solubility, cell permeability, and conformational rigidity. Furthermore, the synthetic route is relatively straightforward, which will make the procedure suitable for the construction of large libraries and high-throughput screening. Therefore, this scaffold could be useful in the discovery of a variety of inhibitors.

The development of small molecules inhibitors remains a challenge for researchers, which leads them to explore new techniques for replicating selective protein interactions.[23] A disruption of interactions by binding to the protein surface instead of directly targeting the active site is one way to achieve this. Additionally, the interface between interacting proteins involves not only electrostatic interactions, but also hydrogen bonds and π- π stacking interactions.

Most molecules examined inhibit protein interaction by binding within active depressions, but less is known about synthetic molecules that inhibit protein function by binding to the external surface. It is possible to develop new therapeutic agents by studying these molecules and to gain a deeper understanding of how protein periphery and surfaces are recognized by proteins.[6,24]

1.6 Calixarene and porphyrin-based receptors

To address the challenges of designing small molecule inhibitors, researchers have investigated large scaffold molecules as potential protein-binding agents. An alternative strategy for inhibiting protein function involves binding to the protein surface near the active site, effectively disrupting protein-protein interactions crucial for maintaining biological processes. The peripheral surface of each protein is characterized by distinct regions with varying hydrophobic, hydrophilic, and charged properties. These regions create a complex landscape of interaction potential, where various intermolecular forces can come into play.

In addition to electrostatic interactions arising from charge complementarity, significant interactions such as hydrogen bonding and π-π stacking also occur at the interface between two proteins. These diverse interactions collectively contribute to the stability and specificity of protein complexes, making them critical targets for therapeutic intervention. By strategically

designing molecules that can bind to these surfaces, researchers can effectively modulate protein functions and develop new therapeutic strategies for diseases driven by dysregulated protein interactions. [6]

Most molecules studied in the context of protein inhibition primarily disrupt protein interactions by binding to active cavities. While this strategy has proven effective, it often overlooks the potential of surface-binding synthetic molecules, which remain largely unexplored. By focusing on the interactions that occur at the protein surface, researchers can investigate alternative binding sites that may offer new avenues for drug design. This surface-binding approach not only has the potential to lead to the discovery of novel drug candidates but also fosters a deeper understanding of protein surfaces and the mechanisms by which they recognize and interact with various ligands.

The exploration of surface-binding molecules may yield valuable insights into the dynamics of protein interactions and contribute to the development of innovative therapeutic strategies. Such insights could ultimately inform more targeted and effective approaches in drug discovery, allowing for the modulation of specific protein interactions involved in various diseases. Overall, the study of large scaffold molecules and their interactions with protein surfaces represents a promising frontier in the field of medicinal chemistry, with the potential to revolutionize how we approach the design of therapeutics for complex biological systems. [24]

It has been demonstrated by Fischer et al. (1985) that a tetracarboxyphenyl porphyrin (TCPP) (Figure 13) mimics the topology of cytochrome-c, binding with a Kd of 5 µM. Cytochrome c is a small heme protein that is loosely associated with the inner mitochondrial membrane and has been extensively studied for its roles in apoptosis and electron transfer. Its heme edge surface contains cationic lysine residues and hydrophobic domains, which play a crucial role in facilitating electrostatic interactions essential for its function.[6]

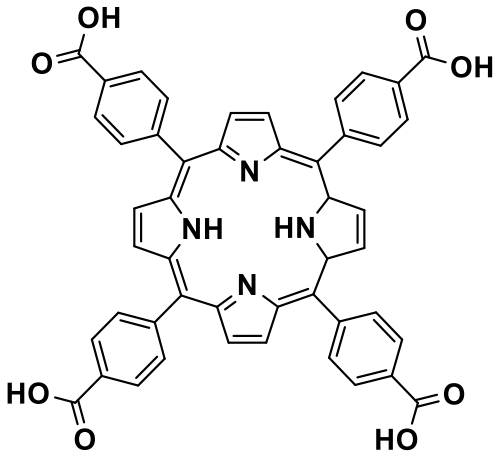

Figure 13- Tetracarboxyphenyl porphyrin structure.

Hamilton et al. extended their research by using fluorescence spectroscopy to investigate tetraphenyl porphyrin and calix[4]arene scaffolds.[24,25] In 1997, the researchers developed a macrocyclic scaffold with covalently attached peptide loops, resulting in an antibody mimic based on calix[4]arene and four peptide loops (Figure 14). The Calix[4]arene was selected because of its availability and ability to adopt a cone shape, thereby forming a binding domain when para substituents are positioned on the same edge.

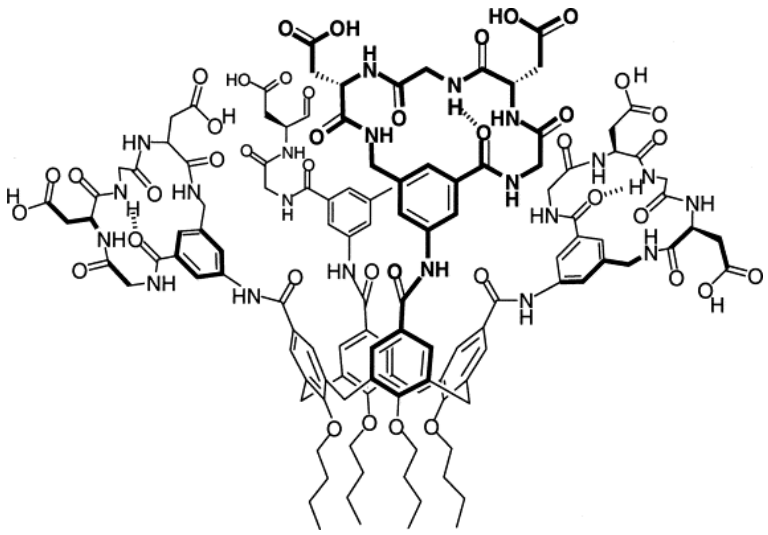

Figure 14- The structure of an antibody mimic based on a calix[4]arene scaffold covalently attached to four peptide loops in the sequence (Gly-Asp-Gly-Asp).

The initial target protein was cytochrome-c, which has a well-defined, positively charged surface. The peptide loops contain a sequence of negatively charged amino acids (Gly-Asp-Gly-Asp). Negative charges are required in order to match and interact with positively charged

surfaces on target proteins. X-ray studies showed that these loops could interact with four lysine residues present, allowing the synthetic receptor to cover a large area of the surface of the protein. According to X-ray studies, the receptor disrupts the formation of cytochrome c/cytochrome c peroxidase complexes. Further research showed that a similar antibody mimic could disrupt chymotrypsin interactions. However, calixarene receptors proved to be impractical due to the difficulty of synthesis and the low yields, prompting further research into other scaffold-based receptors.

Furthermore, Hamilton also demonstrated that an amino acid functionalized tetraphenyl porphyrin (TPP) can recognize cytochrome-c.[26] In addition, since various amino acid and peptide derivatives on the external edge affected fluorescent quenching in different ways, different proteins could be distinguished by their distinctive patterns of fluorescent quenching.[27]

TPP studies have also revealed that the number of hydrophobic and anionic groups on a receptor's surface determines its relative affinity to that surface, as shown in Figure 15. The receptor exhibits a high level of affinity in a liquid environment. A receptor with the highest affinity for cytochrome-c surfaces (20 nM Kd) is receptor (D) because it has the greatest number of carboxylic acids and phenyl groups. The electrostatic and hydrophobic interactions of these groups bind cytochrome-c. This finding suggests that this compound may not only be capable of recognizing protein surfaces but may also possess potential medicinal implications.

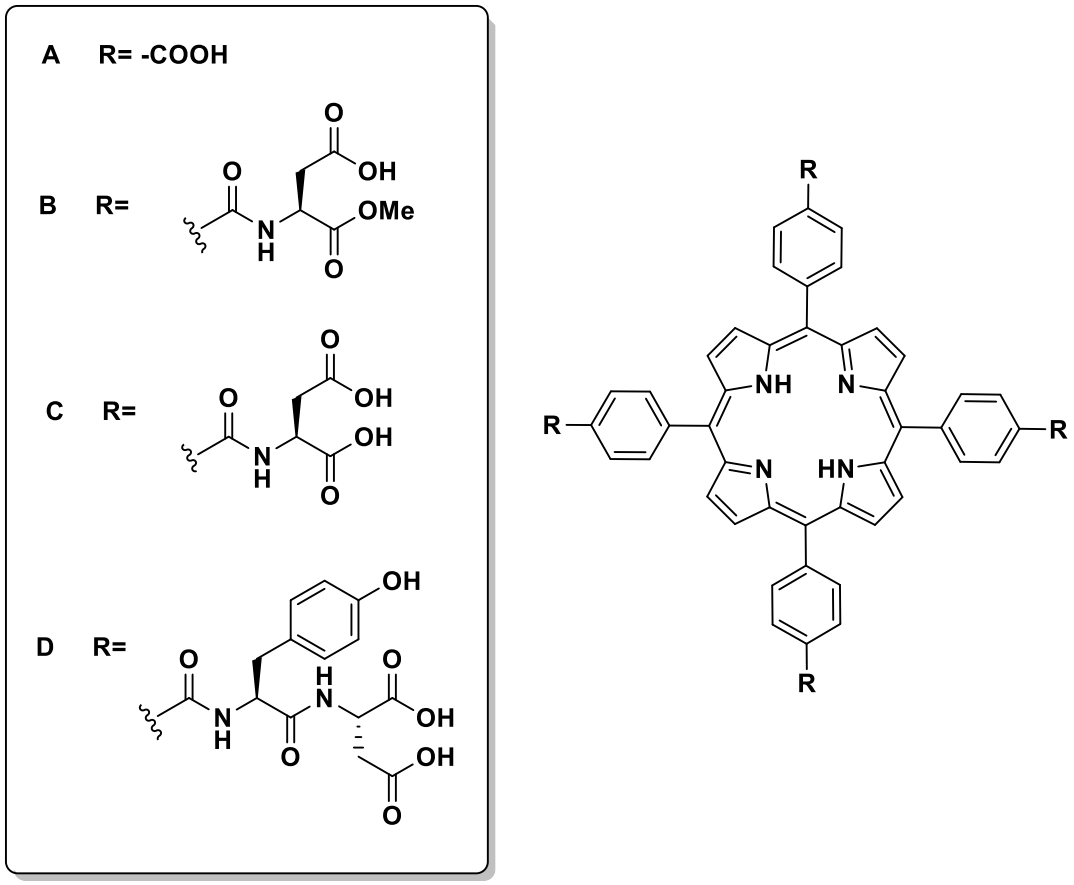

Figure 15- Tetraphenyl porphyrin scaffolds with hydrophobic and anionic groups.

Furthermore, previous studies have shown that cytochrome-c can interact with the apoptopic protease activating factor (APAF1).[28] This interaction can lead to the activation of aptosis. Therefore, receptors like these may be useful in disrupting specific protein-protein interactions.

The peripheral surface of a protein plays a crucial role in the binding of proteins during biological processes such as cell growth. Therefore, synthetic molecule designed to complement this surface can bind and disrupt these interactions rather than targeting the enzyme's active site. According to Hamilton et al. (2003), the tetrabiphenyl porphyrin receptor shows a high affinity for cytochrome-c (Kd = 0.6 nM). The structure of one of the receptors is shown in Figure 16. Using circular dichroism, it was shown that cytochrome-c's melting temperature decreased from 85°C to 35°C in the presence of this receptor, suggesting the potential for developing porphyrin-based receptors for recognizing and denaturing proteins. Further, metalloporphyrin dimers accelerated the degradation of cytochrome-c.

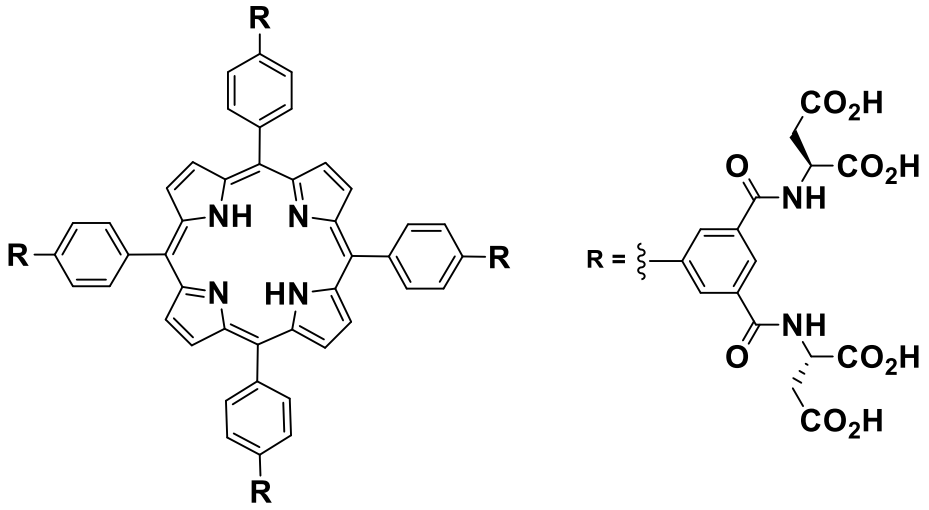

Figure 16- The structure of a tetrabiphenyl porphyrin-based receptor for enhancing cytochrome-c surface recognition and unfolding.

A recent study conducted by the Twyman group has shown that porphyrin-cored dendrimers can bind to the surface of cytochrome-c (Cyt-c) and quench its fluorescence signal.[29] This was achieved by encapsulating the signaling porphyrin within the dendrimer.

1.7 Supramolecular protein scaffold

Using self-assembled systems, Rotello and his colleagues have been able to achieve surface recognition focusing on enzymatic inhibition. This innovative approach involved the functionalization of mixed-monolayer protected gold clusters (MMPCs) with terminal anionic groups, which are designed to bind to the positively charged surface of α-chymotrypsin, a serine protease that plays a vital role in numerous biological processes. Upon interaction, the MMPCs effectively suppress the enzymatic activity of α-chymotrypsin through a two-step mechanism. In the first step, a rapid, reversible binding takes place, which is facilitated by electrostatic interactions between the anionic ligands on the MMPCs and the cationic residues on the enzyme surface. After initial binding, a slower, irreversible process leads to the gradual degradation of the enzyme, ultimately compromising its catalytic capability (Scheme 1). By comparing these electrostatic interactions with elastase, it has been demonstrated that these interactions are highly selective in binding. Circular dichroism (CD) spectroscopy was used to quantify the interaction, and it revealed an apparent inhibition constant K_i(app) of 10 nM, which in turn underscores the high affinity of the MMPCs for α-chymotrypsin. Moreover, it has been determined that the stoichiometry of the binding mechanism is five protein molecules per

MMPC, further emphasizing its strength and specificity. MMPCs demonstrated a marked preference for inhibiting α-chymotrypsin over β-galactosidase,[30,31] indicating their potential as inhibitors in modulating enzymatic activity and therapeutic applications.

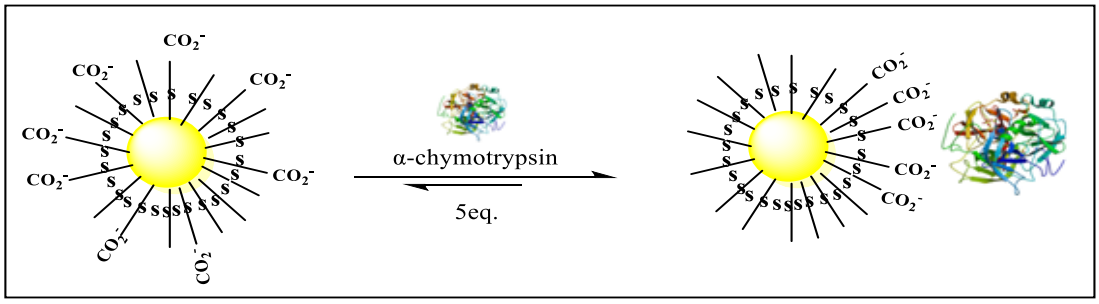

Scheme 1- Chymotrypsin surface recognition by nanoparticle receptors.

Currently, dendrimers are gaining attention for their potential as protein inhibitors due to their unique structural characteristics and terminal functional groups that are capable of enhancing interactions with specific hot spots on target proteins. These dendritic polymers are commonly acknowledged as artificial globular proteins because of their resemblance in size and shape to crucial proteins. According to a study conducted by Twyman, dendrimers have demonstrated the ability to inhibit both chymotrypsin and cytochrome c, indicating the possibility of selective binding mechanisms based on the size compatibility of dendrimers.

The underlying principle suggests that a dendrimer with an addressable area similar to the interfacial area of a given target protein is likely to exhibit the most efficient binding. As shown in Figure 17, a generation 2.5 dendrimer with an addressable surface area of 1200 Å² binds cytochrome c with an optimal affinity, which has an interfacial area of approximately 1000 Å². Furthermore, this principle applies to chymotrypsin, whose interfacial area is approximately 2400 Å². According to these findings, larger ligands, such as dendrimers, can effectively bind to the active sites of enzymes, affecting their activity in a size-selective manner.[32]

Taking advantage of this interaction indicates that dendrimers can be used to develop targeted therapeutic agents, as their design can be tailored to optimize binding interactions with specific proteins, thus modulating the activity of enzymes and offering avenues for developing new therapeutic strategies for a wide range of diseases.

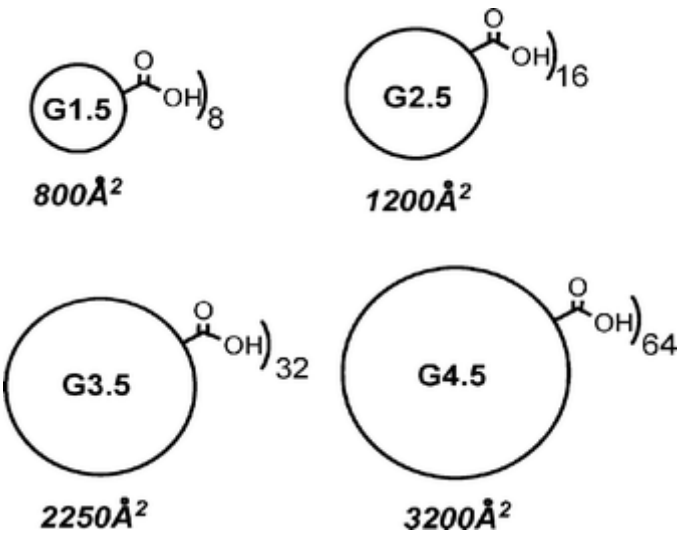

Figure 17- Different generations of PAMAM dendrimers and their addressable areas.[32]

Researchers have been investigating the possibility of developing inhibitors derived from graphene oxide (GO) layers that can function as both artificial receptors and inhibitors of α-chymotrypsin (Chy). GO, in comparison to alternative synthetic inhibitors, exhibited greater suppression of α-chymotrypsin activity based on dose response (by weight). The research conducted by Wang et al. in 2017 demonstrated the potential of combining GO with iron oxide (IO) to create a nanocomposite material for therapeutic purposes, specifically in the treatment of Alzheimer's disease. [33]This innovative approach leverages the unique properties of both materials, enhancing their effectiveness in targeting disease mechanisms.

In addition, Twyman's research has demonstrated that graphene oxide (GO) functionalized with tyrosine monomer and oligomer layers significantly enhances the inhibition of chymotrypsin,[34] a crucial serine protease involved in various biological processes. Studies indicate that this functionalization not only increases the potential for interaction between GO and the enzyme but also improves its specificity as an inhibitor. The enhancement in inhibitory capacity can be attributed to the addition of functional groups to the GO molecules, which facilitate stronger binding to the active site of the enzyme. By effectively occupying this active site, the functionalized GO prevents chymotrypsin from conducting its enzymatic activity, thereby inhibiting its ability to hydrolyse peptide bonds.

These findings collectively underscore the potential of GO and its derivatives as versatile platforms for the development of novel therapeutic agents. The unique structural properties of GO, coupled with its functionalization capabilities, allow researchers to tailor its characteristics for specific applications. By optimizing the structural features and the degree of

functionalization of graphene oxide, scientists can design targeted inhibitors that may offer improved efficacy in modulating enzymatic activity. This approach holds promise for advancing treatment strategies for a wide range of diseases, particularly neurodegenerative disorders such as Alzheimer's disease, where dysregulated proteolytic activity plays a significant role in disease progression. Ultimately, the innovative use of GO as a therapeutic platform could lead to the development of more effective interventions aimed at restoring normal biological function in affected individuals.

1.8 Dynamic Combinatorial libraries

The concept of dynamic combinatorial chemistry[35,36] (DCLs) refers to combinatorial chemistry under thermodynamic control. This approach was developed in the mid-1990s with the aim of identifying molecules with particular desirable properties.[37] These molecules can self-assemble into complexes through covalent or non-covalent interactions including metal-ligand coordination. It is important to note that DCLs are responsive: any alteration in the experimental conditions will typically result in changes to the relative stabilities of the library members, resulting in changes to the distribution of the library. By comparing the distribution of products under various conditions, valuable information about thermodynamic minima can be obtained, aiding in the identification of species and systems with properties of interest in fields such as drug discovery[38], protein folding, materials chemistry[39], and catalysis[40], analyte sensing and the chemistry of interlocked molecules.

Combinatorial libraries are typically made up of a mixture of small and simple molecules capable of reversible reactions in aqueous solution at physiologically relevant pH levels. These molecules are referred to as "building blocks" (Figure 18). When extrinsic factors or templates, such as proteins, interact or bind with certain molecules within the DCL mixture, the equilibrium within the library will shift in response to this interaction, following Le Chatelier's principle.[32] As a result, molecules that interact with the protein become more abundant in the library or "amplified." This allows for the identification of molecules with high affinity for proteins, which can serve as potential ligands or inhibitors. Consequently, it may be possible to utilize proteins as template molecules in order to identify the dendrimer-chain complex with the greatest binding affinity. By analyzing library compositions under different conditions, researchers can identify thermodynamically stable species useful in drug discovery[38] and other fields. Recent studies have further applied DCLs to explore molecular networks and interactions, contributing to the emerging field of systems chemistry. This method offers a

powerful tool for accelerating the drug discovery process by leveraging the flexibility of DCLs in medicinal chemistry.

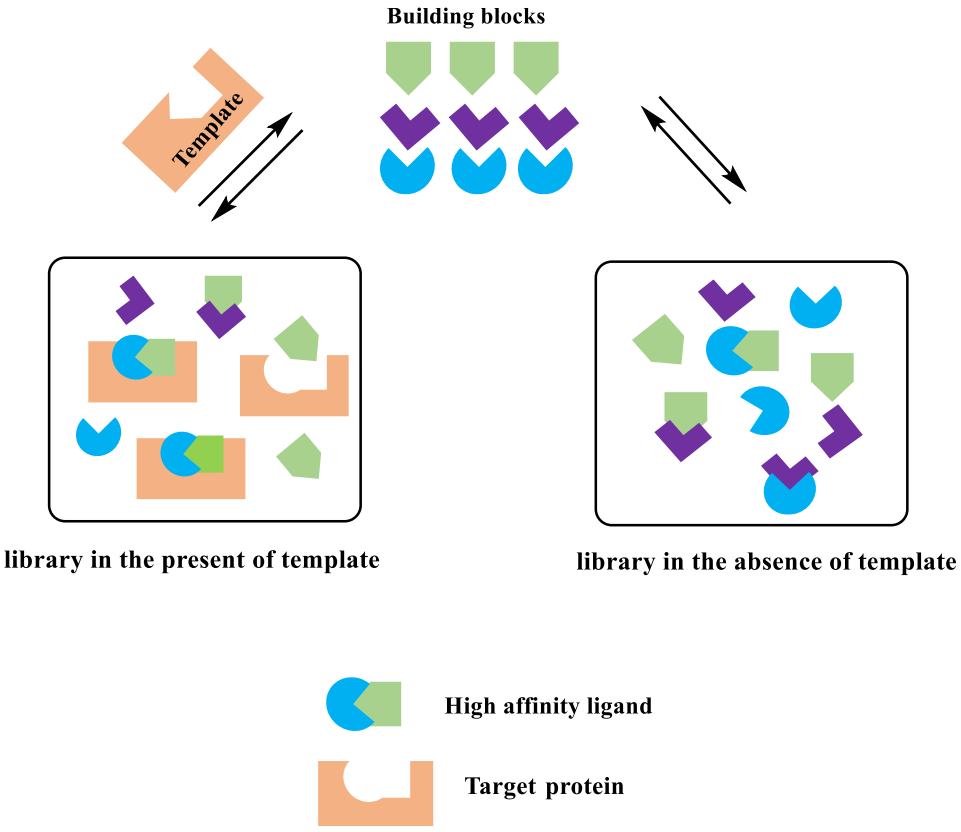

Figure 18- representation of Dynamic Combinatorial Libraries.

Chapter 2

Approach towards the Synthesis and Use of Dendrimers as Scaffolds for Non-Covalent Assembly in Protein Binding and Sensing

2.0 Declaration

This part of my thesis was conducted in collaboration with Dr. Azrah Abdul Aziz. My contribution accounts for 80-90% of the work described and included the synthesis and characterization of all molecules reported, including the dendrimer/chain complexes, encapsulation studies and the improved synthesis of the linear chains. Dr. Azra performed the enzyme assay for protein binding. I was responsible for writing 100% of the chapter.

2.1 Polymers: a general introduction

The main objective of this introduction in this chapter is to provide readers with essential information needed to understand the specific concepts of the subject, which will be utilized in this research area. This review does not provide a comprehensive overview, and readers are directed to several recommended reviews in the literature[41,42].

A polymer is a large molecule that is formed by the repeated linking of smaller units known as monomers, typically through covalent bonds. The term "polymer" derives from the Greek prefix "poly," meaning "many," while "mono" means "single." This distinction highlights the fundamental characteristic of polymers: they are composed of numerous repeating subunits. Polymers can be synthesized through various methods, either artificially in industrial settings or organically through natural processes. For instance, synthetic polymers like plastics, textiles, and rubber are produced on a large scale to meet consumer demands and serve various applications. On the other hand, natural polymers play crucial roles in biological systems and include substances such as proteins (polypeptides), starches, latex, and cellulose, [43] each exhibiting unique properties and functions.

Traditionally, until the late 20th century, polymers were classified into three primary categories based on their structure: linear, branched, and cross-linked (Figure 19). Linear polymers are characterized by monomer units linked together continuously, forming long, unbranched chains. This structure allows for a straightforward arrangement of the molecules. In contrast, branched polymers possess linked monomer units that extend outward from the main polymer chain at various points, creating a more complex structure. Cross-linked polymers, however, are formed when bonds develop between different polymer chains, resulting in a network that enhances the material's strength and stability. [42] Recently, the field of polymer science has seen the emergence of dendritic polymers, which are highly branched structures that offer unique properties and potential applications in drug delivery, materials science, and nanotechnology. These advancements in polymer technology continue to expand the possibilities for innovative applications across various fields.

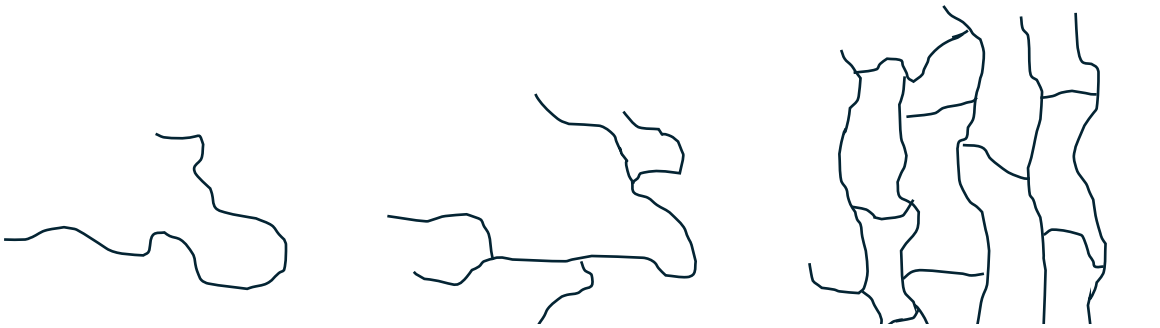

Figure 3- Three traditional classes of polymers

2.2 Dendritic polymers: a general introduction

Dendritic polymers represent a relatively new and exciting field in polymer chemistry that emerged approximately 40 years ago. While linear polymers continue to dominate the research landscape, dendritic macromolecules are increasingly capturing the attention of scientists and researchers. This growing interest is particularly evident in dendritic polymers such as dendrimers and hyperbranched polymers, especially following significant contributions from pioneers like Tomalia,[44]Vogtle,[45] and Newkome.[46]

Dendritic polymers are distinguished by their unique structures, developed through innovative synthetic strategies aimed at creating structure-controlled macromolecules that date back to the 1970s.[47] A fundamental difference between linear and dendritic polymers lies in their functionalization; linear polymers typically have two end groups, whereas dendritic polymers boast a multitude of functionalized end groups. This structural characteristic renders dendritic polymers particularly advantageous for a wide array of biomedical and industrial applications, including drug delivery systems, diagnostic imaging, and materials science.[48]

There are two primary categories of dendritic polymers, both composed of branched repeat units: dendrimers and hyperbranched polymers (HBPs).[48,49] HBPs are created through a polymerization process that results in more complex and less controlled structures, leading to variability in their molecular weights. In contrast, dendrimers are characterized as symmetrical, monodisperse macromolecules, which means they have uniform sizes and precise molar masses. This precision is crucial for many applications where consistency and control are essential.

In this chapter, we will focus specifically on dendrimers, delving into their synthesis, properties, and potential applications, as they will play a central role in the subsequent chapters of this work. Understanding dendrimers' unique characteristics and how they differ from traditional linear polymers is essential for exploring their vast potential in various scientific and technological domains. As research continues to advance, dendritic polymers, particularly dendrimers, hold promise for revolutionizing how we approach challenges in fields ranging from medicine to materials engineering.

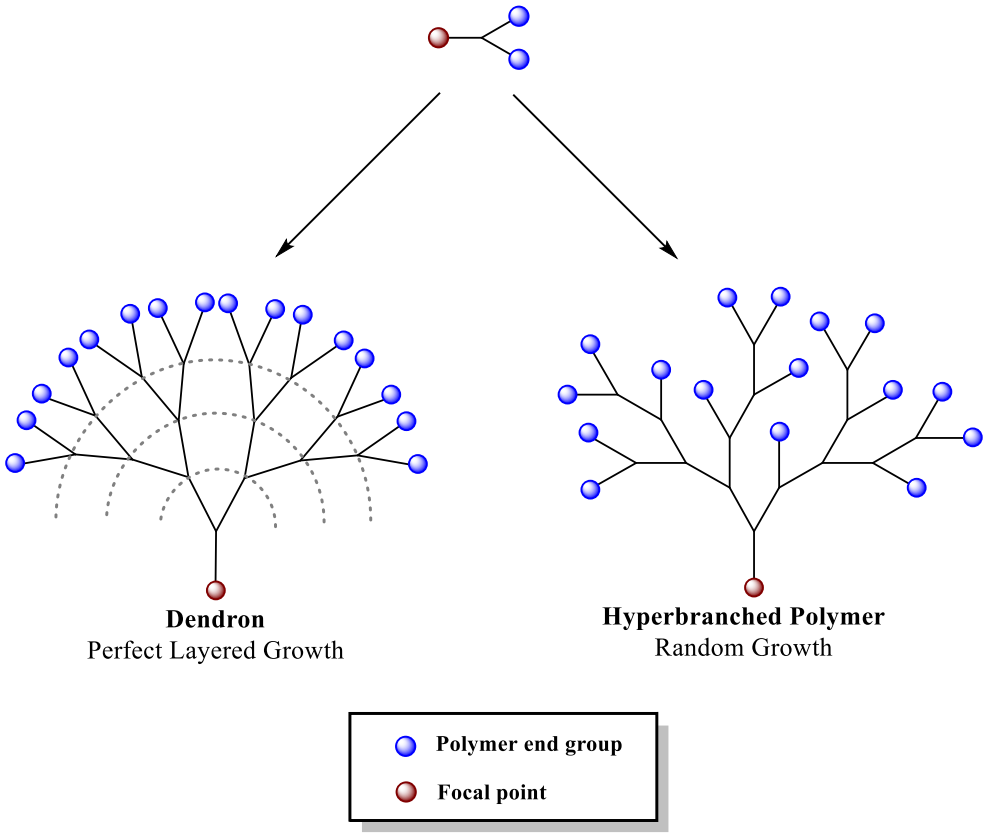

Figure 20- Dendron branching in a dendrimer and a hyperbranched polymer.

2.3 Properties of Dendritic polymers

2.3.1 Dendritic history and terminology

In 1941, Paul Flory made significant contributions to polymer chemistry by publishing papers that provided theoretical evidence for branched three-dimensional molecules.[50] His foundational work laid the groundwork for future advancements in the field. Following Flory's pioneering research, a new class of controlled-branched molecules known as "cascade molecules" was synthesized by Vögtle and his colleagues in the late 1970s.[45] This marked a

significant milestone in polymer science, as researchers began to explore the potential of branched architectures.

In the 1980s, Donald Tomalia and his team further advanced the understanding of branched polymers by discovering hyperbranched molecules, which they aptly named "dendrimers".[44] The term "dendrimer" is derived from the Greek words "dendron," meaning tree, and "meros," meaning part, aptly reflecting the tree-like branching structure of these macromolecules.[51] Around the same time, another research group led by Newkome[52] reported the synthesis of similar macromolecules, which they referred to as "arborols." The term "arborol" is derived from the Latin word "arbor," also meaning tree, emphasizing the resemblance of these structures to tree branches.[48]

While "cascade molecule" is still used in some contexts, "dendrimer" has become the most established and widely recognized term in the field.[53] Over the years, more than 100 different dendritic structures have been reported in the literature. Among the most well-known dendritic families are polyamidoamine (PAMAM) dendrimers, polypropyleneimine (PPI) dendrimers, and those based on polyamide, polyether, polyester, and phosphorus. These families represent a diverse range of dendritic structures, each with unique properties and potential applications.

To further illustrate the breadth of this field, Table 1 provides a summary of some of the most common dendrimers, detailing their chemical compositions, names, and the years they were first reported. This overview highlights the significant progress made in the study of dendritic polymers and underscores their importance in various scientific and industrial applications. As research continues to evolve, dendrimers are expected to play an increasingly vital role in advancing technology, particularly in fields such as drug delivery, nanotechnology, and materials science.

Dendrimer name	**Cascade** in 1978	**PAMAM**. in 1985	**PPI**.in 1993
Chemical Structure	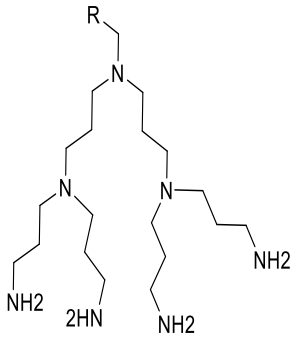	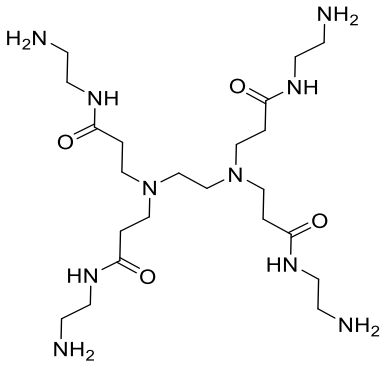	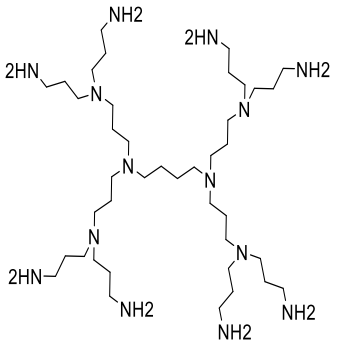
First Synthesis	Vögtle *et al.*	Tomalia *et al.*	Meijer *et al.*

Table 1: Examples of early dendrimers.[51]

2.3.2 Structure of dendrimers

Dendrimers are unique macromolecules characterized by their regular branching monomers, which are systematically arranged around a central inner core. One of the key features of dendrimers is their specific molar mass, which is a result of their symmetrical and monodisperse nature. This means that all dendrimer molecules within a given sample have the same size and weight, ensuring consistency in their properties and behavior.

The precise and highly controlled synthesis required for dendrimer preparation results in a well-defined molecular architecture consisting of two distinct types of monomeric residues. The first type, referred to as the **dendritic unit**, is fully reacted and plays a fundamental role in facilitating branching within the dendrimer structure. The second type, known as the **terminal unit**, is situated at the periphery of the macromolecule and defines its outer surface, often bearing functional groups that enable further chemical modifications and interactions.

Furthermore, dendrimers are composed of multiple fragments known as dendrons. Each dendron contributes to the overall structure and function of the dendrimer. These fragments are typically organized into three distinct subregions, as illustrated in Figure 21: the core, the repeating branching units, and the functionalized terminal groups, commonly referred to as end groups. The core serves as the foundation of the dendrimer, while the branching units expand outward, creating a complex three-dimensional structure.

Each layer of a dendrimer is designated as a generation (G), with an increase in the number of layers corresponding to a proportional increase in both the number of generations and the number of end groups on the dendrimer's surface. As the generation number rises, the

dendrimer becomes increasingly complex, often leading to enhanced properties such as greater solubility, improved stability, and the ability to encapsulate various substances. This unique feature of dendrimers allows researchers to tailor their designs for specific applications in drug delivery, imaging, and various nanotechnology fields, showcasing their potential for innovative solutions in multiple scientific domains.

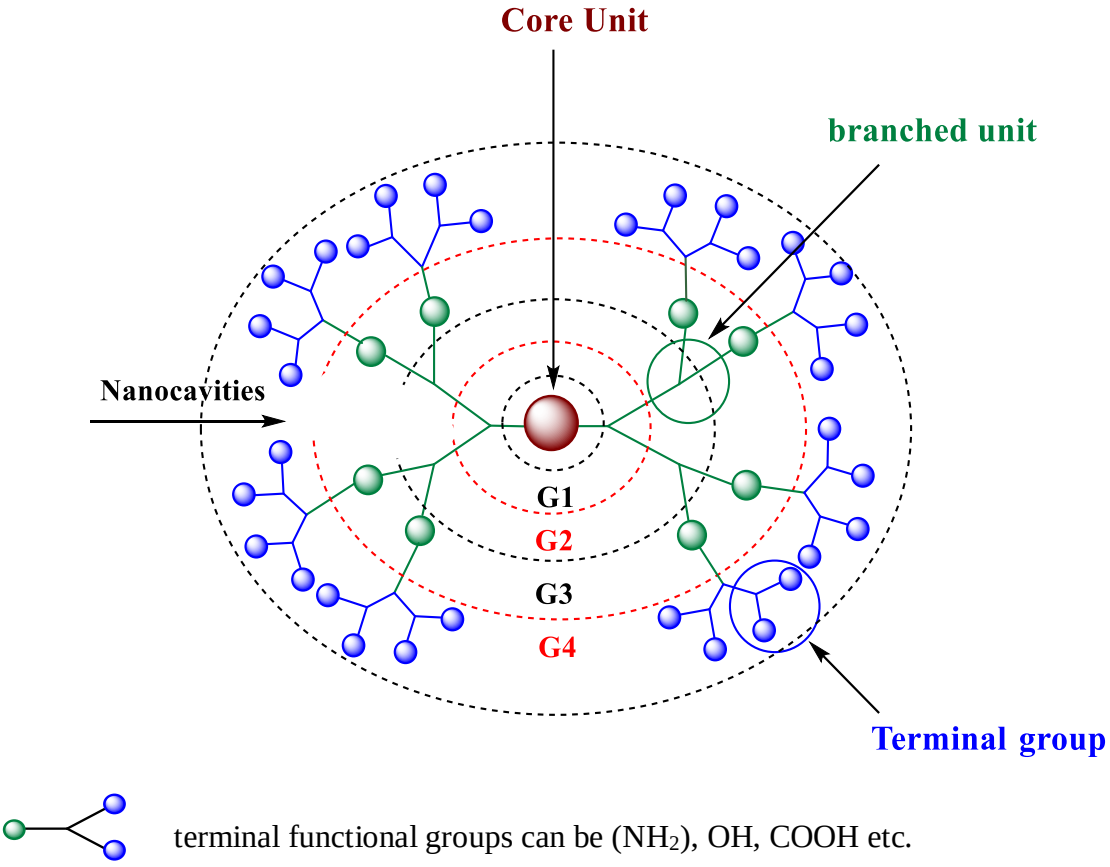

Figure 21- An illustration of a dendrimer's structure, showing the core, branches and terminals.

Dendrimers are sophisticated macromolecules constructed from AB-type monomers,[54] where each step in the synthetic reaction produces a new 'generation' of branching units. These branching units are crucial as they interconnect with one another, contributing to the dendrimer's unique and highly defined molecular shape. The architecture of a dendrimer is primarily influenced by the parameter (n),[48] which indicates the number of branching sites available for further reaction. Consequently, the number of terminal groups—functional groups located at the dendrimer's periphery—can be effectively determined by the value of (n).

As new layers or generations of branching units are added, the number of terminal functional groups increases significantly. For example, when (n = 2), the number of terminal groups doubles, while for (n = 3), it triples. This exponential growth in functional groups is a hallmark of dendrimers, allowing for extensive customization in their applications, particularly in fields such as drug delivery and molecular recognition.

Dendrimers can be classified based on their generation, with low-generation dendrimers typically characterized by more open structures and lower molecular weights. These lower generations are often more flexible, providing easier access to their functional groups for interactions with other molecules. In contrast, high-generation dendrimers display a more branched and denser architecture, resulting from the increased branching that occurs with each new layer. This transition to denser structures is a critical aspect of dendrimer design, as it leads to branch crowding, which can result in the formation of more closed configurations. Such high-generation dendrimers can exhibit unique properties, such as enhanced stability and increased efficacy in various applications, highlighting the importance of understanding the relationship between dendrimer generation and its structural characteristics.

2.4 Synthesis of Dendritic polymers

2.4.1 Synthesis of Dendrimers

Synthesizing dendrimers, which are monodisperse and symmetrical macromolecules, poses significant challenges due to the necessity of high precision and control throughout the process. The construction of these complex structures is achieved through a highly regulated step-by-step methodology, where each monomer layer is added sequentially.[46] This meticulous approach allows for the development of well-defined branching patterns, essential for achieving the desired properties and functionalities of the dendrimer.

A critical aspect of dendrimer synthesis is the need for protection and deprotection of functional groups at every step in the synthetic procedure. This ensures that the reactive sites remain available for further reactions without interfering with the overall structure. Additionally, extreme purification is required at each stage to eliminate any impurities or by-products that could affect the quality and performance of the final product.

Two primary synthetic strategies are employed to construct these perfectly branched dendritic structures: the divergent approach and the convergent approach. The divergent method involves starting from a central core and building outward, layer by layer, while the convergent method assembles dendrons first and then combines them at the core. Each method has its

advantages and challenges, influencing the efficiency and complexity of the synthesis. Overall, the intricate nature of dendrimer synthesis underscores the importance of precision in creating these unique macromolecules, which have diverse applications in fields such as drug delivery, materials science, and nanotechnology.

2.4.2 Divergent Synthesis

The first poly (amidoamine) dendrimers were synthesized by Donald A. Tomalia in 1985,[44] marking a significant milestone in the field of polymer chemistry. At that time, dendrimers were synthesized using a divergent strategy (Figure 22), which involves building layers outward from an initiator core toward the periphery of the molecule. Each layer in this process is commonly referred to as a generation of growth. The growth of dendrimers follows a highly structured procedure that involves two iterative steps: (i) the coupling of the monomers and (ii) the activation of their end groups.[55]

The coupling step begins when the peripheral end groups of subsequent generations react with complementary reactive groups on the monomer units. This reaction not only forms new branch points but also significantly increases the number of terminal functionalized groups on the dendrimer. Importantly, this reaction is fully controlled because the peripheral functionalities on each monomer are protected during the synthesis. Several methods can be utilized to activate these peripheral groups, including converting them into reactive functional groups, coupling them with another molecule, or removing protective groups. This process of coupling and activating is repeated until the desired degree of branching and functionality is achieved.

One major advantage associated with this methodology is that the divergent approach is a relatively straightforward synthetic procedure, making it accessible for various applications. Additionally, dendrimers can be produced in high quantities because their molar masses double with every generation-adding step. This characteristic scalability has led to the divergent approach becoming the preferred commercial route for synthesizing dendrimers, including those of very large sizes.

The implications of this production method extend beyond mere scalability. The ability to control the size and functionality of dendrimers through this systematic approach opens up numerous possibilities for their application in fields such as drug delivery, nanotechnology, and materials science. As researchers continue to explore the potential of dendrimers, the divergent strategy remains a cornerstone in advancing the design and synthesis of these

complex macromolecules, paving the way for innovative solutions in various scientific disciplines.

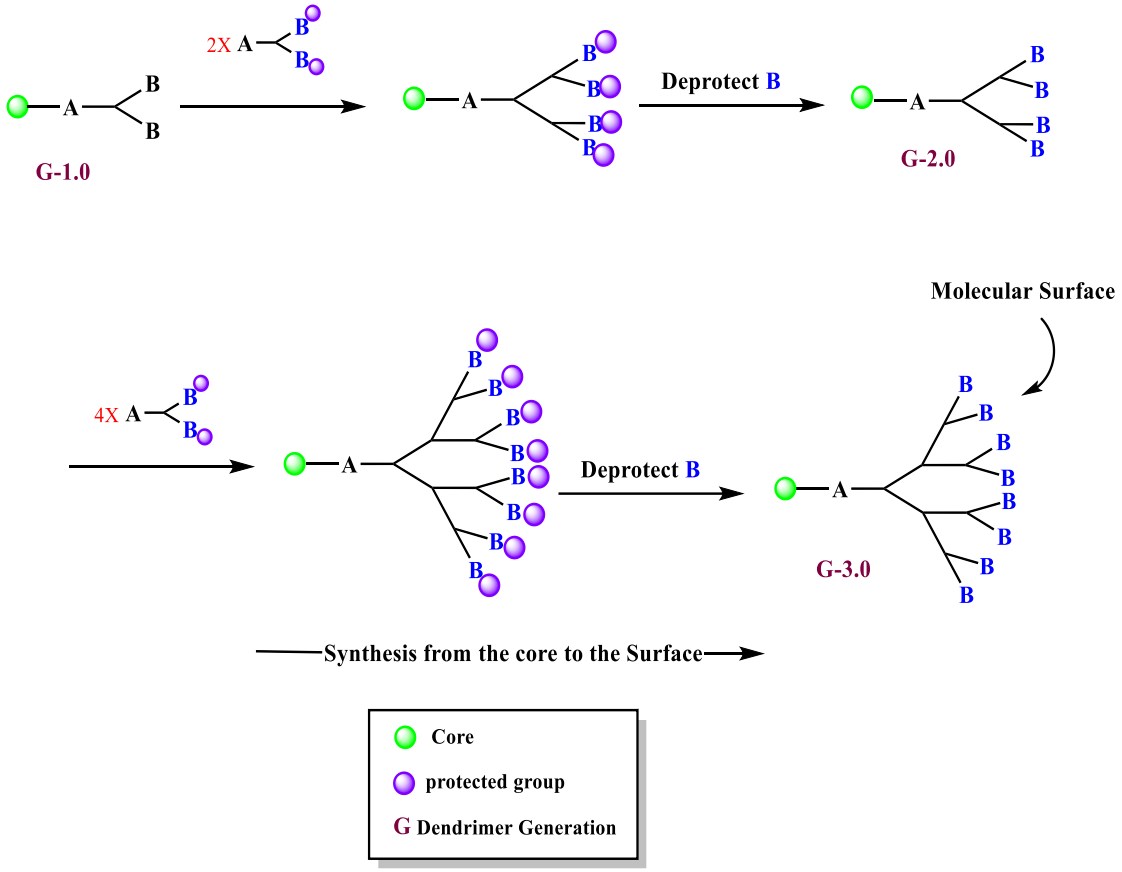

Figure 22- Synthesis of dendrimers by divergent approach.

Despite the advantages of the divergent strategy for synthesizing dendrimers, several notable challenges can complicate the process, particularly regarding purification and achieving well-defined monodisperse structure. One significant issue arises from the repeated activation and coupling reaction steps, which lead to an exponential increase in the number of reactions occurring at the periphery of the dendrimer. As the synthesis progresses, this increased reactivity requires the use of large excesses of reactants to ensure that both coupling and activation steps are successfully completed. The requirement for substantial amounts of reagents can drive up production costs and complicate the overall synthesis process.

Furthermore, as each new generation of the dendrimer is synthesized, the excess reagents left over from previous steps must be meticulously removed from the reaction mixture. This purification process can be time-consuming and may require multiple rounds of filtration or chromatography, making the production of high-purity dendrimers more challenging.

In addition to the purification concerns, increasing the generation of dendrimers also demands a higher number of coupling reactions. This necessity introduces additional complexity to the synthetic route, as each coupling step presents opportunities for unwanted side reactions to occur. These side effects can result in incomplete reactions, leading to by-products that may share similar architectural features with the desired dendrimer. The challenge lies in the fact that these by-products can be particularly difficult to remove, complicating the purification process further. The presence of such by-products not only affects the yield of the desired product but can also influence the overall properties of the synthesized dendrimers, potentially impacting their functionality in applications.[46] Consequently, careful optimization of reaction conditions and purification methods is essential to mitigate these disadvantages and enhance the overall efficiency of dendrimer synthesis.

2.4.3 Convergent synthesis

To address the limitations of the divergent synthesis approach, Fréchet and Hawker developed an alternative technique called the convergent approach (Figure 23).54[46,56] Unlike the outward growth of the divergent method, the convergent approach builds dendrimers from the outer periphery inward toward the core. The process begins with the synthesis of dendrons, which are branched sections of the macromolecule that contain reactive functional groups on their periphery. These dendrons are then combined with a polyfunctional core molecule in a step known as the coupling step, which results in the creation of the globular dendritic structure. After the initial coupling, a functional group within the core of each dendron is activated, preparing the molecule for further growth. This activation step is crucial, as it enables each dendron to react with additional monomer units. By coupling these activated dendrons with further monomers, researchers can systematically increase the generation level, producing higher-generation dendrimers with a controlled structure and functionality.[47,55] This inward-focused process also allows for greater control over purity and the monodisperse nature of the product, addressing some of the challenges encountered in divergent synthesis.

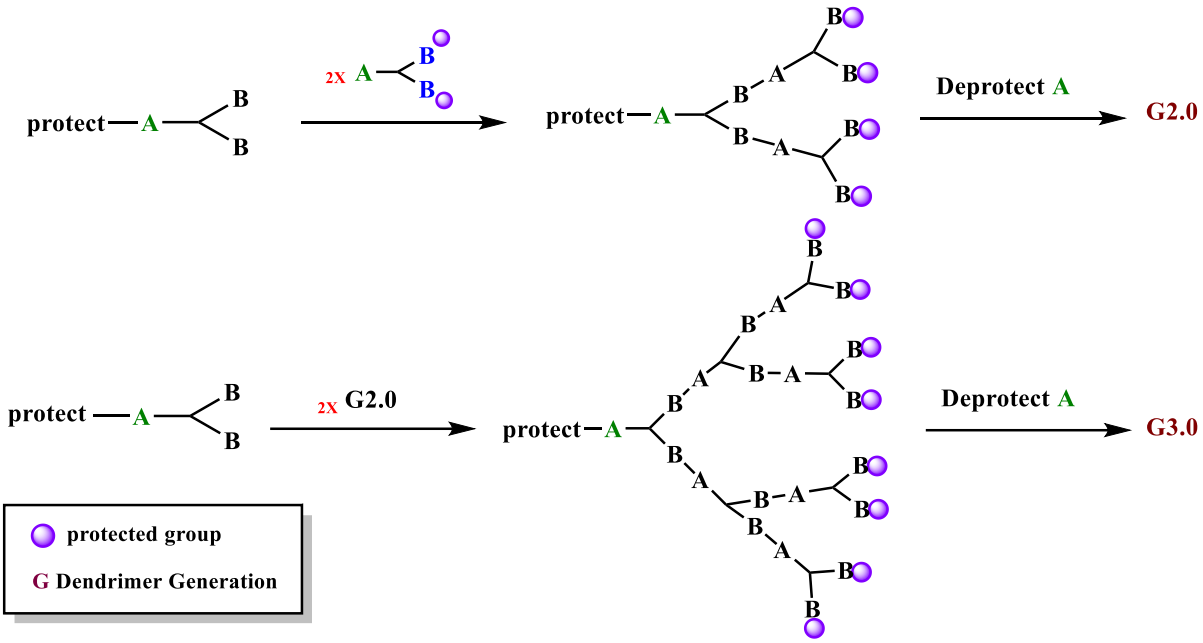

Figure 23- Synthesis of dendrimers by convergent approach.

In contrast to the divergent approach, the convergent approach completes synthesis by using equal molar quantities rather than a large excess of branching units. This method involves fewer coupling reactions at each stage, allowing for more precise control over dendrimer structure and reducing the likelihood of defects. As a result, the products formed through this approach often have fewer imperfections, and the purification process is more straightforward, as there are fewer by-products to remove.

Despite these advantages, the convergent methodology also has limitations, such as steric crowding. This crowding occurs because the reactive groups are situated at the core of the dendrons, which can hinder accessibility, decrease reactivity, and slow down the coupling process, making reactions less efficient. Consequently, producing high-generation dendrimers without significant structural defects is challenging, restricting the synthesis of larger dendrimers through this method.[46] Therefore, the convergent approach is primarily suited for creating smaller dendrimers. Notably, Grayson and Fréchet successfully applied this technique to synthesize poly (benzyl ethers), a class of dendrimers that have found extensive applications due to their stability and functional versatility in various fields.[56]

2.5 Modification of PAMAM dendrimers and their application in biomedicine.

Dendrimers are versatile macromolecules with a wide range of potential applications, including in nanotechnology, biomimicry, diagnostics, catalysis, and various therapeutic formulations. Unlike classical polymers, dendrimers exhibit unique characteristics, largely due to their precise molecular uniformity, multifunctional surface, and well-defined internal cavities. Additionally, dendrimers have a branched structure that forms highly ordered, three-dimensional architectures. This structural design allows for the tuning of dendrimer properties through the use of specific capping reagents on the outermost generation, making it possible to customize dendrimers to suit particular applications. Figure 24 illustrates the three main structural components of dendrimers that can be optimized for specific reactions: the peripheral functional groups, the internal cavities, and the core unit, all of which contribute to their versatility and functionality.

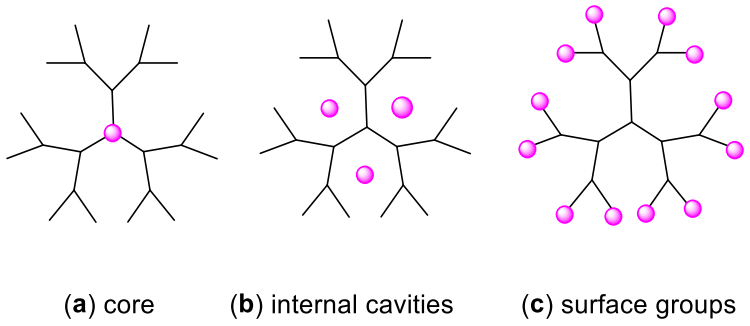

Figure 24- A dendrimer structure component that can be exploited.

Studies have shown that amine-terminated PAMAM dendrimers have the ability to solubilize various families of hydrophobic drugs, enhancing their bioavailability. However, these positively charged surfaces can pose risks, as the cationic charges may disrupt cell membranes and act as crosslinkers, leading to cellular aggregates and potential issues such as haemolysis. To enhance the biocompatibility of dendrimers and mitigate these problems, peripheral amine groups are often modified into a range of surface groups. Common modifications include PEGylation, acetylation, glycosylation, and amino acid functionalization, which help reduce toxicity and improve safety in biomedical applications.[57]

Dendrimers possess a highly functional surface, making them well-suited for applications involving non-covalent interactions, such as in chemical sensing. Due to their branched structure and functional end groups, dendrimers can effectively host various molecules,

enabling them to act as sensors by undergoing measurable changes in properties, such as fluorescence, in response to binding specific analytes. An example of this utility was demonstrated by Balzani, Vögtle, and colleagues, who used a fourth-generation poly (propylene amine) dendrimer decorated with 32 dansyl units to detect small ions like Co^{2+} through a fluorescence response. The presence of Co^{2+} ions caused a detectable fluorescence change, allowing it to act as a selective chemical sensor. Additionally, dendritic sensors show substantial potential in organic detection applications, such as sensing volatile organic compounds and identifying specific chemical structures.[54,58] The high sensitivity and selectivity of dendrimers in these applications make them promising candidates for further development in fields ranging from environmental monitoring to biomedical diagnostics.

In the medical field, dendrimers hold significant potential for applications such as MRI contrast agents, gene therapy, and drug delivery systems. Due to their highly branched structures and ability to be functionalized, dendrimers are being explored as carriers for therapeutic drugs and imaging agents. For instance, gadolinium (Gd)-based contrast agents, when attached to dendrimers, have shown to enhance diagnostic imaging by improving the sensitivity and clarity of MRI scans.[46,53] Dendrimers improve the stability and retention of Gd in the bloodstream, allowing for prolonged circulation and more efficient proton relaxation, which leads to higher-quality imaging of tissues and blood vessels. As a result, dendrimers may serve as an effective alternative to traditional low molecular weight Gd chelates in enhancing MRI image resolution and sensitivity, advancing diagnostic capabilities in clinical settings.[57]

The use of dendrimers as carriers for genetic material has gained considerable attention in the field of gene delivery, especially in the context of gene therapy. This innovative approach is increasingly recognized for its potential to treat a variety of hereditary and acquired genetic disorders. Dendrimers, particularly PAMAM (polyamidoamine) and PPI (polypropylenimine) dendrimers, are being explored as effective non-viral vectors due to their unique properties. They can protect DNA from enzymatic degradation, ensuring the integrity of genetic material during transport. Additionally, dendrimers facilitate effective gene transfer through electrostatic interactions with negatively charged DNA. Their low toxicity, high affinity for genetic material, and relatively small size enhance their suitability for delivering genes safely and efficiently into target cells. [46,54] This capability positions dendrimers as promising tools in the advancement of gene therapy, potentially revolutionizing treatments for genetic disorders.[59]

Drug delivery represents one of the most significant biomedical applications of dendrimers, showcasing their potential in enhancing therapeutic efficacy. There are two primary mechanisms through which drugs interact with dendrimers: encapsulation within their cavity and electrostatic interactions or covalent bonds to their periphery. The unique structural flexibility of dendrimers, especially around the core, allows them to serve as ideal hosts for drug entrapment, which in turn enhances drug solubility, bioavailability, and controlled release profiles. For instance, ibuprofen, a widely used non-steroidal anti-inflammatory drug (NSAID) characterized by its carboxylate functional groups, is often complexed with full-generation PAMAM dendrimers.[46,60] This interaction occurs through the amine groups present on the dendrimer surface, facilitating effective complexation and subsequent drug delivery.

In research conducted by Kolhe et al., the interaction between Generation 3 (G3) and Generation 4 (G4) PAMAM dendrimers and ibuprofen was investigated. The findings revealed that 32 and 48 ibuprofen molecules formed ionic interactions with the dendrimers, indicating a significant capacity for drug loading. Moreover, in vitro studies demonstrated that the release of ibuprofen to cells was slower when the drug was complexed with the dendritic architecture compared to free ibuprofen. [57,61] This slower release rate suggests that dendrimers can not only enhance drug stability but also provide a sustained release mechanism, ultimately improving the therapeutic effectiveness of ibuprofen. By leveraging the unique properties of dendrimers, researchers are paving the way for advanced drug delivery systems that can transform treatment modalities for various diseases.

Boron neutron capture therapy (BNCT) represents an innovative therapeutic application where dendrimers play a crucial role. This specialized treatment modality targets various diseases, particularly cancer, by utilizing a unique mechanism involving boron-10 (^{10}B), a stable isotope. Patients undergoing BNCT receive a pharmaceutical preparation that contains 10B, specifically designed to target and accumulate within cancerous cells. Following the administration of the boron-containing agent, patients are exposed to a low-energy neutron beam. This exposure induces a nuclear reaction that generates highly energetic alpha particles and lithium-3 ($Li3^{+}$) ions, which effectively damage the cancer cells' DNA and inhibit their replication.

To enhance the selectivity and effectiveness of this therapy, researchers have explored the utilization of polymer scaffolds containing boron, such as PAMAM dendrimers. These dendrimers are advantageous due to their well-defined structure and functionalization

capabilities, allowing for optimized delivery and localization of therapeutic agents directly to tumour sites. For instance, Barth et al. have successfully synthesized boron-containing PAMAM dendrimers specifically for BNCT applications. Their research demonstrates the potential of these dendrimers to improve the therapeutic index of BNCT by ensuring that a higher concentration of boron is delivered to cancerous tissues, thereby maximizing the treatment's effectiveness while minimizing damage to surrounding healthy cells. [57] Through ongoing research and development, dendrimers may significantly advance the field of cancer therapy, providing patients with more effective treatment options.

Dendrimers, unique branched macromolecules, are applied widely beyond biomedicine, particularly in industrial catalysis, due to their high solubility and large surface area. Their structure allows dendrimers to act as effective catalytic supports through two primary modifications: (1) attaching catalytic groups to the dendrimer's periphery or (2) embedding a catalytic site within the core, which creates nano-reactor properties. This latter design leverages internal cavities near the core that are shielded from external conditions, offering a protected environment for catalytic reactions.[62]

Dendrimers combine the benefits of both homogeneous and heterogeneous catalysts. Homogeneous catalysts offer highly accessible active sites, yet are often difficult to remove from reaction mixtures, while heterogeneous catalysts are easier to recover but generally less accessible. Dendrimers bridge these properties, providing accessible catalytic sites and ease of recovery through methods like ultrafiltration. Their extensive surface area and controlled structure enable multiple active sites, making them highly versatile in facilitating efficient catalytic processes.

The pioneering work of the Van Koten group, which developed the first catalytic dendrimer for polyhaloalkane addition reactions, highlighted dendrimers' potential in catalysis. This discovery has spurred further research into using dendrimers as multifunctional catalytic platforms, combining accessibility, recovery ease, and reusability—qualities that make them appealing for various industrial applications.

2.6 Aims and Objectives

The aim of this project is to develop macromolecules will improve the selectivity of protein binding. Developing this is a useful strategy in inhibiting undesirable interaction or disease related to protein-protein complexes. In our view, the optimization process to do this is to mimic the nature of protein-protein binding using large molecule. Natural binding means that the proteins bind and recognize each other where there binding surface is complementary and completely matching the binding surface of the other protein. However, one of the problems that may be an obstacle to do this is the surface of the protein which can range from 500 to 5000 Å^2, requiring the design of inhibitors that can interact with most of this area. The Twyman group report the use of dendrimer which are perfectly branched molecules with a highly ordered and well controlled structure. The group have previously shown that these molecules have a size selectivity with respect to protein binding and can be easily modified with good results.[32]Furthermore, specific amino acids can be covalently attached to the dendrimer surface and influence binding either positively or negatively, as shown in Figure 25.

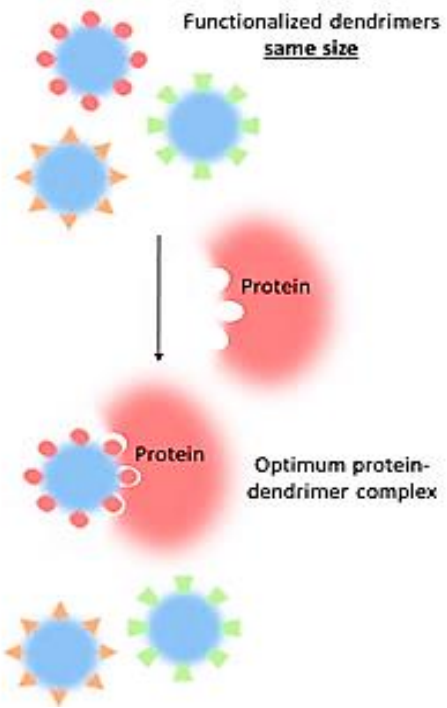

Figure 25- An illustration of how terminal functionality affects protein binding and selectivity.[32]

Even though the approach made progress toward specific dendrimer/protein interactions, it was not yet optimal. For optimised selectivity, we require a variety of different groups to be added to the same dendrimer. However, the main problem is getting all the functional groups positioned in precise 3D locations on the dendrimers surface - so they line up precisely with complimentary groups on the protein surface. This is impossible using a covalent method of functionalization. One of the proposed solutions is to develop a method where the protein helps to synthesis its own binding partner or own ligand. This can be achieved using a dynamic or non-covalent approach where the synthetic method is reversible with respect to the incorporation of these interacting groups. The use of reversible chemistry is important as it can drive the process thermodynamically towards the best ligand for the protein. The design and methodology are shown schematically in Figure 26.

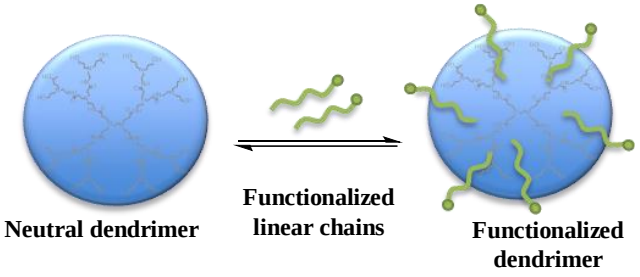

Figure 26- Illustration of neutral dendrimers functionalised with linear chain using a reversible approach.

Our initial plan was to use neutral dendrimers that do not bind unless a targeting or functional group is added non-covalently. Specifically, we will use linear chains terminated with the interacting/binding group. If these chains are hydrophobic and or include functionality that can interact with the interior of the dendrimer, then a self-assembled complex will form, similar to the one shown in Figure 26. This will be a random process, but when a protein is added, the chains can move to maximise their interactions with the protein. Ultimately, we will use a number of different linear chains with different end groups and test these against a variety of protein.

In order to test dendrimer binding and the efficacy of functionalized dendrimers, Cytochrome-c (Cyt-c) was chosen as the target protein due to its well-documented binding surface. Furthermore, it contains a porphyrin moiety that is capable of quenching chromophoric ligands bound to its hotspot region. Therefore, we can quantitatively measure binding using fluorescence spectroscopy. The method was developed by Hamilton in order to directly measure the binding of tetracarboxyporphyrins (TCP) to Cyt-c.[24]

By adding a target protein, the position of these targeting groups can be controlled in order to form an optimized macromolecular through reversible cooperative interactions. This process is illustrated in Figure 27. When the dendrimer, binding units, and sensing component are added to water, they assemble randomly into complex **1**. Upon introducing a protein, the binding units can move and rearrange within the dendrimer to maximize cooperative protein-binding interactions. Binding detection and quantification are achieved by measuring changes in the photophysical properties of the encapsulated sensing groups.

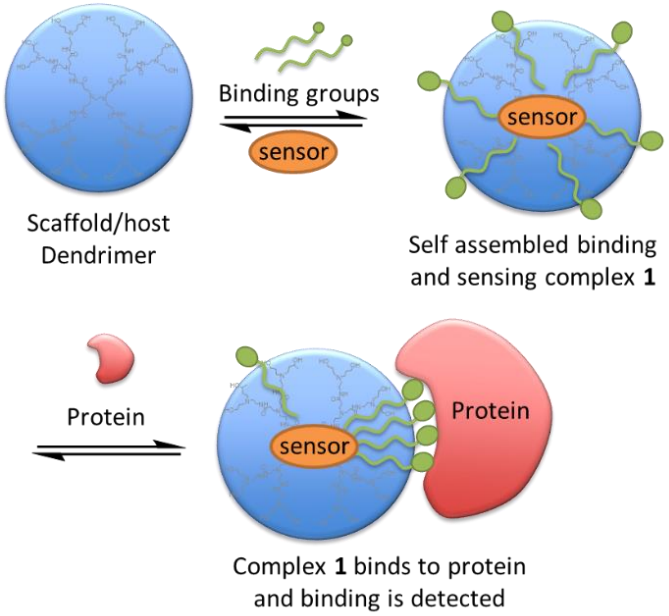

Figure 27- An illustration of the self-assembled protein-binding complex **1**, in which a neutral dendrimer serves as a scaffold to support and encapsulate binding and sensing units. Non-covalent chemistry allows targeting groups to move and optimize binding efficiency when a target protein is present.

2.7 Results and discussion

2.7.1 Synthesis of PAMAM dendrimers

In order to achieve the objectives outlined above, the first step was to synthesise PAMAM dendrimers of different sizes so that the best dendrimer could bind a target protein and create suitable cavities for the encapsulation of functionalized linear chains. These macromolecules have well established physical and chemical properties, as well as synthetic procedures, which make them an appropriate option for these studies. One important factor for selecting PAMAM dendrimers, was their straightforward and simple synthesis via divergent approach. By using a divergent method, minimal generations are formed when preparing PAMAM dendrimers.[44] starting from G0.5 **1**, subsequent reactions lead to larger generations, producing large G3.5 **7** dendrimers.

To synthesize half and whole generation PAMAM dendrimers, two iterative processes were followed: 1) Michael addition and 2) amidation. Scheme 2 shows these steps. Dendrimers with ester terminal groups are generated by Michael addition while dendrimers with amine terminal groups are generated by amidation. These steps are repeated to produce larger dendrimers, or larger generations.

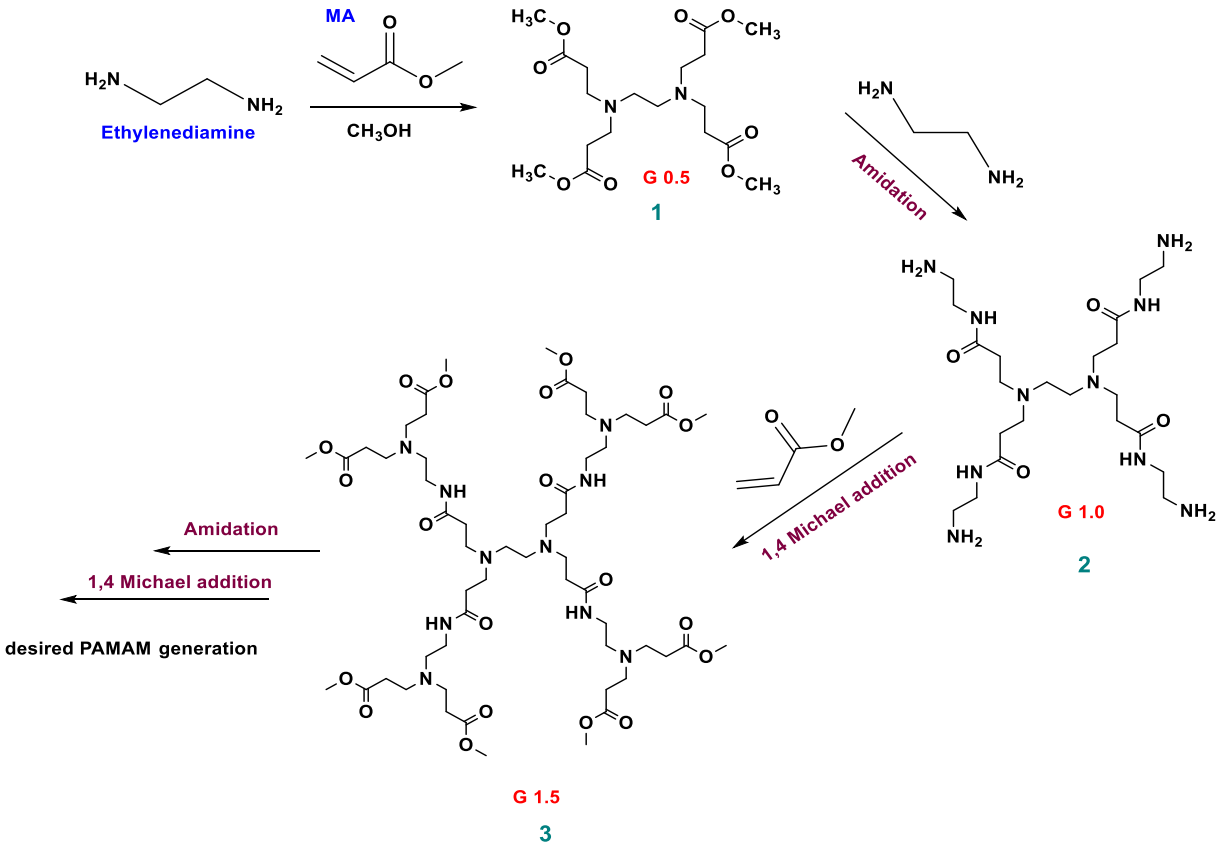

Scheme 2- Steps for PAMAM synthesis.

Half-generation PAMAM preparation begins with the 1,4-Michael addition, shown in Scheme 3. G 0.5 **1** was prepared using ethylene diamine and methyl acrylate in methanol. To prevent incomplete Michael addition and dendrimer imperfections, excess methyl acrylate was utilized. Consequently, the carbonyl substituent induces an electron-withdrawing effect on the alkene, leading to a positive charge (δ+) on the alpha carbon (α) which is eventually stabilized by resonance. As a result of resonance stabilization, the beta carbon (β) becomes electrophilic, rendering it susceptible to nucleophilic attack by NH_2 groups on ethylene diamine (a difunctionalized nucleophile).

The reaction mixture was stirred at room temperature, then rotary evaporation was used to remove the solvent and excess reagents. No additional purification steps were necessary.

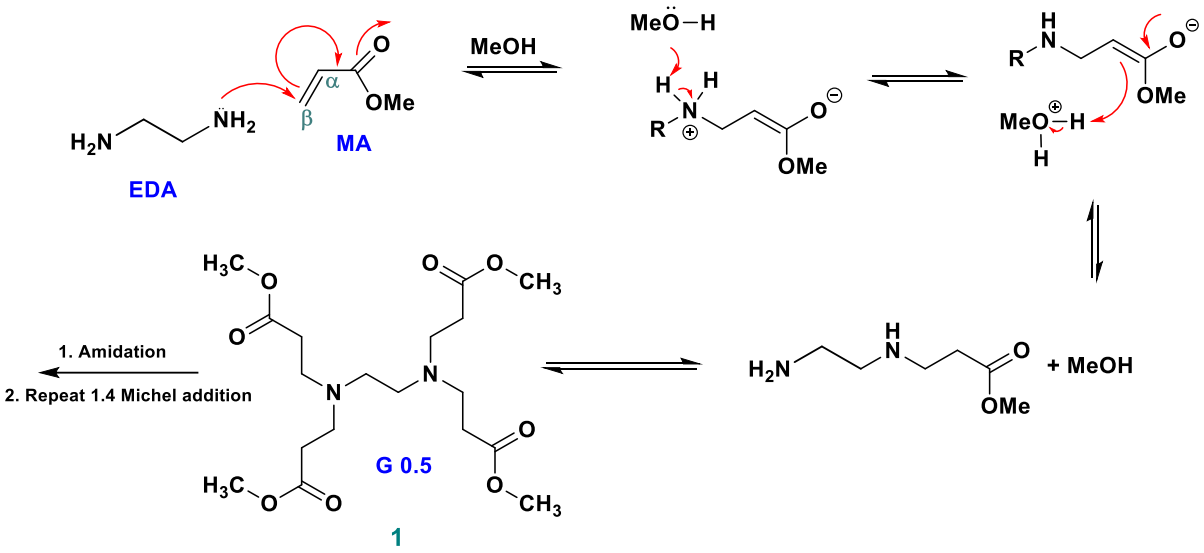

Scheme 3- Michael addition mechanism for synthesis of half-generation dendrimers (ester-terminated PAMAM)

The successful reaction was confirmed via ^{1}H NMR analysis, as shown in Figure 28 below. The Peak at 3.68 ppm associated with methoxy protons (ester group), while two triplets between 2.49 ppm and 2.79 ppm showed the existence of newly formed CH_2 groups. The methylene protons adjacent to the ester functional group will be more shielded, accounting for the lower chemical shift. Additionally, the singlet observed at 2.54 ppm can be assigned to the protons from the core ethylene diamine. An absence of peak around 5-6 ppm in the ^{1}H NMR confirm the complete removal of methyl acrylate from the product. In addition, ^{13}C NMR and

FTIR spectra were used as additional tools to corroborate. The ester carbonyl signal was present at 172 ppm in the ^{13}C spectrum and 1735 cm^{-1} in the FTIR spectrum. Mass spectrometry provided further confirmation via the molecular mass, with a molecule ion observed at 405 (MH^+). Overall, the combined spectral analysis confirmed the structure of the obtained product. After completing the 1,4 Michael addition, new terminal amines were added using an amidation step (Scheme 4). In this step, the nitrogen lone pair from EDA acts as a nucleophile and attacks the electrophilic carbon of the ester (C=O), forming a new tetrahedral intermediate. The intermediate is then deprotonated by the second terminal amine via a stable 5 membered intermediate (a proton transfer), followed by deprotonation of the terminal amine. The carbonyl can then reform, and the methoxy group can leave, to yield a full-generation dendrimer.

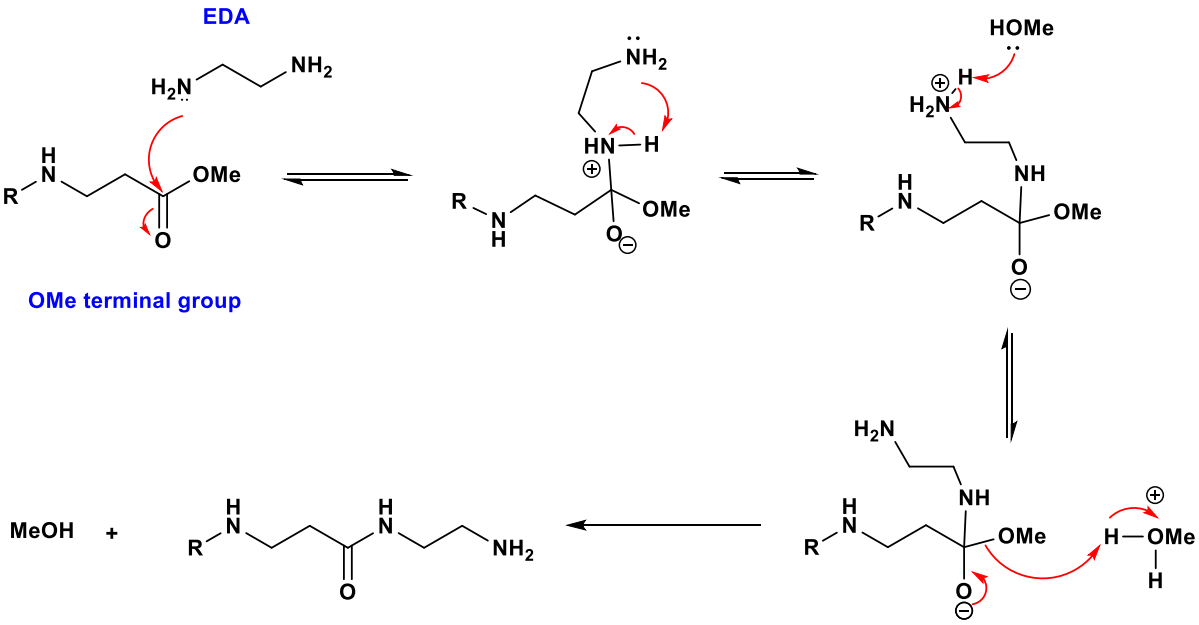

Scheme 4- Amidation reaction mechanism of full-generation PAMAM (amine terminated).

The G1.0 **2** dendrimer was prepared by adding the G0.5 **1** dendrimer to methanol, with a very large excess of EDA. The excess is used to prevent intra and intermolecular reactions, as well as other undesirable side reactions that can lead to structural defects, as illustrated in Scheme 5. However, since EDA acts as a bifunctional reactant during the same step, intramolecular cyclization may occur. Moreover, any residual EDA could serve as a new core, resulting in a half-generation dendrimer. There is also the possibility that two molecules may join together during the amidation process to form a dimer, which could further affect the dendrimer's structure.

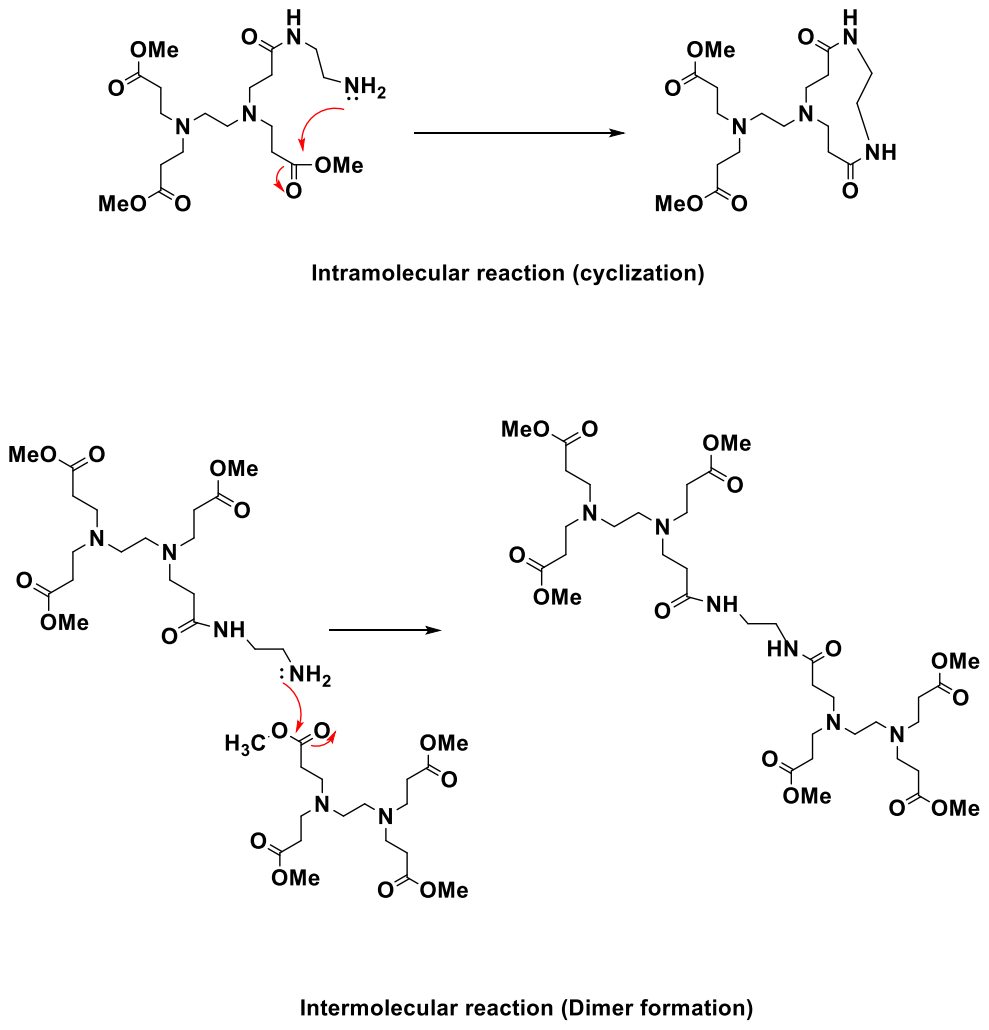

Scheme 5- The possible formation of structural defects during the synthesis of PAMAM dendrimers as a result of various side reactions.

The excess EDA must be completely removed at the end, to prevent it reacting with methyl acrylate in the next steps. However, EDA can form strong hydrogen bonds with the dendrimer (particularly the larger amide dendrimers), which makes it hard to remove by evaporation (Schem 6). Methanol can compete for these hydrogen bonds when in excess, but, due to its low boiling point, ethylene diamine will reoccupy the sites when the methanol concentration decreases. To overcome this, an azeotropic mixture of toluene and methanol (in a 9:1 ratio) was used to eliminate the excess EDA. This solvent can hydrogen bond to the dendrimer and has a boiling point higher than EDA, making it easier to remove the EDA completely. Due to the fact that EDA bonds with amide and amine groups within dendrimers, removing it becomes significantly more challenging as the dendrimers get larger, it is critical to eliminate the substance completely at this stage.

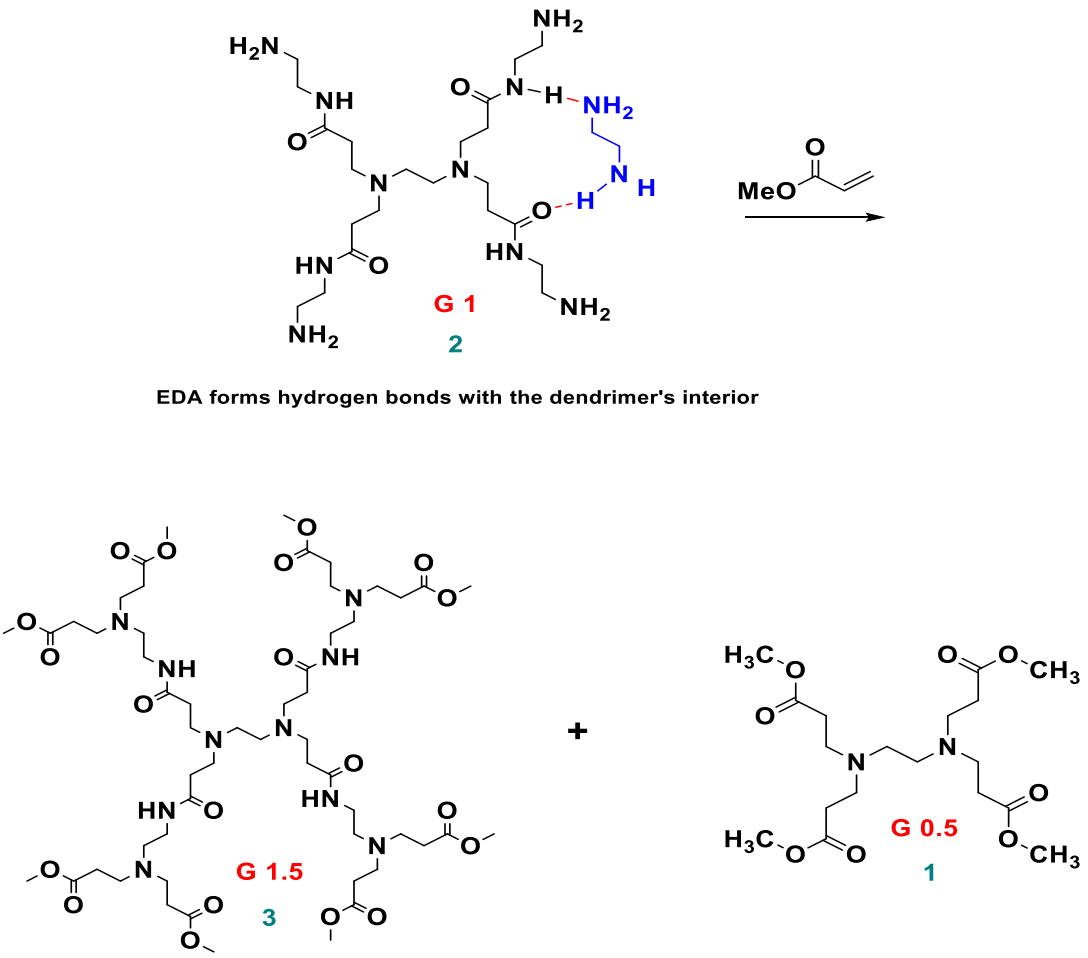

Scheme 6- The hydrogen bonds formed between EDA and the dendrimer's interior, along with the by-products of incomplete EDA removal.

The purified G1.0 **2** dendrimer was confirmed by ^{1}H NMR, revealing the absence of the singlet for EDA at 2.67 ppm. Furthermore, the FTIR peak at 1735 cm^{-1} and the ^{1}H NMR peak at 3.68 ppm, corresponding to the C=O ester, were no longer visible. For the analysis of smaller generations (less than 1000), electrospray ionization mass spectrometry (ES-MS) was employed. A molecular ion with a mass of 517, corresponding to an MH^{+} ion for G1.0 **2**, was determined. These steps were repeated consecutively to build up the size of the dendrimer.

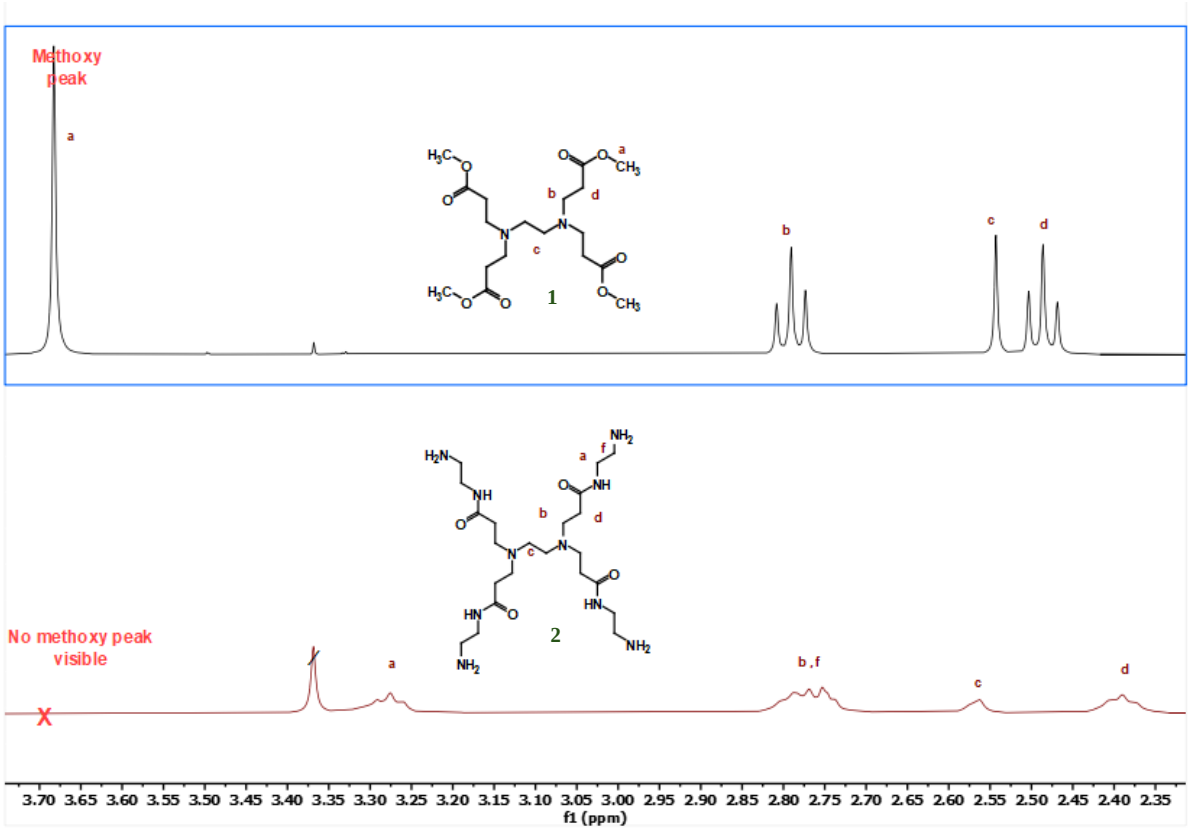

Figure 28- An illustration of the ^{1}H NMR spectrum demonstrates the difference between the half-generation dendrimers (top) and the full-generation dendrimers (bottom).

As the generation increases, many proton environments become very similar, resulting in considerable overlap and peak broadening. Although the classification of larger generation spectra is more challenging than that of smaller generations, it is still possible.

Dendrimers exhibit a uniform structure, making mass spectrometry an ideal technique for determining their molecular weights. The whole and half generations displayed molecular ion peaks at the same positions as calculated from ideal structures, giving confidence in the synthesized model. Smaller generations of dendrimers (fewer than 1000) were analysed using electrospray ionization mass spectrometry (ES-MS), while MALDI was utilized for dendrimers from the largest generation. Table 2 shows the molecular ion peak values for each dendrimer half- and full generation.

Dendrimer Generation	Molecular formula	molecular weight (g/mol)	Terminal Group Type and Number
G 0.5 **1**	C_{18} H_{32} N_2 O_8	405	CO_2Me (4)
G 1.0 **2**	C_{22} H_{48} N_{10} O_4	517	NH_2 (4)
G 1.5 **3**	C_{54} H_{96} N_{10} O_{20}	1206	CO_2Me (8)
G 2.0 **4**	C_{62} H_{128} N_{26} O_{12}	1430	NH_2 (8)
G 2.5 **5**	C_{126} H_{224} N_{26} O_{44}	2806	CO_2Me (16)
G 3.0 **6**	C_{142} H_{288} N_{58} O_{28}	3257	NH_2 (16)
G 3.5 **7**	C_{270} H_{480} N_{58} O_{92}	6014	CO_2Me (32)

Table 2: Characterization of PAMAM generations (both ester and amine terminated)

Infrared spectroscopy further confirmed the correct functional group in both half- and whole-generation dendrimers. When combined with other techniques, infrared spectroscopy proves to be a useful tool for characterization.

Dendrimer Generation	IR Strech (cm^{-1})	
	C=O ester	C=O amide
G 0.5 **1**	1737	-
G 1.0 **2**	-	1647
G 1.5 **3**	1738	1641
G 2.0 **4**	-	1641
G 2.5 **5**	1738	1645
G 3.0 **6**	-	1639
G 3.5 **7**	1738	1642

Table 3: IR Data for PAMAM Dendrimer

2.7.2 Synthesis of dendrimers with hydroxy terminal groups

After synthesizing the half and full generation of PAMAMs, the next step in achieving our aims was to synthesize a non-binding neutral water-soluble PAMAM dendrimer. This was done by converting the half-generation ester terminated PAMAM dendrimers into PAMAM-OH dendrimers through nucleophilic substitution using ethanolamine. Although this reaction is similar to the EDA reaction, a base was needed to deprotonate the tetrahedral intermediate, as the OH group is not sufficiently basic. In our previous studies, DMSO was used as the solvent, along with ethanolamine and potassium carbonate. However, the DMSO was very difficult to remove, as the temperatures required were too high and retro Michael addition was observed. We therefore attempted to avoid the use of DMSO and carried out the reaction using an excess of ethanolamine (as reagent and solvent). Unfortunately, the resulting product was not soluble in water, suggesting that the hydroxy groups were only partially attached. This could be explained by the poor solubility of PAMAM dendrimers in ethanolamine. It was therefore necessary to use some DMSO, however we decided to use this in a very small quantity. This would enable the dendrimer to be dissolved and to react with the ethanolamine and potassium carbonate, as shown in Scheme 7. This subtle change in conditions allowed us to obtain the fully reacted dendrimers in good yield.

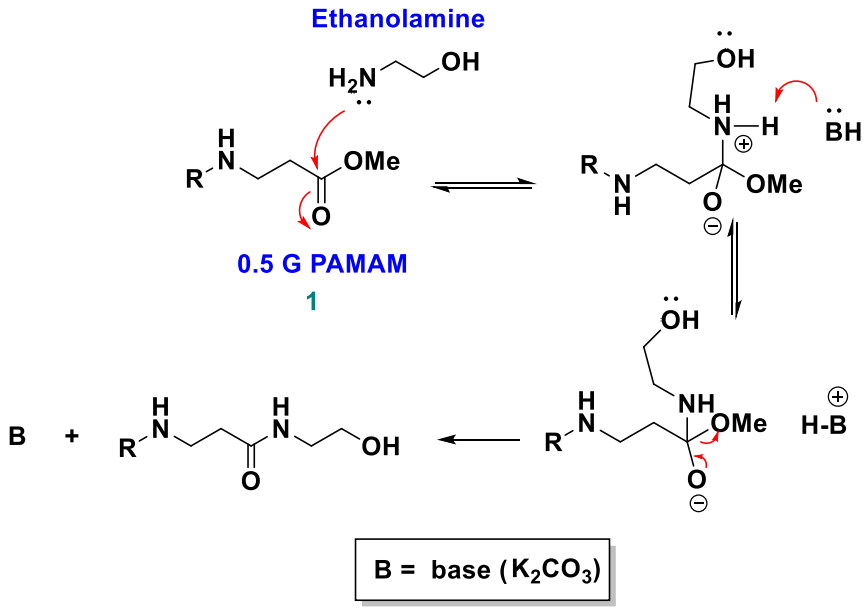

Scheme 7- Mechanism for converting ester/half-generation PAMAM into PAMAM-OH using ethanolamine.

The initial purification of the crude product was achieved through vacuum filtration, to remove excess potassium carbonate. The crude product was then obtained through precipitation using acetone, yielding a thick paste. Subsequently, the product was dissolved in the minimum amount of water, and the purification process was repeated twice, resulting in the neutral PAMAM dendrimer product as a yellow paste in 84% yield. The ^{1}H NMR spectrum showed a new triplet at 3.58 ppm, corresponding to the terminal methylene protons of the ethanolamine, figure 29. Additionally, the ester methyl peak at 3.69 ppm, which was present in starting material was no longer visible. FTIR and ^{13}C NMR spectra were also used to confirm the structures, in which there were no visible peaks for the ester C=O at 1735 cm^{-1} or 175 ppm respectively. A similar procedure and characterization strategy were used for the synthesis of higher-generation neutral dendrimers. The characterization data for all OH terminated dendrimers is summarized In Table 4.

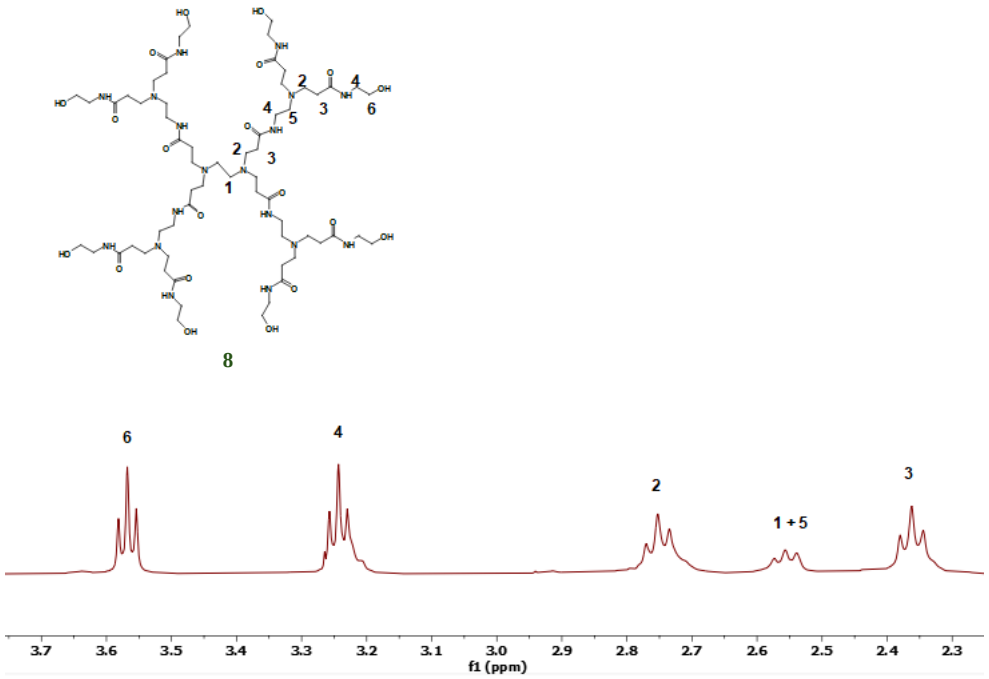

Figure 29- ^{1}H NMR spectrum of G1.5 PAMAM-OH **8** after purification.

Dendrimer generation	Chemical formula	Molecular weight (g/mol)	The number of OH groups
G 1.5-OH **8**	$C_{62}H_{120}N_{18}O_{20}$	1438	8
G 2.5-OH **9**	$C_{142}H_{272}N_{42}O_{44}$	3272	16
G 3.5-OH **10**	$C_{302}H_{576}N_{90}O_{92}$	6940	32

Table 4: Characterization of neutral PAMAM generations.

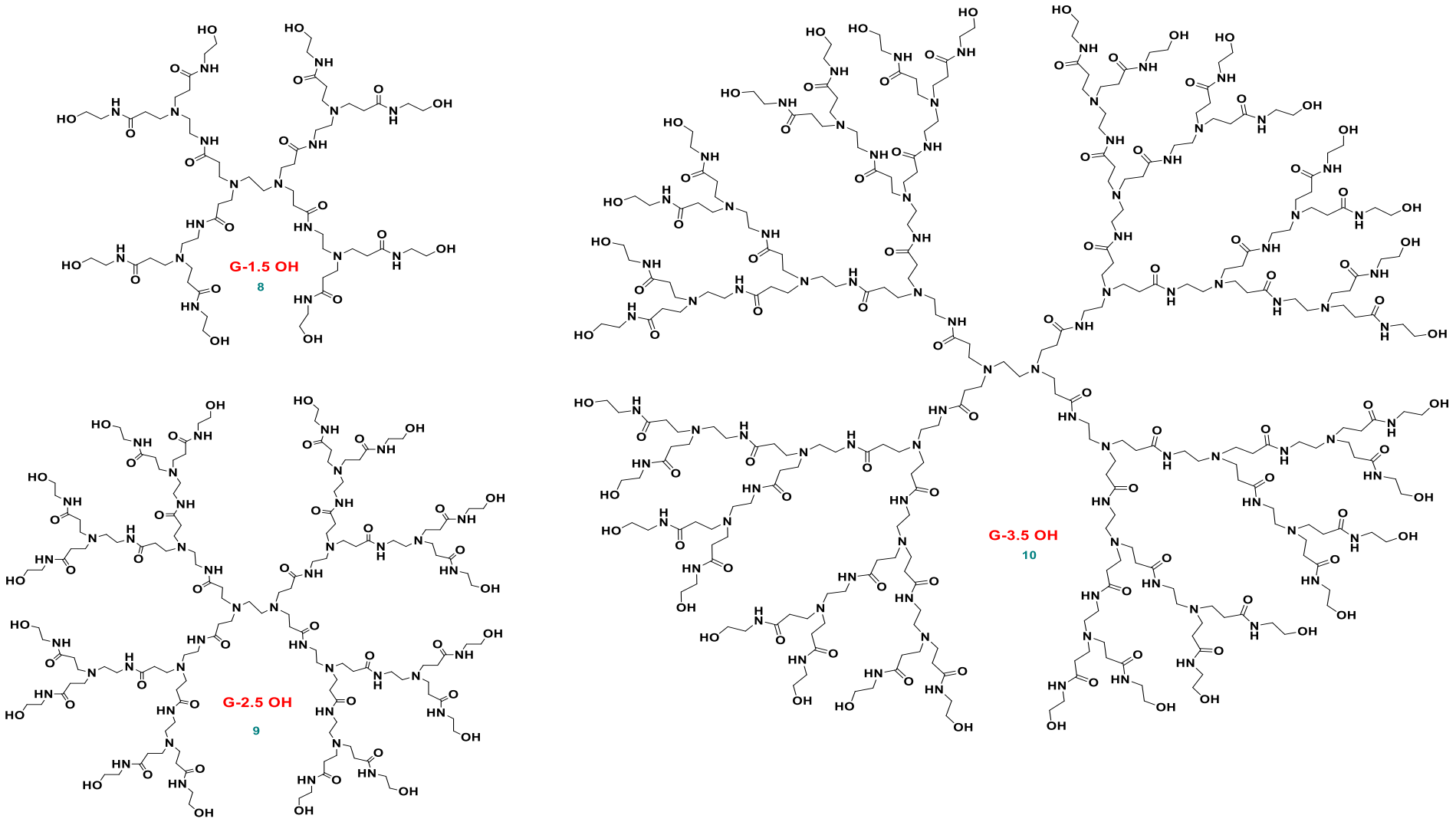

Figure 30- The neutral PAMAM dendrimers synthesised.

2.7.2 Synthesis of linear chain

With the successful synthesis of the neutral dendrimer scaffold required to support the binding and targeting groups, the next step was to synthesize the linear chain that would be used to bind the target proteins. This linear chain was designed to have three amide groups and a terminal binding/terminal group. This chain can be encapsulated/incorporated within the dendrimer's interior by hydrogen bonding between the amide groups on the chain and within the dendrimer, as shown in (Scheme 8), maximizing the number of encapsulated chains. Additionally, these linear chains could interact with the surface groups on the target proteins. Our group found that dendrimers covalently functionalized with tyrosine, phenylalanine, and valine could affect binding positively or negatively.[32] Using functionalized linear copolymers, Giles et al. demonstrated enhanced selectivity for enzyme binding.[63]

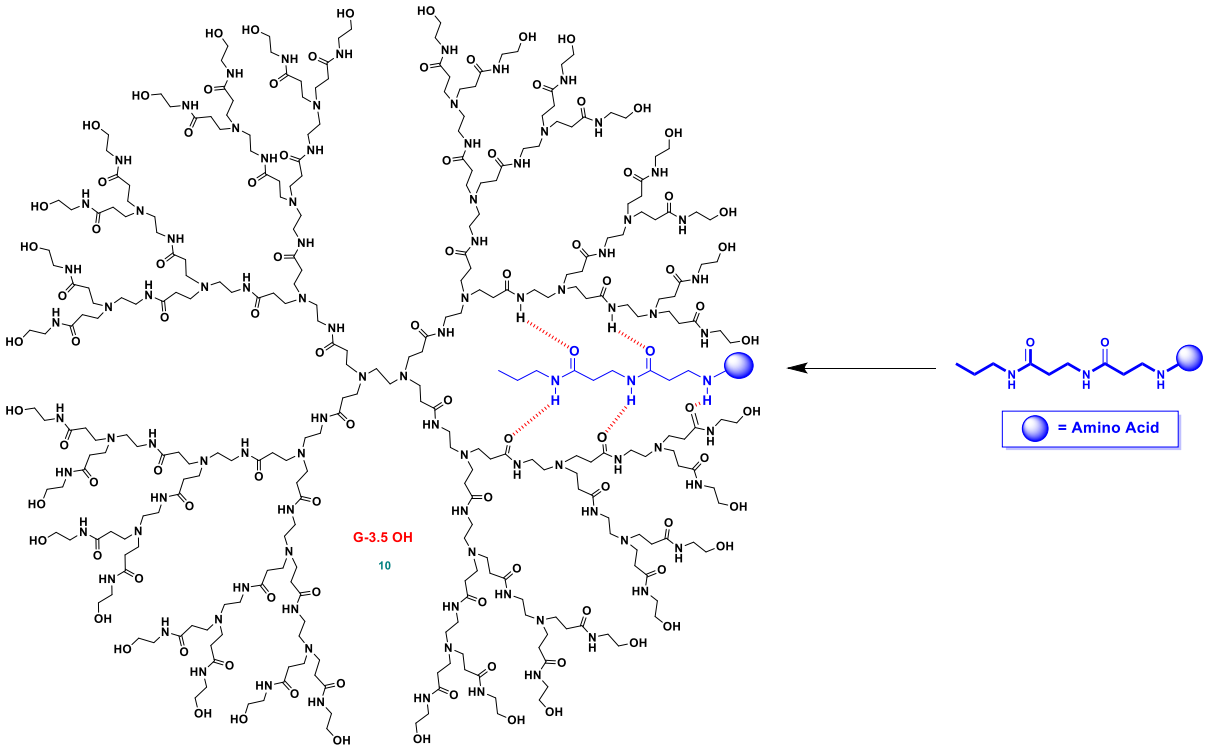

Scheme 8- Possible H-bonding between linear chain and the interior of G3.5-OH **10** dendrimer.

Our group also demonstrated that carboxylic acid terminated dendrimers functionalized with tyrosine chains can inhibit Chy better than the acid terminated dendrimers alone, as shown in Figure 31 and Table 5. However, the acid interactions dominated, with the linear chain functionality possibly being capable of offering some selectivity through additional interactions (albeit weaker interactions). Taking this into account, we decided to incorporate the same key amino acids into our linear chain and use a neutral dendrimer that would not bind.

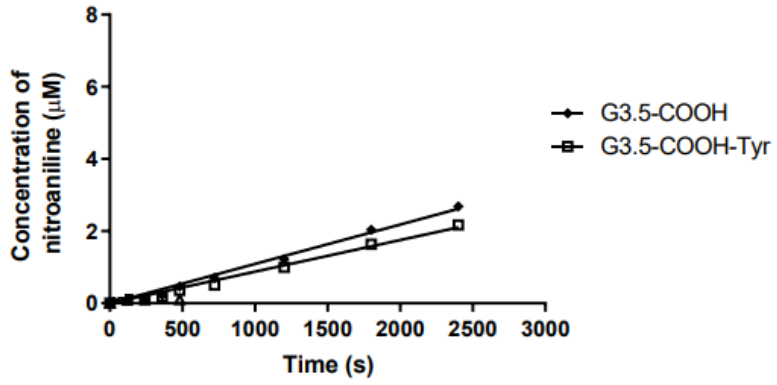

Figure 31- Initial rate plot of chymotrypsin-BTNA hydrolysis in the presence of carboxylic acid-terminated dendrimer inhibitors, functionalized with tyrosine chains.

Dendrimer	3.5-COOH	3.5-COOH -Tyr
Initial velocity (V) nMs^{-1}	1.090	0.876
Percentage Inhibition (%)	66	73

Table 5: Data showing the comparison of relative binding of 3.5-COOH PAMAM before and after functionalization with amino acids.

The linear chains were previously synthesized from an alkyl amine and β-alanine repeat unit. Because of its bifunctionality, it was imperative to protect its amine group to prevent self-polymerization and unwanted side products. Therefore, our previous synthesis used a strategy involving tert-butyloxycarbonyl (Boc) as the protecting group. However, by employing Boc groups, the synthetic process required an aqueous workup. Unfortunately, the deprotected products (obtained after each addition of the β-alanine repeat unit) were water soluble, resulting in considerable loss of product after each deprotection step. For this project, we proposed to overcome this problem using a different protecting group, specifically N-benzyloxycarbonyl (Cbz). Removal of a Cbz-group can be easily achieved through a simple catalytic hydrogenation (Pd/C, H_2.)[64] This method generates CO_2 and toluene, and both can be removed by evaporation. Furthermore, the workup does not involve water, which should result in higher yields and improved purity.

The synthesis began by coupling propylamine **11** with N-Cbz-β-alanine **12** forming a peptide bond. Because the OH group of carboxylic acids is a poor leaving group (it is a good nucleophile), it is necessary to convert it to a better leaving group (a weaker nucleophile). Thus, the acid was converted into an active ester using ethyl-3-(3-dimethylaminopropyl) carbodiimide (EDC.HCl). This is an excellent reagent as it generates a reactive intermediate ester, whilst generating water-soluble byproducts, which can be easily removed through solvent

extraction. Triethylamine (Et_3N) as a base to neutralize the EDC and activate it. The synthetic route of this reaction is shown in Scheme 9. The reaction was conducted at ambient temperature using EDC·HCl, DMAP, and Et_3N in a ratio of 1:2:3, respectively.

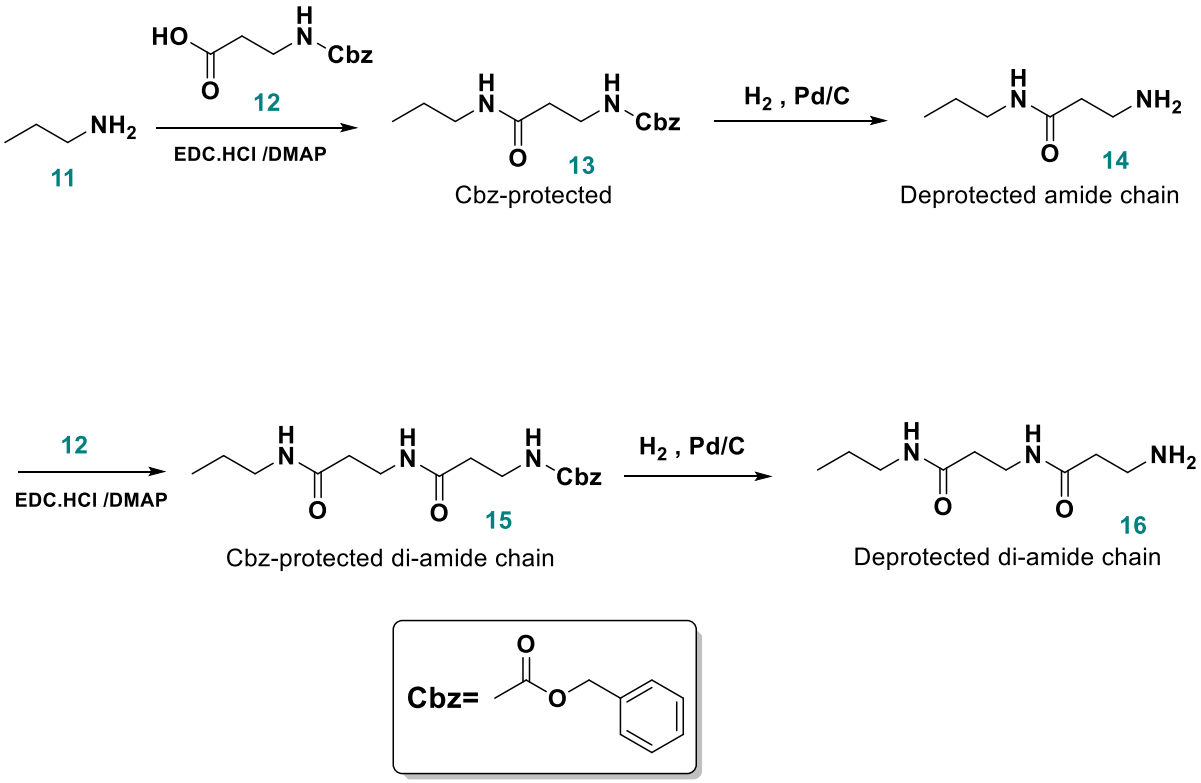

Scheme 9- The planned synthetic route of the linear chain involves an amide coupling reaction and the Cbz deprotection step.

The reaction mixture was allowed to react under nitrogen for 24 hours. The crude product was washed with brine (100 mL x 3) and 2 M of HCl, then the aqueous layers were washed with DCM and dried with Mg_2SO_4. The solvent was concentrated under reduced pressure and dried under high vacuum to give Cbz chain **13** as a white powder (81% yield).

After the reaction was complete, peaks at 7.30 ppm and 7.27 ppm in the ^1H NMR, corresponding to the aromatic protons of the Cbz group were observed. A singlet at 6.23 ppm, which integrated as 2H, was assigned to the $C\underline{H_2}Ar$. The quartets at 3.45 ppm, and 3.17 ppm were assigned as the $NH\underline{CH_2}CH_2$. Additionally, signals at 2.40 ppm, 1.48 ppm, and 0.87 ppm corresponding to $NHCH_2C\underline{H_2}$, $C\underline{H_2}CH_3$, and $CH_2C\underline{H_3}$ respectively, are observed. In addition, ^{13}C NMR and FTIR spectra were used as additional tools to corroborate ^1H NMR results. ^{13}C spectrum showed ester carbonyl signals at 171.28 ppm and 156.66 ppm, while three peaks at

128 ppm were attributed to the Cbz ring carbons. The FTIR spectrum displayed a band at 3078 cm^{-1}, corresponding to aromatic C-H stretching. The protonated molecular ion (MH^+) can be seen at 265 in the ES-MS spectrum, confirming the successful synthesis of the protected chain. The next step involved deprotecting the Cbz group. This was achieved by dissolving the protected amine in methanol, followed by adding Pd/C with hydrogen gas. Once the hydrogenation was complete, the mixture was filtered over Celite to remove the catalyst, and the filtrate was concentrated under reduced pressure, yielding the deprotected chain (**14**) in 84%. Scheme 10 illustrates the deprotection mechanism for the linear chain.

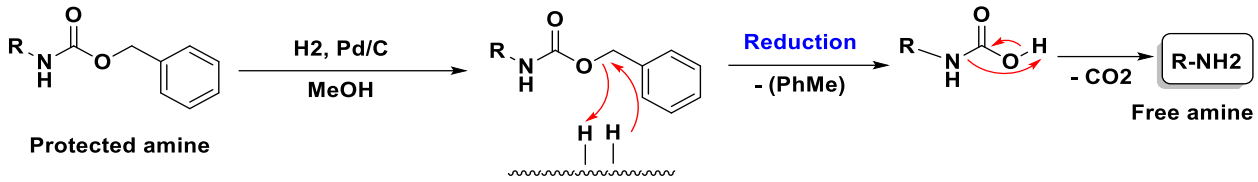

Scheme 10- The general Cbz deprotection mechanism for the linear chain.

The absence of aromatic protons in the ^1H NMR confirmed the successful removal of the Cbz group (Figure 32). Mass spectrometry analysis also confirmed the loss of the protecting group, showing a molecular ion at 130 (MH^+) for the deprotected amide chain.

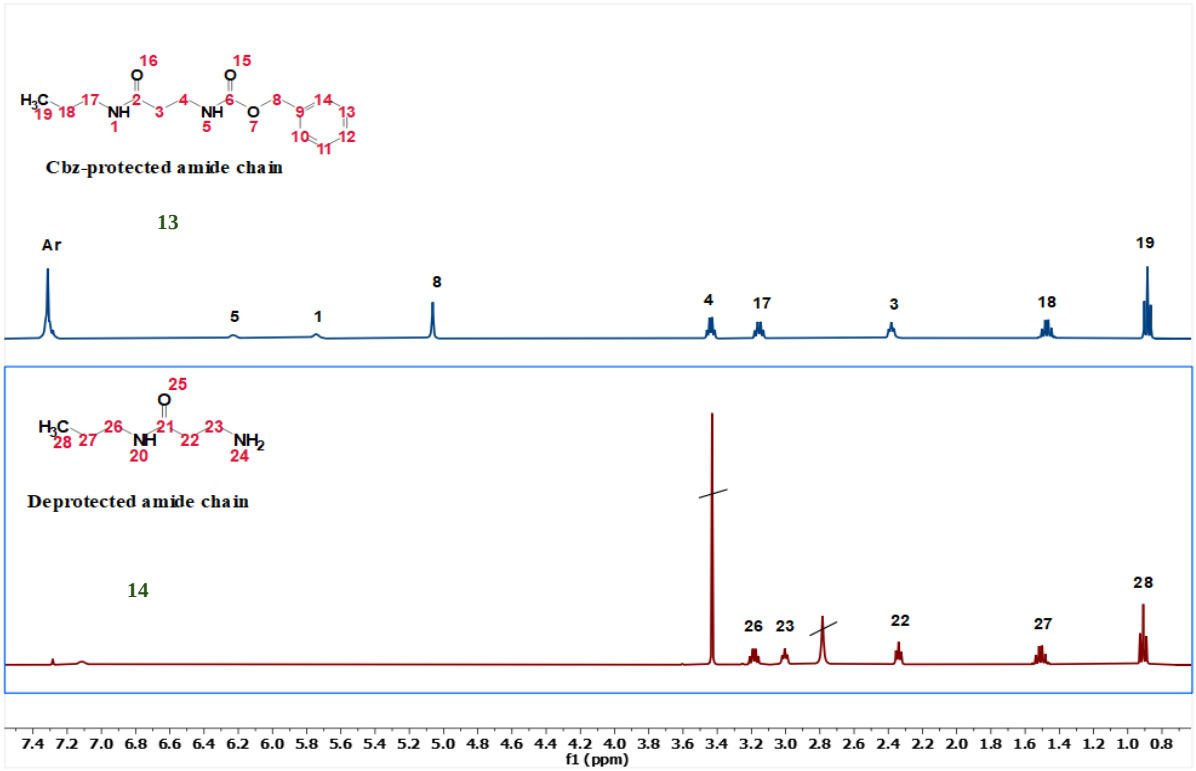

Figure 32- ^1H NMR spectrum of protected (top) and deprotect linear chain (bottom).

To lengthen the chain, a second Cbz-β-alanine group was added using the same EDC procedure. As shown in Scheme 10 above, the compound was subsequently deprotected to yield the longer linear amine terminated amide chain. The characterization data for this chain is summarized in Table 6. Following this, the amino acids tyrosine and valine were added to the terminal amine. The procedure is described in the next section.

Linear chain	Cbz-protected **13**	Deprotected amide chain **14**	Cbz-protected di-amide chain **15**	Deprotected di-amide chain **16**
Chemical Formula	$C_{14}H_{20}N_2O_3$	$C_6H_{14}N_2O$	$C_{17}H_{25}N_3O_4$	$C_9H_{19}N_3O_2$
Expected Molecular weight (g/mol)	264	130	335	201
Obtained Mass ion (MH^+)	265	131	336	202

Table 6: Linear chain characterisation summary.

2.7.3 Addition of Tyrosine and Valine to the linear chain

The amine-terminated chain included a combination of hydrophobic and hydrogen-bonding interactions that would help drive encapsulation. A linear chain with a tyrosine termination (LC-Tyr) was chosen for this initial study, as this amino acid plays a significant role in protein-protein interactions.[65] Valine termination (LC-Val) was also studied, as its amino acid is documented as having a negligible impact on binding.[66] We therefore expected that the inhibitory level would be high when tyrosine was used and low when valine was encapsulated within the dendrimer. Scheme 11 illustrates the synthetic route of both the tyrosine and valine-terminated linear chains.

Tyrosine was then added as its benzyloxy-protected amino acid, to yield a protected tyrosine linear chain (protected LC-Tyr) **17** after a simple deprotection step. A similar procedure was used for the addition of valine, resulting in the formation of protected LC-Val **18**.

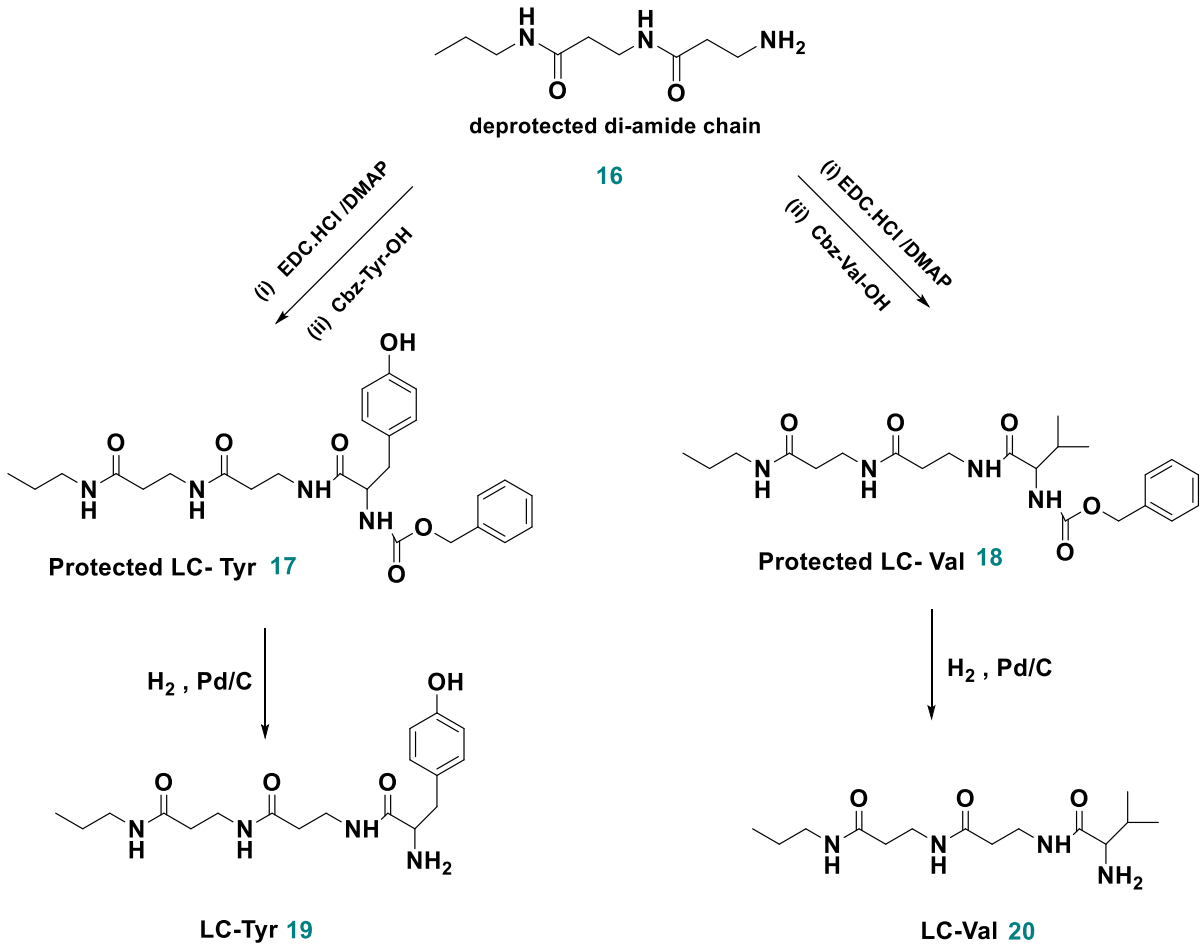

Scheme 11- Reaction scheme for the synthesis of Tyrosine and valine terminated linear chain.

Peaks at 7.05 ppm and 6.71 ppm in the ^{1}H NMR spectrum, corresponding to the aromatic protons of the tyrosine group, confirmed the addition of tyrosine to the amine chain. Mass spectrometry further confirmed the mass with a molecular ion observed at 499 (MH^{+}). The Cbz deprotection of the tyrosine chain **19** was carried out as described in the previous section and the 2D $^{1}H/^{13}C$ HSQC NMR has been conducted for further confirmation of the LC-Tyr **19** structure, as shown in Figure 33 below. The molecular weight of the synthesized LC-Tyr **19** compound was confirmed by high-resolution mass spectrometry (HRMS). The molecular ion $[M+H]^{+}$ was observed at m/z 365.2189, which matches the calculated mass of 365.2183 for $C_9H_{19}N_3O_2$, with a mass error of 1.59 ppm.

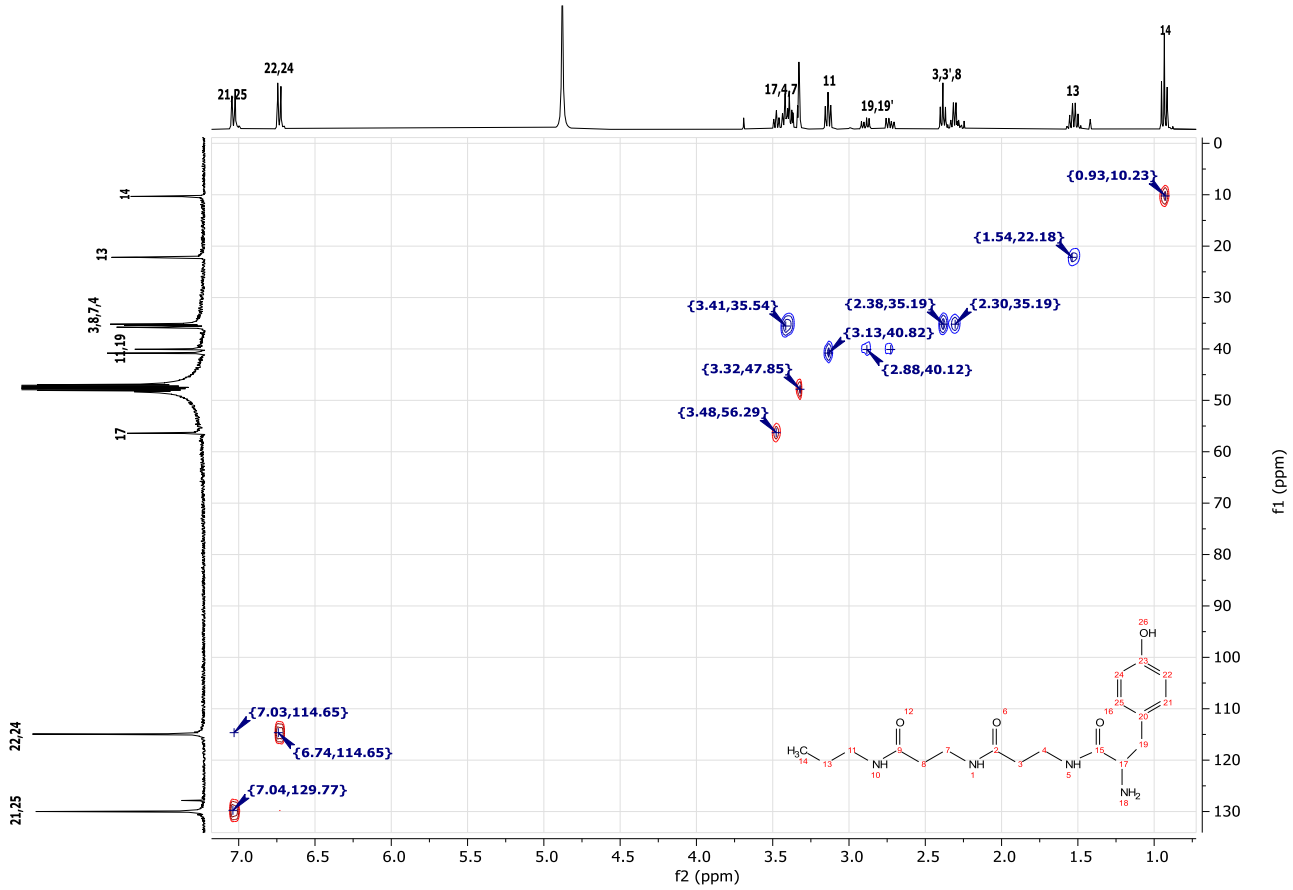

Figure 33- 2D $^{1}H/\ ^{13}C$ HSQC NMR of LC-Tyr chain **19**.

The same addition/deprotection procedure was used to add the valine group. The ^{1}H NMR spectrum of the deprotected valine chain (LC-Val) **20**, showed a small septet at 2.01 ppm, that integrated for one proton, and a large doublet integrating as six protons at 0.99 ppm, this pattern is a characteristic of the C<u>H</u>$(CH_3)_2$ iso-propyl group and confirms addition of valine. The successful preparation of LC-Val **20** was corroborated by the mass spectrum, which displayed a molecular ion at 301(MH^+).

2.7.4 Encapsulation of the functionalised linear chain with neutral PAMAM dendrimer

Encapsulation of the linear chains that would be used to bind the target protein would be achieved using the same techniques our group, and others has used to encapsulate drugs.[67] Drug solubility can be enhanced by encapsulating them with large hydrophobic molecules, in our case a dendrimer. For the proposed methodology, the dendrimer must be water-soluble and serve as a scaffold for the functionalized linear chains. Additionally, the dendrimer's terminal groups should be neutral and inert, preventing any unwanted interactions with the protein's binding surface and ensuring that the only interactions come from the terminal groups on the encapsulated linear chains. The dendrimer must also be large enough to cover the entire

interfacial area of the target protein, while avoiding any dense shell packing that could limit encapsulation of the chain.

To evaluate the potential of the non-covalent methodology using neutral PAMAM-OH dendrimers, we first needed to establish that the systems could encapsulate enough of the linear chains (to achieve a suitable density of functional groups on the dendrimer's surface). Therefore, encapsulation experiments using different generations of neutral PAMAM dendrimers were studied, focusing on G1.5- 8OH **8**, G2.5- 16OH **9**, and G3.5- 36OH **10** (figure 34).

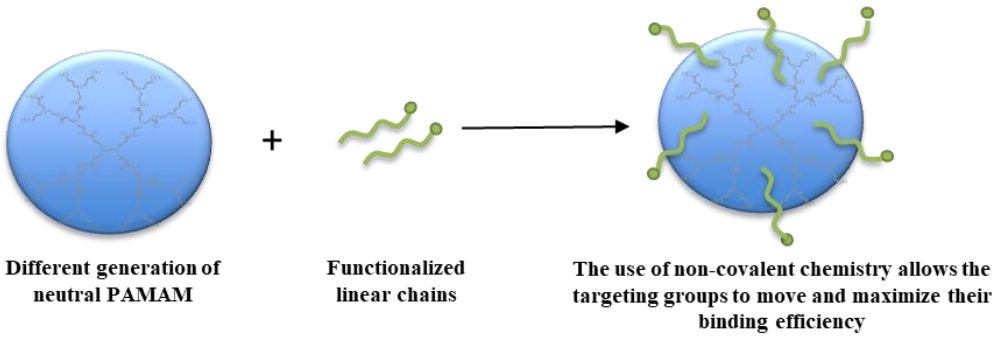

Figure 34-Schematic representation of the components required for the self-assembled macromolecular protein ligand.

Encapsulation was performed using a dendrimer-to-chain ratio with an excess amount of chain. The first experiment was designed to determine maximum solubility of the free chain in phosphate buffer (pH 7.4, 0.01M) without the dendrimer. This value was then subtracted from all subsequent dendrimer measurements, ensuring that only the encapsulated chain was considered.

This was achieved by dissolving an excess of the linear chain in a known volume of methanol and shaking it at room temperature until fully dissolved. Solid residues were removed by vacuum filtration, after which the methanol was evaporated under reduced pressure, and a known volume of 0.01 M buffer solution was added. The absorption was then measured using UV-vis spectroscopy.

For the free tyrosine chain, the concentration of LC-Tyr **19** was calculated as shown in the equation below, and all characterization data for LC-Tyr are provided in Table 7.

$$\text{The concentration of freeTyr } (A) = \frac{\text{Absorbance}}{\text{Ɛ of Tyr}}$$

$$\text{The concentration of freeTyr (A)} = \frac{0.0434}{8480.3} = 5.12\text{E} - 06\ \text{M}$$

Parameter	Free Tyrosine
Extension coefficient	8480.3 $dm^3\ mol^{-1}cm^{-1}$
Concentration of the free Tyr in phosphate buffer	5.12E-06 M

Table 7: Analysis of the characteristics of LC-Tyr **19**.

To prepare the host/guest complex for encapsulation experiments, we used a co-precipitation technique. In the encapsulation experiment, PAMAM-OH dendrimers were used at a concentration of 1.0E-06 M to encapsulate excess amounts of LC-Tyr **19** (10 equivalents). For example, 0.694 mg of PAMAM 3.5-OH **10** and 3.56 mg of LC-Tyr **19** were dissolved in methanol, and then methanol was removed using a rotary evaporator to yield the coprecipitated complex. The concentrations and calculations for the dendrimer and LC-Tyr **19** are shown in Table 8. A buffer solution was then added, and any non-encapsulated or insoluble LC-Tyr **19** was filtered out. Absorbance measurements were taken for each complex, and the encapsulated LC-Tyr concentrations in each generation were determined using Equations 1 below. Using equation 2, the proportion of encapsulated chains within the dendrimer were calculated by subtracting the encapsulated LC-Tyr concentration from the free LC-Tyr concentration and then dividing by the dendrimer concentration.

1. $$\text{The concentration of encapsulated Tyr (A)} = \frac{\text{Absorbance}}{\varepsilon \text{ of Tyr}}$$

2. $$\text{Loading of Tyr chain in PAMAM} - \text{OH (X)} = \frac{[\text{concentration of encapsulated Tyr(A)}] - [\text{concentration of free Tyr(B)}]}{[\text{Dendrimer Concentration (C)}]}$$

PAMAM -OH Generation	Absorbance	The concentration of encapsulated Tyr (A)	Loading of Tyr chain in PAMAM-OH (X)
Free Tyrosine **19**	0.0434	5.12E-06 (B)	/
G 1.5- Tyr complex **21**	0.0721	8.50E-06	3 (±0.23)
G 2.5- Tyr complex **22**	0.0821	9.68E-06	4 (± 0.17)
G 3.5- Tyr complex **23**	0.0979	1.16E-05	6 (±0.18)
Dendrimer Concentration (C) = 1E-06			

Table 8: Encapsulation analysis of different PAMAM generations with tyrosine chains.

As shown in Table 8, the data demonstrate that the tyrosine chains were efficiently encapsulated within the PAMAM-OH dendrimers. There is a clear relationship between the dendrimer's generation size and its encapsulation capacity. The G1.5 dendrimer, which had eight OH groups, encapsulates only 3 chains within its hydrophobic void. By comparison, dendrimers with 36 OH groups, encapsulated 6 chains, demonstrating improved encapsulation efficiency as the dendrimer generation increases.

A G3.5 dendrimer, known for its optimal interaction with the binding area of chymotrypsin Chy[32], also encapsulates the maximum number of targeting chains. After investigating the effect of dendrimer size on encapsulation capacity, the study analyzed the complex's UV absorbance before and after encapsulation. A bathochromic shift of 5 nm in the tyrosine peak was observed in all cases, providing strong evidence for encapsulation and indicating that the absorptions originated from encapsulated chains (figure 35). This shift suggests that the dendrimer's interior groups replace the water solvating the linear chains, providing evidence for encapsulation. It is believed that complexation is driven by a cooperative process involving hydrophobic interactions and hydrogen bonding.

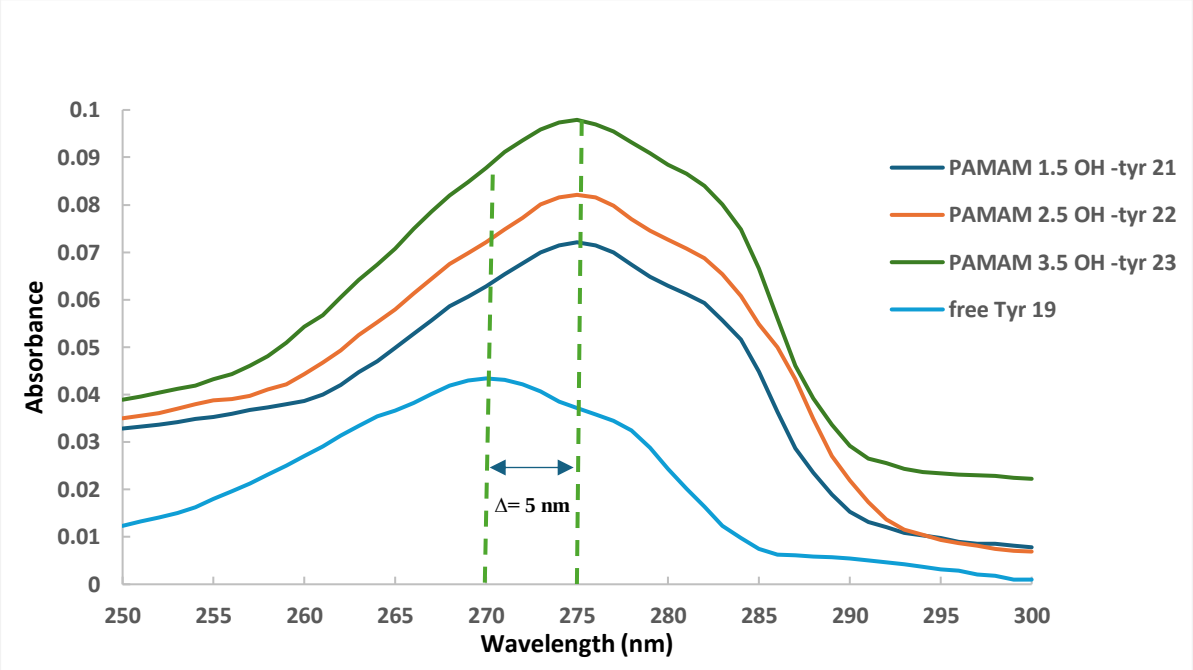

Figure 35- A comparison of UV absorbance before and after encapsulation of the tyrosine chain **19** in different generations of neutral dendrimers.

Increased hydrogen bonding sites in higher-generation dendrimers, as well as their hydrophobic and globular structure, contribute to enhanced encapsulation efficiency. However, the G1.5-8OH **8** and G2.5-16OH **9** dendrimers did not show any significant difference in

loading, possibly because of their relatively open structures, which result in poorly formed hydrophobic cavities. This is a known effect and is associated with the lack of densely packed structure for these small dendrimers.[68,69]

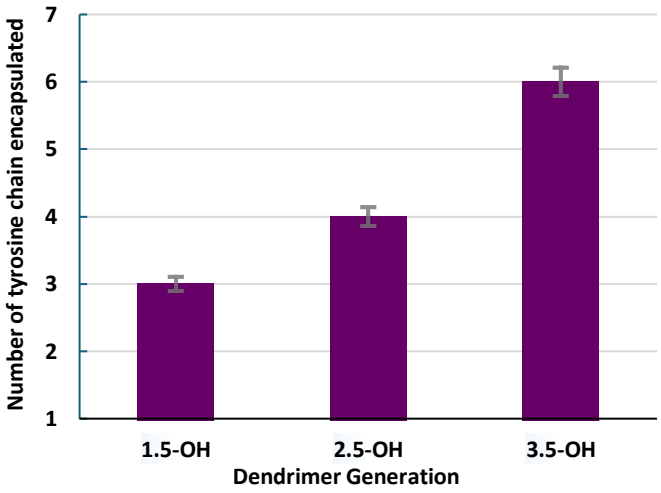

Figure 36- LC-Tyr **19** encapsulated in the different generations of PAMAM dendrimer

The next experiment was conducted to determine the encapsulation of a different functionalized linear chain, which in this case is the valine chain **20**. The same procedure and calculations used to encapsulate LC-Tyr **19** were applied here, and all parameters used are shown in Table 9.

Parameter	Free Valine
Extension coefficient	13402 dm^3 $mol^{-1}cm^{-1}$
Concentration of the free Val in phosphate buffer	5.86E-06 M

Table 9: The characterization data of LC-Val **20**.

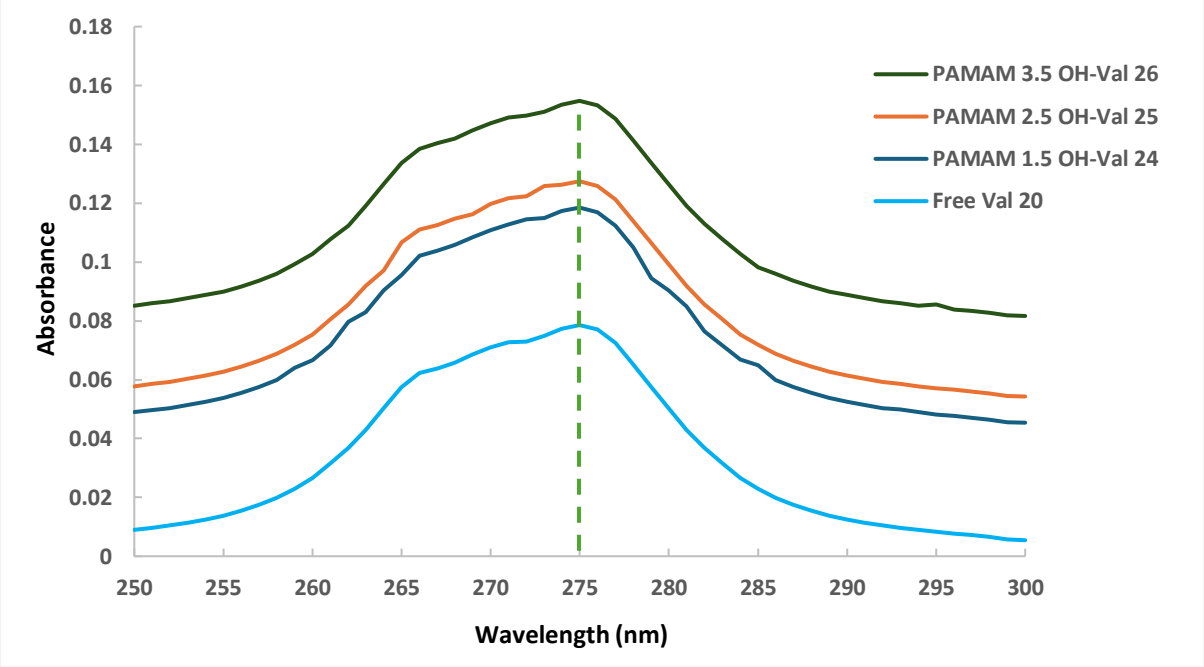

Figure 37- UV absorbance before and after encapsulation of the valine chain.

According to the UV spectral absorbance values presented in Figure 37 for LC-Val **20**, especially at higher generations of PAMAM-OH, the dendrimer's increased size and generation enhance its ability to encapsulate the LC-Val chains. However, no shift in valine λmax was observed after encapsulation. There is no explanation for this, but one possibility is that the encapsulated chains have different orientations; some chains may orient their amino acid end group inside the dendrimer, while others may have their head groups exposed to bulk water, requiring further investigation.

PAMAM -OH Generation	Absorbance	The concentration of encapsulated Val (A)	Loading of Val chain in PAMAM-OH (X)
Free Valine **20**	0.07856	5.86E-06 (B)	/
G 1.5- Val complex **24**	0.1185	8.80E-06	3 (±0.15)
G 2.5- Val complex **25**	0.1274	9.50E-06	4 (±0.43)
G 3.5- Val complex **26**	0.15477	1.15E-05	6 (±0.37)
Dendrimer Concentration (C) = 1E-06			

Table 10: UV absorbance data of Val chain **20** before (free) and after encapsulation by PAMAM-OH generations.

According to the data summarized in Table 10, G3.5-**32** OH **10** encapsulated at least 6 of Val chains **20** within the dendrimer through supramolecular/non-covalent interactions. This confirms that a neutral dendrimer can effectively act as a scaffold for the linear chain.

2.8 Assessment of dendrimer-Cyt-c binding using non-covalent targeting and signaling methods.

2.8.1 Introduction

Cytochrome-c (Cyt-c) (figure 38) is a key mitochondrial protein involved in electron transfer and apoptosis, making it an important target for research.[70] Heme moiety is covalently linked to the protein by thioether groups, while iron in the protein serves as either an electron donor or electron acceptor by switching between ferrous and ferric oxidation states (Fe^{2+} and Fe^{3+}). The changeability between these two states is enabled by the interaction between the electronic orbitals of the heme iron and the π system of the porphyrin.[71] The protein's structure consists of two minor and three major helices that fold into a round shape, forming a heme pocket. The exposed heme edge is surrounded by lysine, arginine, and a variety of hydrophobic residues, giving the domain a positive charge. This surface serves as a site of electron transfer between the heme moiety and a complementary protein partner. This interaction is facilitated by the presence of anionic domains on the partner protein.

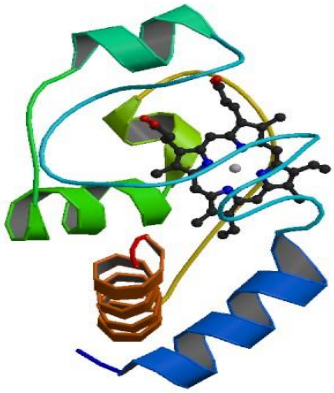

Figure 38- Ribbon structure of human cytochrome-c with a heme moiety.

As part of our research, we propose a new paradigm to achieve our aim through non-covalent self-assembly of binding and sensing units within and around an inert dendrimer scaffold. Although embedded in the dendrimer, the binding units remain mobile and free to move. Upon introducing a target protein, these units reposition themselves in order to optimize cooperative interactions with the protein's binding surface.

During this dynamic process, the protein guides and controls the creation of its own macromolecular ligand.

In this section, we described the synthesis and assembly processes. It is also possible for binding to be detected and quantified when binding and "sensor units" are combined and included in the assembly program. For the experiments, we used both unfunctionalized and non-covalently functionalized dendrimers for binding and control studies. No binding was observed when only the dendrimer, sensing units, or binding units were used individually (figure 39). However, strong binding was detected when all components were used together and allowed to self-assemble (dendrimer, functionalized chains, and sensing porphyrin). Through fluorescence titration techniques, the binding was quantified as nanomolar (nM).

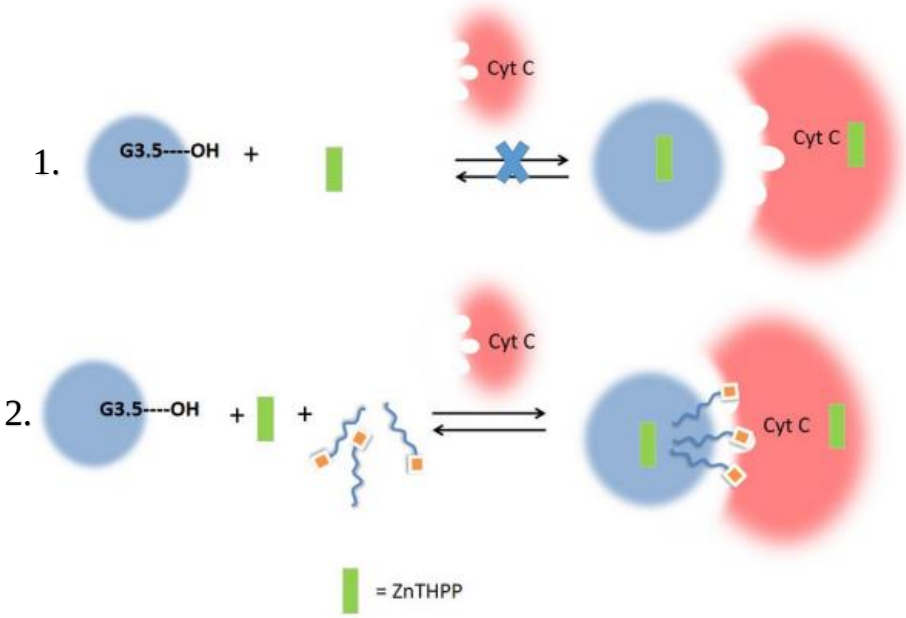

Figure 39- Schematic representation of possible binding complexes that could form when the ZnTHPP **30** /dendrimer complex is added to the protein. (1) No binding occurs between the dendrimer-porphyrin complex, and Cyt-c. (2) A neutral dendrimer **10** could bind to Cyt-c if its functionalized chains were encapsulated.

2.8.2 Design and synthesis of materials.

The proposed approach is based on non-covalent chemistry, which involves the assembly of an optimized macromolecular ligand around a protein template. This design involves three components, as illustrated in Figure 40. It is essential that the dendrimer be water-soluble, in order to ensure that the protein and the assembled ligand are in the same aqueous phase. Dendrimers also need to be big enough to bind the target protein's binding area, while also ensuring that the binding/sensing units can be incorporated without being obstructed by a dense

shell or dense packing structure.[72,73] Our target protein for this study was cytochrome-c which has a well-characterized structure with a binding interface (hot-spot) of approximately 1100 Å². The first component of this study is the neutral G3.5-OH **10** dendrimer, selected for its size and packing density, which allows for maximum guest encapsulation. However, the neutral dendrimer cannot bind to cytochrome-c in the absence of functional groups.

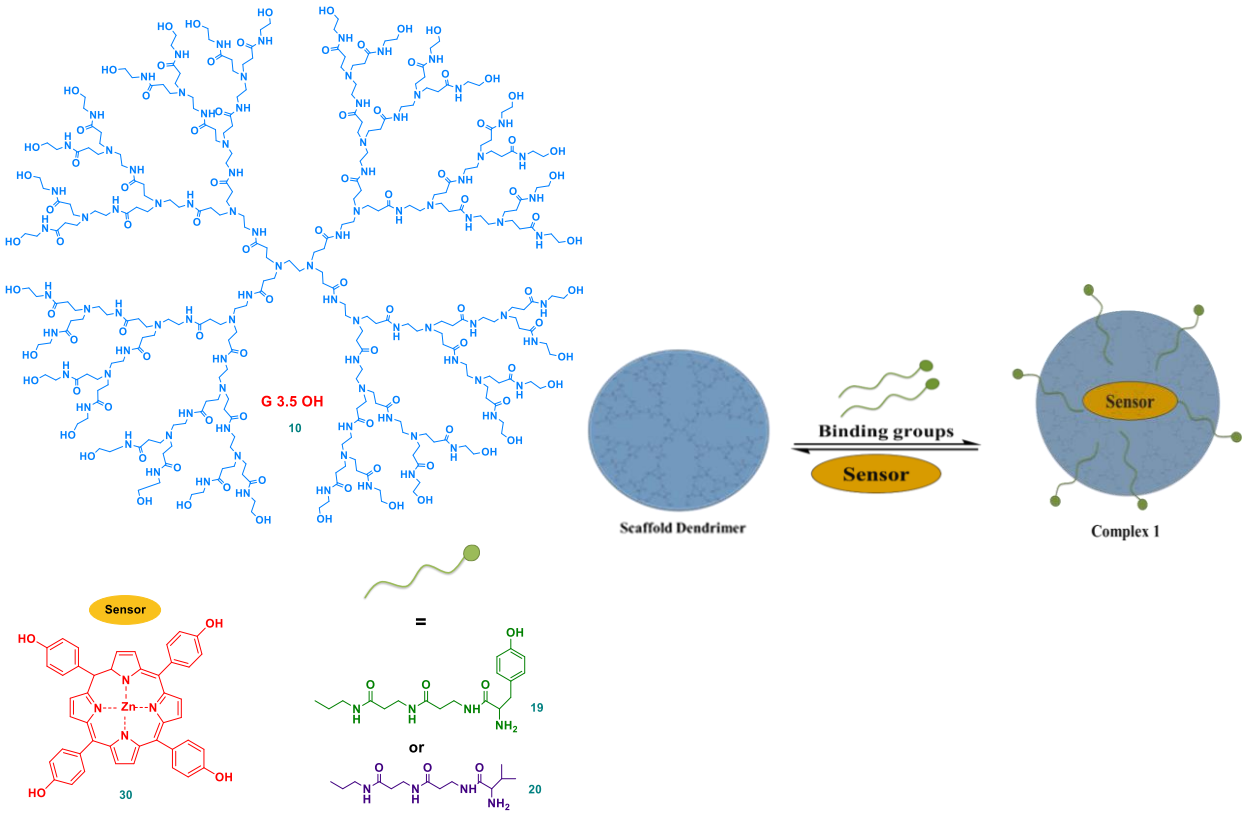

Figure 40- An illustration of the structure of the three components of the self-assembled macromolecular protein ligand.

The second component is a targeting or binding unit that may be encapsulated or incorporated within the dendrimer's interior. To achieve this, the chains were specifically designed and synthesized as described in section (2.7.2). For this proof-of-principle study, tyrosine- and valine-terminated linear chains (LC-Tyr **19** and LC-Val **20**) were selected, as these amino acids are known to play a significant role in facilitating protein-protein interactions.[12,32] the self-assembled macromolecular protein ligand is completed by a simple porphyrin that serves as the sensing/detection unit. Cytochrome-c, the protein used in this study, has a well-characterized binding area and an appropriate size. It also contains a porphyrin group that emits a strong fluorescence signal, which can be disrupted by a bound quencher, allowing for

effective detection of the interaction.[27,29,32] Using this property, a hydrophobic fluorescent reporter can be encapsulated within the interior of neutral dendrimer **10** to detect and quantify binding. It is crucial that the reporter does not bind to the protein independently and stays encapsulated inside the dendrimer. To accomplish this, zinc-tetra(4-hydroxyphenyl) porphyrin (Zn-THPP **30**) was chosen as the internal reporter. Zn-THPP **30** is hydrophobic and is nearly insoluble in water but can be encapsulated within dendrimers by simple hydrophobic interactions. Moreover, Zn-THPP **30** contains a metal center that can coordinate with the dendrimer's internal amines, as well as four phenolic OH groups that can form hydrogen bonds with the dendrimer's amides. The OH groups are acidic enough to undergo deprotonation by the internal amines, which further contributes to electrostatic interactions. Through these cooperative interactions, Zn-THPP **30** remains securely encapsulated within dendrimer **10**. The additional interaction provided by ZnTHPP **30** coordination can be seen in Figure 41.

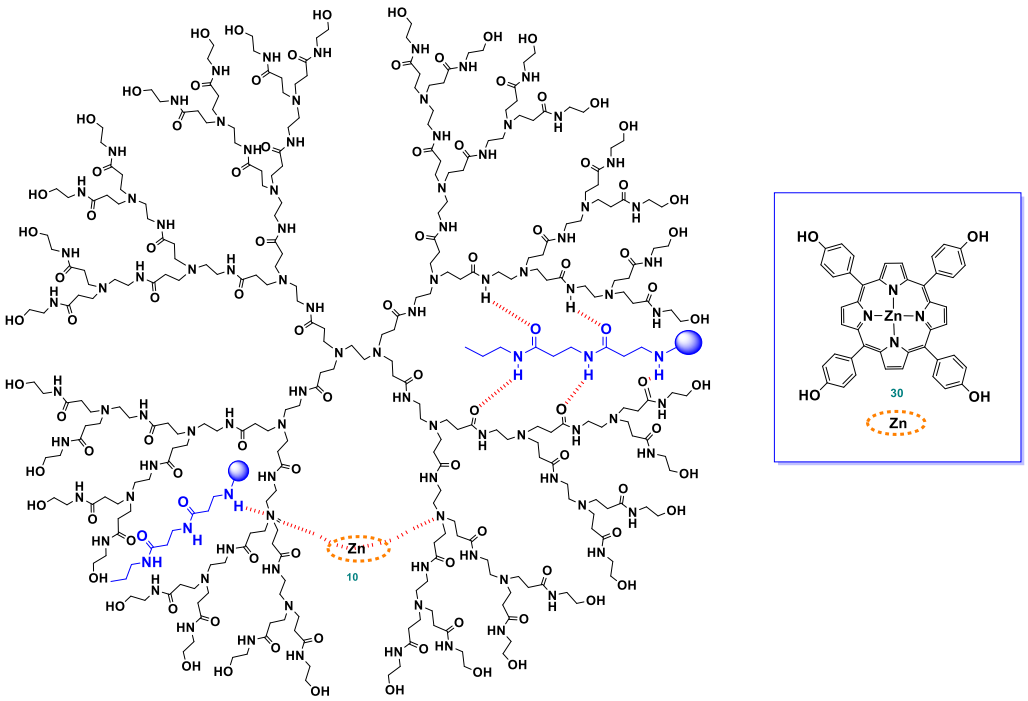

Figure 41- Illustration of the possible coordination interactions between ZnTHPP **30** and the internal amines of the OH dendrimer **10.**

ZnTHPP **30** can be synthesized in two steps, as shown in Scheme 12. Starting with 4-methoxybenzaldehyde **27** and pyrrole **28**, tetra(4-hydroxyphenyl)porphyrin (THPP) **29** was easily obtained, followed by zinc insertion to produce ZnTHPP **30**.

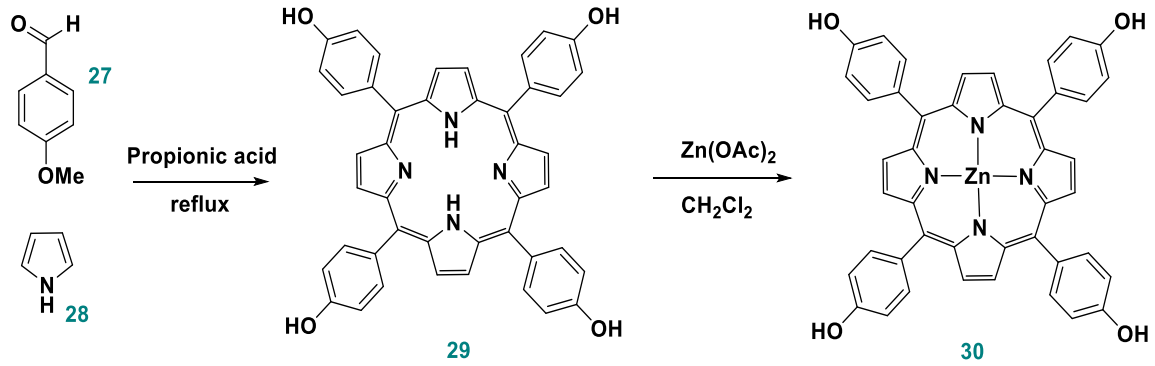

Scheme 12- Synthesis of zinc tetra(4-hydroxyphenyl) porphyrin (ZnTHPP) **30**

2.8.3 Protein interactions and binding affinity quantification between dendrimer and Cyt-c using non-covalent targeting and non-covalent signalling.

The porphyrin-signalling unit Zn-THPP **30** was encapsulated using a similar procedure to that used for the linear chain. An initial series of control experiments was conducted to assess the ability of neutral dendrimers, without functionalized chains, to bind to the protein to establish a baseline for comparison with later experiments. These experiments aimed to determine if adding Cyt-c to ZnTHPP **30** would result in a decrease in the fluorescence or emission of the porphyrin.

It was difficult to carry out the first control with just Zn-THPP **30** due to its low solubility. Despite using a saturated solution, a very weak emission peak was observed, which was not quenched by adding cytochrome-c. This confirms that the porphyrin alone does not bind to the protein independently, as shown in Figure 42 (A).

Figure 42- Control experiments indicated that no binding was detected when using ZnTHPP **30** alone.

In a second control experiment with LC-Tyr **19** or LC-Val **20** dissolved in a saturated Zn-THPP **30** solution, no quenching or binding occurred after the addition of cytochrome-c, as shown in Figure 43 (B). These results clearly indicate that linear chains alone do not bind the protein.

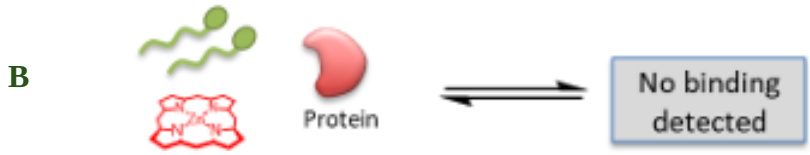

Figure 43- No binding was detected in the control experiments using ZnTHPP **30** and the linear chains.

A final control involved adding cytochrome-c to a solution containing a dendrimer-porphyrin complex (without linear chains), which did not result in any change in the porphyrin emission intensity, indicating no binding for the dendrimer alone, as shown in Figure 44(C).

Figure 44- The mixture system with dendrimer for control experiments also shows no binding was detected.

The next set of experiments would determine whether or not the functionalized dendrimers could bind the protein. Initially a test was done to determine the concentration of Zn-THPP/dendrimer, UV spectroscopy[24]was used, which confirmed a 1:1 stoichiometry. The soret band of the porphyrin was shifted from 412 nm to 425 nm, indicating complexation between Zn and the dendrimer's nitrogens, which confirmed encapsulation within the dendrimer. Following encapsulation and quantification, a series of binding experiments were conducted to determine whether the self-assembled complex could bind to cytochrome c and be detected.

After carrying out the controls, which confirmed that the individual component did not bind the protein, we proceeded to test the binding of the self-assembled protein-binding complex 1. These binding experiments were performed at pH 7.4 by titrating cytochrome c into a solution of the dendrimer complex 1 (Figure 40), which was assembled from all three components in a

1:1:10 ratio of dendrimer **10**, Zn-THPP **30**, and linear chain **19** (1×10^{-6} M for the dendrimer and Zn-THPP, and 1×10^{-5} M for the linear chain). Detection of binding and quantification were measured by monitoring the intensity of the Zn-THPP **30** emission band at 610 nm, which is quenched as cytochrome c binds. With increasing additions of cytochrome c, the emission peak at 610 nm was significantly reduced, confirming the binding of the protein (figure 45).

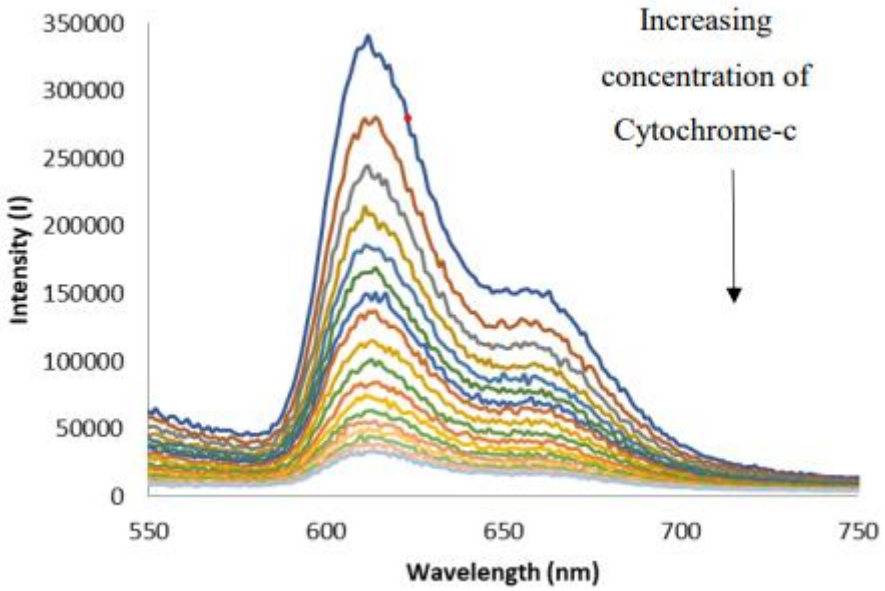

Figure 45- The emission spectra decreased with the addition of each aliquot of 1.0 µM Cyt-c to a solution of the G3.5-OH complex 1 (containing 1.0 µM of dendrimer **10** and Zn-THPP **30**, and 10.0 µM of LC-Tyr **19**).

for LC-Tyr **19** system, a plot of the change in intensity with respect to cytochrome-c concentration was plotted, and the data were fitted to a 1:1 binding model using GraphPad, yielding a dissociation constant (Kd) of 32 nM (Figure 46).

Despite the fact that our self-assembled system does not contain negative charges to interact with cytochrome-c's positively charged surface, it still exhibited comparable binding affinities to other surface-binding ligands. Hamilton, for example, reported Kd values ranging from 120 to 20 nM for porphyrins containing up to eight negative charges,[74] while Wilson observed Kd values between 23 and 2 for metal ligands containing terminal negative charges.[75]

The same experiments, using the same concentrations as in the previous tests, were conducted to examine the binding of a dendrimer complex functionalized with LC-Val **20**, an amino acid generally not involved in protein-protein interactions.[12]

In this case, the porphyrin fluorescence intensity did not change as cytochrome-c was titrated into the dendrimer complex (Figure 46), indicating no binding had occurred. Even with increased cytochrome-c concentration, no decrease in porphyrin intensity was observed. As expected, this result confirms that valine is unfavourable for surface protein binding.

Comparing the binding of these two systems shows that binding occurred only in the system with a suitable binding group—tyrosine. Since the chains are N-terminated, the binding must result from the aromatic ring and the OH groups, either as phenolate or through hydrogen bonding. Additionally, none of the individual components, including the LC-Tyr chain, showed binding on their own. Therefore, the binding was due to the self-assembled complex of dendrimer-OH, LC-Tyr, and ZnTHPP (the probe).

As our system does not possess any negative charges, binding must be a result of other features that combine cooperatively to produce the high binding affinity observed. These include π-π stacking, hydrogen bonding and hydrophobic interactions from the tyrosine linear chain. Based on the titration plots (Figure 46) below, the intensity of fluorescence of the porphyrin in the dendrimer complex functionalized with valine remained unchanged as cytochrome-c was titrated in, indicating that no binding occurred. This result was expected, as valine is not favoured for surface protein binding.

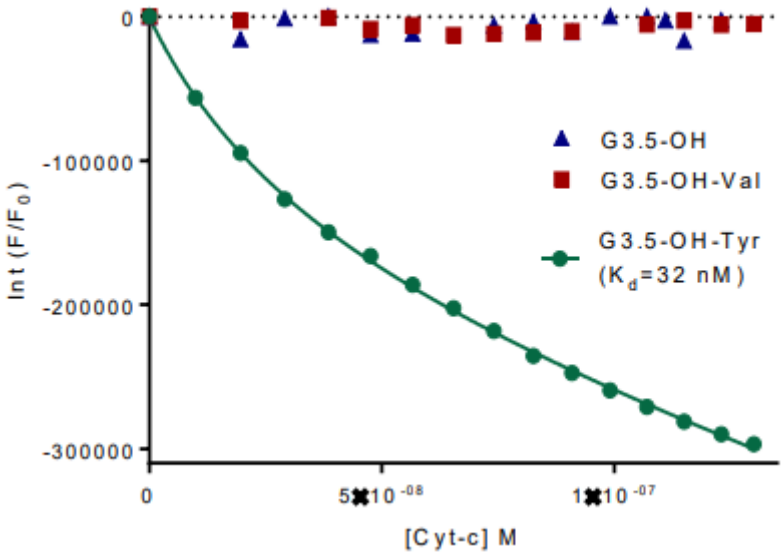

Figure 46- A binding plot showing the emission intensity versus the concentration of Cyt-c titrated with and without chains in the neutral G3.5-OH **30** dendrimer at a 1.0 µM ZnTHPP buffer.

This result provided useful information regarding the arrangement of amino acid chains within dendrimers. According to Figure 47 (top), the head groups extend out of the dendrimer when the dendrimer binds to the protein surface. If the tyrosine and valine head preferred to be within the interior of the dendrimer. If this were true, LC-Tyr **19** and LC-Val **20** would have the same dissociation constant, but it was not the case.

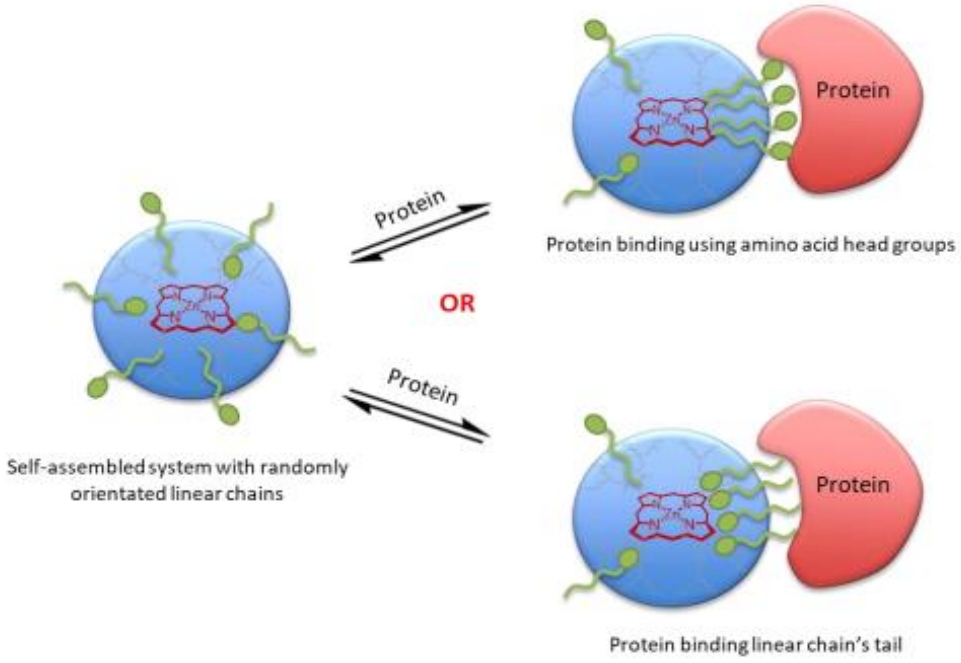

Figure 47- The two possible extreme orientations of linear chains.

2.9 Summary

We have demonstrated a macro-supramolecular methodology that can be used to generate new ligands capable of binding selectively or specifically to the large interfacial binding sites found on the surface of target proteins. Even though covalently functionalized macromolecules have also shown promise in this area, it can be difficult to functionalize their surfaces and impossible to control the relative positions of terminal groups with respect to any 3-dimensional geometric requirements (of functional groups). Several of these problems can be overcome by the use of the supramolecular methodology described herein. This methodology involved encapsulating a targeting/binding group and a sensing group in a dendrimer scaffold. Through a combination of hydrophobic, electrostatic, and hydrogen bond interactions, encapsulation was achieved. Using a 10:1 ratio of linear chains to dendrimer, self-assembly complexes were constructed. Encapsulation resulted in an increase in the linear chain's aqueous solubility, and complexation was confirmed via UV, which indicated a 5 nm bathochromic shift. In order to obtain complexes containing both the targeting groups and the sensing unit, a hydrophobic, insoluble porphyrin (1 equivalent to dendrimer) was added as a quencher for fluorescent measurement of cytochrome-c. Afterward, cytochrome-c was titrated into solutions of these porphyrin/dendrimer complexes containing either valine or tyrosine to assess protein binding. Despite the valine complex not binding, the tyrosine complex bound with a very strong affinity, giving a binding constant of 3.13×10^8 M^{-1} (Kd = 32 nM). In control experiments, no binding was observed between dendrimer/porphyrin complexes without linear chains due to the lack of terminal functionality required for binding to the protein surface. Similar results were obtained with controls using diluted porphyrin, linear chains, or solutions containing both. However, the same neutral dendrimer successfully bound to Cyt-c when the chains were encapsulated, confirming the effectiveness of using non-covalent self-assembly of binding and sensing units within and around an inert dendrimer scaffold.

2.10 Future work

Using the methodology described, it is possible to bind and sense a wide variety of proteins with the same scaffolds and targeting chains by simply modifying the binding and/or sensing components. The flexibility of the system allows for the development of versatile protein recognition systems. The use of dendrimers of different sizes and functional units can be combined with the same binding and/or sensing groups, thereby expanding the range of potential targets. The approach facilitates the development of libraries of dendrimer scaffolds, binding groups, and sensing units that can be systematically combined to selectively bind and sense many different proteins in a variety biological context.

In addition, dendrimers provide unique opportunities due to their branched, multivalent structure, which can host multiple functional groups that can be used for the binding and detection of proteins. These dendritic systems offer increased surface area and the ability to incorporate a variety of sensing units, enabling highly specific protein interactions. Multivalency of dendrimers makes them useful for enhancing their interaction strength and selectivity with target proteins, making them valuable in diagnostics, biosensors, and therapeutic delivery applications.

Future experiments will focus on methods for fixing or trapping linear chains within dendrimers, which may improve the selectivity and recognition capabilities of these systems. It may be possible for dendrimers to achieve better protein binding precision by stabilizing the conformations of their linear chains. Additionally, combining multiple targeting groups within a single dendrimer could allow simultaneous interactions with multiple proteins or multiple sites within the same protein. This multivalent binding could improve specificity and affinity for complex targets.

Further enhancements could be achieved by designing dendrimers or linear chains to contain photochemically reactive groups. Adding photoreactive groups allows specific chemical reactions to be triggered upon exposure to light, such as crosslinking with target proteins or altering dendrimer binding characteristics. The application of photochemical reactions would offer a precise, externally controlled means of modulating dendrimer interactions with proteins, providing new possibilities for proteomic sensing, drug delivery, and controlled release. The combination of structural control, multivalency, and photoresponsiveness of dendrimers promises to make them a powerful tool for protein targeting and therapeutic development.

2.11 Experimental

2.11.1 Instrumentation

UV/Vis spectroscopy

The ultraviolet and visible absorbance of the solution was recorded on GENESYS™ 140/150 Vis/UV-Vis Spectrophotometers.

Infrared spectroscopy (IR)

Infrared spectra were recorded on a Perkin Elmer Paragon 1000 FTIR spectrometer.

NMR Spectroscopy

All NMR samples were prepared using deuterated solvents supplied by Sigma Aldrich. ^{1}H NMR and ^{13}C NMR spectra were recorded using a Brucker AV1400 MHz machine. Chemical shifts are quoted using ppm and referenced to residual solvent signals, coupling constants are quoted in Hertz. The NMR spectra were analysed using Mnova 15.0.1 NMR software.

Mass Spectrometry

For dendrimers, a Bruker reflex III MALDI-ToF mass spectrometer was used. For all other samples, a Waters LCT Premier XE spectrometer, and Electrospray Ionization (ES) was used.

Accurate Mass Spectrometry

A High-Resolution Agilent 6530 Accurate-Mass Q-TQF spectrometer and electrospray ionisation was used.

2.11.2 Synthesis of poly (amidoamine) PAMAM dendrimers:

General procedure for the synthesis of half generation ester terminated PAMAM dendrimers.

Ethylenediamine (EDA) or a complete generation PAMAM dendrimer was initially dissolved in methanol to create a homogeneous solution. Subsequently, methyl acrylate (MA) was added dropwise over a period of 45 minutes into the round-bottom flask containing the EDA or dendrimer solution. This controlled addition was followed by overnight stirring at room temperature to facilitate the reaction between the amine groups of EDA or the dendrimer and the acrylate functionalities. After the reaction was complete, excess solvent and any unreacted methyl acrylate were carefully removed using a rotary evaporator, followed by treatment under ultra-high vacuum to ensure complete removal of volatile components and to obtain the desired product.

General procedure for the synthesis of full generation amine terminated PAMAM dendrimers.

A PAMAM ester-terminated dendrimer was dissolved in methanol, after which ethylenediamine was added dropwise over a 45-minute period while stirring continuously at room temperature. The duration of the reaction varied depending on the generation size of the dendrimer, with larger generations typically requiring a longer time to complete the reaction due to increased steric hindrance and complexity. Once the reaction was deemed complete, excess EDA and methanol were efficiently removed using a rotary evaporator set to 45°C. The resultant product underwent purification by washing with an azeotropic toluene-methanol mixture in a 9:1 ratio, followed by an additional purification step using methanol to ensure the removal of any unreacted materials.

Synthesis of G 0.5 (methyl ester) PAMAM dendrimer 1

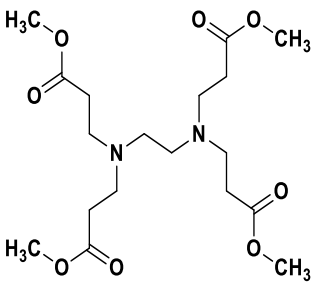

In a 500 mL round bottom flask, ethylenediamine (10 mL, 0.14 mol) was dissolved in 150 mL of methanol to create a homogeneous solution. Subsequently, an excess amount of methyl

acrylate (26.4 g, 0.60 mol) was added dropwise over a period of 45 minutes, ensuring consistent mixing throughout the addition. Following this, the reaction mixture was stirred overnight at room temperature to facilitate the reaction between the amine and the acrylate. After that, the remaining methyl acrylate and methanol were removed under reduced pressure (in vacuo) to isolate the product. The resultant G0.5 **1** was obtained as a light-yellow oil, yielding 55 g (97%)

FTIR (νmax/cm^{-1}), 2955 (O$\underline{CH_3}$, stretch), 1737 (C=O, ester), 1433 (CH_2, bend), 1165 (C-O), 1036 (C-N); ^{1}H NMR (400 MHz, MeOD) δ 3.68 (12H, s, O$\underline{CH_3}$), 2.79 (8H, t, *J*= 7.0 Hz, NC$\underline{H_2}CH_2C$=O), 2.54 (4H, s, NC$\underline{H_2}C\underline{H_2}$N), 2.49 (8H, t, *J*= 7.0 Hz, OC=OC$\underline{H_2}$); ^{13}C NMR (100 MHz, MeOD) δ 173.2 (C=O), 51.6 (-CH_2 Core), 50.7 (-OCH_3), 49.5, 31.7 (CH_2); Mass spec (ES) 405.2 (MH^+), ES-MS C_{18} H_{32} N_2 O_8 = 406 (calculated).

Synthesis of generation 1.0 of PAMAM dendrimer 2

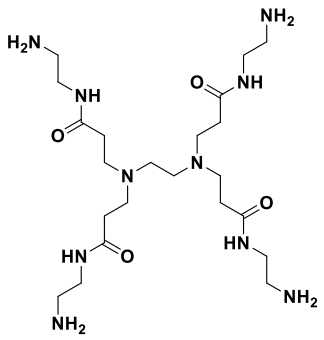

A PAMAM G 0.5 (50 g, 0.123 mol) was dissolved in 150 mL of methanol, then EDA (148.4 g, 2.4 mol) was added dropwise over 45 minutes. The mixture was allowed to react at room temperature for 3 days. Excess solvent and EDA were removed under reduced pressure (in vacuo). The remaining traces of ethylenediamine were purified azeotropically four times using a 2.0 L mixture of 9:1 toluene and methanol, then washed again with 100 mL of methanol. The purification process was repeated several times until the EDA was completely removed, and the product was dried under reduced pressure. The final product, generation 1.0 of PAMAM dendrimer **2**, was obtained as a viscous light-yellow oil (60 g, 97%).

FTIR (νmax/cm^{-1}), 3278 (N-H, stretch), 2931 (C-H, stretch),1642 (C=O, amide), 1578 (N-H, bend), 1473, 1153 (C-N, bend); ^{1}H NMR (400 MHz, MeOD) δ 3.28 (8H, t, *J*= 6.5 Hz, CONHC$\underline{H_2}$), 2.79-2.74 (16H, m, CH_2NC$\underline{H_2}$+$CH_2C\underline{H_2}NH_2$), 2.56 (4H, s, CH_2N), 2.39 (8H, t, *J*= 6.5 Hz, C$\underline{H_2}$CONH); ^{13}C NMR (100 MHz, MeOD) δ 173.6 (C=O), 51.0 (-CH_2 Core), 49.9 ,41.4, 40.6, 33.3 (CH_2); Mass spec (ES), 517.4 (MH^+), 539.4 (MNa^+), ES-MS C_{22} H_{48} N_{10} O_4 = 516 (calculated).

Synthesis of G 1.5 (methyl ester) PAMAM dendrimer 3

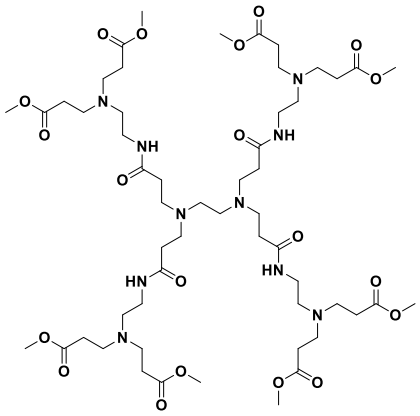

In a 500 mL round-bottom flask, PAMAM G1.0 (40 g, 0.077 mol) was dissolved in 120 mL of methanol. Methyl acrylate (133 g, 1.55 mol) was then added dropwise over 45 minutes. The mixture was allowed to react at room temperature for 72 hours. After the reaction was complete, the residual methyl acrylate and methanol were removed under reduced pressure (vacuum). The final product **3** was obtained as a sticky yellow oil (72.31 g, 85%).

FTIR (νmax/cm^{-1}), 3300 (N-H, stretch), 2950 (C-H, stretch), 2830, 1738 (C=O, ester), 1641 (C=O, amide), 1536 (N-H), 1436 (CH2, bend), 1155 (C-N, bend); ^{1}H NMR (400 MHz, MeOD) δ 3.69 (24H, s, OC$\underline{H_3}$), 3.27 (8H, t**,** *J*= 6.5 Hz, NHC$\underline{H_2}$), 2.79 (24H, t, *J*= 7.0 Hz, NC$\underline{H_2}$), 2.58 (12H, m**,** C$\underline{H_2}$N), 2.48 (16H, t, *J*= 7.0 Hz, C$\underline{H_2}$CO), 2.41 (8H, t, *J*= 7.0 Hz, C$\underline{H_2}$CO)**;** ^{13}C NMR (100 MHz, MeOD) δ 173.33, 172.5, (C=O), 52.39 (-CH_2 Core), 50.8 (CH_3), 49.8 49.0, 47.5, 37.3, 33.1, 32.2 (CH_2); Mass spec (ES), 1205.7 (MH^+), ES-MS $C_{54}H_{96}N_{10}O_{20}$ = 1205 (calculated).

Synthesis of generation 2.0 of PAMAM dendrimer 4

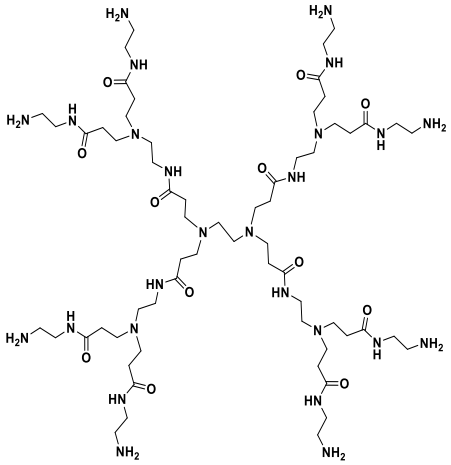

PAMAM G1.5 (50 g, 41 mmol) was dissolved in 150 mL of methanol and stirred. Ethylenediamine (99.7 g, 1.65 mol) was added dropwise over 45 minutes. The mixture was allowed to react at room temperature for 6 days. After the reaction was complete, an azeotropic mixture of 9:1 methanol was used to wash the product several times and remove the unreacted EDA. The final product of generation 2.0 of PAMAM dendrimer **4** was obtained as a sticky yellow oil (55.7 g, 94%).

FTIR (νmax/cm^{-1}), 3284 (N-H, stretch), 2933 (C-H, stretch), 1642 (C=O, amide), 1546 (N-H) ; ^{1}H NMR (400 MHz, MeOD) δ 3.27 (24H, t, *J*= 6.0 Hz, NHCH_2), 2.82 (24H, t, *J*= 7.0 Hz, NCH_2), 2.74 (16H, t, *J*= 6.0 Hz, C$H_2$$NH_2$), 2.60 (12H, t, , *J*= 7.0 Hz, CH_2N), 2.39 (24H, t, *J*= 6.5 Hz, CH_2CO); ^{13}C NMR (100 MHz, MeOD) δ 173.7, 173.3 (C=O), 52.1, 50.9, 49.7, 41.6, 37.2, 33.4 (CH_2); Mass spec MALDI-TOF, 1430 (MH^+), ES-MS C_{62} H_{128} N_{26} O_{12} = 1429 (calculated).

Synthesis of G 2.5 (methyl ester) PAMAM dendrimer 5

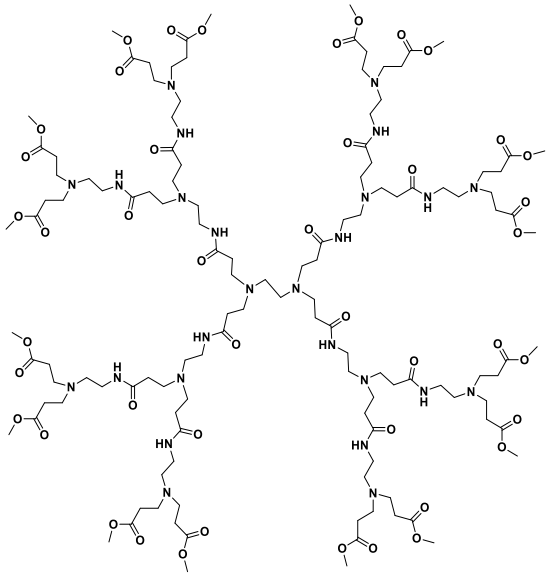

In a 500 mL round-bottom flask, PAMAM G2.0 (40.19 g, 82 mmol) was dissolved in 150 mL of methanol. Methyl acrylate (96.4 g, 1.12 mol) was then added dropwise over 45 minutes. The reaction mixture was stirred at room temperature for 5 days. Methanol and methyl acrylate were removed using a rotary evaporator, and the product was dried under ultra-high vacuum. A sticky yellow oil G 2.5 (methyl ester) PAMAM dendrimer **5** (58.20 g, 74%) was obtained.

FTIR (νmax/cm^{-1}), 3290 (N-H stretch), 2951 (C-H stretch), 1738 (C=O, ester), 1645 (C=O, amide), 1561 (N-H, bend), 1433 (CH_2); ^{1}H NMR (400 MHz, MeOD) δ 3.69 (48H, s,

OC<u>H3</u>), 3.28 (24H, m, NHC<u>H</u>$_2$), 2.89–2.76 (56H, m, 2(NC<u>H</u>$_2$), 2.58 (12H, t, *J*= 7.0 Hz, NC<u>H</u>$_2$), 2.49 (32H, t, *J* = 6.5 Hz, C<u>H</u>$_2$CO), 2.40 (16H, t, *J*= 7.0 Hz, C<u>H</u>$_2$CN); ^{13}C NMR (100 MHz, MeOD) δ 173.0 (C=O), 173.3, 173.2 (C=O), 171.5, 52.4, 52.1 , 50.8 (CH_3), 50.6, 49.9, 49.7, 37.2, 37.1, 33.3, 33.2, 32.2 (CH_2); Mass spec MALDI-TOF, 2806 (MH^+), ES-MS C_{126} H_{224} N_{26} O_{44} = 2807 (calculated).

Synthesis of generation 3.0 of PAMAM dendrimer 6

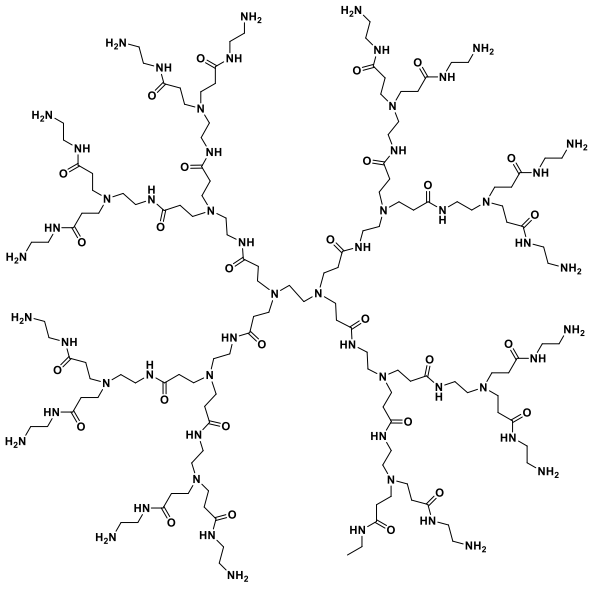

Ethylenediamine (44.96 g, 0.74 mol) was added to a stirred solution of the methyl ester of PAMAM G2.5 dendrimer (35 g, 0.012 mol) in methanol (150 mL). The reaction solution was left to react at room temperature for 10 days. To remove EDA from the crude product, 2.0 L of an azeotropic solution of 9:1 toluene: methanol was used. By repeating the purification after washing with methanol (100 mL), EDA was completely eliminated. The product was dried to yield generation 3.0 of PAMAM dendrimer **6** (38.25 g, 97%) as a sticky dark yellow oil.

FTIR (νmax/cm^{-1}), 3297 (N-H, stretch), 2993 (C-H stretch), 1639 (C=O, amide), 1561 (N-H); ^{1}H NMR (400 MHz, MeOD) δ 3.27 (56H, t, *J*= 7.0 Hz, NHC<u>H</u>$_2$), 2.81 (56H, t, *J*= 6.0 Hz, C<u>H</u>$_2$N), 2.74 (32H, t, *J*= 7.0 Hz, C<u>H</u>$_2$N), 2.60 (28H, t, *J*= 6.0 Hz, NC<u>H</u>$_2$), 2.39 (56H, t, *J*= 7.0 Hz, C<u>H</u>$_2$CO); ^{13}C NMR (100 MHz, MeOD) δ 173.7 ,173.3 (C=O), 52.1, 49.7, 48. 4 , 41.7 , 40.6 , 37.2, 33.4 (CH_2); Mass spec MALDI-TOF, 3257(MH^+), ES-MS C_{142} H_{288} N_{58} O_{28}= 3256 (calculated).

Synthesis of G 3.5 (methyl ester) PAMAM dendrimer 7

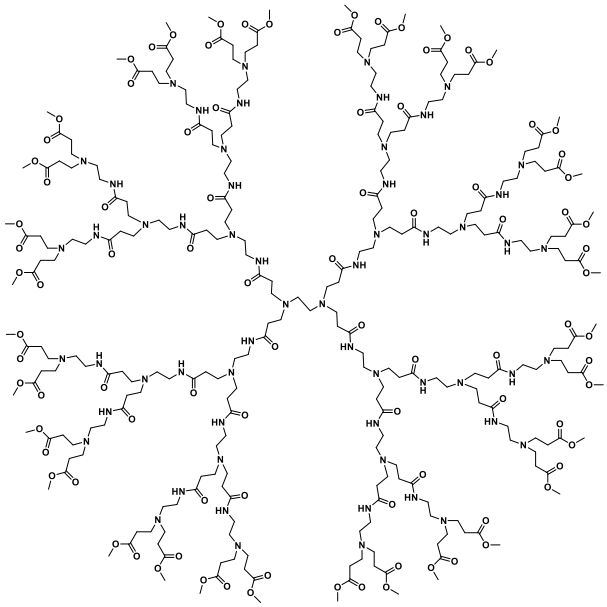

PAMAM dendrimers (35 g, 0.01 mol) were dissolved in 150 mL of methanol, followed by the dropwise addition of methyl acrylate (55.5 g, 0.64 mol). The solution was stirred at room temperature for 6 days. Methyl acrylate and the excess solvent were removed under reduced pressure. The final product of G 3.5 (methyl ester) PAMAM dendrimer **7** was obtained as a sticky dark yellow oil (49.7 g, 82%).

FTIR ($\nu max/cm^{-1}$), 3298 (N-H stretch), 2953 (C-H stretch), 2832, 1738 (C=O, ester), 1642 (C=O, amide), 1550 (N-H bend), 1443 (CH_2); ^{1}H NMR (400 MHz, MeOD), 3.69 (96H,s, OC$\underline{H}_3$), 3.26 (24H, t, *J*= 6.0 Hz, NHC$\underline{H}_2$), 2.90 (32H, t, *J*= 6.0 Hz, NC$\underline{H}_2$), 2.81 (65H,t, *J*= 7.0 Hz, NC$\underline{H}_2$) , 2.63 (64H, t, *J*= 7.0 Hz, NC$\underline{H}_2$),2,54 (32H,t, *J*= 6.0 Hz,C$\underline{H}_2$N), 2.47 (64H, t, *J*= 6.0 Hz, C$\underline{H}_2$CO), 2.36 (65H, t, *J*= 7.0 Hz, C$\underline{H}_2$CO); ^{13}C NMR (100 MHz, MeOD) δ 173.5, 173.1 (C=O), 54.9, 54.5, 53.5, 51.7 (CH_3),38.5, 38.3 , 34.5, 32.0(CH_2); Mass spec MALDI-TOF, 6014 (MH^+), ES-MS $C_{270}\,H_{480}\,N_{58}\,O_{92}$ = 6014 (calculated).

2.11.3 Synthesis of neutral PAMAM dendrimers

A general method for the synthesis of neutral OH terminated dendrimers

A PAMAM half-generation dendrimer was initially dissolved in dimethyl sulfoxide (DMSO) to create a uniform solution. Following this, potassium carbonate and ethanolamine were added dropwise to the mixture. The resulting solution was then stirred and refluxed at 50 °C for three days under a nitrogen atmosphere to facilitate the reaction. After the reflux period, purification of the crude product commenced with filtration to remove any solid residues. The filtrate was subsequently transferred to a large conical flask, and 600 mL of acetone was introduced, leading to the formation of a thick oil or paste at the bottom of the flask. The upper layer of acetone was carefully decanted to eliminate unreacted materials. To further dissolve the product, 5 mL of distilled water was added, and the precipitation procedure was repeated with an additional 300 mL of acetone. Afterward, the product was dissolved in methanol and transferred to a round-bottom flask, where traces of solvent were removed under reduced pressure. Finally, the resulting product was dried, yielding the PAMAM-OH dendrimer.

Synthesis of G 1.5 (neutral) PAMAM dendrimer 8

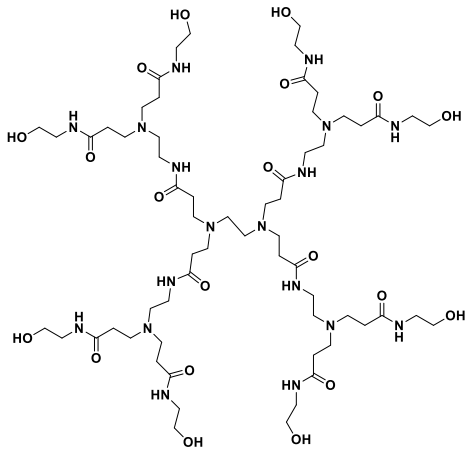

A PAMAM G1.5 dendrimer (22.3 g, 0.018 mol) with 8 terminal methyl ester groups was dissolved in 10 mL of DMSO. Potassium carbonate (25.5 g, 0.18 mol) and ethanolamine (11.08 g, 0.18 mol) were then added. The mixture was stirred and refluxed at 50°C for 72 hours. Purification was performed as previously described. The product was dried to yield G1.5-OH **8** (18.01 g, 69%) as a pale yellow/cream paste.

FTIR (νmax/cm^{-1}), 3295 (N-H stretch), 3096 , 2947, 2841, 1642 (C=O amide), 1560 (N-H), 1445 (CH_2); ^{1}H NMR (400 MHz, D_2O) δ 3.57 (16H, t, *J*= 5.5 Hz, $CH_2C\underline{H_2}OH$), 3.28–3.23 (24H, m, $NHC\underline{H_2}CH_2$), 2.79– 2.70 (24H, m, $N(C\underline{H_2}CH_2)$), 2.56 (12H, t, *J*= 6.5 Hz, $CH_2C\underline{H_2}N$),

2.37 (24H, t, *J*= 6.0 Hz, $CH_2C\underline{H_2}CO$); ^{13}C NMR (100 MHz, D_2O) δ 174.6, 174.1 (C=O), 61.0, 54.7, 53.5 (-CH_2 Core), 49.9 , 43.5 , 38.3, 34.5 (CH_2); Mass spec (ES), 1438 (MH+), ES-MS $C_{62}H_{120}N_{18}O_{20}$ = 1437 (calculated).

Synthesis of G 2.5 (neutral) PAMAM dendrimer 9

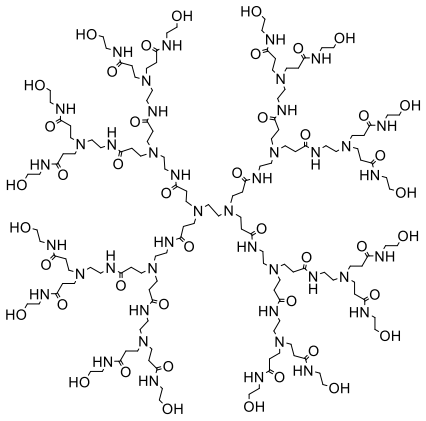

A PAMAM G2.5 dendrimer (17.6 g, 6.3 mmol) with 16 terminal methyl ester groups was dissolved in 8 mL of DMSO. Potassium carbonate (17.3 g, 0.12 mol) and ethanolamine (7.66 g, 0.12 mol) were then added. The mixture was stirred and refluxed at 50°C for 3 days. Purification was performed as previously described. The product was dried to yield G2.5-OH **9** (18.36 g, 89%) as an orange sticky oil.

FTIR (νmax/cm^{-1}), 3393 (N-H stretch), 2955, 1643 (C=O amide), 1564 (N-H), 1445(CH_2); ^1H NMR (400 MHz, D_2O) δ 3.57 (32H, t, *J*= 5.5 Hz, $CH_2C\underline{H_2}OH$), 3.27–3.21 (m, 56H, $NHC\underline{H_2}CH_2$), 2.76 (56H, t, *J*= 7.0 Hz, $N(C\underline{H_2}CH_2)$), 2.56 (28H, t, *J*= 7.0 Hz, $CH_2C\underline{H_2}N$), 2.37 (56H, t, *J*= 7.0 Hz, $CH_2C\underline{H_2}CO$); ^{13}C NMR (100 MHz, D_2O) δ 175.0, 174.8 (C=O), 61.3 , 54.7 ,53.5 (-CH_2 Core), 50.1, 43.0 , 38.3 , 34.5 (CH_2); Mass spec MALDI-TOF, 3272 (MH^+), ES-MS $C_{142}H_{272}N_{42}O_{44}$ = 3271 (calculated).

Synthesis of G 3.5 (neutral) PAMAM dendrimer 10

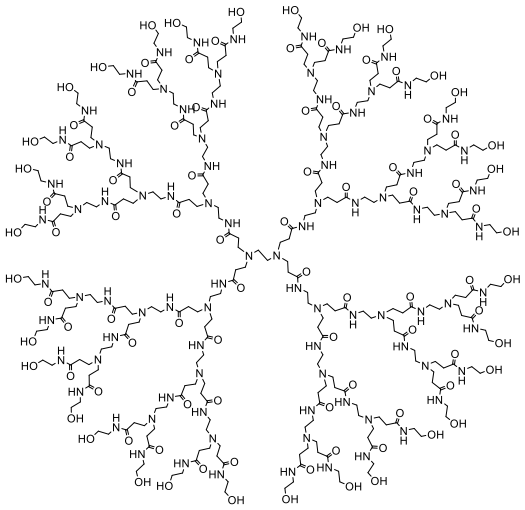

A PAMAM G3.5 dendrimer (15.04 g, 2.5 mmol) with 32 terminal methyl ester groups was dissolved in 8 mL of DMSO. Potassium carbonate (13.8 g, 0.10 mol) and ethanolamine (6.11 g, 0.10 mol) were then added. The mixture was stirred and refluxed at 50°C for 3 days. Purification was performed as described in the general procedure. The product was dried to yield G3.5-OH **10** (14.42 g, 94%) as a dark orange sticky oil.

FTIR (νmax/cm^{-1}) , 3265 (N-H), 3072, 2923, 2830, 1643 (C=O amide), 1551 (N-H), 1438 (CH_2); ^{1}H NMR (400 MHz, D_2O) δ 3.57 (60H, t, *J*= 5.5 Hz, $CH_2C\underline{H_2}OH$), 3.26 – 3.20 (120H, m, $NHC\underline{H_2}CH_2$), 2.77 – 2.71 (120H, m, $N(C\underline{H_2}CH_2)$), 2.55 (60H, t, *J*= 7.0 Hz, $CH_2C\underline{H_2}N$), 2.38 – 2.32 (120H, m, $CH_2C\underline{H_2}N$); ^{13}C NMR (100 MHz, D_2O) δ 175.3, 175.0 (C=O), 61.5, 60.0, 52.0 (-CH_2 Core), 49.3, 48.6, 42.7, 37.1 ,34.0 (CH_2) ; Mass spec MALDI-TOF, 6941 (MH^+), ES-MS $C_{302}H_{576}N_{90}O_{92}$ = 6940 (calculated).

2.11.4 Synthesis of Linear Chain

Cbz-protected amide chain 13

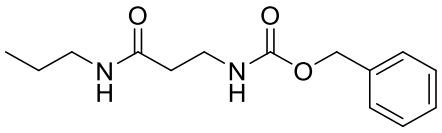

In 500 ml round bottom flask, n-propylamine **(**1.30 g, 0.022 mol), N-Cbz-β-alanine (5.00 g, 0.022 mol) and DMAP (5.38 g, 0.044 mol) were dissolved in DCM (150 mL). EDC.HCl (4.22 g, 0.022 mol) and triethylamine (6.68 g, 0.066 mol) was added to the mixture. The mixture was allowed to react under nitrogen for 24 H. The crude product was washed with brine (100 mL x 3), and 2M of HCl, then the aqueous layers were backwashed with DCM. The organic layers were collected and dried with Mg_2SO_4. The solvent was concentrated at reduced pressure and dried under a high vacuum to give Cbz-protected amide chain **13** as a white powder in (4.7 g, 81%) yield.

FTIR (νmax/cm^{-1}) 3324, 3293 (N-H stretch), 3078 (C-H aromatic) , 2959 (C-H), 1684, 1644 (C=O), 1528 (N-H- bend) 1227 (C-N), 1028 (C-O) ; ^{1}H NMR (400 MHz, $CDCl_3$) δ 7.40 – 7.20 (5H, m, $\underline{CH}_{Ar}$), 6.23 (1H, s CO$\underline{NH}CH_2$), 5.75 (1H, s CO$\underline{NH}$CH2), 5.06 (2H, s, $\underline{CH2}_{Ar}$), 3.44 (2H, q, NH$\underline{CH2}$), 3.16 (2H, q, NH$\underline{CH_2}$), 2.38 (2H, t, *J*= 7.0 Hz, NHCH$_2\underline{CH_2}$), 1.58 (2H, m, $\underline{CH_2}CH_3$), 0.88 (3H, t, *J*= 7.5 Hz, $CH_2\underline{CH_3}$); ^{13}C NMR (100 MHz, $CDCl_3$) δ 171.2, 156.6 (C=O), 136.5-127.9 (*C*-Ar), 66.5, 41.2, 37.2, 36.0, 22.7 (CH_2), 11.3 (CH_3); Mass spec (ES) 265 (MH^+), ESI-MS $C_{14}H_{20}N_2O_3$ = 264.15 (calculated).

Deprotected amide chain 14

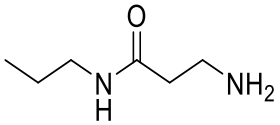

In a 500 mL round-bottom flask, 25 mL of methanol was used to dissolve Cbz-protected chain (4 g, 0.015 mol). A catalytic amount of Pd/C (5% on carbon, 0.4 g) was added to the solution under nitrogen. The reaction mixture was stirred, and an H_2 balloon was placed on top of the flask. After completion, the mixture was filtered over Celite, and the filtrate was concentrated under reduced pressure. The deprotected amide chain **14** was obtained as a viscous yellow oil (1.65 g, 84% yield).

FTIR (νmax/cm^{-1}) 2978 (N-H), 1645 (C=O), 1558 (N-H); ^{1}H NMR (400 MHz, $CDCl_3$) δ 3.19 (2H, q, $CH_2\underline{CH_2}NH$), 3.01 (2H, t, *J*= 6.0 Hz, $CH_2\underline{CH_2}NH_2$), 2.34 (2H, t, *J*= 6.0 Hz, $\underline{CH_2}CH_2NH_2$), 1.50 *(*2H, m, $CH_3\underline{CH_2}$), 0.91 (3H, t, *J*= 7.0 Hz, $CH_2\underline{CH_3}$)*;* ^{13}C NMR (100 MHz, $CDCl_3$) δ 172.19 (C=O), 50.28, 41.07, 37.94, 37.79, 22.73(CH_2), 11.40 (CH_3); Mass spec (ES) 131 (MH^+), ES-MS $C_6H_{14}N_2O$ = 130 (calculated).

Cbz-protected di-amide chain 15

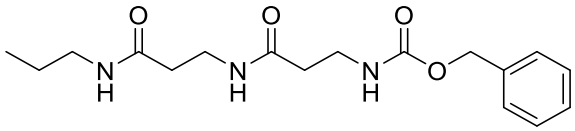

Cbz-deprotected chain (4.26 g, 0.032 mol), N-Cbz-β-alanine (6.69 g, 0.032 mol), and DMAP (7.33 g, 0.06 mol) were dissolved in 150 mL of THF. EDC·HCl (5.73 g, 0.032 mol) and triethylamine (9.19 g, 0.09 mol) were added to the mixture, which was then stirred under nitrogen for 24 hours. After work-up, the Cbz-protected di-amide chain **15** was obtained as a white solid (7.11 g, 66% yield).

FTIR (νmax/cm^{-1}) 3324, 3293 (N-H stretch), 3005 (C-H aromatic), 2911 (C-H), 1680, 1629(C=O), 1528 (N-H- bend) 1227 (C-N); ^{1}H NMR (400 MHz, $CDCl_3$) δ 7.36 (5H, m, $\underline{CH}_{Ar}$), 5.11 (2H, s, $\underline{CH_2}_{Ar}$), 3.49 (4H, m, $NH\underline{CH_2}$), 3.21 (2H, q, *J*= 6.8 Hz, $NH\underline{CH_2}$) 2.40 (4H, m, 2($NHCH_2\underline{CH_2}$),1.54 (2H, m, $\underline{CH_2}CH_3$), 0.93 (3H, t, *J*= 7.5 Hz, $CH_2\underline{CH_3}$); ^{13}C NMR (100 MHz, $CDCl_3$) δ 171.4,171.3, 156.4 (C=O), 136.5-128.0 (*C*-Ar), 66.6, 41.3, 37.1, 36.0, 35.4, 35.4, 22.7 (CH_2), 11.36 (CH_3); Mass spec (ES) 336.16 (MH^+), ESI-MS $C_{17}H_{25}N_3O_6$= 335 (calculated).

Deprotected di-amide chain 16

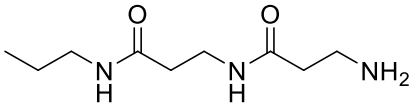

In a 500 mL round-bottom flask, 25 mL of methanol was used to dissolve the Cbz-protected diamide chain (5.50 g, 0.016 mol). A catalytic amount of Pd/C (5% on carbon, 0.5 g) was added to the solution under nitrogen. After work-up, the di-amide chain **16** was isolated as a viscous yellow oil in a yield of 3.1 g (96%).

FTIR (νmax/cm-1) 2938 (N-H stretch), 1645 (C=O, stretch), 1555 (N-H bend), 1178 and 1130 (C-N); ^{1}H NMR (400 MHz, $CDCl_3$) δ 3.56 (2H, q, *J*= 6.4 Hz, $CH_2\underline{CH_2}NH$), 3.22 (2H, q, *J*= 6.5 Hz, $CH_2\underline{CH_2}NH$), 3.01 (2H, t, *J*= 6.8 Hz, $CH_2\underline{CH_2}NH_2$), 2.43 (2H, t, *J*= 6.0 Hz,

$\underline{CH_2}CH_2NH$), 2.32 (2H, t, *J*= 6.0 Hz, $\underline{CH_2}CH_2NH$), 1.51 (2H, m, $\underline{CH_2}CH_3$), 0.94 (3H, t, *J*= 7.0 Hz, $CH_2\underline{CH_3}$); ^{13}C NMR (100 MHz, $CDCl_3$) δ 172.9, 171 (C=O), 50.8, 41.2, 38.8, 38.2, 36.0, 35.4, 22.8 (CH_2), 11.3 (CH_3); Mass spec (ES) 202 (MH^+), ES-MS $C_9H_{19}N_3O_2$ = 201 (calculated).

Cbz-protected tyrosine chain 17

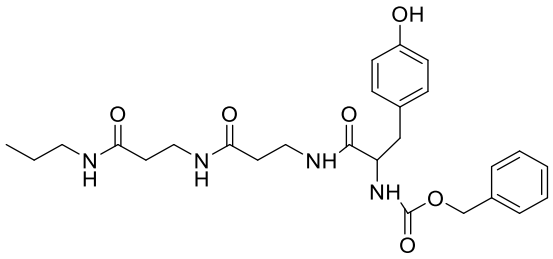

The deprotected diamide chain (3.26 g, 0.016 mol), Cbz-L-tyrosine (5.04 g, 0.016 mol), and DMAP (3.90 g, 0.032 mol) were dissolved in 150 mL of THF in a 500 mL round-bottom flask. EDC·HCl (3.06 g, 0.016 mol) and triethylamine (4.85 g, 0.048 mol) were added to the mixture. The mixture was stirred under nitrogen for 24 hours. After work-up, the Cbz-protected tyrosine chain **17** was obtained as a light-yellow powder in a yield of 5.19 g (66%).

FTIR (νmax/cm-1) , 3288 (N-H, stretch), 3100 (C-H aromatic), 2956 and 2877 (C-H), 1689 and 1638 (C=O stretch), 1542,1513 (N-H bend), 1365 (O-H phenol), 1258 (C-N) ; ^{1}H NMR (400 MHz; MeOD) δ 7.31 (5H, m, $\underline{CH}$Ar), 7.05 (2H, d, *J*= 8.4 Hz, *m*-C$\underline{H}_{Ar(Tyr)}$), 6.71 (2H, d, *J*= 8.5 Hz, *o*-C$\underline{H}_{Ar(Tyr)}$), 5.04 (2H, m, $\underline{CH2}$Ar), 4.28 – 4.21 (1H, m, $\underline{CH}$NH), 3.45 – 3.08 (3x 2H, m , NH$\underline{CH2}$), 2.98 – 2.73 (2H, m, diastereotopic C$\underline{H_2}$), 2.38 (4H, m, NHC$H_2\underline{CH_2}$),1.50 (2H, m, $\underline{CH_2}CH_3$), 0.91 (3H, *t*, *J*= 7.5 Hz, CH2$\underline{CH}$3); ^{13}C NMR (100 MHz, MeOD) δ 172.9, 172.6, 172.3, (C=O $_{Lc}$), 156.40, 156.20 (C=O_{CBZ}), (C-OH), 129.94- 106.83(*C*-Ar), 66.1-22.1(CH_2), 10.3(CH_3); Mass spec (ES) 499.25 (MH^+), ES-MS $C_{26}H_{34}N_4O_6$ = 498.25 (calculated).

Tyrosine linear chain - LC-Tyr 19

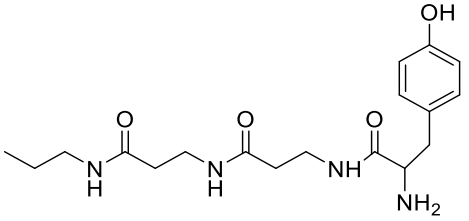

The tyrosine chain was synthesized using the same method described for the Cbz-deprotected chain, using the following amounts: Cbz-protected tyrosine chain (3.6 g, 7.2 mmol) and Pd/C

(5% on carbon, 0.3 g). After workup, the final tyrosine-functionalized linear chain **19** was obtained as a light-yellow powder in a yield of 1.9 g (73%).

FTIR (νmax/cm^{-1}) , 3288 and 3086 (N-H), 2936 (C-H), 1634 (C=O), 1536 and 1512(N-H), 1185 and 1138 (C-N); ^{1}H NMR (400 MHz; MeOD) 7.03 (2H, d, *J*= 8.5 Hz, *m*-CHAr), 6.73 (2H, d, *J*= 8.5 Hz, *o*-CHAr), 3.47 (1H, t, *J*= 7.0 Hz, $CH_2\underline{CH}NH_2$), 3.40 (4H, m,$CH_2\underline{CH_2}NH$), 3.14 (2H, t, *J*= 7.0 Hz, $CH_2\underline{CH_2}NH$), 2.90 (1H, dd, diastereotopic CH_2), 2.74 (1H, dd, diastereotopic CH_2), 2.38 (2H, t, *J*= 6.8 Hz, $NHCH_2\underline{CH_2}$), 2.31 (2H, q, $NHCH_2\underline{CH_2}$), 1.52 (2H, m, $CH_3\underline{CH_2}$), 0.93 (3H, *t*, *J*= 7.5 Hz, $CH_2\underline{CH_3}$);^{13}C NMR (100 MHz; MeOD) δ 175.1, 172.2 ($C=O_{Lc}$), 155.9 (C-OH), 130.0- 114.9 (*C*-Ar), 56.4- 22.1 (CH_2), 10.3(CH_3); Mass spec (ES) 365 (MH^+). HRMS (ES), Calculated for $C_9H_{19}N_3O_2$ [MH^+]: 365.2183, found 365.2189.

Cbz-protected valine chain 18

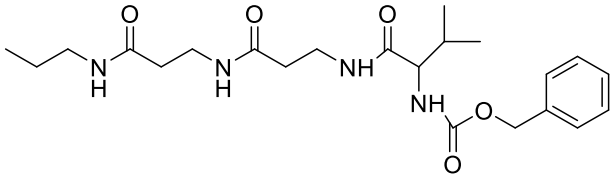

The deprotected di-amide chain (3.12 g, 0.015 mol), N-Cbz-L-Valine (3.7 g, 0.015 mol), and DMAP (3.66 g, 0.03 mol) were dissolved in THF (150 mL). EDC.HCl (2.87 g, 0.015 mol) and triethylamine (4.55 g, 0.045 mol) were added to the mixture. The mixture was stirred under nitrogen for 24 hours. After workup, the Cbz-protected valine chain **18** was obtained as a white powder in a yield of 3.22 g (52%).

FTIR (νmax/cm^{-1}) , 3396, 3287 (N-H, stretch), 2960 and 2866 (C-H), 1687 and 1638 (C=O stretch), 1535 (N-H bend), 1258 (C-N)*;* ^{1}H NMR (400 MHz; MeOD) 7.38 (5H, m, $C\underline{H}_{Ar(Val)}$), 5.11 (2H, s, $C\underline{H_2}Ar$), 3.89 (1H, m, $C\underline{H}NH$), 3.44 (4H, m, $CH_2C\underline{H_2}NH$*)*, 3.14 *(*2H, m, $CH_2\underline{CH_2}NH$*)*, 2.39 (4H, m, $NHCH_2C\underline{H_2}$), 1.52 (1H, sept ,$C\underline{H}(CH_3)_2$), 1.38 (2H, m, $CH_3C\underline{H_2}$),1-0.95 (6H, d, $CH(C\underline{H_3})_2$), 0.93 (3H, t, *J*= 7.0 Hz, $CH_2C\underline{H_3}$)*;*^{13}C NMR (100 MHz, MeOD) δ176.1, 176.0, 175.1 ($C=O_{Lc}$), 152.8($C=O_{Cbz}$), 128.0- 127.4(*C*-Ar), 66.3- 22.1(CH_2), 18.3, 10.3(CH_3); Mass spec (ES), 435.26 (MH^+), ES-MS $C_{22}H_{34}N_4O_5$ = 434.25 (calculated).

Valine linear chain - LC-Val 20

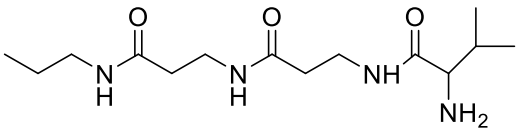

Cbz-protected valine chain (3.2 g, 7.3 mmol) was dissolved in 25 mL of methanol, and Pd/C (5% on carbon, 0.3 g) was added. After workup, the final valine-functionalized linear chain **20** was obtained as a light-yellow powder in a yield of 1.67 g (76%).

FTIR (νmax/cm^{-1}), 2940 (N-H stretch), 1657 (C=O stretch), 1566 (N-H bend), 1280 and 1130 (C-N);^{1}H NMR (400 MHz, MeOD) δ3.49 (1H, m, CH), 3.44 (2H, t, *J*= 7.5 Hz, $CH_2\underline{CH_2}NH$), 3.15 (2H, t, $CH_2\underline{CH_2}NH$), 2.40 (4H, m, $NHCH_2C\underline{H_2}$), 2.01 (1H, sept ,$C\underline{H}(CH_3)_2$), 1.55 (2H, m, $CH_3C\underline{H_2}$), 1-01,0.99 ***(***6H, d, $CH(C\underline{H_3})_2$), 0.94 (3H, t, *J*= 7.0 Hz, $CH_2C\underline{H_3}$);^{13}C NMR (100 MHz, MeOD) 172.40, 172.21, 172.16 ($C=O_{Lc}$), 59.54- 17.96 (CH2)**,** 16.58, 10.35 (CH3)*;* Mass spec (ES) 301 (MH^+). HRMS (ES), Calculated for $C_{14}H_{28}N_4O_3$ [MH^+]: 301.2234, found 301.2248.

Chapter 3

Covalent and Non-Covalent Functionalization of Graphene Oxide: A Dynamic Approach to Protein Binding Studies.

3.0 Introduction to Graphene Oxide (GO)

Graphene has been theoretically studied for decades due to its fundamental role as the building block of graphite and carbon nanotubes. [76],[77] However, isolating a single layer remained a significant challenge. In 2004, Geim and Novoselov successfully isolated monolayer graphene through mechanical exfoliation using adhesive tape, marking a major breakthrough in materials science. Their pioneering work earned them the Nobel Prize in Physics in 2010, significantly advancing research on graphene and its derivatives. [78]

Graphene oxide (GO) is an intermediate product in the synthesis of graphene from graphite. It consists of a single carbon layer arranged in a hexagonal lattice, with oxygen-containing functional groups—hydroxyl, epoxide, carbonyl, and carboxyl—distributed across its surface. [79], [80] These functional groups render GO hydrophilic, allowing it to disperse in water and other polar solvents, a key property distinguishing it from pure graphene. Additionally, the presence of oxygen functionalities enables tunable chemical properties, making GO highly adaptable for various applications. Its large surface area further enhances its suitability for surface modification and adsorption, broadening its potential in materials science and engineering.

GO has attracted significant attention in the biomedical field due to its diverse applications in drug delivery, bioimaging, tissue engineering, and biosensing. [81] Among these, drug delivery is particularly promising due to GO's high surface area and ease of functionalization, which enable it to transport a variety of therapeutic agents, including small-molecule drugs, proteins, and nucleic acids. In addition to its biocompatibility, GO's ability to interact with biological molecules makes it a strong candidate for cancer therapy. [82],[83] Functionalized GO can be loaded with anticancer drugs and targeted specifically to cancer cells through the attachment of targeting ligands such as antibodies or peptides. Moreover, GO's capacity to generate reactive oxygen species (ROS) under light irradiation can be utilized in photothermal and photodynamic therapies, both of which are emerging as effective cancer treatments.

Beyond drug delivery, GO has also been investigated as a scaffold material in tissue engineering due to its excellent mechanical properties and capacity to support cellular growth. The incorporation of GO into polymeric scaffolds not only enhances the mechanical strength of the composite material but also promotes cell adhesion, proliferation, and differentiation. Studies have demonstrated that GO-modified scaffolds support the growth of various cell types, including stem cells, positioning them as valuable tools for regenerative medicine and tissue engineering. [84]

The design of synthetic inhibitors for protein-protein interactions represents a promising therapeutic strategy for treating diseases such as thromboembolism, hereditary angioedema, diabetes, Alzheimer's disease, and Parkinson's disease.[85],[86] The development of these targeted inhibitors enhances therapeutic precision by disrupting harmful protein interactions, thereby mitigating disease progression and improving patient outcomes. Furthermore, their customizable nature allows for the optimization of binding affinity and selectivity, which is crucial for minimizing off-target effects and maximizing therapeutic efficacy.

The nature of protein-protein binding fundamentally relies on electrostatic interactions, where selectivity arises from the specific functional groups of amino acids arranged in precise three-dimensional conformations around the binding surfaces of proteins. Key amino acids, such as tyrosine, tryptophan, and phenylalanine, play pivotal roles in these interactions. Although these amino acids are relatively scarce within the overall protein structure, they are frequently localized on the surfaces of protein-binding sites, enhancing the specificity and affinity of protein interactions.[12]

Graphene oxide has been investigated as a synthetic inhibitor for protein binding.[76] GO is rich with carboxylic acid groups on its surface, which can interact with protein binding surfaces that are rich in cationic functionality. Essentially, it is a simple (non-selective) electrostatic interaction. For instance, in 2011, De and Dravid demonstrated that unfunctionalized GO binds to the active site entrance on the surface of chymotrypsin (Chy), inhibiting its function.[77] Subsequent studies have explored how the inhibition of GO could be improved through its functionalization with amino acids.[78,79] A common method of functionalization involves the use of a coupling agent and an excessive amount of amino acids in their unprotected form. This method leads to the formation of an oligomeric layer on the surface of GO. The oligomeric layer potentially provides a large number of amino acids on the surface, which could lead to stronger interactions. However, the strong π-π interactions between key-aromatic amino acids, such as phenylalanine (Phe), tyrosine (Tyr), and tryptophan (Trp), result in a strong cooperative interaction between the oligomeric "string" of amino acids and the GO surface. As a result, the cooperative interactions must be broken before GO can bind to the target protein. This leads to relatively weak binding. Conversely, a monomeric layer of amino acids (synthesised using a standard protection/deprotection approach) may struggle to bind with a protein surface due to strong steric effects. These two possibilities were studied by Twyman using graphene oxide (GO) functionalized with both monomeric and oligomeric layers of tyrosine. An inhibition assay using chymotrypsin was used to test the binding/inhibition with both systems showing

significantly enhanced inhibition.[34] . In the case of the monomeric system, a Ki value four times greater than that of GO alone was recorded. As such, these results confirmed that a simple monomeric covering of the GO surface was enough to improve the binding of GO to chymotrypsin; steric effects did not hinder or reduce binding.

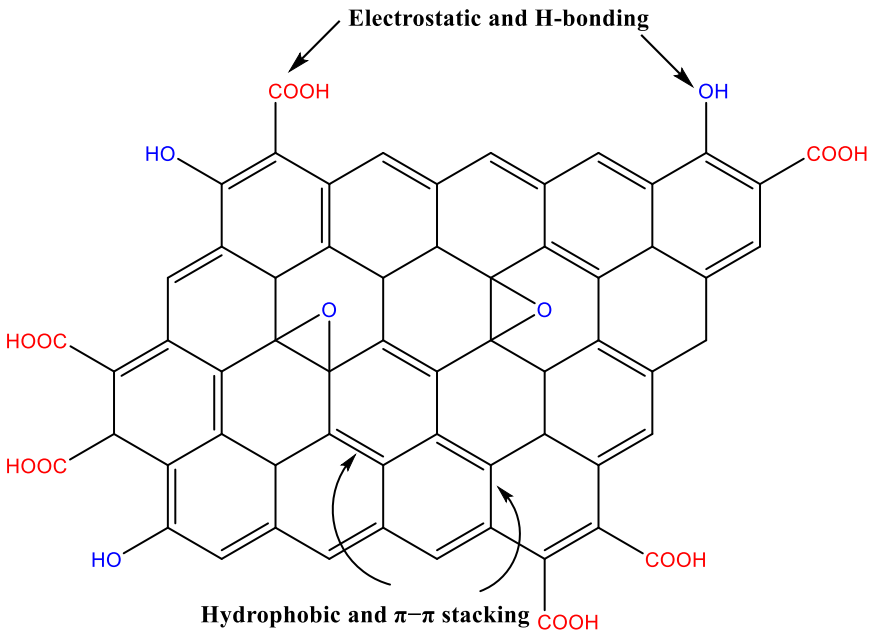

Figure 48- Representative structure of unfunctionalized GO showing the various types of functionalities present.

As discussed above and shown in Figure 48, a combination of electrostatic, π-π, and hydrophobic forces governs all interactions involving graphene oxide (GO). Electrostatic interactions arise from the carboxylic and hydroxyl functional groups located at the edges and surface of GO, whereas hydrophobic and any π-π interactions occur on aromatic patches found on its surface. Subrata and De investigated the inhibitory efficiency between surface-functionalized GO compared to edge-functionalized GO with similar amino acid functionalities for biomolecular interactions.[78] They employed two different strategies: covalent functionalization of the carboxylic acid groups and non-covalent π-π functionalization of the surface through functionalized aromatic groups.

Their results indicated that the non-covalent π-π functionalization exhibited stronger protein binding than covalently functionalized GO. Although amino acid density was not considered in the paper, the results provide some support for our hypothesis that a dynamic approach

towards the synthesis of specific protein binding ligands was possible. To test this proposition, we proposed to functionalise the aromatic compound anthracene with various amino acids and to react these covalently with GO using a Diels–Alder reaction and also non-covalently using π-π functionalization.

3.1 Aims and Objectives

The main aim of this project is to test and develop a dynamic method to investigate the potential of functionalized graphene oxide (GO) as a protein-protein interaction inhibitor. This would be accomplished through a noncovalent system, with the goal of enhancing the selectivity of protein binding. To optimize and test the process, we will compare the results to those of an analogous covalent system. Overall, the development of this approach is valuable for addressing diseases related to protein-protein complexes.

Therefore, we propose to introduce surface recognition sites in GO by functionalizing its surface with anthracene-amino acid ligands using covalent and non-covalent methodologies. The idea behind the non-covalent system is shown in Figure 49. This shows that the protein can "self-select" and direct the synthesis towards an optimized ligand. This is possible due to the dynamic nature of the system, which allows the functionalised groups to move and maximize interactions with the protein (chymotrypsin). This is not possible for an analogous non-covalent system. Specifically, our plan involves functionalizing anthracene with various amino acids and then reacting these with GO via a covalent and non-covalent method. Specifically, a Diels–Alder reaction will be used for the covalent system, and a simple π-π interaction for the non-covalent method. Once synthesized, their protein binding ability will be assessed by inhibiting the activity of the protein a-chymotrypsin, whose active site entrance is located at the centre of its binding area.

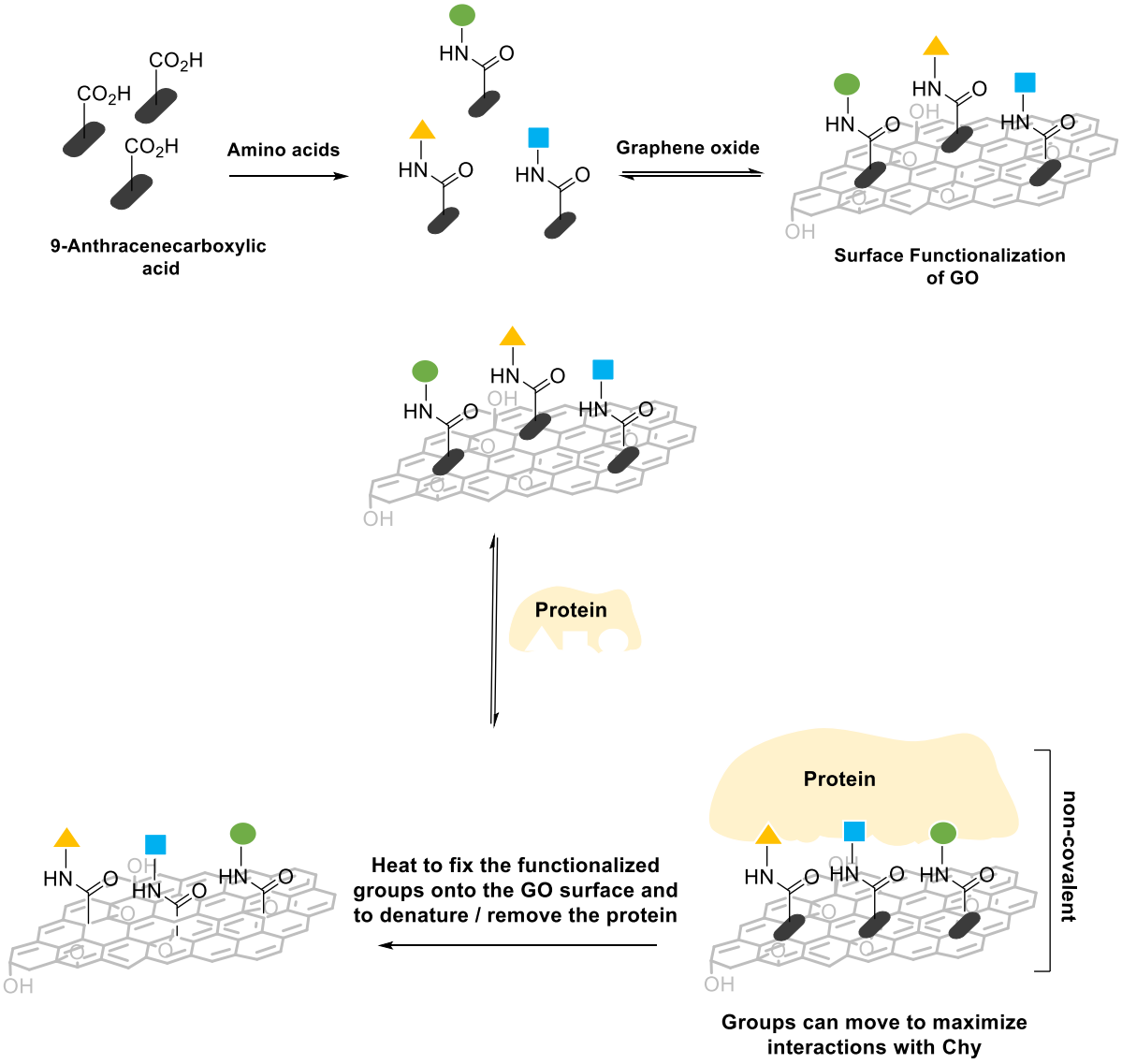

Figure 49- Proposed functionalization of the GO using both non-covalent and covalent methods.

3.2 Results and discussion

To achieve our objectives, the initial step involves synthesizing graphene oxide from graphite powder. While several methods are available for this synthesis, the Tour method is preferred due to its ability to produce a high yield of GO, [80–82] making it an efficient choice for our purposes. The resulting graphene oxide may contain various oxygen functional groups, including alcohols, epoxides, carbonyls, and carboxylates. However, the relative and absolute concentrations of carbon and oxygen (C/O ratio) can vary significantly depending on the synthesis method employed. Therefore, it is essential to characterize GO concerning its carbon and oxygen content before and after functionalization.

Nuclear magnetic resonance (NMR) spectroscopy is not suitable for the characterization of GO due to its paramagnetic properties and the absence of hydrogen atoms. .[81,83] Consequently, alternative characterization techniques are typically employed to analyse GO. These techniques include elemental analysis, which provides insights into the composition of the material; Fourier transform infrared (FTIR) spectroscopy, which is useful for identifying functional groups; X-ray photoelectron spectroscopy (XPS), which can elucidate the chemical state and electronic environment of the elements present; and Raman spectroscopy, which offers valuable information about the structural properties and quality of the graphene oxide. Each of these methods plays a crucial role in providing a comprehensive understanding of GO's characteristics and functionalities.

3.3 Synthesis and characterization of unfunctionalized Graphene oxide

Several methods for synthesising graphene oxide **32** from graphite 31 through oxidation have been elucidated by Brodie[84], Staudenmaier[85], and Hummers.[82] The Tour method[86], introduced in 2010 improved upon Hummers' method by excluding $NaNO_3$ from the reaction, resulting in a safer procedure that does not produce toxic gases. Consequently, we chose to synthesise GO **32** using the Tour method. In the first step, graphite powder was added to the 9:1 mixture of cool, concentrated H_2SO_4/H_3PO_4.This was followed by the gradual addition of $KMnO_4$ in droplets to minimise the risks associated with exothermic reactions. Subsequently, the mixture was stirred for 24 hours at 50 °C, leading to the production of graphene oxide. Scheme 13 represents the GO sheets **32** that result after the strong oxidation of graphite 31.

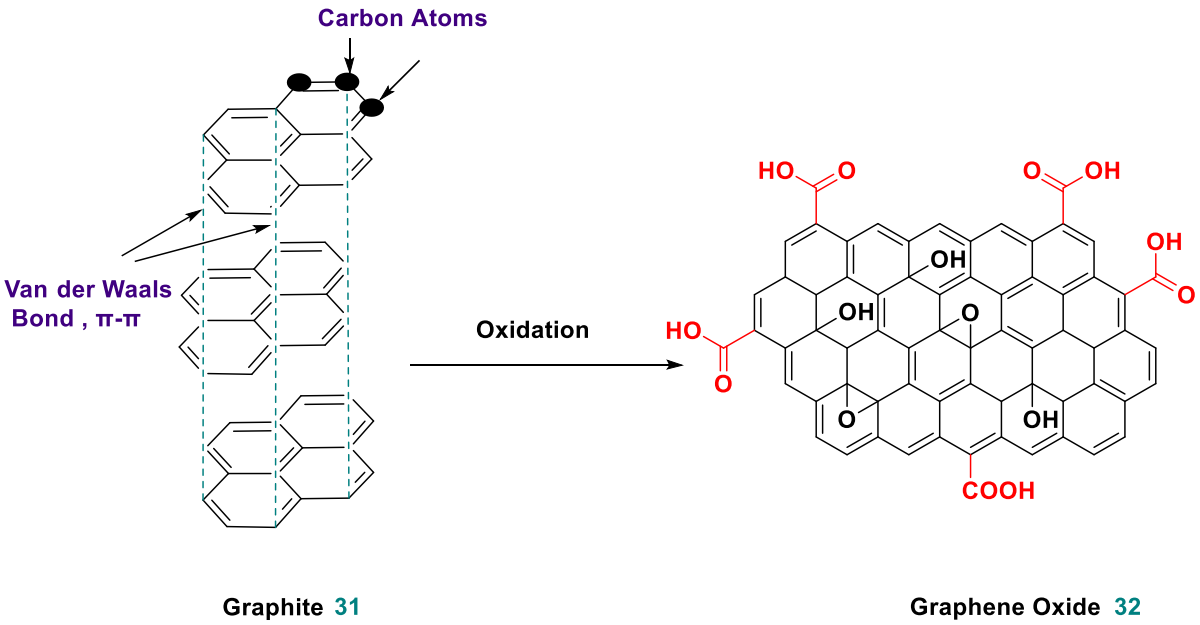

Scheme 13- A schematic showing the structural features of graphite sheets **31** and the oxidation process leading to the formation of graphene oxide **32**.

The structure of the obtained GO **32** was verified by comparing its characterization data with published information. The oxidation process was monitored using FTIR, as shown in Figure 50. The FTIR spectra of graphite exhibited no significant peak, indicating its chemical inertness, whereas those of GO **32** showed the presence of various functional groups. The broad peak observed at 3428 cm^{-1} indicates the presence of OH and/or COOH functional groups. Peaks at 1716 cm^{-1} and 1632 cm^{-1} correspond to (C=O) and (C=C), respectively. Additionally, the (C-OH) group of C-O (epoxy) and C-O (alkoxy) appears at 1200 cm^{-1} and 1038 cm^{-1}, respectively. The FTIR results confirm the presence of various oxygen-containing functional groups in the GO structure.

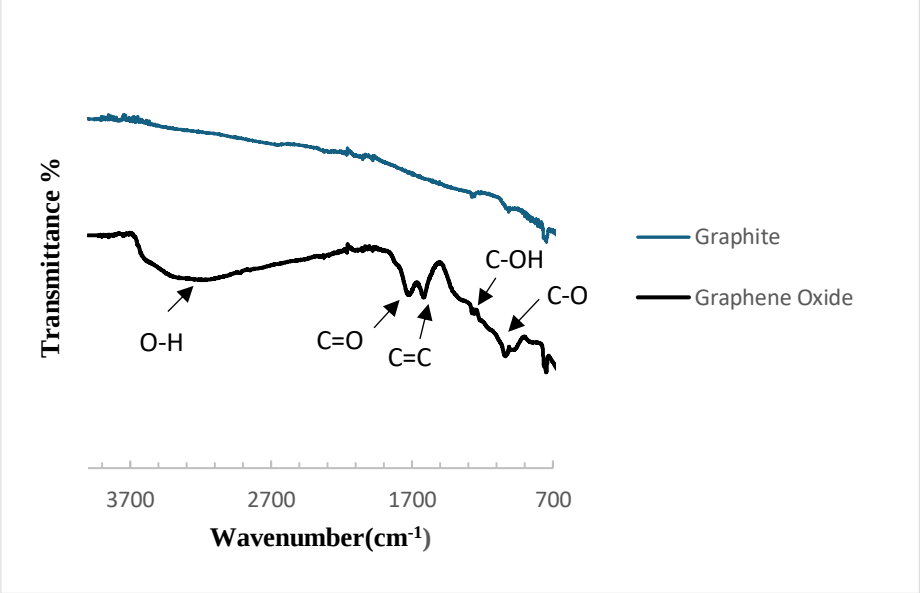

Figure 50- FTIR spectra of graphite **31** and GO **32**.

In Raman spectroscopy, information is obtained by recognising the inelastic scattering of molecules exposed to monochromatic light, which is generally provided by lasers. It has become common practice to use Raman spectroscopy for characterising the molecular structures of carbon products due to the resonance-enhanced Raman scattering inherent in carbon materials. Therefore, graphene exhibits well-defined vibrational bands. In addition, Raman spectral analysis can be used to assess the disorder in carbon materials by measuring the intensity ratio of the D band to the G band (I_D/I_G ratio). Figure 51 illustrates the Raman spectra for both GO **32** and graphite **31**. The spectrum of GO **32** shows two peaks at 1355 cm^{-1} and 1593 cm^{-1}, corresponding to the D and G bands, whereas graphite shows a single sharp peak at 1570 cm^{-1}. The I_D/I_G ratio of GO **32** was measured as 0.87, indicating structural disorder likely due to oxygen-containing functional groups introduced during oxidation, which convert sp^2 carbon bonds to the sp^3-hybridized carbon on the surface of GO. The 2D band in graphite is sharp, but it appears broad and shifted to a higher wavenumber at 2500–3200 cm^{-1} in GO. This suggests the presence of layers of graphene oxide sheets.[87]

X-ray diffraction (XRD) is commonly used to characterize crystalline materials, as it provides information about the atomic spacing and crystal orientation of the materials. Figure 51 displays the d-spacing XRD pattern for synthesized graphene oxide. The presence of a diffraction peak at $2\theta=10^{\circ}$ indicates the formation of GO **32** layers, which is mainly due to the oxidation of graphite. Additionally, there has been an observed increase in the d-spacing of graphite from 0.33 nm to 0.88 nm following GO **32** formation.[82]

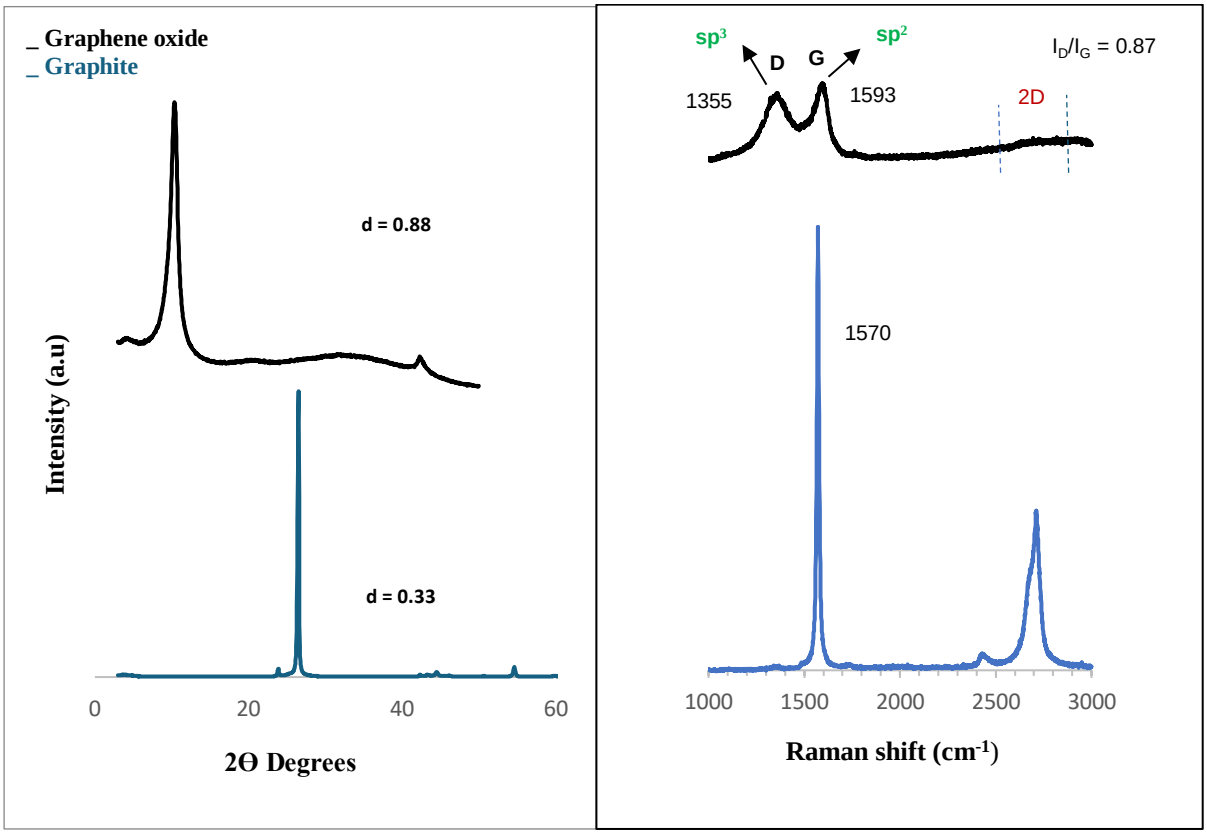

Figure 51- XRD pattern (left) and RAMAN spectra (right) of GO **32** and Graphite **31**.

3.4 Synthesis of anthracene-Amino Acid Ligands

After successfully synthesizing GO **32**, the next step involved synthesizing anthracene-terminated amino acid ligands. To accomplish this, we employed peptide coupling reactions, which facilitate the formation of an amide bond through the reaction of a carboxylic acid group with an amine group. In our previous work, we utilized EDC as a coupling agent; however, this approach necessitated additional purification steps, which could complicate the process. In this chapter, we adopted the HBTU method for peptide coupling, as it has been shown to be more efficient and straightforward, as highlighted in the work of Subrata and De. [78] This method minimizes side reactions and enhances the yield of the desired ligands.

In these reactions, we utilized the (2-(1H-benzotriazol-1-yl)-1,1,3,3-tetramethyluronium hexafluorophosphate (HBTU) as the in situ activation reagent in the presence of N,N-diisopropylethylamine (DIPEA). peptide coupling reactions conducted with HBTU often result in high yields and fewer byproducts.[88] In our goal, we initiated the reaction by interacting

anthracene-9-carboxylic acid with protected amino acids utilizing HBTU as a coupling reagent, as shown in Scheme 14.

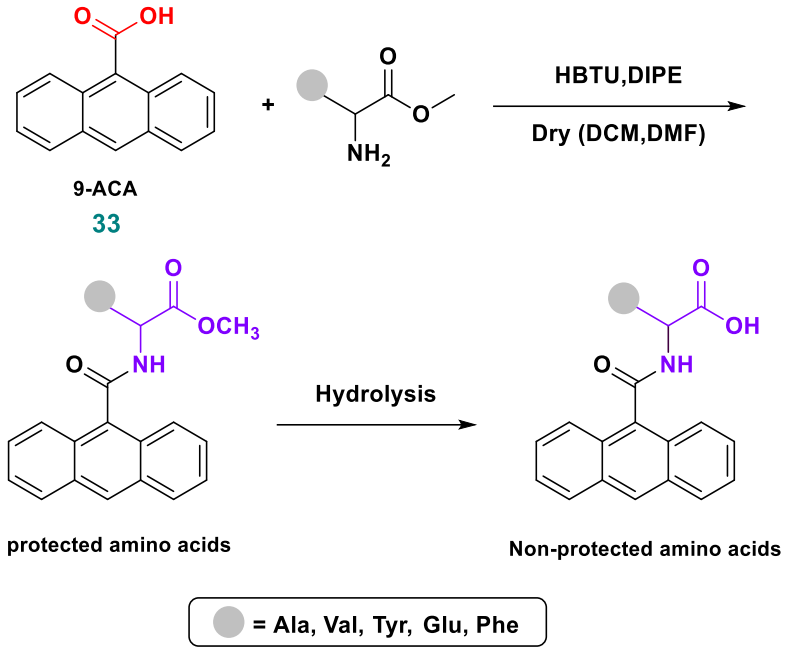

Scheme 14- Peptide coupling reactions of anthracene with a series of L-amino acid ligands.

When HBTU is added to a reaction mixture containing a carboxylic acid, the carboxylate anion, which is formed during deprotonation by a base such as DIPEA, attacks the electrophilic uronium center. The nucleophilic attack displaces the benzotriazolyl group of HBTU to produce an O-acylisourea intermediate. This intermediate then undergoes intramolecular rearrangement to form an active ester "benzotriazolyl ester". Active esters are more reactive than carboxylic acids since the benzotriazolyl group is a good leaving group, making them highly susceptible to amine nucleophilic attack. As a result, the desired amide bond is formed and the benzotriazolyl group is released (Scheme 15).

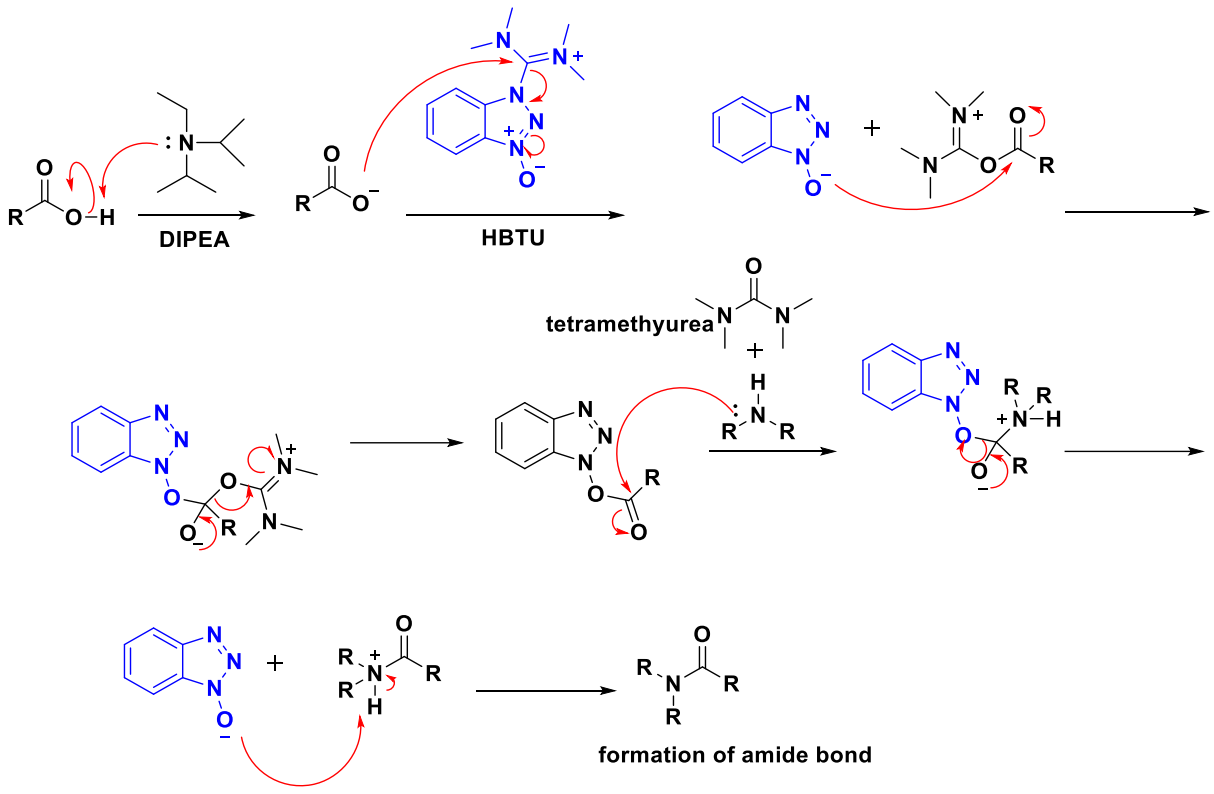

Scheme 15- HBTU, DIPEA Peptide Coupling mechanism.

Several factors are considered when selecting the different amino acids for functionalization of anthracene, including hydrophobicity, hydrophilicity, aromaticity, and negative charge. These features can influence binding affinity and specificity. Alanine (Ala), valine (Val), phenylalanine (Phe), tyrosine (Tyr) and glutamic acid (Glu) were subsequently selected for our study. tyr and Phe are amino acids known to be important with respect to protein binding.[89,90] These amino acids can provide a number of possible interactions. However, we expected that Tyr would bind more strongly than Phe, due to the extra hydrogen bond contributed by the hydroxyl group (-OH) on its aromatic ring. Additionally, the negative charge of glutamic acid-functionalized GO is likely to result in very strong inhibition.

Completion of the reaction was confirmed through ^{1}H NMR, ^{13}C NMR, and FTIR spectra, as each amino acid was easy to recognise within the spectra. For example, Valine was distinguishable by the presence of two doublet signals located in the upfield region, whereas Alanine exhibited a single doublet in the same region. Additionally, the spectrum of Valine showed a septet at 2.22 ppm, indicative of the presence of its characteristic of the CH in the isopropyl group. A distinct chemical shift is observed in the ^{1}H NMR spectrum of Tyrosine and Phenylalanine. The CH_2 protons adjacent to the aromatic ring showed two broad singlets, each integrating as one proton. This is because these protons are diastereotopic. Additionally,

the chemical shifts of protons at the meta, ortho, and para positions in the phenyl ring were observed between 7.27 ppm and 7.40 ppm. The DEPTQ ^{13}C NMR spectrum confirmed these findings, with five peaks between 127.0 ppm and 129.4 ppm corresponding to the aromatic group. For Glutamic acid, the ^{I}H NMR peaks were observed also as a diastereotopic. Additionally, all amino acids exhibited a peak at 4.62 ppm corresponding to the Alpha Hydrogen (Hα). Anthracene peaks were also observed in the aromatic region between 7 and 9 ppm. Furthermore, FTIR analysis showed peaks at 3315 cm^{-1} and 2965 cm^{-1}, corresponding to the N-H and C-H respectively. The vibrational stretching frequency for C=O of ester and amide functional groups were observed at approximately 1735 cm^{-1} and 1647 cm^{-1}, while the aromatic C-C bands were at 1524 cm^{-1}. Table 11 summarizes the molecular weight of different anthracene-amino acid ligands.

Amino acid	Alanine **34**	Valine **35**	Phenylalanine **36**	Tyrosine **37**	Glutamic acid **38**
Chemical Formula	$C_{19}H_{17}NO_3$	$C_{21}H_{21}NO_3$	$C_{25}H_{21}NO_3$	$C_{25}H_{21}NO_4$	$C_{22}H_{21}NO_5$
Expected Molecular weight (g/mol)	307	335	383	399	379
Obtained Mass ion (MH^+)	308	336	384	400	380

Table 11: The molecular weights of various protected anthracene-amino acid ligands.

The next and final step involved the removal of the protecting groups from the amino acids. This deprotection process was achieved by hydrolysing the ester group using sodium hydroxide, resulting in the formation of the corresponding carboxylic acid. The successful formation of the final product was confirmed through NMR analysis. Notably, the methyl ester peak at 3.82 ppm for valine (labelled as **40**) was no longer visible after the deprotection, indicating that the ester had been effectively hydrolysed (Figure 52). This confirms that the intended anthracene-terminated amino acid ligands were successfully synthesized and deprotected, ready for further functionalization or applications.

Amino acid	Alanine **39**	Valine **40**	Phenylalanine **41**	Tyrosine **42**	Glutamic acid **43**
Chemical Formula	$C_{15}H_{21}NO_3$	$C_{20}H_{19}NO_3$	$C_{24}H_{19}NO_3$	$C_{24}H_{19}NO_4$	$C_{20}H_{17}NO_5$
Expected Molecular weight (g/mol)	292	322	370	386	352
Obtained Mass ion (MH^+)	293	321	369	385	351

Table 12: Molecular weights of deprotected anthracene-amino acids.

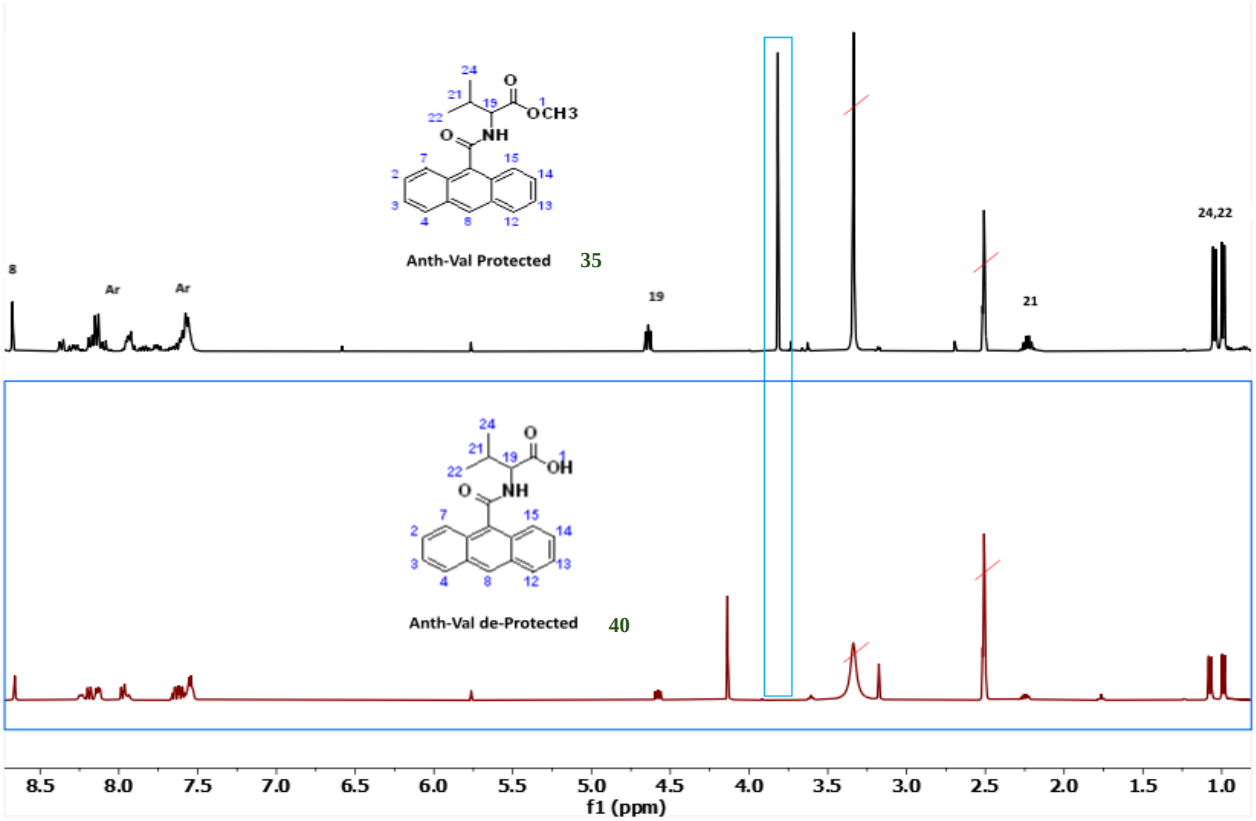

Figure 52- ^{1}H NMR spectrum of anthracene-terminated Valine ligands **35** and **40** in DMSO solvent.

After synthesizing the amino acid-anthracene for covalent and non-covalent functionalization, the next step was to add these to GO **32**. In our first experiment, we achieved this covalent functionalization using the Diels-Alder reaction.

3.5 Covalent Functionalization of the GO surface.

There has been extensive research on the surface functionalization of graphene oxide, both covalently and non-covalently[91]. The non-covalent approach relies on weak interactions between molecules and graphene oxide, such as hydrogen bonding, electrostatic interactions, van der Waals forces, or π-π stacking interactions. This process does not involve the formation of chemical bonds between the molecules and GO but rather relies on reversible physical interactions. Because there is no formation of new chemical bonds, the chemical structure of GO is preserved. In contrast, the covalent functionalization of GO surfaces involves the formation of strong chemical bonds between organic molecules and functional groups on the surface of the GO (Figure 53). Reactions are usually performed between reactive oxygen containing functional groups on GO and specific functional groups on the molecules being attached. For example, an amide formed between an amine and the carboxylic acid groups on

the GO surface.[92] The formation of covalent bonds results in a more stable attachment of molecules to the GO surface. In most cases, this process requires special reaction conditions, a number of reagents and may generate a number of by-products.[93,94]

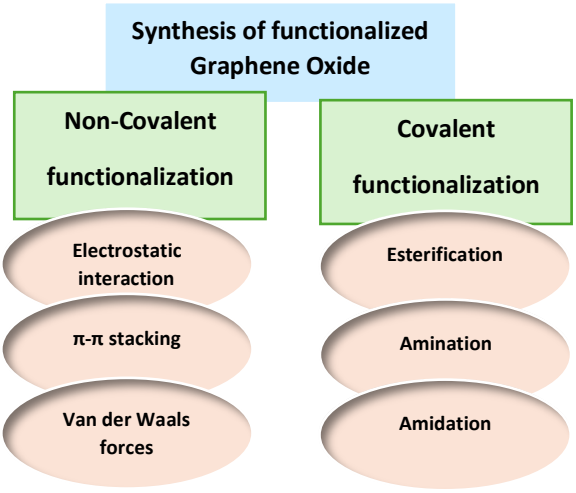

Figure 53- Illustration of the covalent and non-covalent functionalization methods of GO **32**.

In organic chemistry, the Diels-Alder reaction is a [4+2] cycloaddition reaction where a diene and dienophile react with each other to yield a stereospecific cyclic product reaction.[95,96] Graphene oxide can potentially act as a dienophile or diene in such reactions, depending on its specific functionalization and conditions of reaction. Mrinmoy De tested GO as a carbocatalyst for the DA reaction in water at room temperature, which reduces the activation energy and produces high yields (Scheme 16).[97]

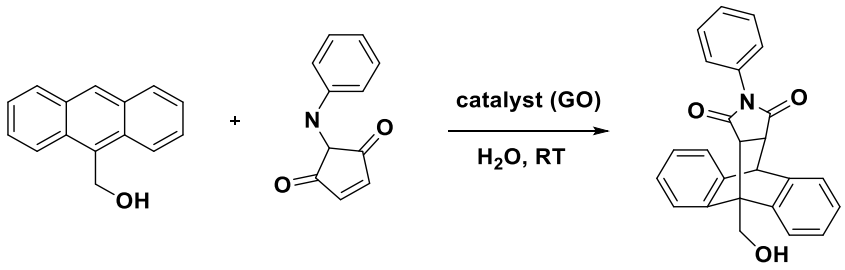

Scheme 16- GO-catalysed Diels-Alder reaction of 9-hydroxymethylanthracene with N-phenylmaleimide.

However**,** some limitations of using GO as a diene include the reversibility of the reaction (defunctionalisation) and the decomposition of GO, particularly at long reaction times.[83] The results of computational simulations examining the reactivity of graphene oxide with certain

molecules in Diels-Alder reactions indicate that graphene oxide functions more as a dienophile than a diene, with the latter leading to exothermic reactions.[98]

To achieve our goal, we covalently functionalized the surface of graphene oxide **32** using the Diels-Alder reaction. This reaction alters the structure of GO while keeping the acid groups (required for binding). Importantly, Diels-Alder reactions do not require additional reagents, thereby eliminating the production of by-products. Following the washing of GO, highly pure compounds are obtained. The general Diels-Alder mechanism between anthracene and GO is represented in Scheme 17 below.

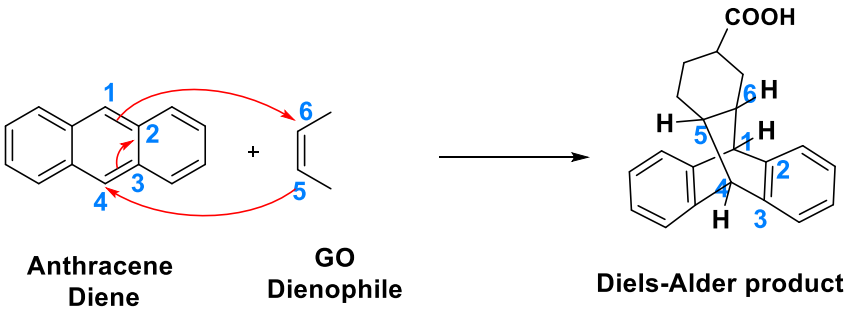

Scheme 17- The Diels-Alder mechanism between GO and anthracene.

The surface functional groups on graphene oxide make it an ideal dienophile for use in Diels-Alder reactions with anthracene. Anthracene acts as the diene, donating electrons to electron-deficient functional groups of GO, resulting in a cyclic intermediate and a fused-ring adduct. This process results in the formation of stable covalent bond at the surface of GO. The proposed mechanism of this reaction is illustrated in scheme 18 below.

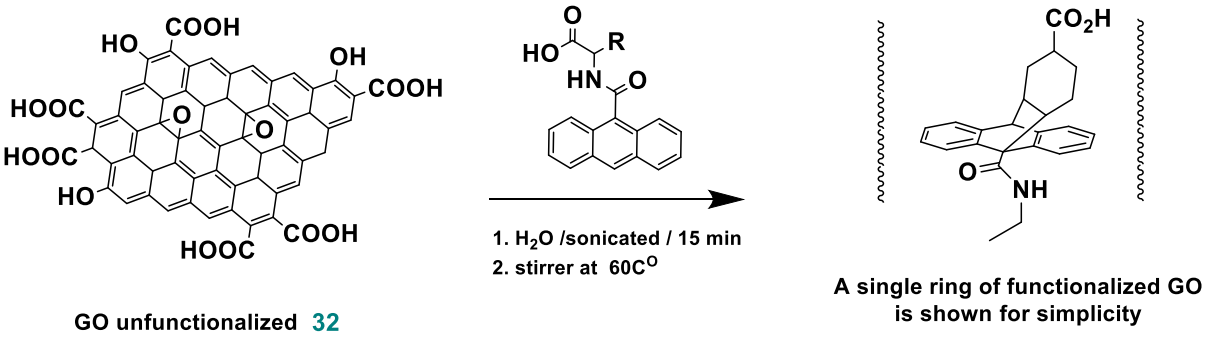

Scheme 18- Systematic representation of the Diels–Alder reaction between anthracene-amino acid ligands and the surface of GO **32**.

The covalent functionalization process began by combining equal amounts of GO and anthracene-amino acid (anthracene-AA) ligands in a small volume of Milli-Q water. The mixture was sonicated for 30 minutes to disperse the nanoparticles evenly, enhance interactions

with the functionalizing agents, and maximize the available surface area. Following sonication, the mixture was stirred at 60°C for 24 hours to allow sufficient reaction time. After cooling, the precipitate was separated by centrifugation and lyophilized.

Fourier-transform infrared spectroscopy was employed to confirm successful functionalization, with spectra showing distinct vibrational stretching frequencies corresponding to the −OH and −NH groups of the amino acid residues attached to the GO sheets. Figure 54 illustrates the FT-IR spectra comparison of 9AC before and after the Diels-Alder (DA) reaction, highlighting the noticeable differences in −OH and −NH stretching frequencies that indicate successful covalent attachment.

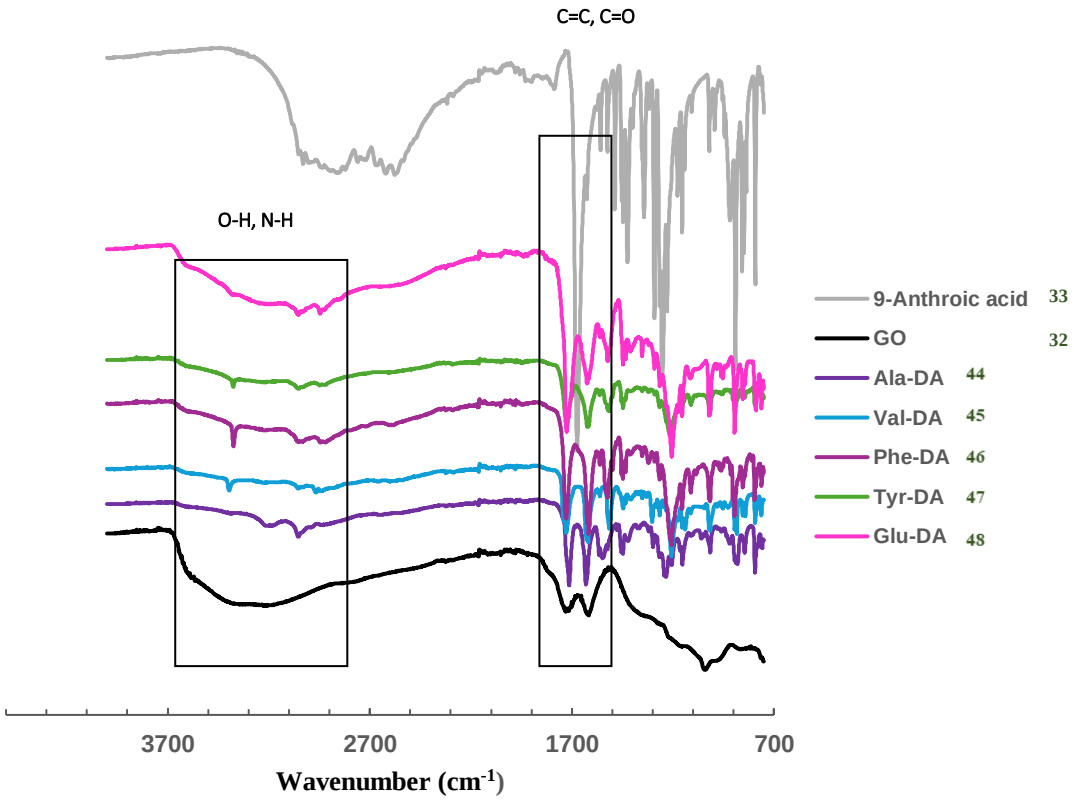

Figure 54- FT-IR spectra of covalently functionalized GO with different amino acids, GO **32** and 9AC **33**, are shown.

After confirming the attachment of anthracene-AA to GO sheets, we utilized elemental analysis and SEM-EDX were employed to probe the top layer and analyze the composition of the compounds. These methods are known to yield different values due to variations in surface and bulk chemical compositions, but they are widely used and reliable. The data confirmed the

presence of nitrogen in all samples after functionalization, and nitrogen can only be derived from an amino acid. Table 13 summarizes the elemental analysis results. The oxygen percentage was estimated by assuming it was the only other atom present and subtracting the sum of all atoms from 100. SEM-EDX element mapping in Figure 55 showed that GO alone contained only carbon and oxygen, whereas images of functionalized GO revealed the presence of nitrogen.

Compound Name	C [%]	H [%]	N [%]	O [%]	C/N [%]
GO **32**	38.20	2.95	n/a	56.73	/
AN - Ala **44**	62.57	4.11	2.32	31	3.7
AN - Val **45**	61.08	4.27	1.69	32.96	2.8
AN - Phe **46**	50.84	3.44	1.27	44.45	2.5
AN – Tyr **47**	63.08	4.28	2.12	30.52	3.4
AN – Glu **48**	53.68	3.43	1.04	41.85	1.9
AN – GO **49**	48.03	2.22	0.02	49.73	0.04

Table 13: Elemental analysis of GO **32** and anthracene – AA, with estimated oxygen % calculated as the difference between 100 and the sum of (C/H/N %).

Each amino acid has a different molecular weight, so we cannot make a direct comparison. However, their molecular weights are very similar with respect to graphene oxide, so element analysis can give us a guide to how the loading is being done. As shown in the table above, all amino acids contain different amounts of carbon and hydrogen, but not significantly. While amino acids contribute to both nitrogen and hydrogen, in our case they are the sole contributors to nitrogen, so we can use nitrogen content to estimate the loading. As a result, we focus on the nitrogen percentage, which provides insights into loading. In most cases, the nitrogen percentage is around $\simeq$ 2%, except for Glu **48** and Phe **46**, which have approximately 1%. Interestingly, the carbon percentage is also lower in these cases. In conclusion, we assume that the loading relatively is similar.

a)	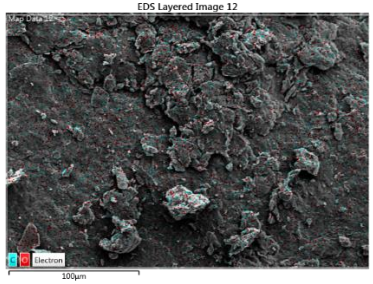 EDS Layered Image 12 Electron 100µm	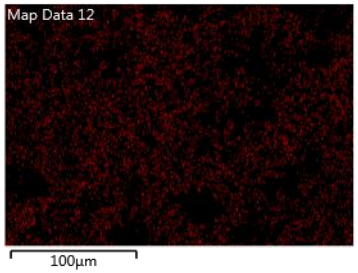 O Kα1 Map Data 12 100µm	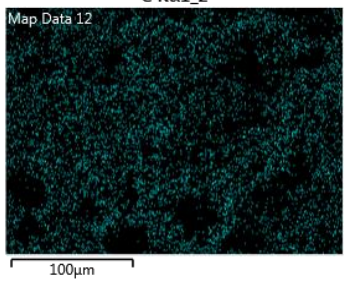 C Kα1_2 Map Data 12 100µm	N/A
b)	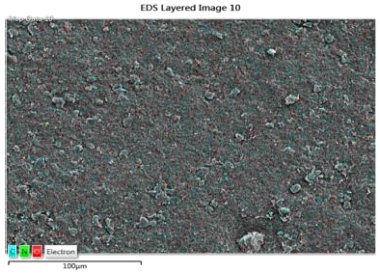 EDS Layered Image 10 Electron 100µm	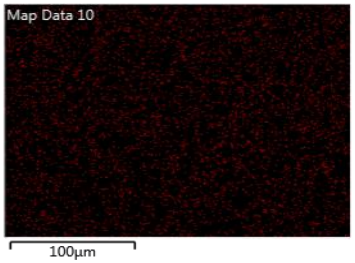 O Kα1 Map Data 10 100µm	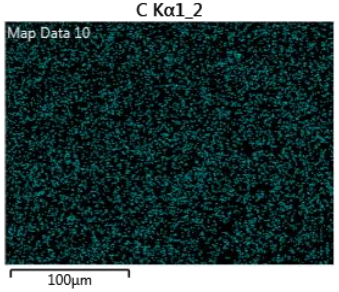 C Kα1_2 Map Data 10 100µm	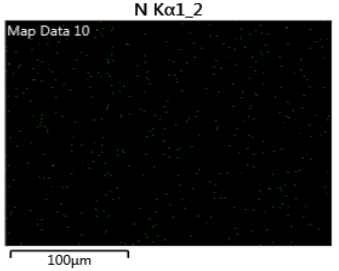 N Kα1_2 Map Data 10 100µm
c)	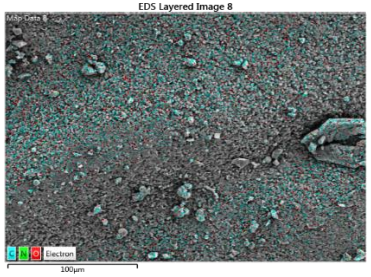 EDS Layered Image 8 Electron 100µm	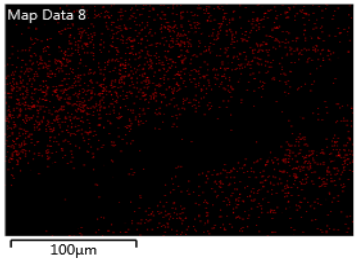 O Kα1 Map Data 8 100µm	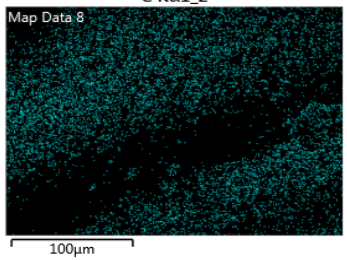 C Kα1_2 Map Data 8 100µm	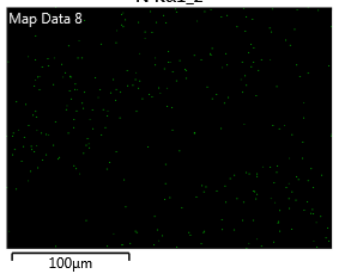 N Kα1_2 Map Data 8 100µm

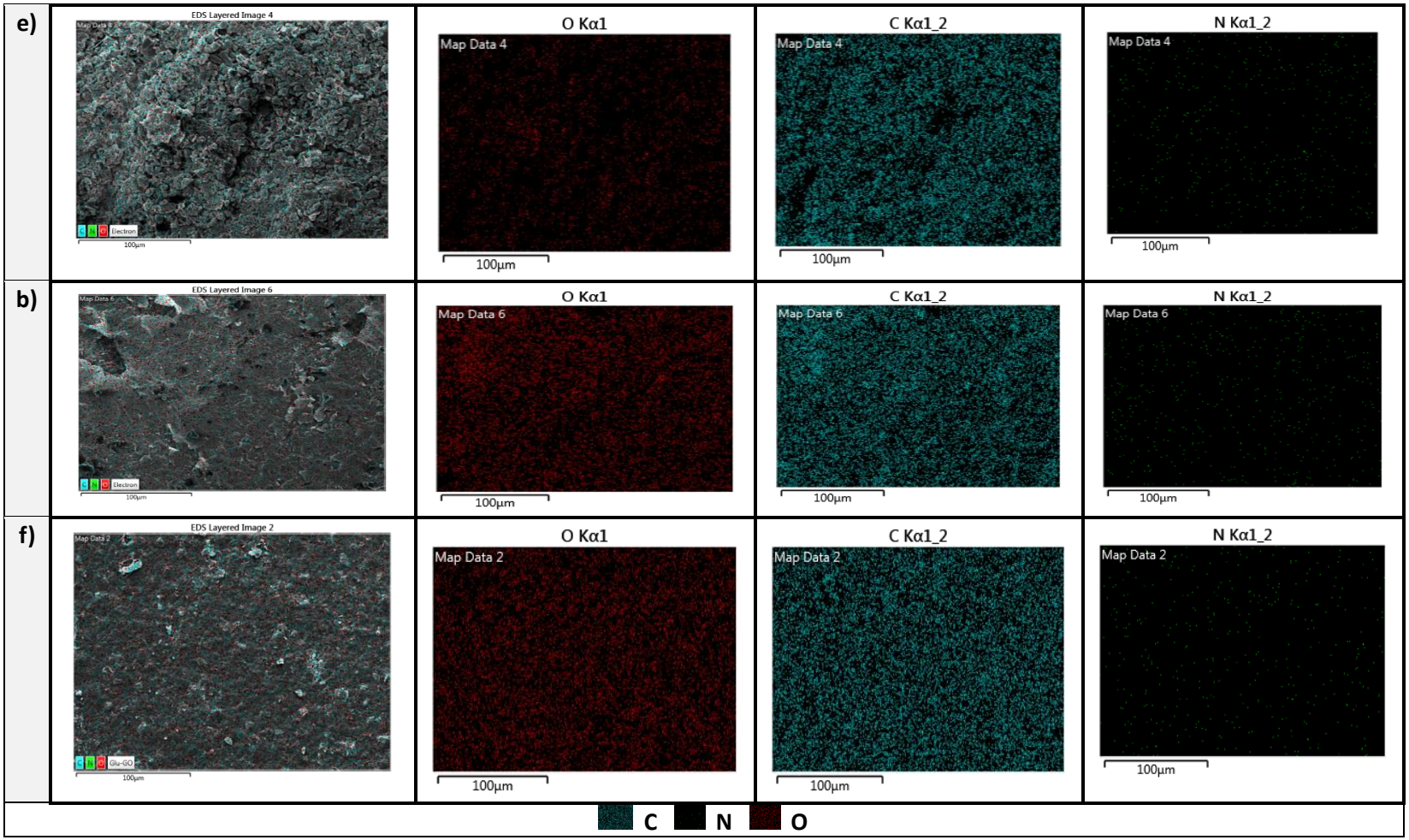

Figure 55- SEM-EDX element mapping graphs for a) GO **32**, b-f) AN - Ala **44**, AN - Val **45**, AN - Phe **46**, AN – Tyr **47** and AN- Glu AN – Glu **48** respectively.

3.6 Determination of GO binding using as α- Chymotrypsin and an inhibition assay.

3.6.1 Introduction

To investigate graphene oxide's ability to bind proteins and engage in specific molecular interactions, we selected α-chymotrypsin as a model enzyme. α-Chymotrypsin is well-studied for its detailed structural features, particularly its active site and substrate recognition properties, making it an ideal candidate for evaluating GO's binding efficacy and specificity in enzyme inhibition studies. [77] The active site of α-chymotrypsin lies centrally within the enzyme's binding pocket. This strategic location implies that any effective interaction between GO and α-chymotrypsin will likely obstruct substrate access to the active site. Such obstruction should result in measurable inhibition of the enzyme's activity, offering a clear indicator of binding interaction strength and specificity. Moreover, the degree of inhibition is expected to provide a direct measure of the affinity and extent of GO binding, as strong interactions would correspond to increased inhibition, confirming GO's potential for modulating protein function through surface interactions.

α-Chymotrypsin, a member of the serine protease family, plays a significant role in medicinal chemistry, making it an appealing target for protein surface recognition applications (Figure 56). Serine proteases like α-chymotrypsin are characterized by their well-defined active sites and substrate specificity, which are essential features for designing selective inhibitors and probes. At a neutral pH, proteins like α-chymotrypsin exhibit highly positive surfaces due to the abundance of lysine and arginine residues on their exterior. These positively charged areas provide an accessible target for binding partners with complementary, anionic functionalities. GO, with its rich array of oxygen-containing functional groups, including carboxylates, can serve as an effective binding partner. The electrostatic attraction between GO’s negatively charged sites and the positively charged regions on α-chymotrypsin facilitates robust binding, underscoring the potential of GO in applications where targeted, reversible protein interactions are advantageous.

It is composed of a polypeptide chain of 245 amino acids, with its biological function being to hydrolyse peptide bonds, particularly those adjacent to aromatic residues like tyrosine, tryptophan, and phenylalanine.[99,100] These aromatic residues are specifically targeted by enzyme because of the hydrophobic pocket located in the active site, which accommodates aromatic side chains and enhances the enzyme's catalytic efficiency. Therefore, inhibition

studies with GO are not only intended to reveal GO's ability to bind to proteins, but also to provide insight into how surface modifications may enhance its inhibitory potential. These insights may prove useful in drug development and other biomedical applications, where selective enzyme inhibition plays an integral role.

Our group has previously used this assay to show that dendrimers and proteins can selectively bind when their surface and binding areas are compatible in size, [29] demonstrating the importance of surface complementarity for selective binding interactions. A comparable approach was employed by De and Dravid to confirm that GO can interact electrostatically with α-chymotrypsin. [77] However, protein binding is influenced by more than just size and electrostatic attraction; the entrance to α-chymotrypsin's active site also has functional groups that can engage in hydrogen bonding, π-π stacking, and hydrophobic interactions. These additional interactions contribute to the specificity and strength of binding, enhancing GO's potential as a tool for selective protein interaction studies.

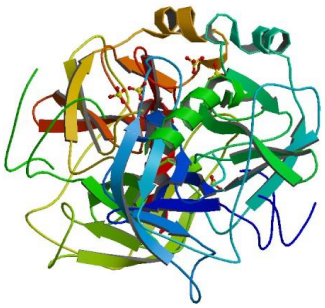

Figure 56- The native bovine chymotrypsin ribbon structure.

3.6.2 Control inhibition experiments with and without unfunctionalized GO.

In this part of the project, the catalytic activity of α-chymotrypsin is assessed by its ability to hydrolyse the substrate N-benzoyltyrosine-p-nitroanilide (BTNA) **50**, which results in the production of a UV-active species (as depicted in Scheme 19). The hydrolysis reaction produces a distinct colour change, providing an easily monitored indicator of enzymatic activity: the initial colourless solution of BTNA transitions to a yellow solution as it converts to p-nitroaniline **52**. This colour change can be tracked over time using UV-Vis spectroscopy, offering a straightforward and quantifiable means to measure the enzymatic reaction rate. By introducing functionalized GO to the system, we aim to demonstrate its effectiveness as a synthetic inhibitor, potentially slowing or reducing the rate of BTNA hydrolysis catalysed by

α-chymotrypsin. This assay thus allows for a direct comparison of inhibition efficiencies and insights into how surface modifications on GO might enhance or diminish enzyme inhibition.

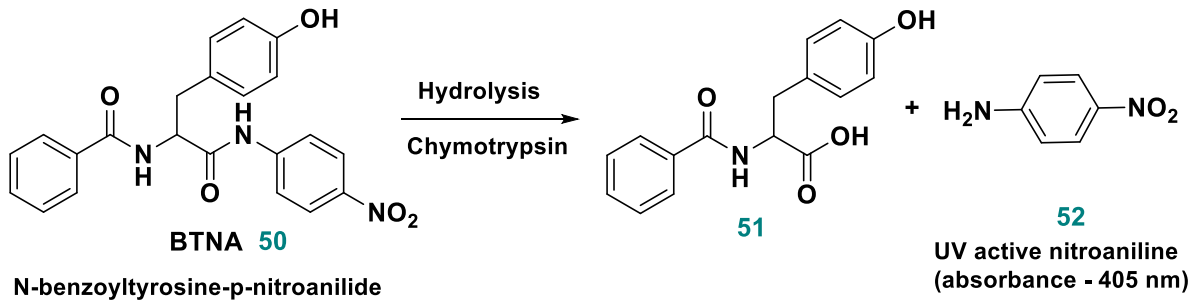

Scheme 19- The generation of UV active p-nitroaniline **52** by the hydrolysis of BTNA **50** by chymotrypsin.

Before conducting studies on GO **32**, it is necessary to confirm that any apparent inhibition is the result of GO **32** binding rather than interaction between the GO **32** and the BTNA **50** substrate. Therefore, a control reaction carried out in the absence of any GO **32** inhibitor is required. This was performed where a solution of the BTNA **50** substrate in methanol was added to an aqueous solution of α-chymotrypsin (in sodium phosphate buffer, 5 µM at pH 7.4). The final concentrations for the substrate and the enzyme were $1x10^{-4}$ M and $1x10^{-6}$ M, respectively, and the experiment was conducted at room temperature. The hydrolysis of the BTNA **50** substrate was monitored using UV spectroscopy by measuring the absorbance of the nitroaniline **52** leaving group at λ = 405 nm. Measurements were recorded at 20-second intervals for a period of 5 mins. Each experiment was conducted three times, and the raw data from these experiments is shown in the table 14 and Figure 57.

Time (Sec)	Abs (run 1)	Conc	Abs (run 2)	Conc	Abs (run 3)	Conc	Average	SD	ES
0	0	0	0	0	0	0	0	0	0
20	0.092	1.03E-05	0.0662	7.4E-06	0.089	1E-05	2.1E-05	1.59E-06	9.16E-07
40	0.1453	1.63E-05	0.1102	1.2E-05	0.1436	1.6E-05	3.4E-05	2.23E-06	1.28E-06
60	0.1822	2.05E-05	0.1437	1.6E-05	0.1793	2E-05	4.3E-05	2.41E-06	1.39E-06
80	0.2105	2.37E-05	0.1692	1.9E-05	0.2078	2.3E-05	5E-05	2.6E-06	1.5E-06
100	0.23	2.59E-05	0.1914	2.2E-05	0.2303	2.6E-05	5.6E-05	2.52E-06	1.45E-06
120	0.2448	2.75E-05	0.2111	2.4E-05	0.2484	2.8E-05	6.1E-05	2.31E-06	1.34E-06
140	0.2577	2.9E-05	0.2277	2.6E-05	0.2632	3E-05	6.5E-05	2.15E-06	1.24E-06
160	0.2677	3.01E-05	0.2407	2.7E-05	0.2755	3.1E-05	6.8E-05	2.05E-06	1.19E-06
180	0.2748	3.09E-05	0.2519	2.8E-05	0.2853	3.2E-05	7.1E-05	1.92E-06	1.11E-06
200	0.2814	3.16E-05	0.2634	3E-05	0.2933	3.3E-05	7.3E-05	1.69E-06	9.77E-07
220	0.287	3.23E-05	0.2724	3.1E-05	0.3	3.4E-05	7.5E-05	1.55E-06	8.96E-07
240	0.2906	3.27E-05	0.2795	3.1E-05	0.3052	3.4E-05	7.7E-05	1.45E-06	8.37E-07
260	0.2933	3.3E-05	0.2876	3.2E-05	0.3106	3.5E-05	7.8E-05	1.35E-06	7.77E-07
280	0.2972	3.34E-05	0.2948	3.3E-05	0.3156	3.5E-05	8E-05	1.28E-06	7.39E-07
300	0.3	3.37E-05	0.3012	3.4E-05	0.3201	3.6E-05	8.1E-05	1.27E-06	7.32E-07

Table 14: Raw data for the hydrolysis of N-benzoyltyrosine-p-nitroanilide by α-Chymotrypsin, yielding UV-active p-nitroaniline, with concentration values from three independent control runs.

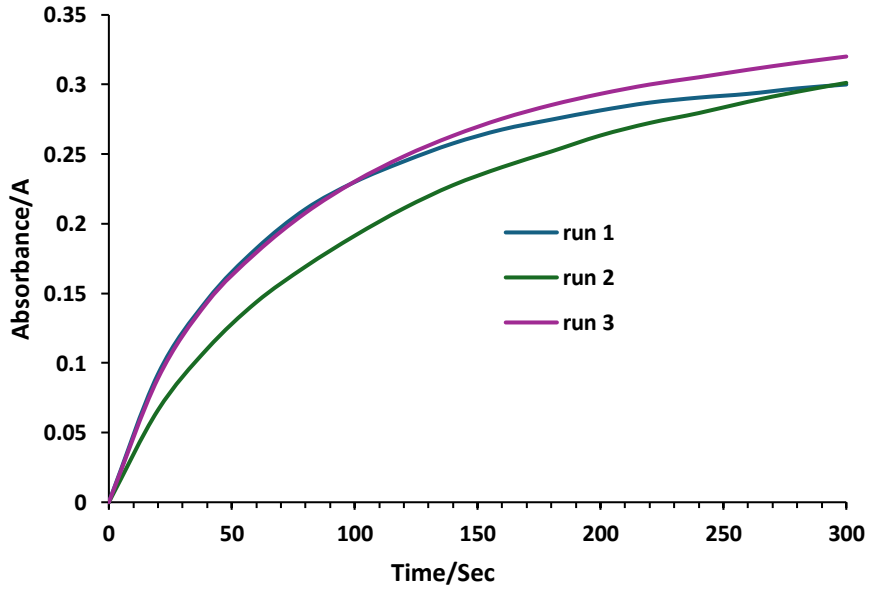

Figure 57- A graph showing the hydrolysis of BTNA by α-Chymotrypsin across three experimental runs.

The initial velocity (V_0) of the control reaction was determined by measuring the concentration of nitroaniline **52** (M) against time (s) by taking the gradient of the linear region during the early part of the reaction (Figure 58). It is important to note that the initial velocity is not constant and will vary with the concentration of various species (substrate, enzyme, and inhibitor).

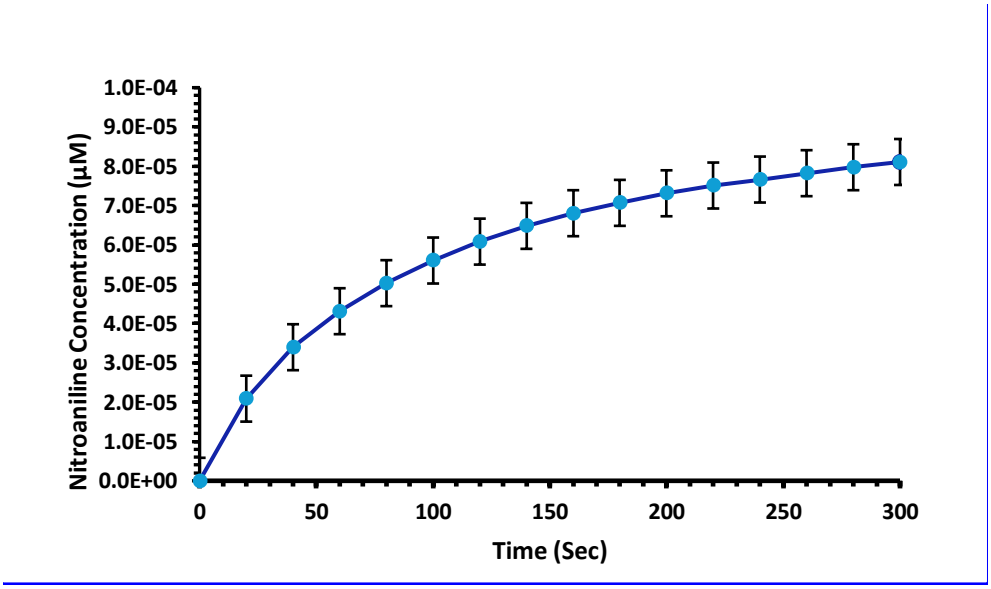

Figure 58- The rate of reaction plots for the hydrolysis of 50 µM BTNA (substrate) with the Chy (enzyme) without inhibitor, referred to as the control reaction.

A second control experiment was then carried out, but in the presence of unfunctionalized GO **32** (inhibitor). This was prepared by using a Chy solution to make a 0.025 mg/mL solution of GO **32**. The mixture was incubated and shaken for 30 minutes. The inhibition experiment was conducted by adding 50 µM of the enzyme-substrate **50** to the cuvette containing 2.0 mL of the pre-incubated protein-GO solution. The reaction profiles show the initial velocity for the enzyme control (V_o) and the GO **32** control are shown in Figure 57. The initial rates were 5.6 x 10^{-7} Ms-1 and 4.89 x 10^{-7} $Ms^{-}1$, respectively, indicating that the presence of the small amount of GO **32** decreased the initial rate in a measurable way.

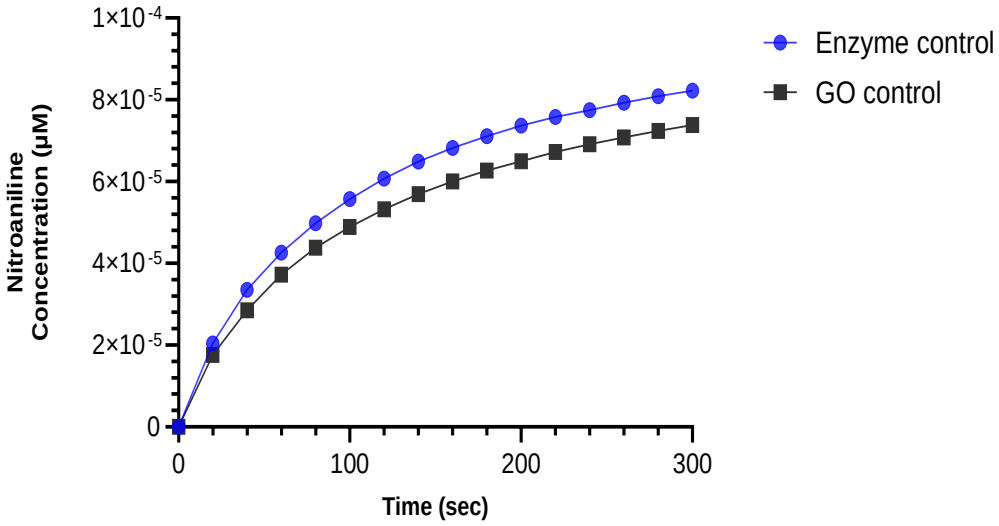

Figure 59- Initial rate plot over 5 minutes for chymotrypsin-BTNA hydrolysis in the presence and absence of unfunctionalized GO **32**.

In order to quantify GO **32** binding on a relative scale, the ratio of initial rates multiplied by 100 gives the percentage of inhibition.

a) For the enzyme only control we have;

$$\frac{5.60 \text{ x } 10 - 7}{5.60 \text{ x } 10 - 7} \text{ x } 100 = 100\ \%$$

b) For the GO **32** control we have;

$$\frac{4.89 \text{ x } 10 - 7}{5.60 \text{ x } 10 - 7} \text{ x } 100 = 87\ \%$$

Subtracting the inhibition percentage from 100 allows for easy determination of the extent of binding (as a percentage). The summary of initial velocities (V_o) and relative binding data is provided in Table 15. Based on these findings, inhibitors can be directly compared. The results obtained indicate that the reaction of graphene oxide is inhibited by 10%. Therefore, it is expected that higher levels of inhibition will be observed after functionalization.

$$\text{Inhibition } \% \ = \frac{\text{V0 (obtained)}}{\text{V0 enzyme control}} \text{ x } 100$$

BTNA [S]= 50 µM	**Enzyme Control**	**GO Control**
Initial velocity (V_o) (x 10^{-7} Ms^{-1})	5.60	4.89
Extent of Reaction %	100	87
Relative Binding %	0	13

Table 15-Initial rates and binding data for the Chy and unfunctionalized inhibitor **32**.

3.6.3 Inhibition using functionalized GO.

Having established the results from the control experiments, the next step was to assess protein binding using the covalently functionalised GO samples. The covalent functionalization process was described in section (3.5). Further experiments were conducted, repeating the reaction using GO functionalized with various amino acids. Elemental analysis data confirmed that the loading of each functionalized anthranilic acids onto the GO surface was similar, allowing us to make direct comparisons. The solutions were prepared in the same way as described previously in the control experiment. Figure 60 below shows the hydrolysis data of 50 µM BTNA (substrate) with different functionalized GOs over 300 seconds.

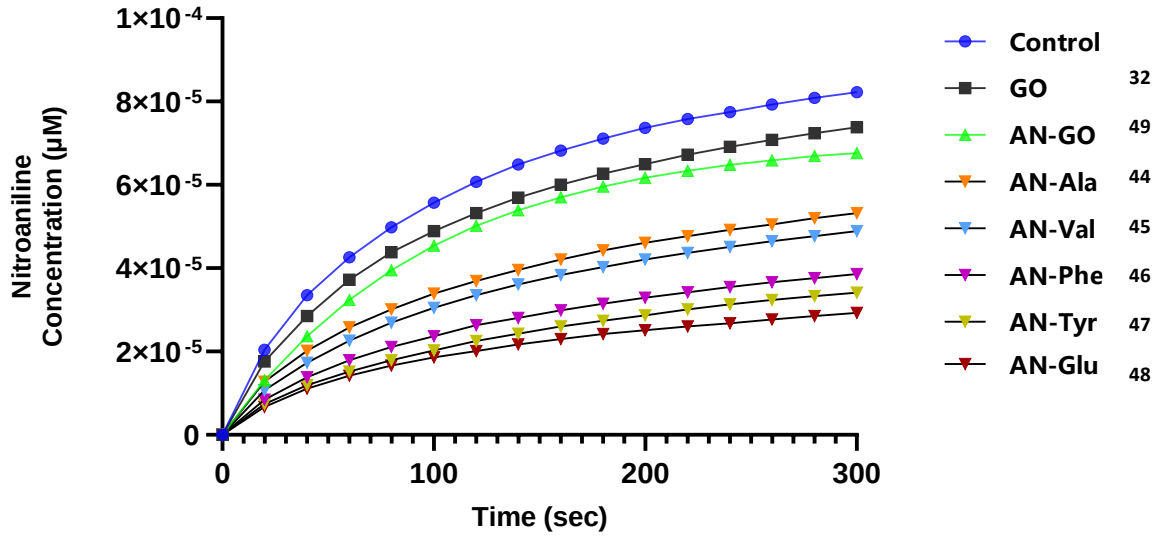

Figure 60- Rate plots comparing the hydrolysis of BTNA with various functionalized GOs.

During the enzyme reaction, there is an initial burst. During the initial burst stage, the hydrolyzed product from the first reaction remains within the active site and only moves away slowly, preventing the new substrate entering. Therefore, the second (and all other) hydrolysis events are slower than the first. Initial velocities were therefore obtained from the gradient of the linear region between 20 and 60 seconds.

Table 6 and Figure 61 illustrate the initial velocities that are calculated using data obtained over the first 60 seconds. In all cases, the reaction profiles and initial velocities were reduced when compared to the reaction rate of the GO control.

BTNA [S]= 50 µM	Control	GO **32**	AN-GO **49**	AN-Ala **44**	AN-Val **45**	AN-Phe **46**	AN-Tyr **47**	AN-Glu **48**
(V_o) (x $10^{-7}Ms^{-1}$)	5.60	4.89	4.82	3.25	2.97	2.37	1.95	1.87
Extent of Reaction %	100	87	86	58	53	42	34	33
Relative Binding %	0	13	14	42	47	58	66	67

Table 16-The summary of initial velocity data of various functionalised GO.

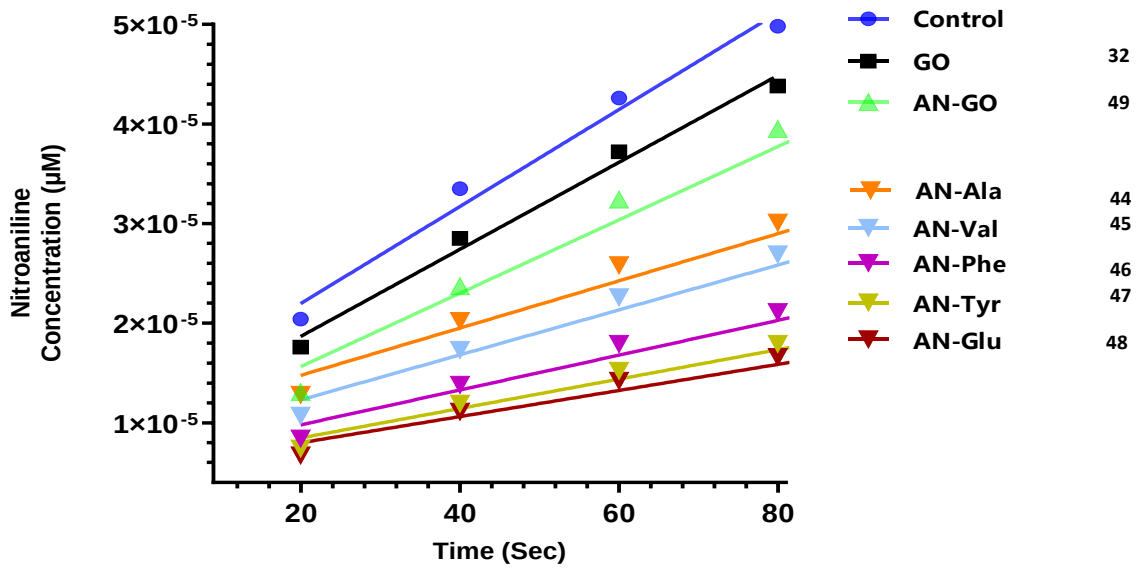

Figure 61- Initial rate plots for the hydrolysis of BTNA (substrate) with various functionalized GOs over 60 sec.

It is clear from the data presented in Figure 59 and Table 15 that surface-functionalized GOs exhibit stronger inhibition compared to native GO. The introduction of additional carboxylic moieties to the surface of GO using anthracene-GO (AN-GO) **49** increases their interaction with proteins due to the addition of negatively charged carboxylate groups. However, there is no significant difference in the inhibition percentage between GO **32** and AN-GO **49**, because the carboxylic acid group lies flat against the surface and is limited in geometry when binding

to the enzyme. Notably, the double carboxylic acid glutamic acid-functionalized GO **48** exhibited a remarkable relative binding percentage of approximately 67%. Tyrosine **47** performs better than phenylalanine **46** due to the additional hydrogen bonding capacity provided by the phenolic hydroxyl groups (-OH) in tyrosine. It is often reported that valine **45** and alanine **44** not important with respect to protein binding, because they do not contain suitable functionality to interact electrostatically with the protein.[32] However, alanine **44** and valine **45** do provide hydrophobic interactions, help GO interact with the protein. Alanine 44 demonstrated less inhibition than valine **45**, which has a larger hydrophobic side chain and can presumably provide a stronger hydrophobic interaction.

Although these covalent systems bind well to the target protein, binding is not optimised. The functional groups (amino acids) are fixed to the GO surface, and the protein must "explore" the GO surface to try and maximise binding. As a result, some of the functional groups may not be in a suitable position to bind. To maximise binding, the functional groups would need to move and find their optimum interactions with the target protein. In principle, this is possible if we adopt a non-covalent/dynamic approach. In this approach, the functional groups will be able to move and form the strongest GO-protein complex. The following section describes our initial efforts towards proving that a dynamic approach may work.

3.6.4 A dynamic, non-covalent functionalization of GO

In the previous section, we discussed the inhibition properties of the covalent systems on the surface of GO **32**, through Diels Alder reactions.

In contrast, non-covalent functionalization can be achieved through hydrogen bonding, ionic bonding, and electrostatic interactions. These are straightforward procedures that can be performed under mild conditions. Furthermore, the use of non-covalent reactions preserves the structure and properties of GO.[80]

In order to achieve our aim of developing a dynamic process for enhanced protein binding, we need to synthesise a library of non-covalently functionalised GOs and compare the inhibitory efficiency with the data obtained using the covalently surface-functionalized GOs described above. For a direct comparison, it is important that we use the same amino acids and achieve a GO coverage that is similar in both cases. We propose to obtain a noncovalently functionalized graphene oxide using the same amino acid functionalised anthracenes. However, in this functionalisation would be achieved using non-covalent π-π interactions between the amino acid anthracenes and the aromatic GO surface. Assuming the surface coverage/loadings are the same for the non-covalent and covalent systems, then we would expect to observe

stronger interactions for the non-covalent GO systems. This is because the non-covalent functionalised anthracenes should be able to move across the GO surface, which enables optimum binding to occur (between GO and the target protein).

The non-covalent GO systems were prepared by dispersing exfoliated GO in Milli-Q water and adding an equal amount of the amino acid functionalised anthracenes, followed by a 30-minute sonication in cold water. The mixture was then stirred for 24 hours, before the mixture was dialyzed using a 5 mM sodium phosphate buffer at pH 7.4. The final product was obtained after the solution was lyophilized.

To investigate our proposed dynamic hypothesis, graphene oxide functionalized both covalently and non-covalently with valine and phenylalanine were evaluated for their protein binding capabilities. Comparing the elemental analysis data and the amount of amine allows us to estimate the level of coverage, which is important if we want to make a direct comparison. The elemental analysis and carbon to nitrogen ratio for both systems are shown in Table 17.

Based on the elemental analysis, these systems have relatively similar nitrogen content and therefore similar coverage over the GO surface.

Compound Name	C [%]	H [%]	N [%]	O [%]	C/N
AN-Val covalent **45**	61.08	4.27	1.69	32.96	36
AN-Val non-covalent **53**	58.90	4.37	1.71	35.02	35
AN-Phe covalent **46**	50.84	3.44	1.27	44.45	39
AN-Phe non-covalent **54**	52.96	4.11	1.52	41.41	35

Table 17-The elemental analysis of GO functionalized with anthracene-Val (**45**,**53)** and Phe (**46**,**54**) both covalently and non-covalently.

The inhibition study for both systems was conducted using the same procedure and concentration as described in section (3.6.3). The data in Table 18 and Figure 62 summarises the results and highlight the parameters for both systems. The data clearly shows a decreased rate of reaction for the non-covalent system suggests compared to the equivalent covalent system. The inhibition efficacy between these systems differs by approximately 7% in favour of the non-covalent system. This result clearly supports our hypothesis that a dynamic approach can provide the optimum binding environment. In contrast, static nature of the covalent system limits binding.

BTNA [S]= 50 µM	AN-Val Covalent **45**	AN-Val non-covalent **53**	AN-Phe Covalent **46**	AN-Phe non-covalent **54**
(V_o) (x $10^{-7}Ms^{-1}$)	2.9	2.5	2.3	1.9
Extent of Reaction %	52	45	41	34
Relative Binding %	48	55	59	66

Table 18- Summaries the kinetic parameters for reactions inhibited by functionalized GO covalently and non-covalently with (**45**,**53)** and Phe (**46**,**54**).

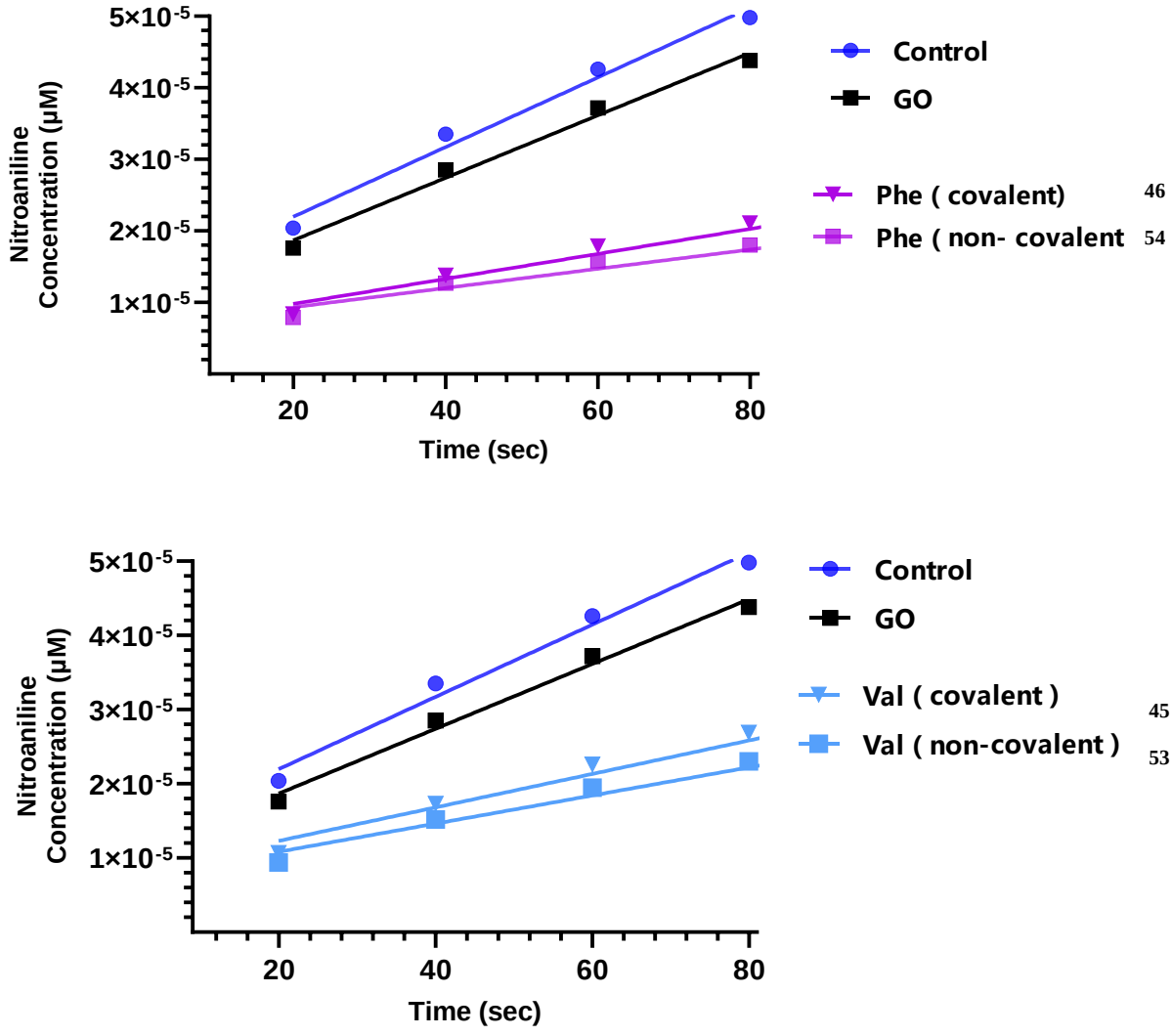

Figure 62- Rate plots comparing the hydrolysis of BTNA using GO functionalized in different ways with Phe (**46**, **54**) at the top and Val (**45**, **53**) at the bottom.

3.6.5 A comparison of Homo and Hetero functionalised systems for protein binding

In the previous experiments, the GO was functionalized with a single amino acid – a homo functionalization. After successfully studying the binding in different systems, we need to test our hypothesis that the interaction of less effective amino acids can be enhanced by using a hetero GO system, which is functionalized with a mixture of amino acids. This hypothesis predicts that a combination of amino acids may result in greater inhibition than using a single amino acid. The reason behind this is the various interactions and forces generated on the protein surface, such as π-π stacking, electrostatic, hydrogen bonding, and hydrophobic binding. For instance, within the homo system, primary interactions on the surface of α-chymotrypsin involve individual amino acids like glutamic acid through a single interaction (electrostatic in this case). In contrast, it is possible to have many different types of interactions using a hetero system. This can be achieved using GO functionalized with a mixture of amino acid anthracenes. It is predicted that these hetero complexes will exhibit an overall stronger binding through cooperative interactions involving electrostatic, hydrophobic, and π-π stacking (Figure 63).

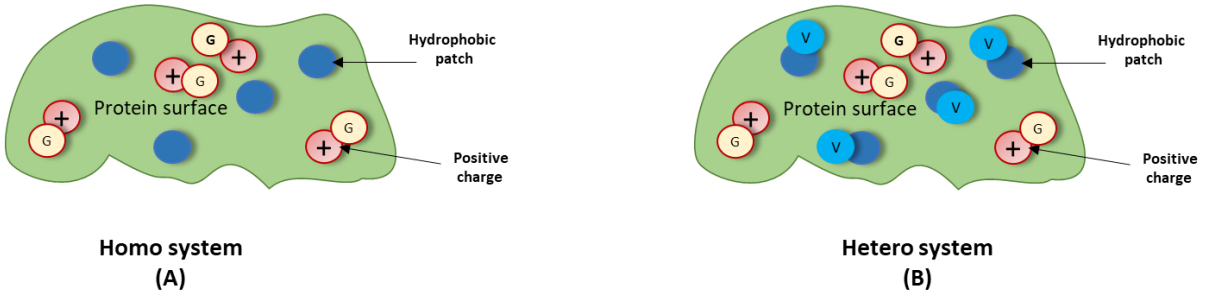

Figure 63- Schematic showing a 2D "top down" representation of a protein hotspot.

For a homo system, there is only one functional group on the GO, and this can only bind to one type of complementary group on the protein surface. For example, (A) shows the carboxylates from the glutamic acid-functionalized GO (shown as G) interacting with the ammonium groups on the protein's surface (shown as "+" on the schematic). However, a hetero system has several functional groups that can interact with many more types of complementary groups on the protein surface. Therefore, even weakly interacting groups can contribute significantly to the overall binding through cooperative interactions. For example, (B) shows a hetero system with carboxylates from the glutamic acid functionalized GO and hydrophobic interactions from valine functionalized GO (shown as G and V, respectively) interacting with

ammonium groups and hydrophobic patches on the protein's surface (shown as "+" and blue circles on the schematic).

To evaluate the impact of a hetero/mixed system, enzymatic inhibition assays were performed using graphene oxide covalently modified with a blend of amino acid anthracenes. The anthracene concentration was consistent with that of the homogeneous system. Anthracenes modified with phenylalanine, glutamic acid, and valine were chosen for their capacity to form strong electrostatic interactions via their carboxylic acid groups. Glutamic acid contributes an additional powerful electrostatic interaction, and phenylalanine provides a substantial π-π interaction, facilitating the formation of robust bonds with chymotrypsin. Valine's hydrophobic side chain, however, has a lesser influence on the overall binding affinity with chymotrypsin.

Comparing the elemental analysis data with the amount of amine allows us to determine the level of coverage, which is crucial to making direct comparisons. Table 19 presents the elemental analysis and carbon-to-nitrogen ratios for both systems.

Compound Name	C [%]	H [%]	N [%]	O [%]	C/N
Mixed anthracene (covalent)	46.5	4.2	1.4	47.8	33
Mixed anthracene (non-covalent)	50.7	4.36	1.9	34.0	27

Table 19-The elemental analysis data of Hetero system functionalised covalently and non-covalently (with phenylalanine, glutamic acid, and valine).

Based on the elemental analysis, the non-covalent systems show a higher nitrogen content, indicating more extensive coverage of the GO surface (higher N% and lower O%). This suggests that the relative binding affinity of the non-covalent system will be higher.

To explore the impact of nitrogen content on binding, we performed inhibition studies on both non-covalent and covalent hetero systems, adhering to the same procedures and concentrations detailed in section (3.6.3), ensuring consistent amino acid concentrations across experiments. The findings, depicted in Table 20 and Figure 64, are encouraging; they clearly indicate that the dynamic non-covalent method is the most effective system. Notably, there is an 8% increase in inhibitory efficiency favoring the non-covalent system. This outcome not only corroborates the previous results but also solidly establishes a proof of concept for selective protein binding via dynamic combinatorial chemistry. The dynamic nature of this method permits the functionalized anthracenes to traverse the surface of the graphene oxide. Consequently, upon

introducing a protein, the anthracenes re-position to optimize interactions, thereby reducing the Gibbs free energy of the resulting anthracene/GO/protein complex.

BTNA [S]= 50 µM	Control	GO	Mixed anthracene (covalent)	Mixed anthracene (non-covalent)
(V_o) (x $10^{-7}Ms^{-1}$)	5.60	4.89	1.2	0.74
Extent of Reaction %	100	87	21	13
Relative Binding %	0	13	79	87

Table 20- Kinetic and inhibition parameters for reactions inhibited by functionalized GO using hetero system covalent and non-covalent (with phenylalanine, glutamic acid, and valine).

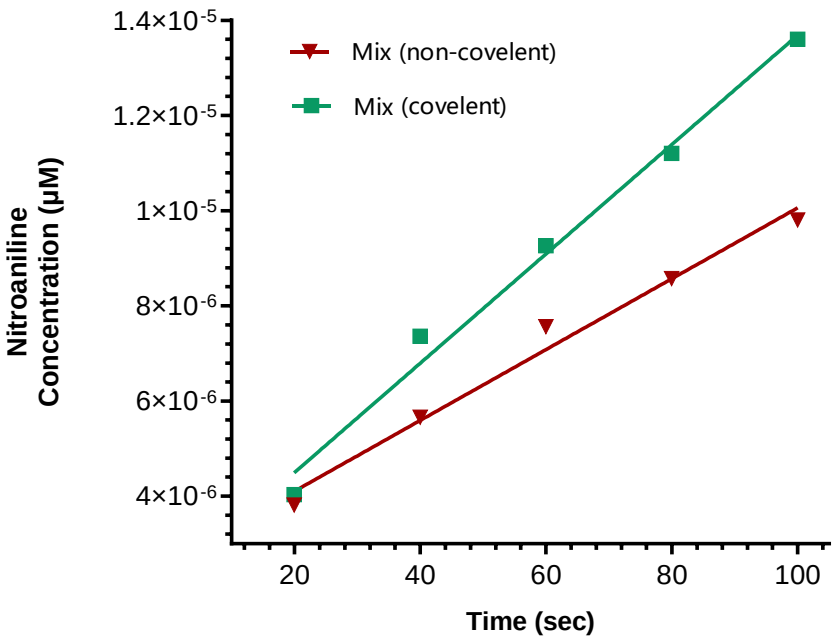

Figure 64-Illustration of the rate plots for the hydrolysis of BTNA using different hetero system of GO functionalized (with phenylalanine, glutamic acid, and valine).

Upon confirming the superior inhibition of the non-covalent hetero system over the covalent hetero system, our research expanded to include a comparison between hetero/mixed systems and individual/homogeneous systems. The binding studies followed the same protocol as outlined in section (3.6.3), maintaining the anthracene concentration remained consistent with that used in the homogeneous system. Initial rate data for the hetero/mixed system, presented in Figure 64 were compared with that of the glutamic acid-modified GO —the most effective

homogeneous GO system. The comparison of data between the hetero/mixed and individual/homogeneous systems, as detailed in Table 21, clearly indicates the superior performance of the mixed system over the glutamic acid-modified GO. This finding highlights the enhanced binding affinity achieved through combining different of amino acids, supporting the viability of a selective binding strategy using a mixed or combinatorial approach. Nevertheless, due to the limitations of controlling functional group via covalent modification, we explored a dynamic mixed strategy to potentially yield superior ligands for selective protein interaction.

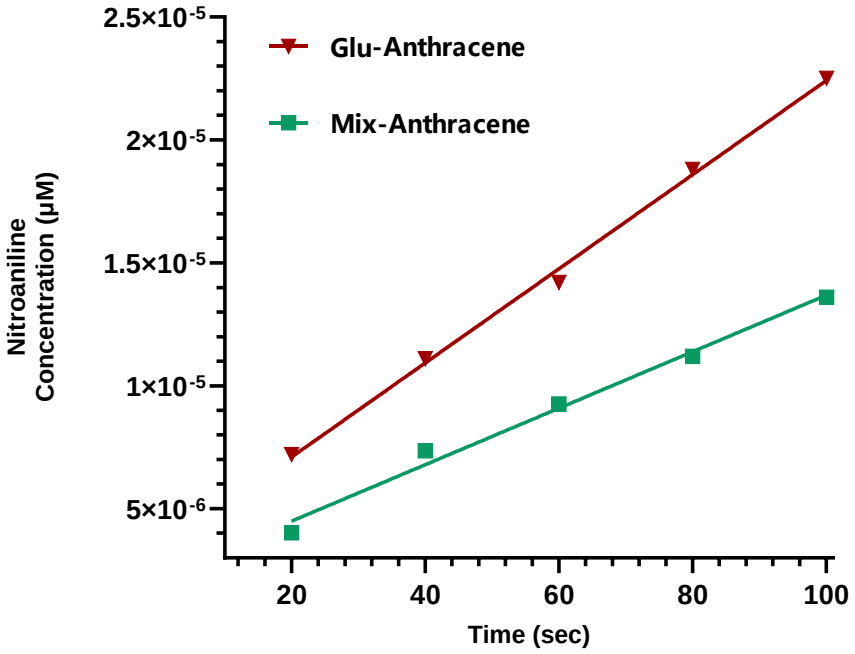

Figure 65- Initial velocity plots for covalent Glu- anthracene and the hetero system of GO functionalised (with phenylalanine, glutamic acid, and valine)- [S]= 50 µM.

	Control	Val-anthracene	Phe-anthracene	Glu-anthracene	Mixed anthracene (covalent)
(V_o) (x $10^{-7}Ms^{-1}$)	5.60	2.9	2.37	1.87	1.2
Extent of Reaction %	100	53	42	34	21
Relative Binding %	/	47	58	66	79

Table 21- Initial velocity data for covalent homo and hetero/mixed systems of (AN-Val **45**, AN-Phe **46** and AN-Glu **48)**

3.7 Summary

Our research aimed to develop a "proof of principle" for a dynamic approach to protein binding, focusing on the potential advantages of non-covalent interactions over traditional covalent methods. To accomplish this, we needed to devise a method to non-covalently functionalize graphene oxide (GO). This functionalization was critical, as it would enable us to explore the dynamic nature of protein binding through reversible interactions. Additionally, it was essential to develop a control experiment where the same functionalization could be achieved using covalent chemistry. This control setup would allow us to make a direct comparison between the two approaches and assess whether the non-covalent, dynamic method provided superior binding capabilities. Effectively, the covalent approach served as a benchmark for evaluating the efficacy of the dynamic interactions. For both methods to yield comparable results, it was crucial that they targeted the same region of GO—either the surface or the edges, but not both. To achieve this specificity, we employed aromatic molecules that could bind non-covalently to the aromatic surface of GO through π-π interactions. Moreover, these same aromatic molecules could also be covalently grafted to the GO surface via a Diels-Alder reaction, allowing for a systematic comparison of the binding properties achieved through these distinct methodologies.

This study concluded that the surface functionalization of graphene oxide (GO) could be utilized to specifically or selectively influence binding interactions with the interfacial areas of target proteins. The promising results obtained through covalent functionalization suggest that it can enhance binding affinity; however, its inherent rigidity and lack of movement may restrict its practical application in dynamic biological environments. This limitation could potentially be addressed by employing a hetero/mixed functionalization strategy on the GO surface, which could introduce flexibility while maintaining binding efficacy.

Our comparative analysis of non-covalent and covalent functionalized GO supports the notion that the non-covalent method is generally more effective. This is evidenced by the reduction in Gibbs free energy observed in the resulting complexes formed with the non-covalently modified GO. In addition, we employed inhibition assays as a tool to measure protein binding quantitatively. Our results revealed that several properties of amino acids—including hydrophobicity, hydrophilicity, aromaticity, and negative charge—significantly influence the degree of inhibition during binding interactions. These findings have substantially enhanced our understanding of the critical role of functionalization in optimizing graphene oxide for

protein binding applications. By highlighting the interplay between various molecular characteristics, we aim to pave the way for more effective use of GO in biotechnological and therapeutic contexts.

3.8 Future wark

Our findings approve that the dynamic approach that could “fix” the anthracenes after protein binding. This is important, because we need the anthracenes to remain fixed in their positions after the protein has been removed. This leaves behind the perfect GO ligand for the protein that was used to form the initial anthracene/GO/protein complex.

Circular dichroism (CD) is a valuable technique for examining the conformations of nucleic acids and the secondary structures of proteins, such as alpha helices and beta sheets. It enhances scientific understanding of the folding and functionality of these biomolecules. At 232 nm and 204 nm, two characteristic minima of α-chymotrypsin conformations appear in the CD spectra. Our group has utilized CD to assess whether complex formation has altered or denatured the protein structures[101,102]. By comparing the structure of the protein/dendrimer or GO complex with that of the native protein, it will be possible to identify any structural changes.[101,103]

Notably, our results indicate that both unfunctionalized and functionalized GO do not induce denaturation of Chy, preserving its functional state. We also applied the same CD technique to evaluate the impact of binding on protein stability across various temperatures. This investigation is essential to ascertain whether the GO systems, when complexed with proteins, exhibit enhanced or diminished stability under elevated temperature conditions, further contributing to our understanding of the dynamic interactions between GO and proteins.

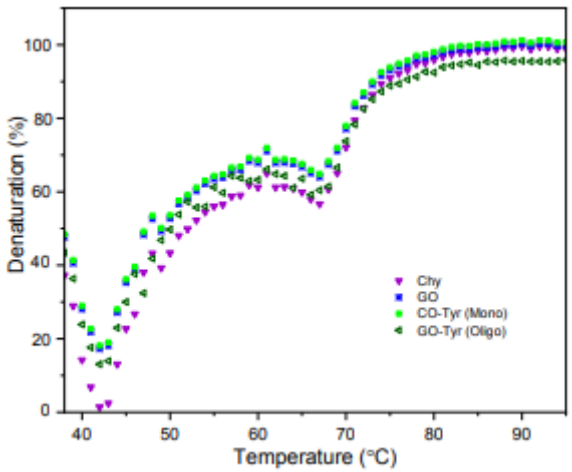

Figure 65 - Circular Dichroism (CD) spectra for chymotrypsin and complexes of chymotrypsin with different GO-Tyr systems.

Figure 65 presents the results, showing no differences in the extent of denaturation concerning temperature, as they generate similar plots. As a result, the GO systems' binding does not destabilize or stabilize the protein structures.[34]

In future studies, it would be valuable to examine the thermal stability of chymotrypsin when bound to a covalently linked graphene oxide (GO) system at elevated temperatures. Covalently bound GO systems are anticipated to offer increased selectivity in binding interactions compared to non-covalent methods. This experiment would involve incubating the samples and progressively increasing the temperature, while monitoring the intensity of the characteristic peak at 224 nm in the circular dichroism spectra. This approach aims to reveal any changes in protein stability and secondary structure under elevated thermal conditions.

3.9 Experimental

3.9.1 Instrumentation

RAMAN spectrometer

Raman spectra of samples were recorded from 500 to 3500 cm^{-1} on a Renishaw inVia Raman Microscope using a green laser operating at wavelength of 514.5 nm and laser power at 20 mV.

X-ray diffractometer (XRD)

XRD patterns were collected using a Bruker, D8 Advanced diffractometer with a copper target at the wavelength of λ CuKα = 1.54178 Å and a tube voltage of 40 kV and tube current of 35 mA, in the range of 5–100° at the speed of 0.05°/min

Elemental Analysis (EA)

The elements analysed using a Vario MICRO Cube CHN/S analyser and solid samples were used.

UV/Vis spectroscopy

The ultraviolet and visible absorbance of the solution was recorded on GENESYS™ 140/150 Vis/UV-Vis Spectrophotometers.

Infrared spectroscopy (IR)

Infrared spectra were recorded on a Perkin Elmer Paragon 1000 FTIR spectrometer.

Scanning Electron Microscope (SEM)

The samples were analysed by a JEOL-7001F operated at 15 kV. Solid samples were used for the SEM and EDX analysis.

Synthesis of Graphene Oxide (GO) 32

In a 1000 mL round bottom flask, graphite flakes (3.0 g, 1 wt. equiv) were added to a 9:1 mixture of concentrated H_2SO_4 / H_3PO_4 (360:40 mL). The reaction was stirred, and (18.0 g, 6 wt. equiv) of potassium permanganate ($KMnO_4$) was added slowly. The reaction was then heated and refluxed at 50 °C for 24 h. The reaction was cooled to room temperature, then poured onto ice (400 mL) with (3 mL) of 30% H_2O_2. The obtained suspension was centrifuged at 4000 rpm for 30 min. The, and the supernatant produced has been then decanted away to give. Then, the crude product. This was washed thoroughly with 400 mL of deionized water (DIW), 400 mL of HCl (37%), and 400 mL of ethanol until the pH of the rinsed water remained constant. The obtained product was coagulated using 400 mL of diethyl ether, and the and the suspension formed was collected by filtration. The resulting graphene oxide (GO) on the filter was dried at room temperature. The product (6.2 g) was obtained as a dark brown solid.

3.9.2 Synthesis of 9- carboxylic anthracene -Amino Acid Ligands

General synthesis procedure for the preparation of amino acid-conjugated 9-carboxylic anthracene:

9-Carboxylic anthracene (1.5 g, 6.74 mmol) was dissolved in a mixture of dry DCM and dry DMF (10:1). The reaction mixture was cooled for 15 minutes under ice conditions. After that, 2 equivalents of the coupling reagent (HBTU) were added to the reaction mixture and stirred for 15 minutes. The ester protected amino acids (double equivalent) were added along with N, N-diisopropylethylamine (0.026 mol, 3.48 g). The mixture was stirred under nitrogen for 24 hours. Then, deionized water (20 mL) was added, and the crude product obtained after extraction with DCM (4 × 15 mL). After collecting the organic layers, the solvent was dried and evaporated. The desired compound was characterized by ^{1}H-NMR.

Alanine conjugated 9- carboxylic anthracene 34

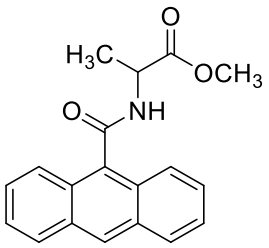

A double-neck round-bottom flask was used to dissolve 9-carboxylic anthracene (1.5 g, 6.74 mmol) was dissolved in a dry DCM and dry DMF (10:1) mixture. Then the reaction mixture was cooled for 15 minutes in an ice bath. After that, (5.11 g, 0.013 mol) of the coupling reagent (HBTU) was added to the reaction mixture and stirred for 15 minutes. The L-Alanine methyl ester (0.0134 mol, 1.88 g) was added in the basic condition in the presence of N-diisopropylethylamine (0.026 mol, 3.48 g). The mixture was stirred under nitrogen for 24 hours. The extraction and purification were followed as mentioned above. The product **34** (1.5 g, 73%) was obtained as a sticky yellow oil.

FTIR (vmax/cm^{-1}), 3219 (N-H), 2997(C-H), 1742 (C=O, ester), 1635 (C=O, amide), 1446 (C=C), 1206 (C-N amine); ^{1}H NMR (400 MHz, DMSO) δ 8.68 (1H, s, *p*-C<u>H</u>Ar), 8.13 (4H, m, Ar), 7.57 (4H, m, Ar), 4.71 (1H, m, C<u>H</u>) , 3.81 (s, 3H), 1.44 (d, , *J*= 7.2 Hz, 3H); ^{13}C NMR (100 MHz, DMSO) δ 173.6, 169.2 (C=O), 128.7- 125.7, 52.5 (-OCH3), 48.79 (C)17.02 (CH_3); Mass spec (ES) 308 (MH^+), ES-MS $C_{19}H_{17}NO_3$ = 307 (calculated).

Valine conjugated 9- carboxylic anthracene 35

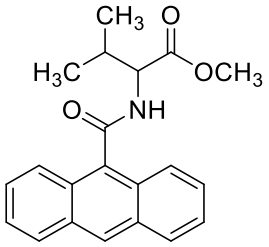

A double-neck round-bottom flask was used to dissolve 9-carboxylic anthracene (1.5 g, 6.74 mmol) was dissolved in a mixture of dry dichloromethane (DCM) and dry N,N-dimethylformamide (DMF) in a 10:1 ratio, then cooled in an ice bath for 15 minutes. To this, HBTU (0.013 mol, 5.11 g) was added, and the solution was stirred for an additional 15 minutes. L-valine methyl ester (0.013 mol, 2.26 g) and N,N-diisopropylethylamine (0.026 mol, 3.48 g) were then added, and the mixture was stirred under nitrogen atmosphere for 24 hours.

Following extraction and purification, a sticky yellow oil of valine-conjugated 9-carboxylic anthracene **35** was obtained, yielding 1.7 g (82%).

FTIR (νmax/cm^{-1}), 3315 (N-H), 2955 (C-H), 1732 (C=O, ester), 1647 (C=O, amide), 1524 , 1436 (C=C), 1207.6 (C-N); ^{1}H NMR (400 MHz, DMSO) δ 8.68 (1H, s, *p*-C<u>H</u>$_{Ar}$), 8.11 (4H, m, Ar), 7.56 (4H, m, Ar), 4.62 (1H, m, C<u>H</u>), 3.82 (3H, s, OC<u>H</u>$_3$), 2.22 (1H, m, C<u>H</u>), 1.05 (3H, *J*= 7.2 Hz, d), 0.98(3H, *J*= 7.2 Hz, d); ^{13}C NMR (100 MHz, DMSO) δ 172.6, 169.5 (C=O), 133.2-124.0(*C*-Ar), 58.9(C), 52.3 (-OCH_3), 29.2 (<u>C</u>-CH_3)$_2$,19.6, 18.9(CH_3); Mass spec (ES) 336 (MH^+), ES-MS $C_{21}H_{21}NO_3$ = 335 (calculated).

Phenylalanine conjugated 9- carboxylic anthracene 36

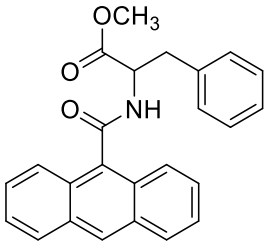

A double-neck round-bottom flask was used to dissolve 9-carboxylic anthracene (1.5 g, 6.74 mmol) was dissolved in a mixture of dry dichloromethane and dry dimethylformamide in a 10:1 ratio. The solution was cooled in an ice bath for 15 minutes before adding HBTU (0.013 mol, 5.11 g) with continued stirring for another 15 minutes. Under basic conditions provided by N,N-diisopropylethylamine (DIPEA) (0.026 mol, 3.48 g), L-phenylalanine methyl ester (0.013 mol, 2.19 g) was then added. The reaction mixture was stirred under a nitrogen atmosphere for 24 hours, followed by extraction and purification. This process yielded a sticky yellow oil of phenylalanine-conjugated 9-carboxylic anthracene **36** (1.41 g, 68% yield).

FTIR (νmax/cm^{-1}) , 3162 (N-H), 2319 (C-H), 1726 (C=O, ester), 1627 (C=O, amide), 1449 (C=C aromatic), 1223 (C-N); ^{1}H NMR (400 MHz, MeOD) δ 8.54 (1H, s, *p*-C<u>H</u>$_{Ar}$), 8.14 (4H, m, Ar), 7.79 (4H, m, Ar), 7.39 (5H, m, C<u>H</u>$_{Ar(Phe)}$), 5.33 (1H, m, C<u>H</u>), 3.93 (3H, s , OC<u>H3</u>), 3.51 (m, 1H, diastereotopic C<u>H</u>$_2$), 2.98 (m, 1H, diastereotopic C<u>H</u>$_2$); ^{13}C NMR (100 MHz, MeOD) δ 171.8, 167.4 (C=O), 132.2- 125.1(*C*-Ar), 52.3 (*C*), 51.5 (-OCH_3), 36.5 (CH_2); Mass spec (ES) 384 (MH^+), ES-MS $C_{25}H_{21}NO_3$ = 383 (calculated).

Tyrosine conjugated 9- carboxylic anthracene 37

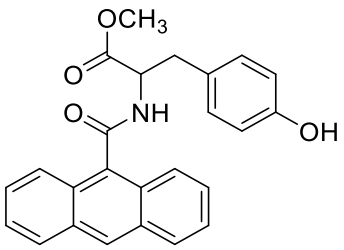

9-Carboxylic anthracene (1.5 g, 6.74 mmol) was dissolved in a combination of dry DCM and dry DMF (10:1) in a double-neck round bottom flask. Subsequently, the reaction mixture was stirred for 15 minutes in an ice bath. This was followed by the addition of the coupling reagent HBTU (0.013 mol, 5.11 g), and the mixture was stirred for another 15 minutes. L-tyrosine methyl ester (0.013 mol, 2.46 g) was then added under basic conditions in the presence of N-diisopropylethylamine (0.026 mol, 3.48 g). The mixture was stirred under nitrogen for 24 hours. The extraction and purification procedures were carried out as previously described, resulting in a sticky yellow oil product **37** (1.36 g, 66% yield).

FTIR (vmax/cm^{-1}) , 3261 and 3034 (N-H), 2319 (C-H),1713 (C=O, ester), 1638 (C=O, amide), 1515 (C=C), 1219 (C-N); ^{1}H NMR (400 MHz, DMSO) δ 8.63 (1H, s, *p*-C$\underline{H}_{Ar}$), 8.10 (4H, m, Ar), 7.54 (4H, m, Ar), 7.15 (2H, d, *J*= 8.4 Hz, *m*-C$\underline{H}_{Ar(Tyr)}$), 6.77 (2H, d, *J*= 8.4 Hz, *o*-C$\underline{H}_{Ar(Tyr)}$), 5.04 (1H, m, C$\underline{H}$), 3.82 (3H, s, OC$\underline{H3}$), 3.17 (1H ,m, diastereotopic C$\underline{H_2}$), 2.83 (1H ,m, diastereotopic C$\underline{H_2}$); ^{13}C NMR (100 MHz, MeOD) δ 172.5, 171.1 (C=O), 164.6 (C-OH), 130.0-115.1(*C*-Ar), 54.3(*C*), 51.5 (-OCH_3), 37.8 (CH_2); Mass spec (ES) 400 (MH^+), ES-MS $C_{25}H_{21}NO_4$ = 399 (calculated).

Glutamate conjugated 9- carboxylic anthracene 38

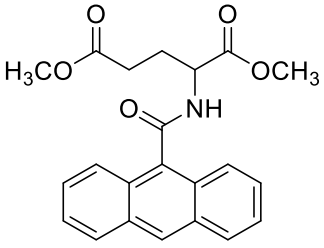

After dissolving 9-carboxylic anthracene (1.5 g, 6.74 mmol) in a dry DCM and dry DMF (10:1) mixture in a double-neck round-bottom flask, the mixture was cooled in an ice bath for 15 minutes. Subsequently, the reaction mixture was combined with the coupling reagent HBTU (0.013 mol, 5.11 g) and stirred for 15 minutes. L-glutamic acid dimethyl ester (0.013 mol, 2.85 g) was then added under basic conditions with N,N-diisopropylethylamine (0.026 mol, 3.48 g),

and the mixture was stirred under nitrogen for 24 hours. The extraction and purification were carried out as previously described, yielding a sticky yellow oil **38** (1.08 g, 53%).

FTIR (νmax/cm^{-1}), 3225 (N-H), 2951 (C-H),1734 (C=O, ester), 1628 (C=O, amide),1554 (C=C aromatic) and 1437 (N-H), 1206 (C-N amine); ^{1}H NMR (400 MHz, DMSO) δ 8.69 (1H, s, *p*-C$\underline{H}_{Ar}$), 8.14 (4H, m, Ar), 7.58 (4H, m, Ar), 4.72 (1H, m, C$\underline{H}$), 3.82- 3.56 (2x 3H, s , OC$\underline{H3}$), 2.62 – 2.57 (m, 2H, diastereotopic C$\underline{H_2}$), 2.17 – 1.97 (m, 2H, diastereotopic C$\underline{H_2}$); ^{13}C NMR (100 MHz, DMSO) δ 173.0, 172.7, 169.2 (C=O), 132.8- 125.5(*C*-Ar), 52.6, 51.9 (-OCH_3), 30.3- 25.9 (CH_2); Mass spec (ES) 380 (MH^+), ES-MS $C_{22}H_{21}NO_5$ = 379 (calculated).

General procedure for deprotected anthracene-amino acid conjugates

Each methyl ester amino acid-conjugated 9-carboxylic anthracene was dissolved in a solvent mixture consisting of MeOH, THF, and 3M NaOH in a (2:2:1) ratio. The reaction mixture was then stirred at room temperature for a duration of 16 hours, allowing for the complete hydrolysis of the methyl ester to yield the corresponding carboxylic acid. Following this, the pH of the mixture was carefully adjusted to 7 using a 2 M HCl solution, ensuring a neutral environment for subsequent processing. After concentrating the mixture, the residue in the aqueous solution was acidified to pH 3 by the gradual addition of 2 M HCl, which facilitated the precipitation of the desired compound. The resulting solid was then filtered, thoroughly washed with deionized water to remove any impurities, and finally dried to yield the target product.

Hydrolysis of 9- anthracene with alanine methyl ester 39

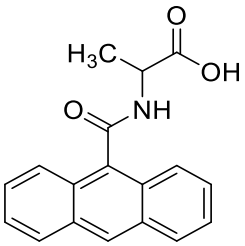

Anthracene-alanine methyl ester (1.03 g, 3.35 mmol) was dissolved in a solvent mixture consisting of 20 mL MeOH, 20 mL THF, and 10 mL 3M NaOH. The resulting mixture was stirred at room temperature for a duration of 16 hours, allowing for the hydrolysis of the methyl ester to occur. This process was conducted under conditions similar to those previously described to ensure consistency in the reaction environment. After the reaction was completed, the mixture was processed to isolate the product. The yield obtained from this procedure was 0.88 g, 86% yield, and the final product **39** was characterized as a yellow powder.

FTIR (νmax/cm^{-1}) 3195 (O-H), 3053 (N-H),1712 (C=O, ester), 1629 (C=O, amide), 1543, 1447 (C=C), 1243 (C-O), 1207 (C-N); ^{1}H NMR (400 MHz, DMSO) δ 8.67 (1H, s, *p*-C$\underline{H}_{Ar}$), 8.13 (4H, m, Ar), 7.56 (4H, m, Ar), 4.64 (1H, m, C$\underline{H}$), 1.43 (3H, *J*= 6.8 Hz, d); ^{13}C NMR (100 MHz, DMSO) δ 172.2, 167.9 (C=O), 129-125.1 (*C*-Ar), 44.1(*C*), 17.1 (CH_3); Mass spec (ES) 294 (MH^+), ES-MS $C_{15}H_{21}NO_3$ = 293 (calculated).

Hydrolysis of 9- anthracene with valine methyl ester 40

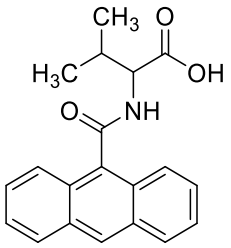

Anthracene-phenylalanine methyl ester (1.1 g, 2.7 mmol) was solubilized in a solvent mixture of 20 mL MeOH, 20 mL THF, and 10 mL 3M NaOH. The resulting solution was subjected to stirring at ambient temperature for a duration of 16 hours to facilitate the hydrolysis of the methyl ester functionality. Upon completion of the reaction, the mixture was processed to isolate the target product. The resultant yield was determined to be 0.82 g, corresponding to an 82% yield, with the final product **40** characterized as a yellow powder.

FTIR (νmax/cm^{-1}) 3203 (O-H), 3053 (N-H), 1725 (C=O, ester), 1624 (C=O, amide), 1521, 1446 (C=C), 1206 (C-O), 1153 (C-N); ^{1}H NMR (400 MHz, DMSO) δ 8.60 (1H, s, *p*-C$\underline{H}_{Ar}$), 8.11 (4H, m, Ar), 7.54 (4H, m, Ar), 4.79 (1H, m, C$\underline{H}$), 2.37 (m, 1H), 1.20 (3H, *J*= 7.2 Hz, d), 1.09 (3H, *J*= 7.2 Hz, d); ^{13}C NMR (100 MHz, DMSO) δ 173.5, 172.0 (C=O), 128.36 - 124.4 (*C*-Ar), 51.7 (*C*), 29.8 ($\underline{C}$-CH_3), 18.6, 17.34 (CH_3); Mass spec (ES) 322 (MH^+), ES-MS $C_{20}H_{19}NO_3$ = 321 (calculated).

Hydrolysis of 9- anthracene with phenylalanine methyl ester 41

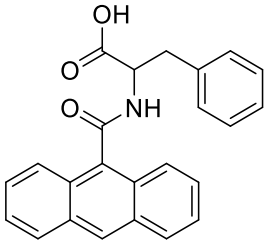

Anthracene-phenylalanine methyl ester (1.1 g, 2.7 mmol) was dissolved in a solvent mixture of 20 mL MeOH, 20 mL THF, and 10 mL 3M NaOH. The reaction mixture was stirred at room temperature for a period of 16 hours to facilitate the hydrolysis of the methyl ester group. Following this period, the mixture was processed to isolate the product. The final yield was determined to be 0.82 g, representing an 82% yield of the desired anthracene-phenylalanine conjugate **41**, characterized as a yellow powder.

FTIR (νmax/cm^{-1}) 3348 (N-H), 1720.30 (C=O, ester), 1612 (C=O, amide), 1511, 1442 (C=C), 1217 (C-O), 1203 (C-N); ^{1}H NMR (400 MHz, DMSO) δ 8.61 (1H, s, *p*-C<u>H</u>$_{Ar}$), 8.19 (4H, m, Ar), 7.64 (4H, m, Ar), 7.37 (5H, m, C<u>H</u>$_{Ar(Phe)}$), 5.05 (1H, m, C<u>H</u>), 3.57 – 3.52 (m, 1H, diastereotopic C<u>H</u>$_2$), 2.93 (m, 1H, diastereotopic C<u>H</u>$_2$); ^{13}C NMR (100 MHz, DMSO) δ 171.2, 167.3 (C=O), 133.9-124.2 (*C*-Ar), 52.3 (*C*), 31.7 (CH_2); Mass spec (ES) 370 (MH^+), ES-MS $C_{24}H_{19}NO_3$ = 369 (calculated).

Hydrolysis of 9- anthracene with tyrosine methyl ester 42

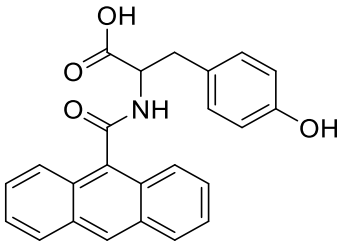

Anthracene-tyrosine methyl ester (1.1 g, 2.7 mmol) was dissolved in 20 mL MeOH, 20 mL THF, and 10 mL3M NaOH and stirred at room temperature for 16 hours, yielding 0.89 g (86%) of non-protected of 9- anthracene with tyrosine methyl ester **42** as yellow powder.

FTIR (νmax/cm^{-1}) 3252 (N-H), 1717 (C=O, ester), 1612 (C=O, amide), 1514, 1445 (C=C), 1209 (C-O), 1153 (C-N); ^{1}H NMR (400 MHz, DMSO) δ 8.61 (1H, s, *p*-C<u>H</u>$_{Ar}$), 8.18 (4H ,m, Ar), 7.59 (4H, m, Ar), 7.14 (2H, d, *J*= 7.5 Hz *m*- C<u>H</u>$_{Ar(Tyr)}$), 6.76 (2H, d, *J*= 7.2 Hz *o*-C<u>H</u>$_{Ar(Tyr)}$), 4.98 (1H ,m,), 3.20 (1H ,m, diastereotopic C<u>H</u>$_2$), 2.80 (1H ,m, diastereotopic C<u>H</u>$_2$); ^{13}C NMR (100 MHz, DMSO) δ 173.6,168.6 (C=O), 156.5 (<u>C</u>-OH), 133.4- 125.1 (*C*-Ar), 115.1 (*C*-Ar $_{tyr}$), 54.4 (*C*), 35.9 (CH_2); Mass spec (ES) 386 (MH^+), ES-MS $C_{24}H_{19}NO_4$ = 385 (calculated).

Hydrolysis of 9- anthracene with glutamate methyl ester 43

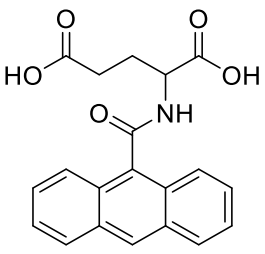

Anthracene-glutamate methyl ester (1.5 g, 3.9 mmol) was dissolved in 20 mL MeOH, 20 mL THF, and 10 mL 3M NaOH, then stirred at room temperature for 16 hours, the final product of **43** was 1.15 g (84%) obtained as yellow powder.

FTIR (νmax/cm^{-1}) 3278 (N-H), 1718 (C=O, ester), 1623 (C=O, amide), 1515, 1445(C=C), 1206 (C-N); ^{1}H NMR (400 MHz, DMSO) δ 8.67(1H, s, *p*-C$\underline{H}_{Ar}$), 8.14(4H, m, Ar), 7.57(4H, m, Ar), 4.65 (1H, m, C$\underline{H}$), 2.44 (m, 2H, diastereotopic C$\underline{H_2}$), 2.14 (m, 1H, diastereotopic C$\underline{H_2}$), 1.92 (m, 1H, diastereotopic C$\underline{H_2}$); ^{13}C NMR (100 MHz, DMSO) δ 147.31,173.51, 169.01 (C=O), 131.13-125.11(*C*-Ar), 52.32 (*C*), 31.06, 26.36 (CH_2); Mass spec (ES) 352 (MH^+), ES-MS $C_{20}H_{17}NO_5$ = 351 (calculated).

Covalent Functionalization of 9-Carboxylic Anthracene-Amino Acid Ligands with GO

An equivalent amount of graphene oxide and anthracene-terminated amino acid ligands were carefully weighed and subsequently dissolved in 5 mL of Milli-Q water. The mixture was then subjected to sonication for 15 minutes. Following sonication, the mixture was stirred continuously for 24 hours at a controlled temperature of 60 °C. Upon completion of the stirring period, the mixture was allowed to cool to room temperature. The resulting precipitate was then separated from the solution by centrifugation. The supernatant was carefully decanted, and the precipitate was subjected to freeze-drying to obtain the final product.

Non-covalent Functionalization of 9-Carboxylic Anthracene-Amino Acid Ligands with GO

To noncovalently functionalize GO with anthracene-terminated amino acid ligands, GO was first dispersed in Milli-Q water, followed by the addition of 9-carboxylic anthracene-conjugated amino acids to the solution. The mixture was sonicated in an ice bath for 30 minutes and then stirred for 24 hours. Subsequently, the reaction mixture was dialyzed in a 5 mM sodium phosphate buffer at pH 7.4, and the dialyzed solution was lyophilized to obtain the final product.

The Inhibition of α-Chymotrypsin using Functionalized GO with Anthracene-Amino Acid Ligands

Preparation of Phosphate Buffer

Disodium hydrogen phosphate (1.011 g) and monosodium dihydrogen phosphate (169.7 mg) were weighed and added to a 1 L volumetric flask. Then, 1000 mL of distilled water was added to give a buffer solution with a pH of 7.4. The pH was further adjusted to 7.46 using HCl or NaOH, resulting in a buffer solution with a concentration of 5 mM.

Preparation of Protein solutions

α-chymotrypsin (25 mg) was dissolved in 1000 mL sodium phosphate buffer (5 mM, pH 7.4) at 25 °C to give (1 x 10^{-6}M) solution of protein.

Preparation of 4 nitroaniline solution (Beer -Lambert)

A series of solutions containing 4-nitroaniline in methanol with different concentrations was prepared. The Δ absorption values were used at 405 nm and Beer- Lambert was employed to establish the relationship between absorbance and concentrations of 4-nitroanaline.

Assay of Chymotrypsin Activity

N-Benzoyl-L-tyrosine p-nitroanilide (BTNA) (0.045 g), was added to 10 mL of MeOH. Then, 2.5 mg of each specimen was dissolved in 100 mL of protein solutions and incubated for 30 min at 25 ºC.

For control experiment, a mixture of (1.0 mL α-chymotrypsin and 1.0 mL phosphate buffer) or 2.0 mL protein-GO/functionalised solution and was added to the cuvette containing 50 µL of BTNA. Hydrolysis was monitored by measuring product formation at 405 nm over a time periods of 300s. All absorption readings are recorded at least three times.

Chapter 4

Conclusions

4.0 Conclusion

In this thesis, two primary macromolecules were investigated for their capacity to bind to proteins: dendrimers and graphene oxide. Dendrimers, with their highly branched, tree-like structures, provide a unique platform for functionalization, allowing for the incorporation of various functional groups that can enhance their interactions with proteins. Similarly, graphene oxide, known for its two-dimensional structure and exceptional surface area, offers significant opportunities for modification and functionalization to improve protein recognition and binding.

In recent years, dendrimers have demonstrated significant potential for enhancing protein affinity, making them increasingly valuable in various biomedical applications. One of the primary advantages of dendrimers lies in their unique architecture, which allows them to encapsulate small host molecules within their globular structures, particularly at higher generations. This encapsulation capability not only increases the solubility of hydrophobic drugs but also facilitates the controlled release of therapeutic agents, thereby improving bioavailability and efficacy.

In this study, we focused on the synthesis of hydroxyl-ended (OH-ended) neutral dendrimers derived from ester-terminated dendrimers. This synthesis involved a strategic addition of ethanolamine, which facilitated the conversion of ester groups to hydroxyl groups, resulting in the formation of OH-ended dendrimers, specifically designated as 8OH, 16OH, and 32OH. This modification not only changed the chemical nature of the dendrimers but also enhanced their solubility and biocompatibility, making them more suitable for various biomedical applications.

Following the synthesis of these OH-ended dendrimers, we conducted a comprehensive evaluation of their ability to encapsulate several linear chains within their structure. This encapsulation capability is crucial as it allows the dendrimers to serve as functionalized systems capable of transporting biologically relevant molecules. The study specifically aimed to investigate the interaction between the dendrimer structures and different amino acid chains, as amino acids play a vital role in numerous biological processes and can influence the overall properties of the dendrimer-based systems.

To assess the encapsulation capabilities of the synthesized dendrimers, three distinct generations were selected for analysis: G1.5-OH **8**, G2.5-OH **9**, and G3.5-OH **10**. Each of these

generations was prepared at a concentration of 1×10^{-6} M. Our investigation included a variety of amino acid chains, which were chosen based on their unique properties and potential interactions with the dendrimer structures.

These chains were synthesized and functionalized with two amino acids: tyrosine and valine. Tyrosine is known to enhance protein-protein interactions due to its hydrophilic nature and ability to engage in hydrogen bonding, while valine tends to contribute less effectively to these interactions. The synthesis process commenced with propyl amine, followed by the stepwise addition of two β-alanine repeat units. This sequential addition was coupled with subsequent deprotection steps to yield the amine-terminated chain. For this purpose, the protecting group employed was N-benzyloxycarbonyl (Cbz), a strategy that allows for facile removal through catalytic hydrogenation using palladium on carbon (Pd/C) in the presence of a hydrogen atmosphere (H_2). Following the synthesis of the chain, the amino acids were introduced in their benzyloxy-protected forms, resulting in the synthesis of LC-Tyr **19** and LC-Val **20**. These compounds were obtained after a straightforward deprotection step, facilitating their incorporation into the functionalized dendrimers for further studies on protein interactions.

The encapsulation results demonstrated that the G3.5-OH**10** generation was the most effective at loading functionalized chains, achieving a loading capacity of 6. This suggests that G3.5-OH**10** dendrimers have an optimal combination of size, functionalization, and flexibility, enhancing their ability to interact with and encapsulate target chains.

A similar encapsulation experiment was undertaken to explore the incorporation of the porphyrin-signalling unit, zinc tetra(4-hydroxyphenyl)porphyrin (Zn-THPP), into the dendrimer architecture. The focus of this investigation was to evaluate how effectively the porphyrin unit could be integrated into the dendrimer system and how this integration could enhance the overall functionality of the resulting assembly.
When the binding and sensing units were integrated into the assembly program, the interaction between the two components allowed for effective detection of binding events. This enabled not only the qualitative assessment of the binding process but also the quantitative measurement of the binding affinity, as illustrated in Figure 66.

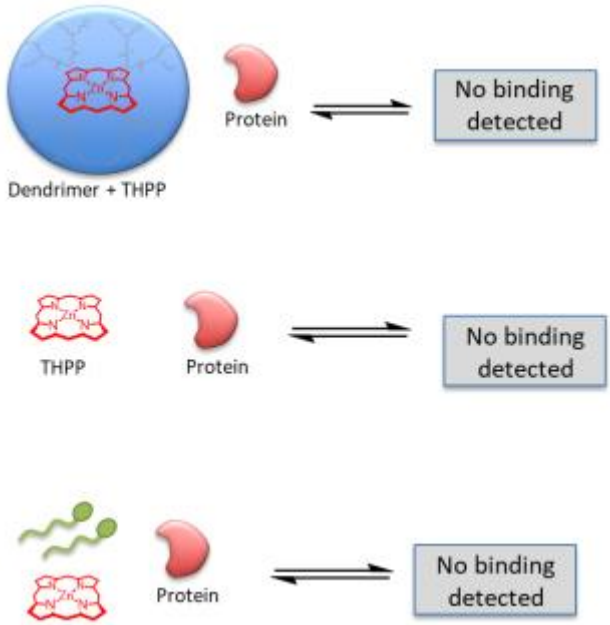

Figure 66 - No binding was detected when using the dendrimer, sensing, or binding units individually.

Detection and quantification of binding interactions were achieved by monitoring changes in the intensity of the emission band of Zn-THPP at 610 nm. This specific emission signal exhibits a quenching effect when cytochrome-c binds to the sensing unit, serving as a reliable indicator of the binding event. Notably, no binding was detected when the dendrimer, sensing unit, or binding unit was used individually, highlighting the necessity of the complete assembly for effective interaction. However, when all components—the dendrimer, functionalized chains, and sensing porphyrin—were combined and allowed to self-assemble, a significantly strong binding interaction was observed. As cytochrome-c was introduced in increasing concentrations, a marked decrease in the emission peak at 610 nm was recorded, further confirming the occurrence of protein binding. This correlation between the decrease in emission intensity and the concentration of cytochrome-c demonstrates the potential for precise quantification of protein interactions through this sensing mechanism.

It is important to note that the linear chain in the complex was oriented with the 'head' group facing outward, allowing it to interact with the protein surface. However, there is also a possibility that the linear chain's 'tail' of the linear chain may be exposed, enabling it to bind to the protein as well. By comparing the changes in porphyrin fluorescence intensity when cytochrome-c was added to the dendrimer complex for both LC-Tyr **19** and LC-Val **20**, we can assess the binding interactions. As the concentration of cytochrome-c was increased, the

intensity of the porphyrin signal did not decrease, indicating that no binding occurred. This was expected because valine is not typically effective in binding to protein surfaces, so that the system did not show any interaction.
The result served as a useful control, confirming the orientation of the amino acid chains within the dendrimer and demonstrating that the tyrosine head groups point outward to interact with the protein surface. If the tyrosine and valine head groups were buried within the dendrimer, both linear chains (LC-Tyr **19** and LC-Val **20**) would exhibit the same functionality at the surface, leading to identical dissociation constants, which was not observed.
Synthetic inhibitors of protein-protein binding offer promise for treating diseases like thromboembolism and hereditary angioedema.

Graphene oxide (GO) has garnered considerable attention as a synthetic inhibitor for protein binding due to its rich surface chemistry, particularly the abundance of carboxylic acid groups. These functional groups enable GO **32** to interact effectively with protein surfaces that are enriched in cationic functionalities, thereby facilitating potential inhibition of protein activity. Notably, in a landmark study conducted by De and Dravid in 2011, it was demonstrated that unfunctionalized GO **32** could bind to the active site of chymotrypsin, leading to a significant inhibition of its enzymatic function. This pioneering work laid the foundation for subsequent investigations aimed at enhancing the inhibitory capabilities of GO **32** through strategic functionalization with amino acids.

In exploring the mechanisms underlying GO's interactions with proteins, it is essential to recognize that these interactions are governed by a combination of electrostatic, π-π, and hydrophobic forces. The electrostatic interactions arise from the presence of carboxylic and hydroxyl groups on the GO surface, while the hydrophobic and π-π interactions are facilitated by the aromatic patches present on the material. These diverse interactions contribute to the complex nature of GO's binding behaviour and its potential applications in biological systems.

Further studies conducted by Subrata and De investigated the inhibitory effects of various types of GO on protein interactions. They focused on comparing surface-functionalized GO with edge-functionalized GO, both of which were modified to incorporate similar amino acids. The researchers employed two distinct modification methods: the covalent attachment of carboxylic acid groups and the establishment of non-covalent π-π interactions with aromatic groups. Their findings revealed that the non-covalent approach was more effective in facilitating protein

binding compared to the covalent method. This observation suggests that utilizing a flexible, non-covalent strategy could be advantageous for the development of specific protein-binding ligands, enabling the design of tailored materials for various biomedical applications.

Our goal was to functionalize the aromatic compound anthracene with a selection of amino acids, followed by the covalent attachment of these functionalized compounds to graphene oxide (GO) via a Diels–Alder reaction. In addition to covalent bonding, we aimed to explore the potential for non-covalent interactions through π-π functionalization, capitalizing on the inherent properties of both anthracene and the amino acids.

When selecting amino acids for attachment to anthracene, we carefully considered several crucial properties, including hydrophobicity, hydrophilicity, aromaticity, and negative charge, as these characteristics play a pivotal role in influencing binding affinity to proteins. The amino acids chosen for this study included alanine, valine, phenylalanine, tyrosine, and glutamic acid. Among these, tyrosine and phenylalanine stand out for their significance in protein binding interactions. Tyrosine, in particular, is anticipated to exhibit stronger binding due to the presence of its hydroxyl group (-OH), which can engage in additional hydrogen bonding with protein surfaces, thus enhancing the overall affinity. Furthermore, the introduction of glutamic acid, characterized by its negative charge, is expected to facilitate stronger interactions with positively charged regions on protein surfaces, thereby further enhancing binding and inhibiting undesired interactions.

The covalent functionalization procedure began by mixing equal amounts of graphene oxide and anthracene-amino acid ligands in a small volume of Milli-Q water, followed by 30 minutes of sonication to ensure even dispersion and enhance interactions. The mixture was then stirred at 60°C for 24 hours. After cooling, the precipitate was separated by centrifugation and lyophilized.

The molecular weights of amino acids vary significantly, which complicates direct comparisons of their loading capacities in functionalization processes. However, their structural similarity to graphene oxide allows for effective elemental analysis, simplifying the assessment of loading efficiency. Given that amino acids serve as the only source of nitrogen in this context, we can estimate the loading based on their nitrogen content. Generally, most amino acids contain approximately 2% nitrogen, with the exception of glutamic acid and phenylalanine, which exhibit a lower nitrogen content of around 1%. Additionally, these two amino acids are characterized by reduced carbon percentages compared to others in the series.

Consequently, we can conclude that the loading capacities across the different amino acids are relatively comparable, despite the variations in their molecular weights and elemental compositions. This similarity provides a basis for understanding the effectiveness of functionalization with these amino acids in enhancing the properties of graphene oxide

We assessed the binding affinity of functionalized graphene oxide to proteins through an enzyme inhibition assay. This approach is particularly relevant because binding to the enzyme's surface can restrict substrate access to its active site, which is especially critical in positively charged enzymes. While electrostatic interactions play a significant role in this binding process, other types of interactions, such as hydrogen bonding and hydrophobic interactions, may also occur within the active site. Therefore, incorporating specific functionalities into graphene oxide could enhance selectivity for protein binding. To test this hypothesis, we evaluated the hydrolysis of BTNA by α-chymotrypsin, which served as a model enzyme for assessing the effectiveness of the functionalized graphene oxide in inhibiting enzymatic activity. This study not only highlights the potential of functionalized GO in modulating enzyme interactions but also provides insights into the mechanisms underlying selective protein binding.

Kinetic analysis revealed that surface-functionalized graphene oxides exhibit significantly stronger inhibition compared to native graphene oxide. Notably, glutamic acid-functionalized graphene oxide demonstrated an impressive binding efficiency of approximately 67%. In comparisons between amino acids, tyrosine outperformed phenylalanine, primarily due to its capacity to form additional hydrogen bonds through its hydroxyl groups, enhancing its binding affinity. Although both alanine and valine contribute to hydrophobic interactions with proteins, alanine displayed less inhibitory capacity than valine, which possesses a larger hydrophobic side chain that may facilitate greater interaction with the protein surface. However, it is important to note that the binding mechanisms within these covalent systems are not fully optimized. The fixed nature of the functional groups on the GO surface necessitates that the protein must explore its environment to achieve maximum binding, indicating a need for further refinement in the design of these functionalized graphene oxide systems for improved efficacy.

To establish a dynamic process aimed at enhancing protein binding, we propose the synthesis of a diverse library of non-covalently functionalized graphene oxides. This library will be compared to covalently surface-functionalized graphene oxides in terms of their inhibitory efficiency. By utilizing the same amino acids across both approaches and ensuring similar

coverage of graphene oxide, we anticipate that the non-covalently functionalized anthracenes will demonstrate stronger interactions with proteins. This is primarily attributed to their ability to move freely across the graphene oxide surface, thereby optimizing binding interactions. Such a comparative analysis will not only provide insights into the effectiveness of different functionalization strategies but also contribute to the development of more efficient protein-binding systems. Through this work, we aim to leverage the advantages of dynamic interactions to enhance functionality and specificity.

The non-covalent GO systems were created by dispersing exfoliated GO in Milli-Q water and mixing it with amino acid-functionalized anthracenes, followed by 30 minutes of sonication in cold water. The mixture was stirred for 24 hours, dialyzed using a 5 mM sodium phosphate buffer at 7.4 pH, and then lyophilized to obtain the final product.

To validate our dynamic hypothesis, we assessed the protein binding capabilities of (GO) functionalized with both covalent and non-covalent methods using valine and phenylalanine. We compared the elemental analysis data alongside the amine content to estimate the required level of coverage for a meaningful direct comparison.

The inhibition study for both covalent and non-covalent systems was carried out under identical conditions, with the results summarized in Table 8. The non-covalent system demonstrated an inhibition efficacy that was 7% higher than that of the covalent system. This finding supports our hypothesis that a dynamic approach enhances the binding environment, allowing for greater flexibility and adaptability in protein interactions. In contrast, the static nature of the covalent system appears to restrict its binding capabilities, limiting the potential for optimal protein interactions. These results underscore the importance of considering the dynamics of binding when designing functionalized systems for improved protein affinity and highlight the potential advantages of non-covalent functionalization strategies in biological applications.

BTNA [S]= 50 μM	**AN-Val covalent**	**AN-Val non-covalent**	**AN-Phe covalent**	**AN-Phe non-covalent**
(V_o) (x $10^{-7}Ms^{-1}$)	2.9	2.5	2.3	1.9
Extent of Reaction %	52	45	41	34
Relative Binding %	48	55	59	66

Table 8- Kinetic and inhibition parameters for reactions inhibited by different functionalization systems.

After successfully investigating binding in various systems, our focus has transitioned from utilizing single amino acid-functionalized graphene oxide (homo-functionalization) to examining mixed amino acid-functionalized graphene oxide (hetero-functionalization) to enhance protein binding. This new approach is grounded in the hypothesis that the combination of different amino acids will result in stronger inhibition owing to a broader range of interactions. These interactions may include electrostatic forces, hydrophobic effects, and π-π stacking, which collectively could facilitate more robust binding compared to systems functionalized with a single amino acid. By leveraging the unique properties and affinities of multiple amino acids, we aim to create a more versatile and effective platform for protein binding, potentially leading to improved performance in applications such as biosensing and therapeutic targeting.

To evaluate the impact of a mixed amino acid system, enzymatic inhibition assays were performed using graphene oxide that was covalently modified with a combination of phenylalanine, glutamic acid, and valine anthracenes. In this system, phenylalanine and glutamic acid are expected to significantly enhance binding through their strong π-π interactions and electrostatic attractions with chymotrypsin. Conversely, while valine's hydrophobic side chain may contribute to the overall binding affinity, its role is comparatively limited. This study aims to elucidate the synergistic effects of the mixed amino acids in facilitating stronger protein interactions, thus providing valuable insights into optimizing the functionalization of graphene oxide for enhanced enzyme inhibition.

The binding studies demonstrated that the hetero/mixed amino acid system exhibited superior performance compared to the homogeneous glutamic acid-modified graphene oxide, highlighting the enhanced binding affinity achieved through the combination of different amino acids . This improvement suggests that the diverse interactions provided by the mixed system—encompassing electrostatic, hydrophobic, and π-π interactions—contribute to a more favourable binding environment. However, the challenges associated with controlling the precise placement of functional groups in covalent modifications prompted the exploration of a dynamic mixed strategy. This approach aims to facilitate more selective protein interactions, leveraging the inherent mobility of non-covalently functionalized systems to optimize binding. By allowing the amino acids to adaptively engage with the protein surfaces, we anticipate improved efficacy in protein binding and inhibition.

Chapter 5

References

5.0 References

1 H. Lu, Q. Zhou, J. He, Z. Jiang, C. Peng, R. Tong and J. Shi, *Signal Transduct Target Ther*, 2020, 5, 213.

2 C.-S. Goh, D. Milburn and M. Gerstein, *Curr Opin Struct Biol*, 2004, 14, 104–109.

3 D. Reichmann, O. Rahat, M. Cohen, H. Neuvirth and G. Schreiber, *Curr Opin Struct Biol*, 2007, 17, 67–76.

4 S. Algar, M. Martín-Martínez and R. González-Muñiz, *Eur J Med Chem*, 2021, 211, 113015.

5 D. Vasudevan, S. S and K. Vaidyanathan, in *Textbook of Biochemistry for Medical Students*, Jaypee Brothers Medical Publishers (P) Ltd., 2016, pp. 36–36.

6 H. Yin and A. D. Hamilton, *Angewandte Chemie International Edition*, 2005, 44, 4130–4163.

7 M. W. Peczuh and A. D. Hamilton, *Chem Rev*, 2000, 100, 2479–2494.

8 L. Lo Conte, C. Chothia and J. Janin, *J Mol Biol*, 1999, 285, 2177–2198.

9 E. Fischer, *Berichte der deutschen chemischen Gesellschaft*, 1894, 27, 2985–2993.

10 D. E. Koshland, *Proceedings of the National Academy of Sciences*, 1958, 44, 98–104.

11 K. H. Pearce, M. H. Ultsch, R. F. Kelley, A. M. de Vos and J. A. Wells, *Biochemistry*, 1996, 35, 10300–10307.

12 A. A. Bogan and K. S. Thorn, *J Mol Biol*, 1998, 280, 1–9.

13 D. Baker and A. Sali, *Science (1979)*, 2001, 294, 93–96.

14 M. F. PERUTZ, *Nature*, 1970, 228, 726–734.

15 B. Ghebremedhin, *Infectious Diseases: Research and Treatment*, 2012, 5, IDRT.S7597.

16 D. Wu, Y. Li, L. Zheng, H. Xiao, L. Ouyang, G. Wang and Q. Sun, *Acta Pharm Sin B*, 2023, 13, 4060–4088.

17 W. K. ALDERTON, C. E. COOPER and R. G. KNOWLES, *Biochemical Journal*, 2001, 357, 593.

18 M. A. Cinelli, H. T. Do, G. P. Miley and R. B. Silverman, *Med Res Rev*, 2020, 40, 158–189.

19 M. M. He, A. S. Smith, J. D. Oslob, W. M. Flanagan, A. C. Braisted, A. Whitty, M. T. Cancilla, J. Wang, A. A. Lugovskoy, J. C. Yoburn, A. D. Fung, G. Farrington, J. K. Eldredge, E. S. Day, L. A. Cruz, T. G. Cachero, S. K. Miller, J. E. Friedman, I. C. Choong and B. C. Cunningham, *Science (1979)*, 2005, 310, 1022–1025.

20 D. Jang, A.-H. Lee, H.-Y. Shin, H.-R. Song, J.-H. Park, T.-B. Kang, S.-R. Lee and S.-H. Yang, *Int J Mol Sci*, 2021, 22, 2719.

21 M. Lanning and S. Fletcher, *Biology (Basel)*, 2015, 4, 540–555.

22 C. G. Cummings and A. D. Hamilton, *Curr Opin Chem Biol*, 2010, 14, 341–346.

23 W. Guo, J. A. Wisniewski and H. Ji, *Bioorg Med Chem Lett*, 2014, 24, 2546–2554.

24 R. K. Jain and A. D. Hamilton, *Org Lett*, 2000, 2, 1721–1723.

25 H. S. Park, Q. Lin and A. D. Hamilton, *Proceedings of the National Academy of Sciences*, 2002, 99, 5105–5109.

26 H. Zhou, L. Baldini, J. Hong, A. J. Wilson and A. D. Hamilton, *J Am Chem Soc*, 2006, 128, 2421–2425.

27 L. Baldini, A. J. Wilson, J. Hong and A. D. Hamilton, *J Am Chem Soc*, 2004, 126, 5656–5657.

28 S. J. Riedl, W. Li, Y. Chao, R. Schwarzenbacher and Y. Shi, *Nature*, 2005, 434, 926–933.

29 F. Chiba, T.-C. Hu, L. J. Twyman and M. Wagstaff, *Chemical Communications*, 2008, 4351.

30 N. O. Fischer, C. M. McIntosh, J. M. Simard and V. M. Rotello, *Proceedings of the National Academy of Sciences*, 2002, 99, 5018–5023.

31 N. O. Fischer, A. Verma, C. M. Goodman, J. M. Simard and V. M. Rotello, *J Am Chem Soc*, 2003, 125, 13387–13391.

32 F. Chiba and Lance. J. Twyman, *Bioconjug Chem*, 2017, 28, 2046–2050.

33 I. Ahmad, A. Mozhi, L. Yang, Q. Han, X. Liang, C. Li, R. Yang and C. Wang, *Colloids Surf B Biointerfaces*, 2017, 159, 540–545.

34 A. A. Aziz and L. J. Twyman, *ACS Appl Mater Interfaces*, 2019, 11, 44941–44948.

35 J. N. H. Reek and S. Otto, Eds., *Dynamic Combinatorial Chemistry*, Wiley, 2010.

36 F. Schaufelberger, B. J. J. Timmer and O. Ramström, in *Dynamic Covalent Chemistry*, Wiley, 2017, pp. 1–30.

37 P. Frei, R. Hevey and B. Ernst, *Chemistry – A European Journal*, 2019, 25, 60–73.

38 D. E. Scott, G. J. Dawes, M. Ando, C. Abell and A. Ciulli, *ChemBioChem*, 2009, 10, 2772–2779.

39 J. M. A. Carnall, C. A. Waudby, A. M. Belenguer, M. C. A. Stuart, J. J.-P. Peyralans and S. Otto, *Science (1979)*, 2010, 327, 1502–1506.

40 F. Schaufelberger and O. Ramström, *Chemistry – A European Journal*, 2015, 21, 12735–12740.

41 A. W. Bosman, H. M. Janssen and E. W. Meijer, *Chem Rev*, 1999, 99, 1665–1688.

42 D. E. Heath and S. L. Cooper, in *Biomaterials Science: An Introduction to Materials: Third Edition*, Elsevier Inc., 2013, pp. 64–79.

43 S. Koltzenburg, M. Maskos and O. Nuyken, *Polymer Chemistry*, Springer Berlin Heidelberg, Berlin, Heidelberg, 2017.

44 D. A. Tomalia, H. Baker, J. Dewald, M. Hall, G. Kallos, S. Martin, J. Roeck, J. Ryder and P. Smith, *Polym J*, 1985, 17, 117–132.

45 E. BUHLEIER, W. WEHNER and F. VÖGTLE, *Synthesis (Stuttg)*, 1978, 1978, 155–158.

46 G. M. Dykes, *Journal of Chemical Technology & Biotechnology*, 2001, 76, 903–918.

47 Roseita Esfand and Donald A. Tomalia, *Elsevier Science Ltd*.

48 K. Inoue, *Functional dendrimers, hyperbranched and star polymers*, .

49 L. J. Twyman, A. S. H. King and I. K. Martin, 2002, preprint, DOI: 10.1039/b107812g.

50 P. J. Flory, *J Am Chem Soc*, 1952, 74, 2718–2723.

51 J. Wang, B. Li, L. Qiu, X. Qiao and H. Yang, *J Biol Eng*, 2022, 16, 18.

52 G. R. Newkome, Z. Yao, G. R. Baker and V. K. Gupta, *J Org Chem*, 1985, 50, 2003–2004.

53 B. Klajnert and M. Bryszewska, *Acta Biochim Pol*, 2001, 48, 199–208.

54 M. J. Cloninger, *Curr Opin Chem Biol*, 2002, 6, 742–748.

55 P. Patel, V. Patel and P. M. Patel, *Journal of the Indian Chemical Society*, 2022, 99, 100514.

56 S. M. Grayson and J. M. J. Fréchet, *Chem Rev*, 2001, 101, 3819–3868.

57 N. Taghavi Pourianazar, P. Mutlu and U. Gunduz, *Journal of Nanoparticle Research*, 2014, 16, 2342.

58 V. Balzani and F. Vögtle, *Comptes Rendus Chimie*, 2003, 6, 867–872.

59 S.-E. Stiriba, H. Frey and R. Haag, *Angewandte Chemie International Edition*, 2002, 41, 1329–1334.

60 A. DEMANUELE and D. ATTWOOD, *Adv Drug Deliv Rev*, 2005, 57, 2147–2162.

61 P. Kolhe, *Int J Pharm*, 2003, 259, 143–160.

62 L. J. Twyman, A. S. H. King and I. K. Martin, *Chem Soc Rev*, 2002, 31, 69–82.

63 P. Gilles, K. Wenck, I. Stratmann, M. Kirsch, D. A. Smolin, T. Schaller, H. de Groot, A. Kraft and T. Schrader, *Biomacromolecules*, 2017, 18, 1772–1784.

64 K. Vanlaldinpuia, H. A. Sema, L. Rokhum and G. Bez, *Chem Lett*, 2010, 39, 228–229.

65 T. Pawson and P. Nash, *Science (1979)*, 2003, 300, 445–452.

66 J. M. Shifman and S. L. Mayo, *Proceedings of the National Academy of Sciences*, 2003, 100, 13274–13279.

67 K. T. Savjani, A. K. Gajjar and J. K. Savjani, *ISRN Pharm*, 2012, 2012, 1–10.

68 M. T. Morgan, Y. Nakanishi, D. J. Kroll, A. P. Griset, M. A. Carnahan, M. Wathier, N. H. Oberlies, G. Manikumar, M. C. Wani and M. W. Grinstaff, *Cancer Res*, 2006, 66, 11913–11921.

69 B. Yavuz, S. Bozdağ Pehlivan and N. Ünlü, *The Scientific World Journal*, DOI:10.1155/2013/732340.

70 Y.-L. P. Ow, D. R. Green, Z. Hao and T. W. Mak, *Nat Rev Mol Cell Biol*, 2008, 9, 532–542.

71 M. Allhorn, A. Klapyta and B. Åkerström, *Free Radic Biol Med*, 2005, 38, 557–567.

72 A. Ellis and L. J. Twyman, *Macromolecules*, 2013, 46, 7055–7074.

73 D. Boris and M. Rubinstein, *Macromolecules*, 1996, 29, 7251–7260.

74 R. K. Jain and A. D. Hamilton, *Org Lett*, 2000, 2, 1721–1723.

75 J. Muldoon, A. E. Ashcroft and A. J. Wilson, *Chemistry – A European Journal*, 2010, 16, 100–103.

76 Y. Zhao, H. Chen, Y. Yang, Q. Wu and D. Wang, *Science of The Total Environment*, 2020, 700, 134492.

77 M. De, S. S. Chou and V. P. Dravid, *J Am Chem Soc*, 2011, 133, 17524–17527.

78 S. Pandit and M. De, *ACS Appl Nano Mater*, 2020, 3, 3829–3838.

79 W. Zhou, W. Zhuang, L. Ge, Z. Wang, J. Wu, H. Niu, D. Liu, C. Zhu, Y. Chen and H. Ying, *J Colloid Interface Sci*, 2019, 546, 211–220.

80 D. J. Joshi, J. R. Koduru, N. I. Malek, C. M. Hussain and S. K. Kailasa, *TrAC Trends in Analytical Chemistry*, 2021, 144, 116448.

81 F. T. Johra, J.-W. Lee and W.-G. Jung, *Journal of Industrial and Engineering Chemistry*, 2014, 20, 2883–2887.

82 P. B. Arthi G and L. BD, *J Nanomed Nanotechnol*, DOI:10.4172/2157-7439.1000253.

83 S. Guo, S. Garaj, A. Bianco and C. Ménard-Moyon, *Nature Reviews Physics*, 2022, 4, 247–262.

84 *Philos Trans R Soc Lond*, 1859, 149, 249–259.

85 L. Staudenmaier, *Berichte der deutschen chemischen Gesellschaft*, 1898, 31, 1481–1487.

86 D. C. Marcano, D. V. Kosynkin, J. M. Berlin, A. Sinitskii, Z. Sun, A. Slesarev, L. B. Alemany, W. Lu and J. M. Tour, *ACS Nano*, 2010, 4, 4806–4814.

87 D. Graf, F. Molitor, K. Ensslin, C. Stampfer, A. Jungen, C. Hierold and L. Wirtz, *Nano Lett*, 2007, 7, 238–242.

88 T. I. Al-Warhi, H. M. A. Al-Hazimi and A. El-Faham, *Journal of Saudi Chemical Society*, 2012, 16, 97–116.

89 C. Bissantz, B. Kuhn and M. Stahl, *J Med Chem*, 2010, 53, 5061–5084.

90 M. L. Waters, *Curr Opin Chem Biol*, 2002, 6, 736–741.

91 N. Borane, R. Boddula, N. Odedara, J. Singh, M. Andhe and R. Patel, *Nano-Structures & Nano-Objects*, 2024, 39, 101282.

92 W. Yu, L. Sisi, Y. Haiyan and L. Jie, *RSC Adv*, 2020, 10, 15328–15345.

93 C. Sainz-Urruela, S. Vera-López, M. Paz San Andrés and A. M. Díez-Pascual, *J Mol Liq*, 2022, 357, 119104.

94 A. M. Díez-Pascual and A. L. Díez-Vicente, *ACS Appl Mater Interfaces*, 2016, 8, 17902–17914.

95 V. N. Huynh, M. Leitner, A. Bhattacharyya, L. Uhlstein, P. Kreitmeier, P. Sakrausky, J. Rehbein and O. Reiser, *Commun Chem*, 2020, 3, 158.

96 R. Breslow, U. Maitra and D. Rideout, *Tetrahedron Lett*, 1983, 24, 1901–1904.

97 Y. R. Girish, S. Pandit, S. Pandit and M. De, *Chem Asian J*, 2017, 12, 2393–2398.

98 S. Tang, W. Wu, L. Liu, Z. Cao, X. Wei and Z. Chen, *Physical Chemistry Chemical Physics*, 2017, 19, 11142–11151.

99 P. Hudáky, , Gyula Kaslik, , István Venekei and L. Gráf, *Eur J Biochem*, 1999, 259, 528–533.

100 D. M. Blow, *Acc Chem Res*, 1976, 9, 145–152.

101 S. M. Kelly and N. C. Price, in *Encyclopedia of Life Sciences*, Wiley, 2009.

102 S. Gault, M. W. Jaworek, R. Winter and C. S. Cockell, *Commun Biol*, 2020, 3, 550.

103 C. M. Romero, J. S. Abella, A. Velázquez and J. Sancho, *J Therm Anal Calorim*, 2015, 120, 489–499.